Design, fabrication and stiffening of soft pneumatic robots

Jan Fras

April 2023

Thesis submitted in partial fulfillment
of the requirements of the Degree of Doctor of Philosophy

School of Engineering and Materials Science
Advanced Robotics at Queen Mary (ARQ)
Queen Mary University of London

Supervised by Prof. Kaspar Althoefer

I, Jan Fras, confirm that the research included within this thesis is my own work or that where it has been carried out in collaboration with, or supported by others, that this is duly acknowledged below and my contribution indicated. Previously published material is also acknowledged below.

I attest that I have exercised reasonable care to ensure that the work is original, and does not to the best of my knowledge break any UK law, infringe any third party's copyright or other Intellectual Property Right, or contain any confidential material.

I accept that the College has the right to use plagiarism detection software to check the electronic version of the thesis.

I confirm that this thesis has not been previously submitted for the award of a degree by this or any other university.

The copyright of this thesis rests with the author and no quotation from it or information derived from it may be published without the prior written consent of the author.

06 July 2022

Abstract

In many cases, soft material robots are safer and more dexterous than rigid ones. On account of their compliance and adaptation capabilities, their interaction forces with the environment can be significantly lower than those of their rigid-bodied counterparts. These qualities also often lead to a reduction in task complexity, as they can work when under-actuated, significantly reducing the number of inputs required for their control.

Despite those advantages, they also present many challenges. Traditional manufacturing methods developed for stiff-material robots do not work for soft materials. Soft parts are difficult to shape, align and assemble, and their design processes have to address these limitations.

Although compliance allows the soft robot to be under-actuated and generalise its control, it also impacts the ability of the robot to exert forces on the environment. There is a trade-off between robots being compliant or precise and strong. Many mechanisms that change robots' stiffness on demand have been proposed, but none are perfect, usually compromising the device's compliance and restricting its motion capabilities.

Keeping the above issues in mind, this thesis focuses on creating robust and reliable pneumatic actuators, that are designed to be easily manufactured with simple tools. They are optimised towards linear behaviour, which simplifies modelling and improve control strategies.

The principle idea in relation to linearisation is a reinforcement strategy designed to amplify the desired, and limit the unwanted, deformation of the device. Such reinforcement can be achieved using fibres or 3D printed structures. I have shown that the linearity of the actuation is, among others, a function of the reinforcement density and shape, in that the response of dense fibre-reinforced actuators with a circular cross-section is significantly more linear than that of non-reinforced or non-circular actuators.

I have explored moulding manufacturing techniques and a mixture of 3D printing and moulding. Many aspects of these techniques have been optimised for reliability, repeatability, and process simplification. I have proposed and implemented a novel moulding technique that uses disposable moulds and can easily be used by an inexperienced operator.

I also tried to address the compliance-stiffness trade-off issue. As a result, I have proposed an intelligent structure that behaves differently depending on the conditions. Thanks to its properties, such a structure could be used in applications that require flexibility, but also the ability to resist external disturbances when necessary. Due to its nature, individual cells of the proposed system could be used to implement physical logic elements, resulting in embodied intelligent behaviours.

As a proof-of-concept, I have demonstrated use of my actuators in several applications including prosthetic hands, octopus, and fish robots. Each of those devices benefits from a slightly different actuation system but each is based on the same core idea - fibre reinforced actuators.

1

I have shown that the proposed design and manufacturing techniques have several advantages over the methods used so far. The manufacturing methods I developed are more reliable, repeatable, and require less manual work than the various other methods described in the literature. I have also shown that the proposed actuators can be successfully used in real-life applications.

Finally, one of the most important outcomes of my research is a contribution to an orthotic device based on soft pneumatic actuators. The device has been successfully deployed, and, at the time of submission of this thesis, has been used for several months, with good results reported, by a patient.

ACKNOWLEDGEMENTS

The work described in this thesis would not have been possible without the help and support of many people.

Firstly I want to thank my supervisor, Professor Kaspar Althoefer, who initially offered me this opportunity and kept his trust in me throughout. He not only helped me overcome all the challenges along the way, but allowed me room for independence and creativity. Without his help, I would not be where I am, neither academically nor professionally.

I am grateful to all my colleagues at ARQ, especially Fabrizio Putzu, Liza Konstantinova and Taqi Abrar, for their company and support.

I am also thankful to all my teammates from the STIFF-FLOP project, where my soft robotics adventure began. I want to thank Yohan Noh for his inspiration and all the discussions we had over the years. I should also like to acknowledge my former company co-workers Mateusz Macias, Jakub Glowka and Jan Czarnowski. The skills I learned from them helped me enormously during my PhD journey and indeed beyond.

One of the people who significantly impacted my early development was the aircraft model instructor, the late Andrzej Oporowski. He created a remarkable space for young people in which he taught us not only how to make flying machines but also, perhaps even more importantly, conscientiousness and attention to detail.

I also want to thank my wife for all the support she offered and for all the care she gave to our children when I was working long evenings and travelling to University. She was always willing to listen to my lengthy explanations of how my next idea might work and has always been my primary source of motivation.

Finally, I thank my parents for all the hard work they put into my development. Whatever creativity and patience I have is down to them!

Contents

List of Figures

LIST OF TABLES

LIST OF ABBREVIATIONS

CAD	Computer-Aided Design
DOF	Degrees of Freedom
EAP	Electro Active Polymers
EMG	Electromyography
EPAM	Eversive Pneumatic Artificial Muscle
FDM	Fused Deposition Modelling
FEM	Finite Element Method
MIS	Minimally Invasive surgery
MRI	Magnetic Resonance Imaging
PWM	Pulse Width Modulation
SMA	Shape Memory Alloys
SPA	Soft Pneumatic Actuator

1

INTRODUCTION

Soft robotics is a relatively young discipline within robotics which aims to create systems that are fundamentally different from standard, rigid-element-based systems. That fundamental difference relates to the physical compliance of these new systems, the creation of which is being driven by a number of reasons, including the need for safe interaction between robots and the environment and between robots and humans [1, 2], ability to reduce task complexity [3], or extended dexterity [4].

This physical compliance, due to their soft and flexible properties, makes these machines ideal candidates for tasks involving complex motions as traditional devices composed of links and joints can become unmanageably complex or require overly sophisticated control strategies [5].

For this reason, soft robots are often considered for medical applications [6] (minimally invasive surgery [7], diagnostics [8, 9], rehabilitation [10]) in cooperative human-robot activities [1, 2, 11], grasping [12, 13, 14] or prosthetics [15, 16, 17].

Despite having great potential, soft robotics has not yet become a well-established discipline. This can be attributed to various factors, including numerous challenges associated with soft actuation. Soft-bodied robots deform in a variety of ways that are difficult to model or predict [18], and precise control of their movements is a non-trivial task. Furthermore, the relatively nascent and rapidly evolving concept of soft robots necessitates the development of new materials and techniques to meet emerging design requirements. In this thesis, I aim to address these issues, and my motivation is outlined in more detail below.

1.1 Motivation

My journey in soft robotics began in 2013 when I joined the STIFF-FLOP project (STIFFness controllable Flexible & Learnable manipulator for surgical OPerations [7]). The project's objective was to create a soft, minimally invasive surgical robot capable of bending in any direction and elongating while remaining soft and squeezable. My primary responsibility involved the sensory data fusion from available sensors, which included force/torque and length sensors embedded within the device's body. I proposed an approach to create a simplified physical model of the device, using the sensor data as model inputs. The early STIFF-FLOP robot prototype was a silicone cylinder with three pneumatic chambers symmetrically arranged around its central axis and a braided sleeve enveloping the entire device to constrain ballooning during operation, as depicted in Fig. 1.1.
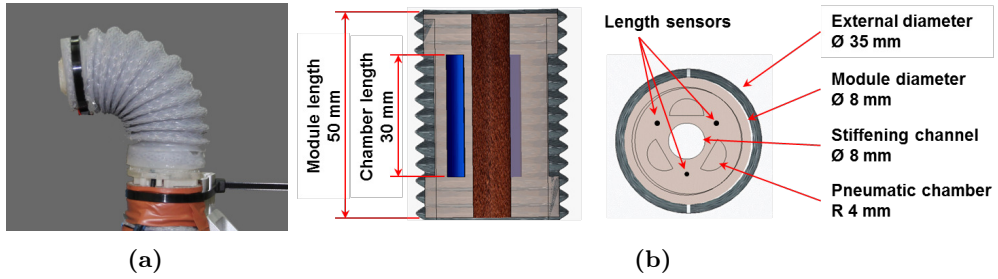
Figure 1.1: The early prototype of STIFF-FLOP module. (a) actual device, (b) design.

Without physical access to the device, I made some assumptions and developed the model by discretizing both Hooke's law and the Euler-Bernoulli beam theory, see Fig. 1.2, [19].
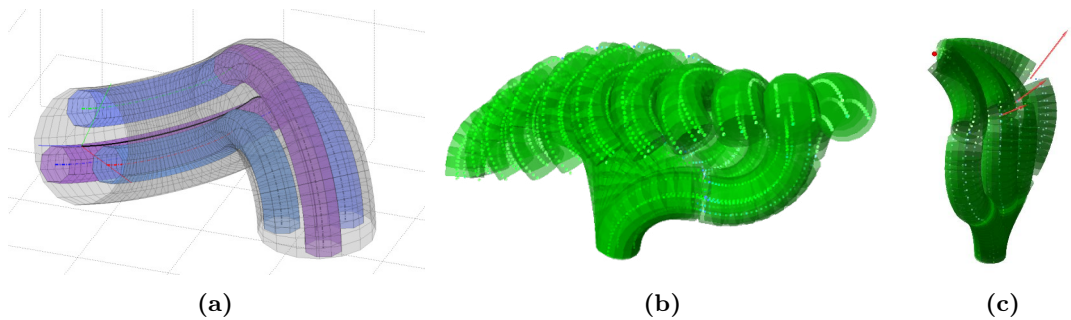
Figure 1.2: Physical model of the STIFF-FLOP manipulator, based on the fundamental principles of Hooke's law and the Euler-Bernoulli beam theory. (a) Shape reconstruction based on the model, with sensor data as input, implemented in MATLAB. (b) Line-following based on inverse kinematics derived from the physical model. (c) Disturbance rejection (indicated by the red arrow) based on the model. Both (b) and (c) are implemented in Python.

Upon receiving one of the prototypes to validate the model, I discovered that my assump-

tions were incorrect. The module exhibited various deformations within the external sleeve, with the chambers not only affecting each other but also the sensors located inside the device. After a thorough investigation, I concluded that it would be better to improve the device rather than alter the model. This led to my involvement in enhancing soft robotic devices' performance, refining fabrication techniques, and applying them to new areas.

1.1.1 Actuation performance

The initial STIFF-FLOP module exhibited high nonlinearity, as seen in Fig. 1.3. I realised that such nonlinearity would impact all aspects of the project, including control strategies, sensing, and shape and position tracking. In my opinion, the best solution was to simplify the device's behaviour rather than complicate all the other system components. I began exploring how the reinforcing structure and actuator geometry could be tuned to enhance the device's response. Alongside improvements in the geometry and structure of multi-DOF STIFF-FLOP modules, I also started investigating more efficient ways of motion generation, leading me to more specific actuators that generate rotation, bending, and two-dimensional bending.
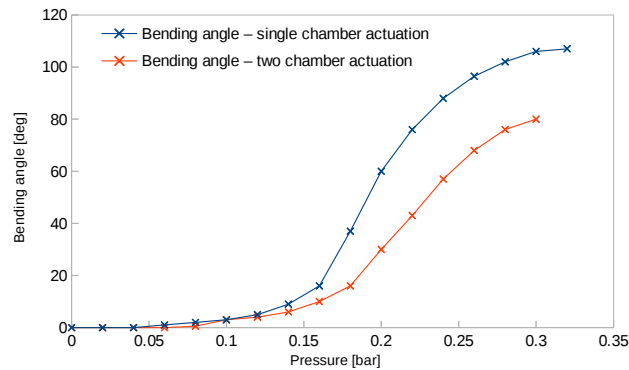
Figure 1.3: The early prototype of STIFF-FLOP module response.

1.1.2 Fabrication

While working on the design of soft actuators, I observed that fibre reinforcement fabrication techniques had several drawbacks and limitations in their current state. The process was very labour-intensive and prone to errors due to the purely manual thread application. Moreover, it was limiting the design space, as some structures were not achievable using the state-of-the-art

procedure. For this reason, I applied some improvements to the existing techniques and proposed new ones.

1.1.3 Stiffening

Stiffening is a significant issue in soft robotics in general. In STIFF-FLOP, stiffening was one of the main research points, even mentioned in the project name. The approach we followed in the project was granular jamming. Multiple stiffening chambers were located in the flexible module body. These chambers were filled with coffee granules that jammed whenever a vacuum was pulled from the stiffening chambers. In practice, this solution had several drawbacks. Stiffening chambers, even when not activated, caused resistance for the bending motion and were a source of significant hysteresis. When active, the device would not only become stiffer but essentially locked. That said, this approach was more 'shape locking' than 'stiffness control'. In fact, most of the proposed stiffening mechanisms in soft robotics are more or less binary systems that lock the shape and disable any further actuation changes. Such suboptimal stiffening technology motivated my research towards smarter stiffening mechanisms that could not only change the effective stiffness of the device but also coexist with the actuation.

1.2 Research questions

Driven by the motivation outlined in the previous sections, this thesis poses the following questions:

1. How can the performance of soft actuators be improved? Is it possible to make their response more linear and reduce undesired deformation effects? Can this be achieved by adjusting their geometry and employing reinforcing structures?

2. Can the manufacturing process be made more repeatable and less labour-intensive? Is it feasible to utilise rapid fabrication techniques, such as 3D printers, whilst maintaining the performance of platinum cure silicone?

3. Is it viable to develop a stiffening mechanism that coexists with actuation, as opposed to current approaches which lock the shape of the actuator and restrict any further actuation?

1.3 Contributions

The main contributions of this thesis fall into three areas, described below.

1.3.1 Actuator design and fabrication

I proposed several design and fabrication ideas that improve the performance and reduce the fabrication complexity of soft fibre-reinforced pneumatic actuators. The proposed design requires circular geometry for the pressure chambers and the application of dense, fibre-based reinforcement. This leads to a more linear actuator response and greater actuator robustness in comparison to other commonly applied approaches. In addition, the proposed manufacturing procedure introduces the idea of applying the reinforcement before the fabrication of the actuator body, significantly simplifying the process while providing more consistent and more reliable results.

I also proposed changes that reduce manufacturing complexity by using a single material Fused Deposition Modelling (FDM) 3D printer. The proposed solution involves printing the reinforcement and the mould in one go as a single-use structure. After filling the mould with silicone, the outer part can be removed and disposed of, while the reinforcement remains attached to the silicone body of the actuator.

1.3.2 Stiffening

I proposed a soft pneumatic actuator that can vary its stiffness in a smart way. The design allows for the coexistence of high actuation compliance alongside stiff response to disturbance at any operating point. Thanks to the smart internal structure, the mechanical resistance of the actuator depends on the direction and characteristics of the external forces acting on its surface. It allows for an efficient change in its compliance on the fly without locking its shape. The actuator I propose can continuously adjust in one spatial direction (towards the inner side of the actuator), remaining soft and compliant while resisting significantly higher forces in the opposite direction (towards the outer side of the actuator). Thanks to the design, the actuator can resist considerably higher forces than it can actively exert at a given input pressure.

The actuator is inspired by the mechanical structure of the mammalian penis, in which

a soft structure can be efficiently stiffened with a relatively low input pressure of blood thanks to a constant-volume cavity and a directional flow of blood. The corpus cavernosum is composed of small sinusoids that fill with blood during an erection and trapping it so that it cannot escape [20]. Blood, being a liquid, has very low compressibility, so any external force compressing it generates a localised increase in pressure that in turn results in high bending resistance of the hydraulic structure of the penis, despite the relatively low inflation pressure.

1.3.3 Robotic system demonstrators

I designed and constructed several soft robotic system demonstrators based on actuation solutions I had developed. Those systems focused on the application of developed actuators into various use case scenarios, such as soft manipulation (soft manipulation modules), soft grasping (soft hands - Section 5.1), and soft locomotion (soft octopus and fish robots, Sections 5.2 and 5.3), as well as rehabilitation (Icarion active orthosis, Section 5.4). The latter system incorporated soft pneumatic actuators, and at the time of writing, has successfully been used by a real patient who has reported very good results over a period of several months.

1.3.4 List of Publications

Most of the work entailed in this thesis has been presented in the following publications:

Papers

J. Fras, J Glowka, and K Althoefer. "Instant soft robot: A simple recipe for quick and easy manufacturing". In: *2020 3rd IEEE International Conference on Soft Robotics (RoboSoft)*. IEEE. 2020, pp. 482–488.

J. Fras and Kaspar Althoefer. "Soft fiber-reinforced pneumatic actuator design and fabrication: Towards robust, soft robotic systems". In: *Annual Conference Towards Autonomous Robotic Systems*. Springer. 2019, pp. 103–114.

J. Fras, Y. Noh, Macias M., H Wurdemann, and K. Althoefer. "Bio-inspired octopus robot based on novel soft fluidic actuator". In: *International Conference on Robotics and Automation*. IEEE. 2018.

J. Fras, M. Macias, Y. Noh, and K. Althoefer. "Fluidical bending actuator designed for soft octopus robot tentacle". In: *2018 IEEE International Conference on Soft Robotics (RoboSoft)*. IEEE. 2018, pp. 253–257.

J. Fras and K. Althoefer. "Soft biomimetic prosthetic hand: Design, manufacturing and preliminary examination". In: *2018 IEEE/RSJ International Conference on Intelligent Robots and Systems (IROS)*. IEEE. 2018, pp. 1–6.

Jan Fras and Kaspar Althoefer. "Soft pneumatic prosthetic hand". In: *Towards Autonomous Robotic Systems: 19th Annual Conference, TAROS 2018, Bristol, UK July 25-27, 2018, Proceedings 19*. Springer. 2018, pp. 112–120.

J. Fras and K. Althoefer. "Bio-mimetic pneumatic soft prosthetic hand". In: *UK-RAS Conference on 'Robotics and Autonomous Systems', Bristol*. UK-RAS, 2017.

J. Fras, Y. Noh, H Wurdemann, and K. Althoefer. "Soft fluidic rotary actuator with improved actuation properties". In: *International Conference on Intelligent Robots and Systems*. IEEE. 2017.

Book Chapters

J. Fras, Alberto Arezzo, Ali Shiva, and Kaspar Althoefer. "Soft Robotics Solutions for Minimally Invasive Surgery: The Need for Stiffness Controllability". In: *Soft Matter for Biomedical Applications*. 2021, pp. 684–719.

J. Fras, Mateusz Macias, Jan Czarnowski, Arianna Brancadoro Margherita Menciassi, and Jakub Glowka. "Soft Manipulator Actuation Module – with Reinforced Chambers". In: *Soft and Stiffness-controllable Robotics Solutions for Minimally Invasive Surgery: The STIFF-FLOP Approach*. Ed. by Jelizaveta Konstantinova, Ali Shafti, and Kaspar Althoefer. River Publishers, 2018. Chap. 3.

J. Fras, Mateusz Macias, Jan Czarnowski, and Jakub Glowka. "Modelling and Position Control of the Soft Manipulator". In: *Soft and Stiffness-controllable Robotics Solutions for Minimally Invasive Surgery: The STIFF-FLOP Approach*. Ed. by Jelizaveta Konstantinova, Ali Shafti, and Kaspar Althoefer. River Publishers, 2018. Chap. 10.

1.3.5 Popular Science

In addition to traditional scientific publications, my work has featured in several showcases as well as a variety of popular science articles.

Showcases:

- London Tech Week 2017,

- International Robotics Showcase 2017 in London,

- International Robotics Showcase 2018 in Liverpool,

- AI UK 2021 in London,

Popular science articles:

- Evening Standard: *Scientists develop robo-octopus that mimics real sea creature*[21],

- Evening Standard: *'Robohand' developed for children who have lost a limb*[22],

- UT2 Magazine: *SOFT MACHINE*[23],

- Mashable: *Scientists built a robot octopus that moves its tentacles like the real thing* [24].

It was also featured on the BBC's Sunday Morning show [25] and used in promotional materials and videos for ICRA 2023.

My PhD work was also recognised by my inclusion in The Evening Standard's *The Progress 1000: London's most influential people 2019* list [26].

1.4 Thesis outline

The structure of this thesis is as follows:

- **Chapter 2** provides background and discusses related work.

- **Chapter 3** describes soft actuators. Firstly general design and fabrication procedures are presented. Then two specific actuators are discussed: rotational and bending actuators. Finally advancement in fabrication using 3D printing is presented along with relevant design strategies.

- **Chapter 4** presents a stiffening mechanism for bending soft actuators. The stiffening structure is inspired by mammalian erectile tissue. The concept, the stiffening principle, its design and fabrication, along with expected and experimental stiffening effects are provided.

- **Chapter 5** discusses soft robotic systems that utilise the soft robotic actuators described in the previous chapters. These systems are:

    - **Soft prosthetic hands** that are entirely soft and aim to mimic real hand morphology. The hand is based on an extending actuator whose motion is converted to bending by an external non-stretchable palm structure. The hand provides 6 DOF and can be controlled using various interfaces

    - **Soft octopus and fish robots** that are created with submarine exploration in mind. These robots can navigate through water in a very natural manner. Design and fabrication details are provided as well as experimental data on velocities and thrust.

    - **A rehabilitation exoskeleton** that was created jointly with Icarion inc. The device uses soft pneumatic actuators in the passive mode for the generation of bending motion in patients' joints. The device is being certified, having already been tested by a patient who has reported very good results over a period of several months.

    - A pressure control system that was designed for the hand, but then successfully implemented in the other projects.

- **Chapter 6** summarises the thesis and provides propositions for future work.

Background and related work

What makes soft robots unique is their physical compliance. Traditional robots are rigid, and they have finite joints and stiff links. They move in response to rotations or linear motions along well-defined axes. To navigate safely through the environment, they need to be aware of their surroundings and equipped with several sensors and sophisticated controllers. Soft robots, however, are compliant by design. As a result, they can passively adapt to the environment ensuring that interactions are inherently safe.

The compliant nature of soft robots requires novel approaches to actuation. Various solutions, each based on specific physical principles have been proposed, among them electrically-driven actuators like Dielectric Elastomers [27], shape memory alloys (SMA) that change their shape when heated [28, 29], light-driven polymers [30], tendon-driven devices [15], and fluidic actuators that can work under positive [31] or negative pressure [32].

Due to their unique properties, soft robots are considered ideal for tasks in which that kind of adaptivity is crucial, such as in human-robot interactions, medical applications, and agricultural tasks.

2.1 Application areas of soft robotic devices

2.1.1 Grasping devices

An example of compliance in action can be found in grasping devices [33], see Fig. 2.1. In [34] a soft gripper is presented, in which the fingers are made of silicone. Each finger is composed of a bellow-like chamber constrained with a flat silicone surface on the inner

side. The geometry of the finger makes it expand on the outer side, while the internal layer constrains this elongation resulting in a bending motion. On account of its passive adaptivity, distributed deformation and compliance, the gripper can grasp various objects using just a very simple (binary) control strategy and without the need for any complex sensing. The expansion of the pressure chamber is constrained on the inner side by the strain-resistant layer but unrestricted on the other side of the gripper. Some of that expansion contributes to the bending, but a part of it, the radial component, is essentially wasted energy. For that reason, researchers have tried to vary the geometry of the actuator to limit that effect.
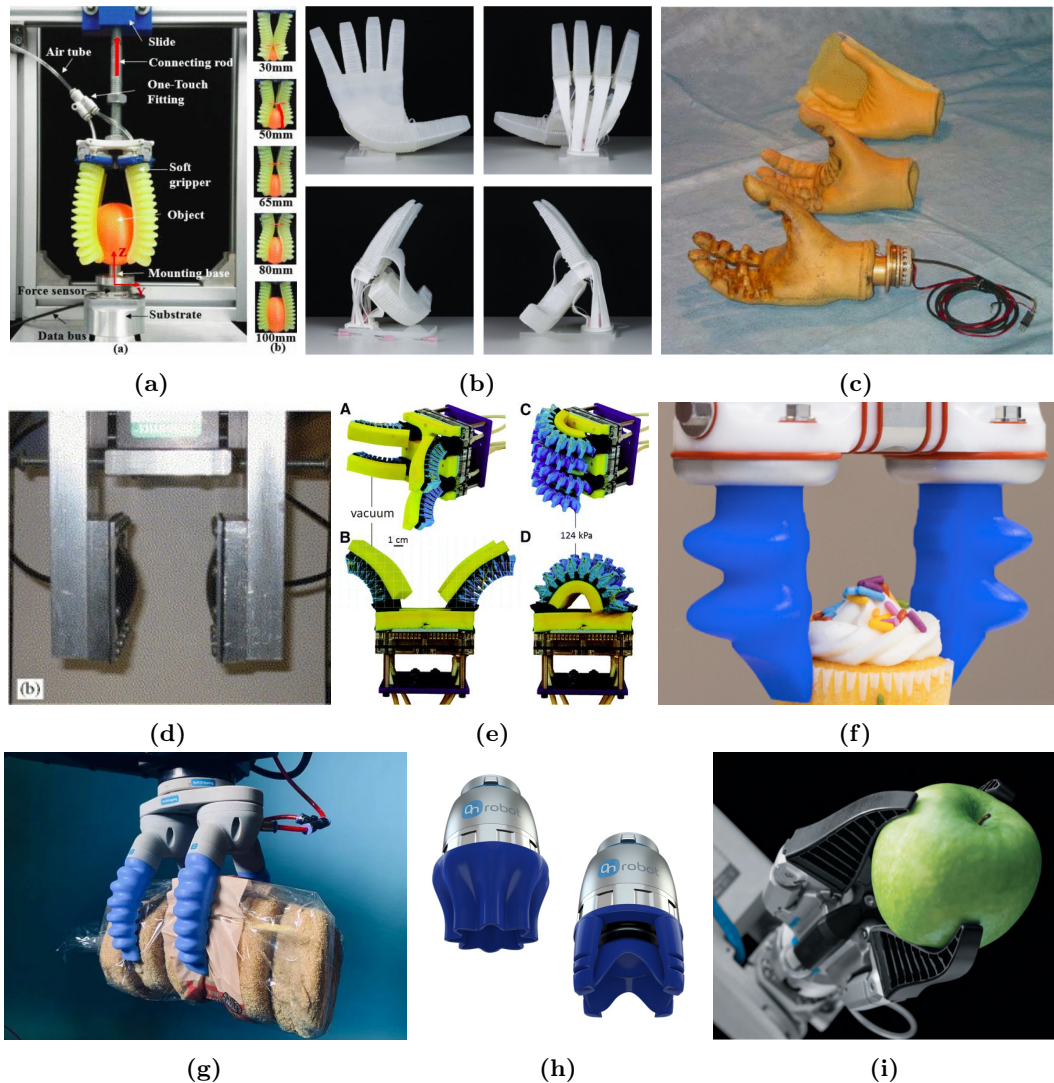
Figure 2.1: Examples of compliant grasping devices: (a) Universal soft pneumatic robotic gripper [34], (b) Underactuated robotic hand for dexterous grasping, image taken from [35], (c) a cosmetic prosthetic hand, image taken from [15], (d) a gripper based on inflatable rubber pockets, image taken from [36], (e) a grippers for sampling on deep reefs, image taken from [37], (f),(g),(h) and (i) commercial grippers from Soft Robotics Inc, Wegard, OnRobot and Festo, respectively,, image taken from [38, 39, 40, 41].

A similar physical principle is used in a human-like hand device presented in [35, 42]. In that instance, the gripper is shaped like a human hand, and its radial expansion is limited due to fibre embedded into the actuator walls. This efficiently constrains the expansion and makes the strain distribution more even than can be achieved via the geometry-based approach alone.

Another soft hand device has been proposed in [15]. In this instance the device is tendon-driven, but thanks to its soft and under-actuated structure it can be driven with a single motor and passively adapt to the object it handles.

Physical compliance of pneumatic actuators has also been utilised in [36]. In that work, the authors propose a gripper that has fingers equipped with inflatable areas. Pressure in those areas can be controlled, enabling adjustment of the fingers' compliance that is dependent on the manipulated object. In the presented design, despite the traditional mechanics of the gripper, this soft modification - the introduction of passive compliance areas - reduces the complexity of its control.

Mechanical compliance is especially important when interacting with delicate objects. Although most soft grippers are still early stage prototypes created as academic proof-of-concepts, there are examples of soft grasping devices used extensively in real-live conditions. One area that is particularly well suited to the gentle touch of soft robots is underwater sample collection [37].

There are also food handling soft grippers commercially available from companies such as SoftRobotics Inc [38] and Wegard GmbH [39], and general purpose soft grippers that have been developed by OnRobot [40].

Another commercially available examples are Festo Fin Ray robotic fingers that are actuated just like traditional rigid fingers but thanks to their smart structure not only conform to the objects they grasp, providing better pressure distribution, but also wrap around them resulting in better grasp stability [41].

2.1.2 Human-robot interaction

The inherent compliance of soft robots is a highly desirable feature, not just because it facilitates control and passive adaptation to unstructured environments but also because it is fundamental to human-robot interaction.

Collaborative devices

Robotic devices have helped humans for decades. Since the industrial revolution they have populated manufacturing environments, medical operating theatres and domestic homes. They execute tasks repeatedly, precisely and do not tire - indeed often outperforming their human counterparts. But in many cases, there remains a need for human-robot collaboration. This is a problem, because robots are usually unable to adapt to changing environment, and therefore pose a significant threat to humans around them.

Recent trends in robotics have tried to address this with the creation of collaborative robots, also known as cobots. This is achieved by introducing sensors and safety algorithms, while also limiting the power of these devices. As a consequence, collaborative robots can feel force and impact and react accordingly, but sacrifice their payload and speed as compared to heavy industrial robots. The upside is that this increases, though doesn't mitigate, safety for humans working alongside them - they can still move at considerable speed and impact with their rigid bodies can be dangerous.

While the integration of sensors and other instruments alongside power limitation has a place, the way in which soft robotics is trying to address these issues is by creating fundamentally different soft-bodied robots.

In [2, 43, 44] robots utilising soft pneumatic links are presented, Fig. 2.2. The main motivation of the work presented in [44] is the reduction of the payload-to-weight ratio of the system, with the improved user safety a value-adding bonus, whereas [2] focuses mainly on the human-robot interaction safety aspect. Both systems are based on inflatable links that can control their rigidity by varying their internal pressure, which can be released when human-robot contact occurs, rendering these robots soft and harmless to the user. The proposed design provides proof-of-concept for the stiffness-controllable links, but still uses rigid, traditional joints. It is noted that robots with inflatable links [43, 44] have been proposed as early as in 1990s.

Some other robots offer entirely soft structures, such as in [45] in which a robotic arm composed of inflatable links and semi-inflatable rotary joints is proposed, Fig. 2.3. The robot utilises traditional rotary joints that simplify its control while the actuators that are embedded in the joints are inflatable. The robot's links contain four chambers parallel to
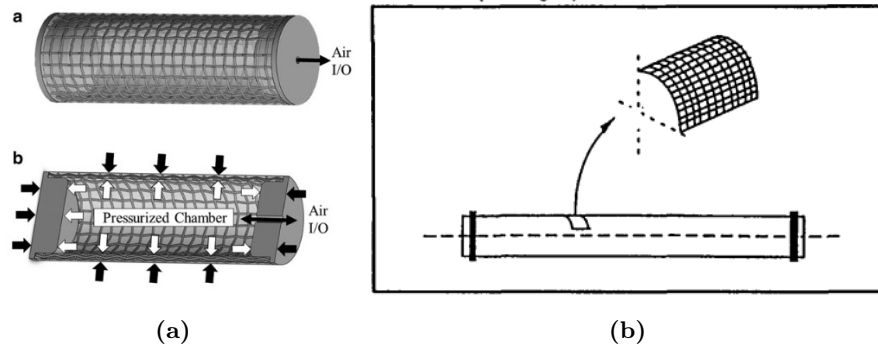
Figure 2.2: Inflatable robotic links, (a) inflatable link structure proposed in [2], (b) inflatable link structure proposed in [43, 44].

the central axis of the link. This design allows for greater rigidity of the link when inflated and simplifies passing pressure tubes to subsequent components. However, while the research aims to provide a safe solution for human-robot interaction with high positioning accuracy, the rigid structures in the joints are still create potential hazards for users.
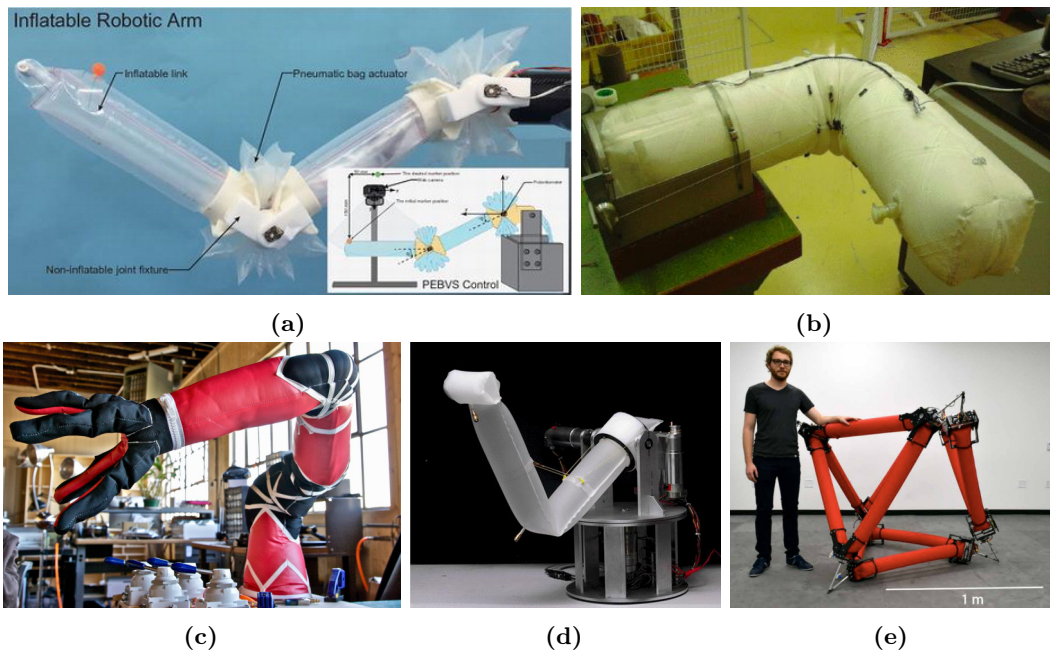
Figure 2.3: Inflatable robots: (a) a robot with inflatable links and semi-inflatable joints, image taken from [45], (b),(c) and (d) fully inflatable robots, image taken from [46, 47, 48], (e) a robot with inflatable links and rolling joints, image taken from [49].

In [46] another inflatable robot is presented. It contains no rigid elements at all; even the joints are entirely pneumatic. As a result the robot is very compact when packed and easy to deploy. Moreover, the robot can bend its joints with tendons thanks to a clever folding design. A similar device is being developed by OtherLab [47].

A fully inflatable design is also presented in [48] in which a movie-inspired robot has been

proposed. It is composed of links made of inflatable plastic film and is actuated by tendons.

An interesting robot design that aims to provide safe human-robot interaction while addressing soft robots' limitations (such as limited mobility) is presented in [49]. This robot is based on inflatable links, but its motion is generated via rollers that change the joints' positions rather than the lengths of the tubes. The overall length of the links in the system remains constant so that once pressurised, the volume does not change over time and does not require pressure supply when operating.

Wearable devices

Human-machine interaction is particularly relevant in relation to wearable devices. In applications like rehabilitation or prosthetics, interaction is, in essence the key issue. As a consequence, soft material robotic devices have been extensively examined in these areas, as they offer as potential solutions on account of their properties [50],.

One of most explored areas is hand rehabilitation. In a review article [51] forty four unique soft robotic hand rehabilitation devices were gathered, most of which use soft pneumatic actuators to help patients close and open their hands. In [52] a soft glove is presented, which is designed to augment hand motion for patients with grasping disabilities Fig. 2.4. It uses pneumatic actuators reinforced with fibres, which have mechanically programmed motions that match the requisite motion types and ranges.

In [10] a similar device was proposed, but to assist not only the closing, but also the opening motion of the patient's hand. The device uses pneumatic tube actuators that straighten when pressurised for the opening motion and tendons for closing. The antagonistic actuation mechanism enables motion adjustment, in turn, maximising rehabilitation effectiveness.

Another field of research are entire limb assistance devices. In [53] a soft exosuit is presented that reduces users' effort while walking. The device is tendon-driven.

A similar device, but one that uses pneumatic power and is designed for hip rehabilitation is presented in [54]. The design uses rotary actors, and helps to reduce the muscle effort for patients suffering from lower limb immobility.

Soft wearable suits are explored not only from rehabilitation perspectives. In [55] a lower-body suit is presented. It is based on Bubble Artificial Muscle and designed to help space travellers maintain physical fitness when prolonged low gravity conditions could cause
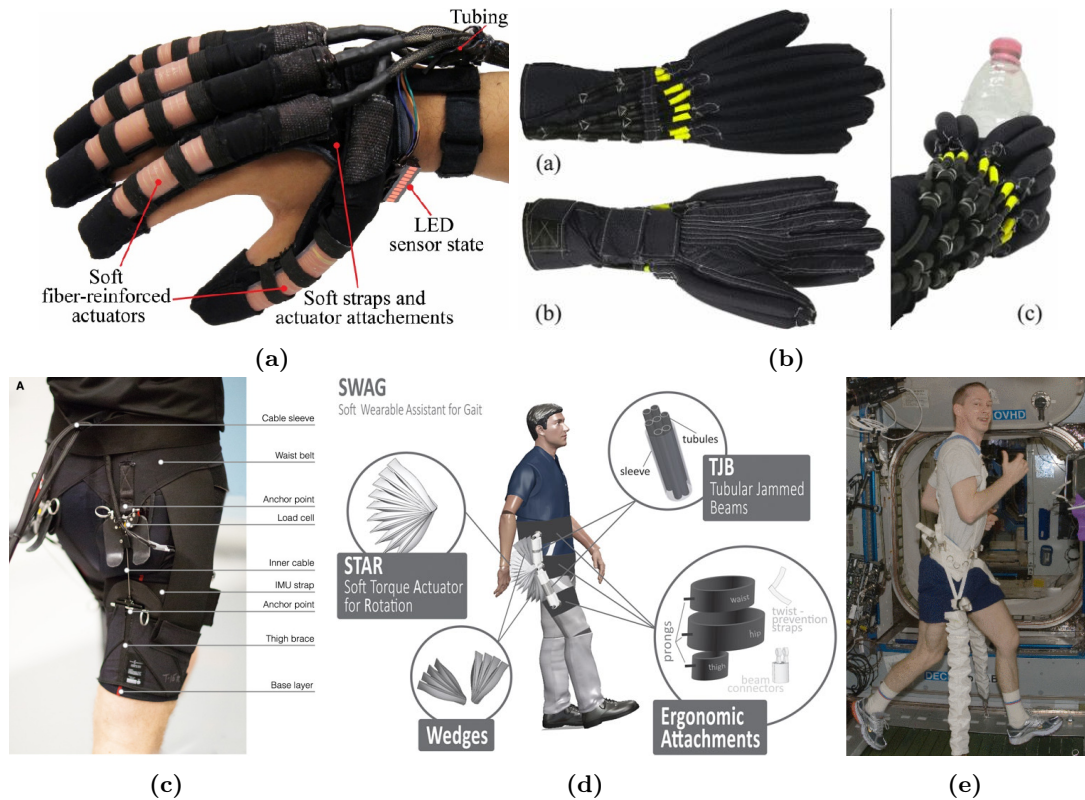
Figure 2.4: (a) and (b) assistive gloves for patients with grasping disabilities, image taken from [52, 10], (c) and (d) walking assistive devices, image taken from [53, 54], (e) astronauts' fitness device, image taken from [55]

health issues.

2.2 Motion generation

2.2.1 Motion principles

Soft actuators come in a variety of shapes and offer various types of motion. They can expand or contract, generating translation, bending, twisting, or rotation. These actuators are classified according to their working principle and medium. Examples include those powered by pressure [56, 57], those that are tendon-driven [58, 15], temperature-driven actuators such as shape memory alloys (SMA) that change their shape when heated [28, 29], state transition-based actuators [59], dielectric elastomer actuators (DMA) [27], mixed actuators [60], or even light-driven ones [30], as shown in Fig. 2.5.

As my research builds upon my prior work in the Stiff-Flop project [61], the focus of this thesis is on pressure-based fluidic actuators. However, it's worth noting that even within this
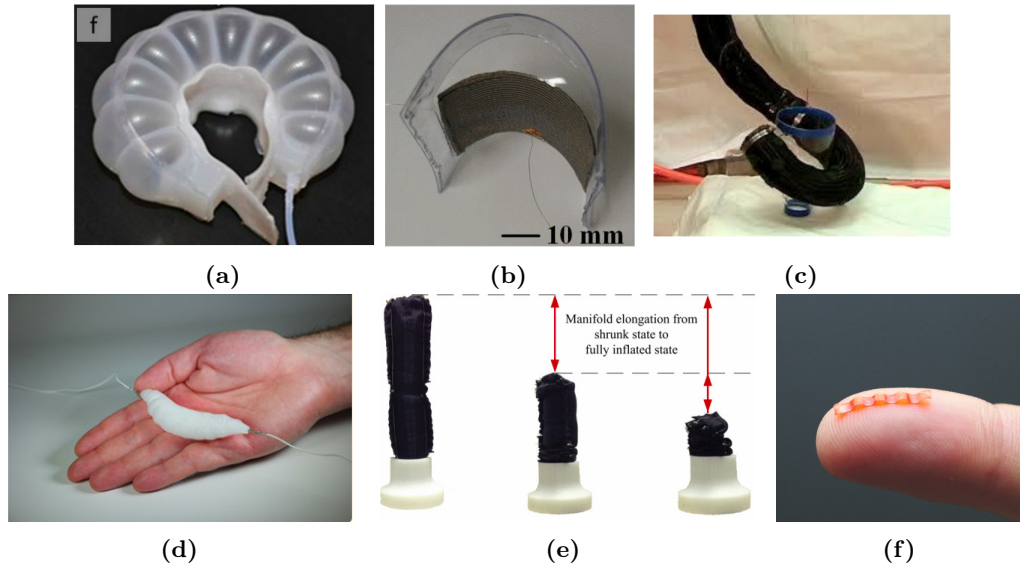
Figure 2.5: Actuation principles: (a) pressure-driven actuator, image taken from [57], (b) dielectric elastomer, image taken from [27], (c) tendon-driven manipulator, image taken from [58], (d) temperature-driven actuator, image taken from [59], (e) actuator driven by both pressure and tendons [60], (f) light-driven actuator, image taken from [30]

category, there can be variations in the actuation principles used, as summarized in the next section.

2.2.2 Fluidic actuators motion primitives

The most basic motion generated by soft actuators is expansion and contraction, as shown in Fig. 2.6. One of the most popular soft pneumatic actuators of this type is known as McKibben's muscle [62, 63]. During actuation with positive pressure, their volume increases, but the arrangement of fibres around the chamber causes the longitudinal dimension of the actuator to contract. They are very well suited for generating high forces, but their stroke is very limited.

Some efforts are being made to try to expand the contraction capabilities of McKibben's muscles [64]. The authors of the cited paper propose to compose the actuator of multiple thin McKibben muscles braided together. Such an approach allows for an increase in the experimental contraction ratio from 28% to 41%. The improvement is significant, but considering different soft actuators, even the improved stroke is very limited.

Although there are many applications in which such a small stroke (41% of the initial actuator's length) is not a problem, there are other situations where greater flexibility is required.
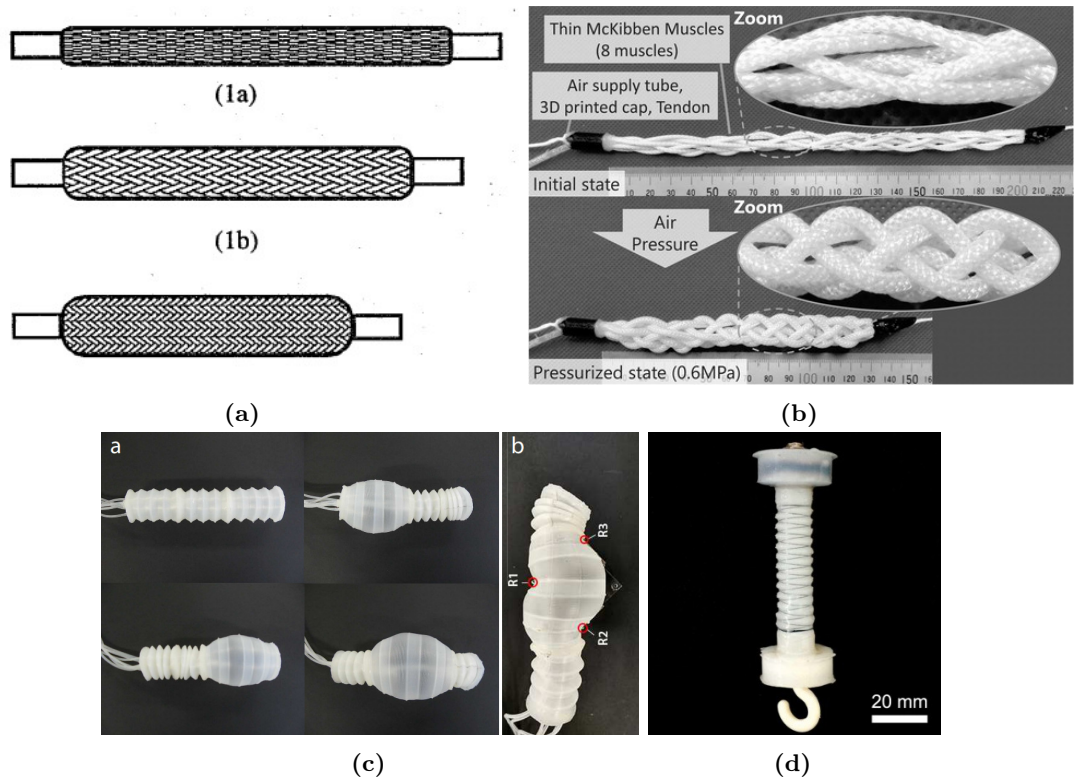
Figure 2.6: Expanding and contracting actuators: (a) McKibben muscle, image taken from [63], (b) braided McKibben muscle, image taken from [64], (c) highly-deformable soft actuator, image taken from [65], (d) fiber-reinforced actuator, image taken from [66]

A good solution for expanding the actuation range is elongating rather than contracting linear actuators. Their design makes them elongate under pressure. They can be made of a soft material that stretches or expands via a geometrical transformation of their structure, when pressure is applied.

In [65] a highly deformable actuator is proposed. The actuator is a soft-material bellow that expands when pressurised. Initially it just elongates, as would any other bellow, but once a critical pressure is reached, it balloons, offering a totally different mode of actuation. The idea is inspired by nature and the actuator can work under both positive and negative pressure ranges. It is capable of volume change by a factor of 300.

Other good examples of expanding actuators are fibre-reinforced actuators [67, 66] whose radial expansion is constrained with fibres so that they expand in the desired direction only.

Another commonly used motion type in soft robotics is bending deformation. Within pressure-driven bending actuators, there are many possible bending principles, Fig. 2.7. One working principle is that of bending due to asymmetrical actuation [61, 68, 69, 32]. In this case, the structure of the actuator makes the acting forces accumulate in a specific area of

the device. This area either elongates or shrinks to a greater extent than the other side, and consequently, the device bends. It is worth noting that the pressure acting in the chambers can also reach negative values. An example of an actuator working within a negative pressure range is a vacuum actuator [32].
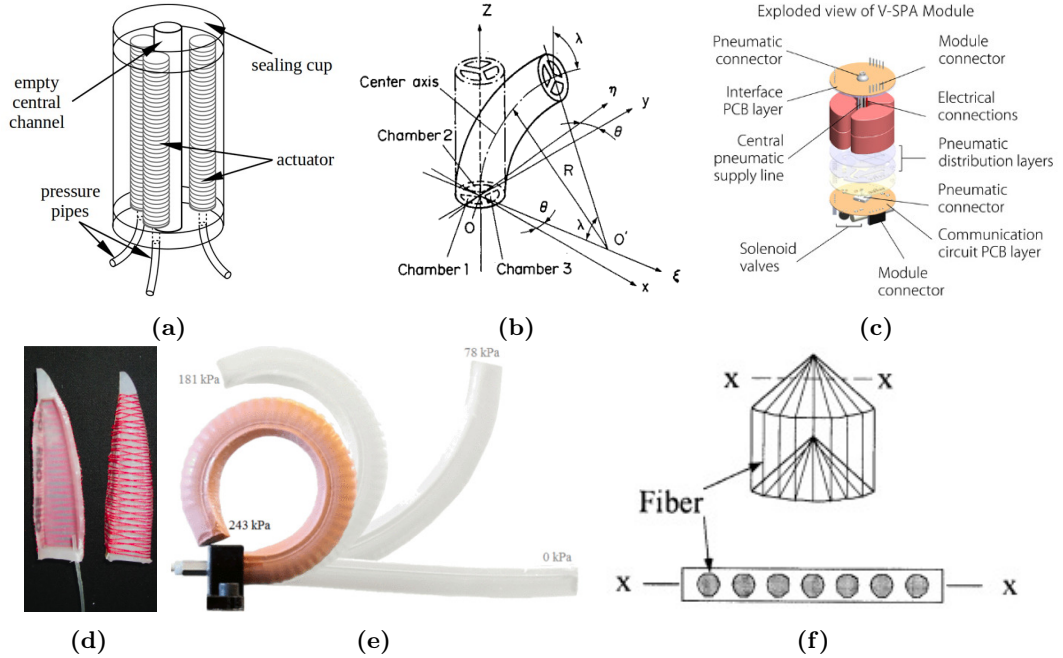
Figure 2.7: Bending actuation principles: (a), (b) and (c) asymmetrical actuation, images taken from [61, 69, 32], (d) and (e) non-uniform rigidity, images taken from [35, 56], (f) geometry-induced bending, image taken from [70]

The bending motion can also be caused by non-uniform rigidity [35, 56]. In this case, one side of the actuator is less extensible than another, so it elongates less when pressurised. These devices can provide pure bending if the less extensible side is in fact not extensible at all [35] or can combine elongation and bending in materials that can extend.

Another principle is that of bending due to the geometry of the device. In [70] an actuator is described that has a symmetrical cross-section and no special layers of less extensible materials (and therefore is equally affected by the actuation pressure) but is curved from the outset. On account of its shape, it is therefore designed to bend when pressurised.

Each bending principle has certain advantages. The first of those outlined above, for example, enables multiple actuation channels to be housed in the same part of the robot, equipping it with more than one degree of freedom (DOF). Consequently, not only the curvature but also the bending direction, twist, and elongation can be controlled [61]. In the second method the robot can use the full actuator cross-section to generate motion making it

more effective, although the bending pattern cannot be controlled and has to be prescribed during the manufacturing process [56].

Along with the actuators that provide one kind of motion, there are actuators that combine many primitives, or deform in more complex way . A good example of an actuator that does not fall into any of the proposed categories is the rapidly expanding actuator proposed in [71] in which a soft robot powered by explosions is proposed Fig. 2.8. The actuator in this case is a soft structure that expands rapidly in response to internal explosions of gas, causing the robot to jump.
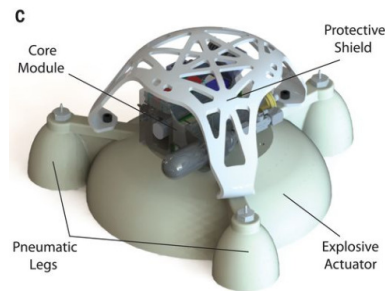
Figure 2.8: Explosion-driven soft robot, image taken from [71].

It is noted that all the motions mentioned above involve deformation of the soft material in the device. This is, however, not the only option. Actuator expansion can also be realised by the displacement of material Fig. 2.9. The entire new class of growing/everting actuators provide expanding motion of the actuator at one of its ends, effectively creating new portions. In [72] a "reel actuator" composed of a pneumatic tube rolled on a reel is proposed. To achieve extension, the tube is simply unrolled and filled with pressurised gas. Similarly, in [73, 74] linear expansion is generated by filling a pneumatic structure that initially is folded up inside of the activated part of the actuator. The folded part inside the active region is pulled towards the tip and everts, adding length to the actuator. The whole process can be repeated, giving a theoretically infinite expansion range.

Reel actuators expand by adding more material at their base, by unrolling previously rolled-up tubing and filling with air. Everting and growing actuators are somewhat similar, but the added material passes internally through the entire length of the actuator and forms at the tip.

The eversion principle of growing robots can be used not only to expand the robot itself forward but also to generate another kind of motion. In [75] an Eversive Pneumatic Artificial
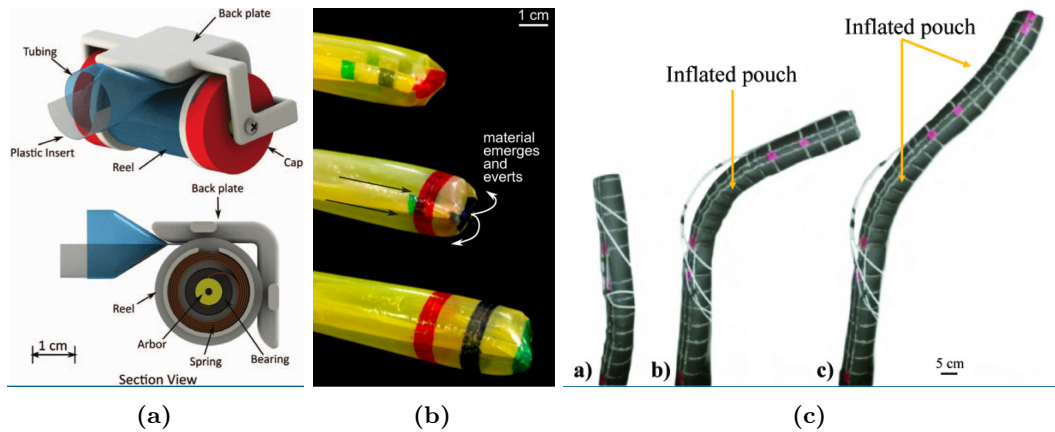
Figure 2.9: "Growing" actuators: (a) reel actuator, image taken from [72], (b) growing actuator, image taken from [73], (c) Eversive Pneumatic Artificial Muscle, image taken from [74]

Muscle (EPAM) has been introduced. It utilises the eversion principle of growing robots to generate pulling force on a tendon.

2.3 Design and Fabrication

Due to its short history, there are, as yet, no well-defined accepted standards in soft robotics. There are various designs of soft actuators and, equally, a variety of manufacturing procedures [76], which include sewing (fabric-based designs [77]), 3D printing [78], and silicone moulding [61]. Each technique uses specific materials and has its own particular advantages, but most of them require considerable effort and a high degree of manual skill from the manufacturer. One of the most commonly used techniques is moulding which usually consists of several moulding steps to manufacture the device. If reinforcement is required, it is usually achieved through additional steps.

There are reasons as to why silicone-based designs are so popular. First and foremost, they are cheap and easy - the only things needed are silicone, 3D-printed moulds and certain manual fabrication skills. Soft pneumatic robots can be actuated with a simple compressor or even a syringe.

The problem however is that the simplest silicone-based robots are very limited in their motion capabilities and performance. One option to improve them is to add thread or fabric to constrain the deformation of the silicone and shape the robot structure in the desired way.

Non-extensible fibres embedded into the soft material ensure that deformation only occurs in the direction perpendicular to the fibre. Any other deformation of the area around the

fibre is limited. There are several soft robot examples that use this system, Fig. 2.10. For example, in [67, 61, 56] fibres are used to pre-program the actuators' behaviour, ostensibly to control the direction and extent of deformation, but also to constrain the final shape of the device. In [79] a non-stretchable mesh is used to constrain the deformation and [2] uses fabric to constrain the deformation of flexible pneumatic cylinders allowing for high actuation pressures. In some cases, the addition of rigid reinforcing structures enhances soft actuators' performance [80].
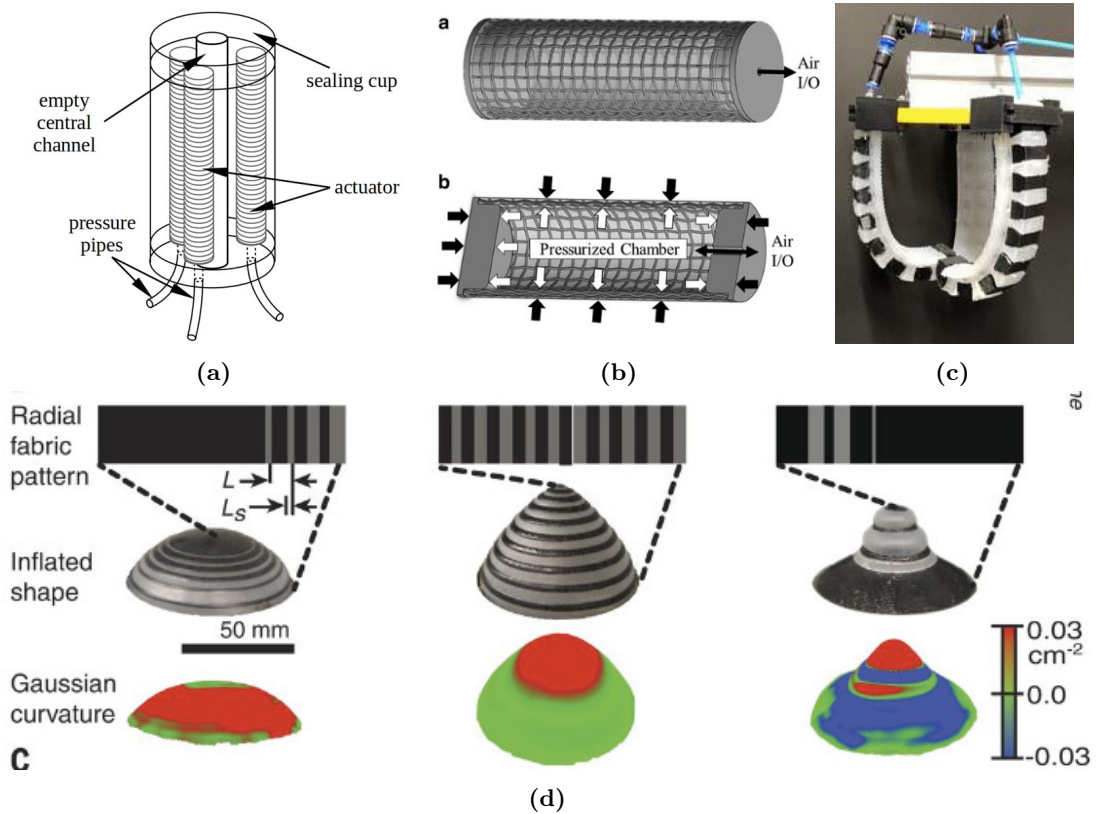
Figure 2.10: Examples of reinforcement in soft actuators: (a) fibers constraining radial expansion of actuation chambers, image taken from [61], (b) fabric mesh constraining expansion of structural pneumatic robotic links, image taken from [2], (c) elastomeric pneumatic fingers reinforced with rigid structures, image taken from [80], (d) fabric mesh constrains and pre-defines the morphing shape of 2D elastomer sheet into 3D shapes, image taken from [79].

The reinforcement can be added to the actuator at any stage of the manufacturing process. The most straightforward approach is to make the soft structure and then wrap it with fibre or fabric, as proposed in [52], Fig. 2.11. This is, however, a very time-consuming task. In many cases, given that an inextensible structure (e.g. a thread) is applied to a soft surface (e.g. a soft actuation chamber wall made of silicone), it is highly likely to create unwanted stresses and tensions in the actuator body. Another option is to incorporate the reinforcement

within the soft structure. In the case of cylindrically-shaped robots, this can be achieved by wrapping a thread around a rigid cylindrical rod, covering it with soft material, removing the rod, and then creating a secondary soft layer inside the reinforcement. In this way no stresses are induced, as the rod does not deform while being wrapped and the thread itself does not stretch even if some tension is required during the wrapping process. This approach improves reinforcement manufacture. However, it requires additional core wrapping operations and an extra moulding step to create both sides (internal and external) of the actuator.
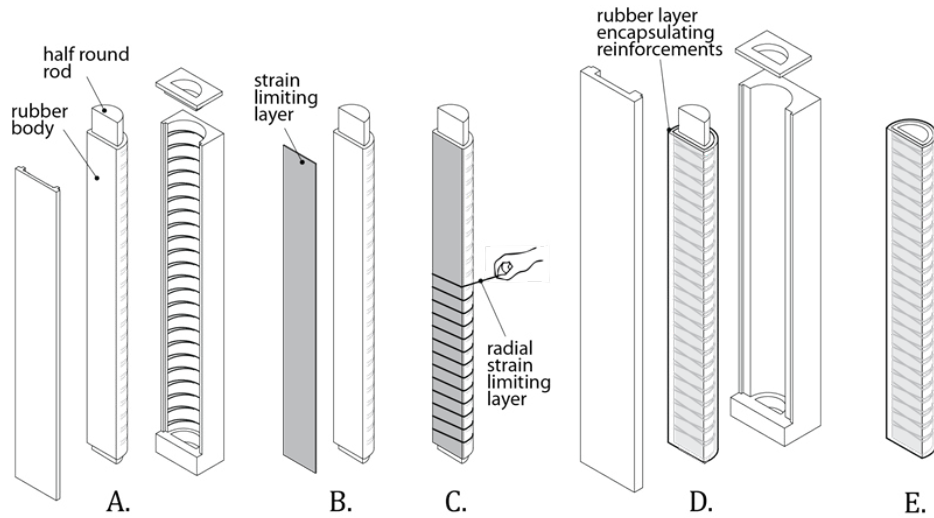
Figure 2.11: Fiber reinforced actuator fabrication procedure proposed in [52]

Embedding any reinforcement into the actuator adds complexity to the manufacturing process. Moreover, due to manufacturing constraints, most of the reinforcement methods proposed so far lead to relatively basic structures that constrain the deformation in a very simple way, and as the process is currently still largely involves manual effort, repeatability is poor.

An ideal solution would be to fabricate soft robot prototypes using additive methods such as 3D printing. Some technologies enable printing with very stretchable materials [78, 81, 82], but parts with complex shapes and internal voids are still challenging to achieve via this approach. In [83] a 3D printer modification that enables printing with silicone and reinforcing it with thin layers of filament has been proposed. The structures are printed on a rotating rod which limits the geometry to that of a cylinder. In [84], a printing technique is proposed using a combination of various materials thereby enabling the printing of soft

structures that are reinforced with fibres.

The key problem is that all the aforementioned approaches rely on custom-made 3D printers that are either not commercially available or very expensive, making them inaccessible to the wider soft robotics engineering community.

2.4 Stiffening of soft pneumatic actuators

Soft robots have enormous potential in fields where interaction between device and environment needs to be gentle. They are compliant and adapt easily to surrounding objects - seemingly ideal alternatives to traditional rigid robots. The problem, however, is that for many potential applications, while there is a requirement for robot-environment interaction to be gentle and compliant, there is also a need for force exertion. A trade-off situation therefore exists between compliance and maintaining shape, position and force exertion. The goal is therefore to develop stiffening mechanisms that allow for an on-demand reduction in compliance in favour of an increase in strength.

One of the popular research approaches in soft robotics is to draw inspiration from nature, as there are many examples of highly efficient soft-bodied animals and animal body parts - among them elephant trunks, octopus arms and snakes - that are all soft-structured but able to stiffen and exert force when required. With this in mind, several stiffening mechanisms have been proposed, all providing capabilities similar to their biological counterparts.

These can be arbitrarily classified as 'passive stiffness change' or 'active stiffness change' systems. Passive stiffness change devices are those whose physical properties change as the device moves from one working point or state to another - in which it has different characteristics - and maintain that (stiffer) state as long as required.

One of the most popular approaches within this category is based on jamming. Jamming refers to the locking of the structure's shape by squeezing physical elements together so that the structure's body stiffens due to the increased friction caused by the jamming force [85, 86, 87], Fig. 2.12. There are various systems of this type, among them devices based on granular jamming [88, 89], layers jamming [90, 91] or jamming of macro-scale structural elements like scales or ossicles [92, 93]. Another approach is based on stiffness or state transition as a function of the temperature of the material used ([94, 95, 96, 97]). These methods, however,

are energy sapping and relatively slow, due to the need to factor in heating and cooling times.
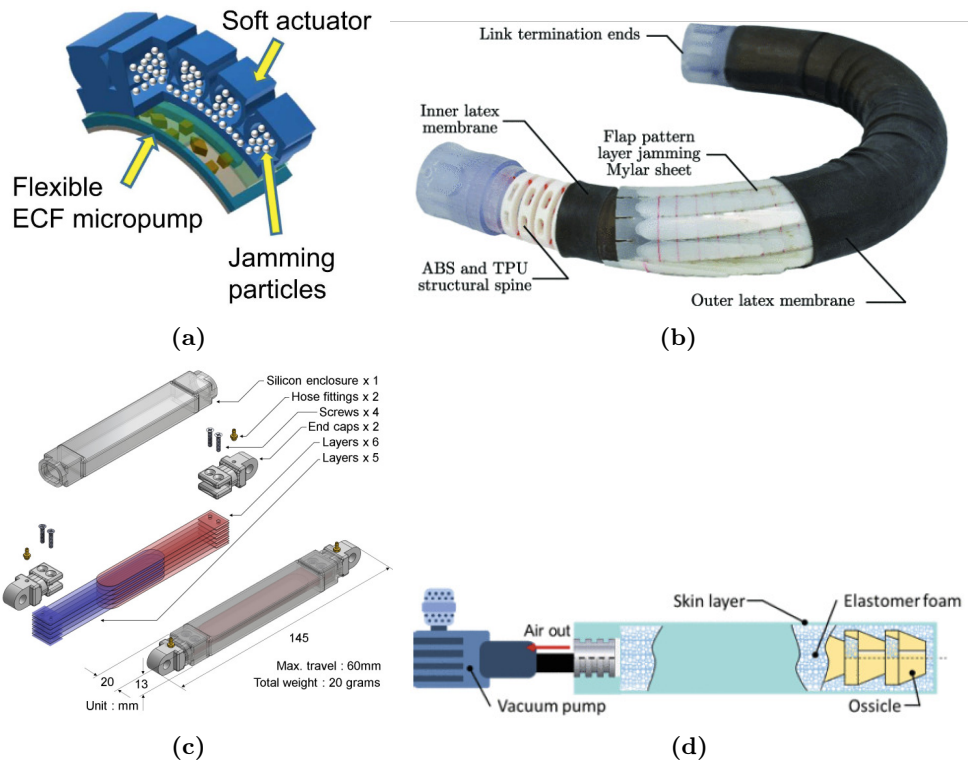
Figure 2.12: Examples of passive stiffening mechanisms: (a) granular jamming mechanisms, image taken from [89, 88], (b), (c) layer jamming devices, image taken from [91, 90], (d) macro-scale ossicles jamming, image taken from [90].

Another approach to stiffening, which could be classified as an active mechanism, is to combine antagonistic actuation methods, Fig. 2.13. In this scenario two or more actuators act against each other and the change in stiffness is achieved by increasing their actuation magnitude simultaneously so that they cancel each other out while their working point moves in a non-linear way towards lower or higher stiffness. This approach allows the geometrical configuration to remain unchanged, while the effective stiffness increases. One such example is the combination of pneumatic pressure applied to chambers along with pulling tendons [60, 98]. The chambers try to expand when pressurised, but the opposing tension of the tendons pulling back increases stress in the system, making it more rigid. This effect can also be achieved by using two similar actuators acting against each other, just like muscles powering joints in human bodies, or pneumatic actuators moving a rotary joint as presented in [99, 100].

Stiffening based on the antagonist principle requires some redundancy in the system as it entails at least two actuation elements acting against one another. Passive stiffening
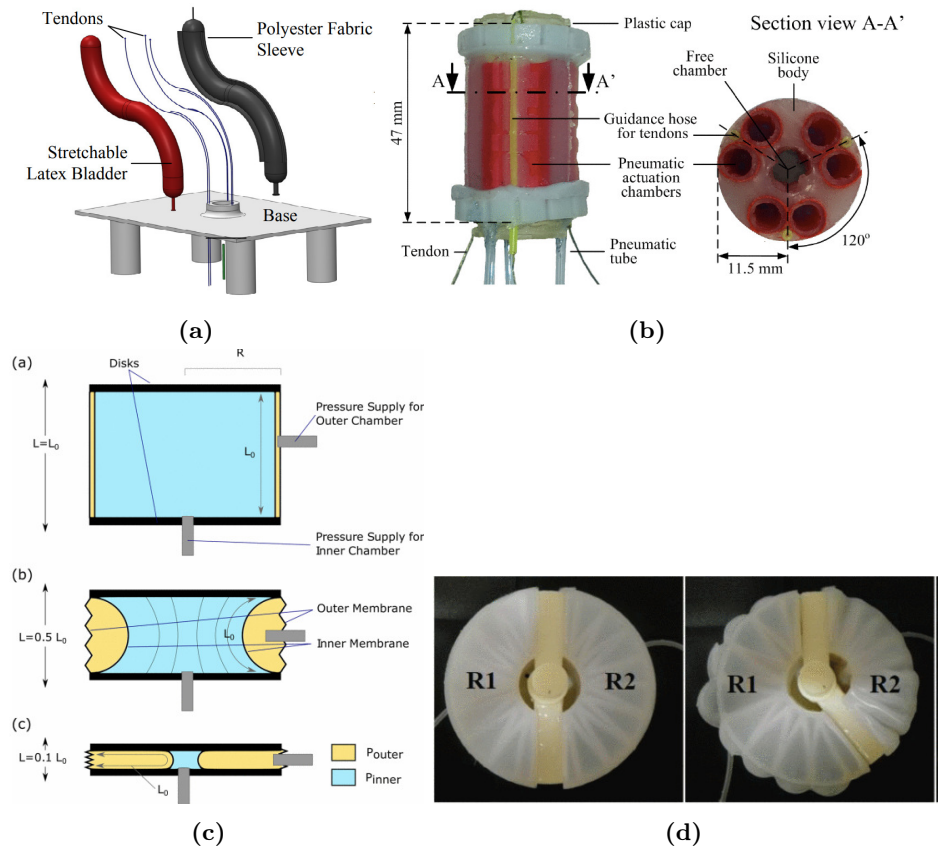
Figure 2.13: Active stiffening mechanisms. (a) and (b) antagonistic pressure and tendon driven actuation, images taken from [60, 98], (c) and (d) same kind actuators (pressure driven) acting against each other, images taken from [100, 99]

mechanisms are simpler in that they require just one actuation method and no active control, but also suffer from significant drawbacks. These mechanisms work both in parallel with, and independently from, the actuation mechanism, so that they can be in compliant mode during actuation, but then rigid once stiffened. Stiffening affects the whole structure so that actuation is increasingly limited as the device stiffens. There is no possible way to gain advantages from both modes simultaneously, i.e. the device has to move while in its soft state, but to resist significant external disturbances it has to then shift into its stiffened state. This kind of stiffening mechanism works independently of the actuation, and can be activated regardless of the current actuation state. It doesn't however work in reverse - once the device is stiffened, actuation is limited accordingly.

There are recently published works that try to improve this situation and couple both actuation and stiffening by taking advantage of jamming, Fig. 2.14. One of the examples is [88] in which particles are squeezed by expanding an actuation chamber. A similar mechanism

is presented in [101] in which an inflatable structure is equipped with patches composed of many layers that are connected via valves to both the atmosphere and the internal chamber volume. Those patches can be selectively jammed depending on the valve states. The last two examples allow for smarter stiffness control as they do not require an energy source beyond the actuation mechanism itself. They are, however, still parallel mechanisms.

<div align="center">(a)   (b)</div>
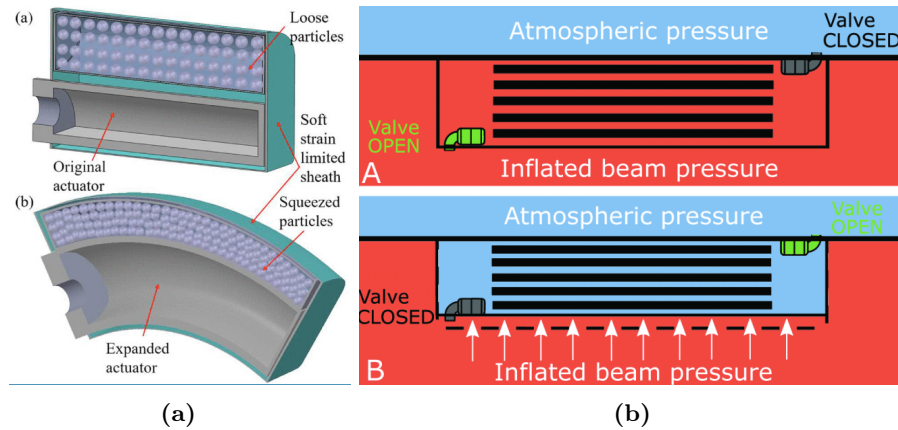
Figure 2.14: Stiffening mechanisms co-existing with actuation. (a) granular jamming based on the actuation chamber expansion, image takend from [88], (b) stiffening based on the actuation pressure and activation valve, image taken form [101].

2.5 Bio-inspiration and bio-mimetics

In nature, many organisms use compliant joints, soft structures, and distributed deformation. As researchers in soft robotics need to achieve similar features and effects in their designs, it is unsurprising that many devices have bio-inspired origins [102, 103, 60, 104, 105, 106, 107]. Certain organisms and biological structures have been of particular interest, examples being octopuses, jellyfish, mantas, fishes and snakes, elephant trunks, muscles and tongues.

One of the oldest bio-inspired soft robotic mechanisms driven with pneumatic power is McKibben muscle [62]. These muscles are composed of an extensible pneumatic tube constrained with a mesh. The fibres in the mesh are arranged so that the pressurisation of the internal bladder leads to an increase in the diameter of the device and, in turn, to a decrease in its length caused by reorientation of the fibres. This particular design has aroused a great deal of research interest due to its workings which are highly analogous to how actual human and animal muscles work.

One of the bio-inspired soft robotics trends worth mentioning is the antagonistic actuation

principle. Many animals can change their physical properties through simultaneous activation of complementary systems. For example, an octopus' tentacle contains various muscles that enable several types of motion, including contraction and extension. Simultaneous actuation of those muscles leads to a change in stiffness of the tentacle's tissue [108].

Indeed the octopus's ability to control stiffness underlies many soft robotic designs. In [109] an octopus robotic arm is presented that uses two types of pneumatic actuators in its continuously deforming segments. One of the actuator types enables extension while the other one contraction. In [1] a pneumatic tentacle equipped with tendons is presented. The internal pressure makes it expand, while tendons enable contraction. Simultaneous actuation of both systems leads to stiffening.

Another example of a bio-inspired soft pneumatic device is the Stiff-Flop robot [68]. This medical manipulator, designed for minimally invasive surgery, is inspired by the elephant trunk and octopus tentacle. The manipulator consists of several consecutive modules, each of which can bend in any arbitrary direction as well as elongate, providing three degrees of freedom per module. Each robot module is composed of three independent actuation chambers reinforced with fibres that elongate when pressurised. Modules of the robot can be customised by increasing the number of actuation chambers to increase the actuation capabilities, by adding stiffening chambers alongside the actuation chambers, or by equipping them with sensors.

In many cases, it is the overall structure of the organism rather than the working principle that is the source of inspiration. For example, in [31] a pneumatically driven soft manta robot is presented, Fig. 2.15. The main part of the robot's body are the wings that generate forward thrust when actuated. They bend up and down thanks to embedded soft fluidic actuators arranged in an antagonistic manner to achieve actuation in both directions. As with the actuators, the wings are composed of a passive, compliant membrane that follows the motion of the actuators and generates the flow in the surrounding water. The actuators are reinforced with fibres that help enhance the actuation process and minimise any side effects of pressure acting on the soft walls of the pressure chamber. A soft robotic fish presented in [110] is also powered with compressed air, although the required medium is stored onboard, making it a self-contained, cordless device.

Beyond animal and body-part inspired ideas, there have been recent developments in
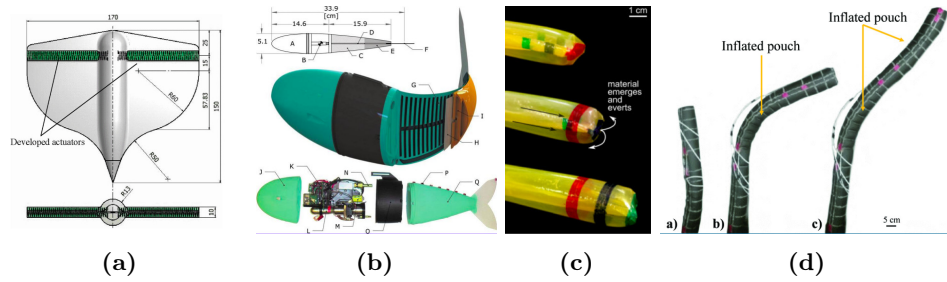
Figure 2.15: Bio-inspired soft devices. (a) bio-inspired manta robot, image taken from [31], (b) bio-inspired fish robot, image taken from [110], (c) and (d), plant-inspired growing robots, images taken from [73, 74]

regard to plant-inspired designs. In [73] a robot composed of an inverted thin-walled vessel that everts from the tip when pressurised is presented. Its working principle mimics the growing mechanism of plants and enables friction-less manoeuvering in clattered environments.

A device based on a similar growing principle, but also capable of bending is presented in [74]. In this instance, the robot features an integrated actuation mechanism composed of inflatable patches that can be filled with air after deployment of the main robot's structure, causing its wall's effective length to shorten and, as a result, bend.

2.6 Summary

Soft robotics is an emerging field that holds great potential, particularly in the realms of wearable and collaborative devices where safe interaction with humans is crucial. Soft robots also present a promising alternative to their rigid counterparts in unstructured environments, as their compliance and adaptivity can potentially simplify complex tasks.

However, this compliance and adaptivity come with certain drawbacks. A trade-off exists between compliance and strength; when a significant amount of force must be exerted, the softness of these robots becomes problematic. Consequently, numerous stiffening mechanisms and strategies have been proposed.

Soft robots exhibit a wide range of shapes and employ various actuation technologies and stiffening mechanisms, each with its own set of challenges. Various fabrication techniques for soft devices have been proposed, many of which are adopted from other fields such as sewing, silicone moulding, or 3D printing. These techniques, however, were originally intended for purposes other than soft robotics, necessitating adaptation and the establishment of new design principles.

Designing soft robots is challenging for several reasons, one of which is that the material deformation required to actuate soft robotic devices often results in not only the desired deformation but also undesirable outcomes, such as ballooning. As a result, soft robot design frequently necessitates some form of reinforcement, further complicating the design and fabrication process.

One approach to addressing these issues is bio-inspiration. Biology has produced numerous highly effective soft structures that have subsequently been emulated by soft robotic researchers, examples being animal muscles, elephant trunks, and plants.

The objective of this thesis is to advance the design and fabrication of soft actuators and improve their stiffening capabilities, thereby bringing the practical application of soft robots closer to reality.

3

SOFT FLUIDIC ACTUATORS DESIGN AND FABRICATION

3.1 Introduction

The soft and compliant nature of soft robots calls for non-standard actuation methods. Traditional actuators, such as electric motors and hydraulic cylinders, can not easily be used in conjunction with soft robotic systems without introducing an element of rigidity - precisely the feature that we are trying to eliminate in soft devices. For that reason, novel actuation methods need to be developed. Several options have already been proposed, including those that use tendons, shape memory alloys, or electroactive polymers. One of the most popular ideas is that of fluidic actuators reinforced with fibres, which offer several advantages when compared to other solutions.

My investigation into soft actuators stems from the STIFF-FLOP project, which aimed to create a device for minimal-invasive surgery (MIS) that fulfilled specific criteria, including small dimensions, flexibility, and squeezability, while also conforming to the requirement of avoiding the use of metallic parts or electrical components to maintain compatibility with Magnetic Resonance Imaging (MRI) scans [111]. A comprehensive examination of the available actuation technologies conducted in the period 2013-2014 resulted in soft fluidic actuators being selected as the target solution.

In table 3.1, a concise comparison of various soft actuators from the perspective of MIS is presented.

My PhD research builds on my work in the STIFF-FLOP project, and for that reason, it focuses mainly on soft fluidic actuation and stiffening.

Table 3.1: Comparison of different soft actuation technologies, based on [111].

Technology	Advantages	Disadvantages

Tendons	- High force-to-weight
	- Compact
	- Miniaturization possible
		- Some rigidity required:
		  - Tendons attachment
		  - Tendons shielding
		- No elongation possible

SMA	- Compact - Low voltage activation - High force-to-weight	- High activation temperatures - Low fatigue life - Need of efficient heat dissipation
EAP	- Scalable - Fast response	- High activation voltage

Vacuum actuators	- Soft
	- Actuated with vacuum
	  no risk of contamination
	- High force to weight ratio
		- Limited actuation pressure range
		- No elongation possible
		- Not squeezable
		- Not very well known
		  at STIFF-FLOP times

Fluidic actuators	- Entirely soft and squeezable - Can be actuated with a human-safe medium - Elongation possible	- External pressure source required - Risk of leakage/burst

3.2 Fibre reinforced actuators

The most basic soft fluidic actuators are able to provide linear actuation (expansion and contraction), bending, and twisting. In fact, any airtight tube made of flexible material can be considered an extendable actuator [65], Fig. 3.1(a). Adding a braided sheath converts it to a contracting McKibben pneumatic muscle [62], Fig. 3.1(b), while adding a fibre reinforcement perpendicular to its central axis makes it a linearly expanding actuator with limited radial expansion [66], Fig. 3.1(c). The further addition of strain limiting layers or fibres at certain angles allow for bending or twisting motion [35], Fig. 3.1(d), though these capabilities can also be induced by the actuator's geometry, such as asymmetrical actuation chambers or a curved, toroidal shape.
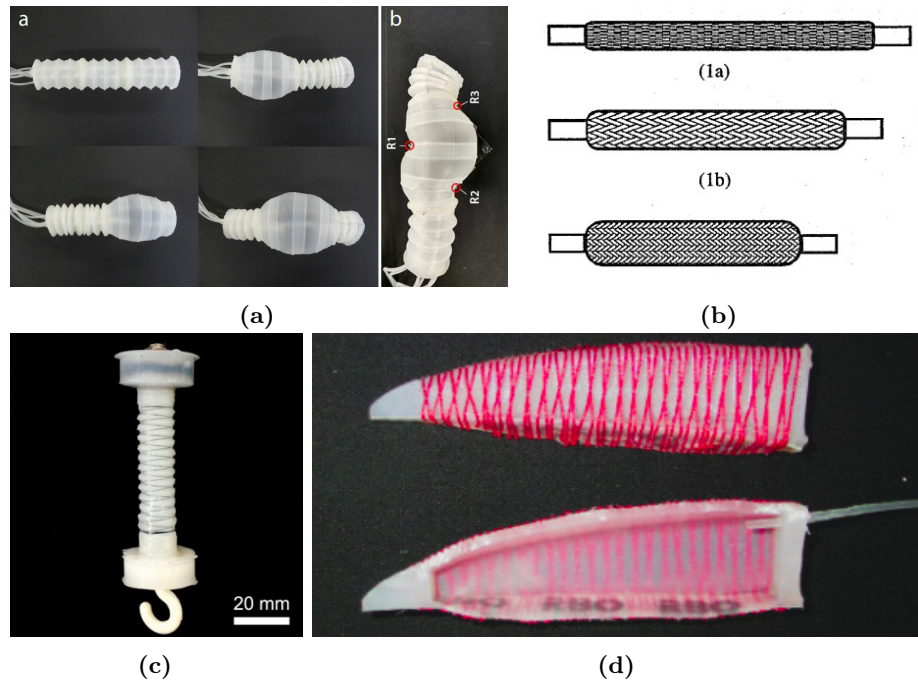
Figure 3.1: Examples of pneumatic actuators. (a) pneumatic 'giant deformation' bellow actuator [65], (b) McKibben muscle [63], (c) double-helix fiber-reinforced linear actuator [66], (d) double-helix fiber reinforced bending actuator[35].

Each technology has its benefits and limitations. For example, bellows-based actuators have a very simple structure in the sense that they do not require any additional reinforcing structures. They deform purely due to their geometry and the flexibility of the material they are made of. On the other hand, since their working principle is based on their folded body, they cannot be simply submerged into a more complex soft robotic device, and their outer geometry needs to be able to unfold during actuation. Fiber-reinforced actuators, on

the other hand, rely on the stretch of the material they are made of. They can be easily integrated into a soft robot body without violating their working principle. Their outer surface can be smooth, which helps to decontaminate the soft robotic device when needed and reduces the interaction forces when actuators need to move relative to external objects, while they could create significant forces with the indentation of bellow actuator.

Advantages and disadvantages of various fluidic actuator technologies have been briefly summarized in table 3.2.

Table 3.2: Comparison of fluidic actuators

Actuator	Advantages	Disadvantages
McKibben muscle	high forces	limited stroke, only contraction
Bellow actuators	positive and negative pressure actuation range, simple fabrication	not trivial integration, complex external surface
Fiber reinforced actuators	smooth outer surface, high pressures possible	complex fabrication, easy integration with complex structures

Given the ease of integration into a silicone structure and the capability of elongation, which were the requirements in the STIFF-FLOP project, as well as the smooth outer edge being a desired advantage, fiber-reinforced actuators were chosen as the most promising actuation technique.

3.2.1 Linearity of the actuator's response

One of the considerations when discussing actuators in general is their response characteristics. Such characteristics describe the actuator's output as a function of the input signal. In the case of the discussed fluidic actuators, the input signal can be pressure or volume of actuation media and the output, depending on the specific design, can be translation, rotation, force, etc. One of the features of such a response is its linearity, meaning how similar the output is as a function of input to a linear function. In work prior to my PhD, I have been working with soft actuators that had non-linear characteristics that led to a number of issues.

The actuator I worked on was specifically an early prototype of the STIFF-FLOP manipulator. Its bending angle was controlled with pressure, and its bending response is

presented in Fig. 3.2.
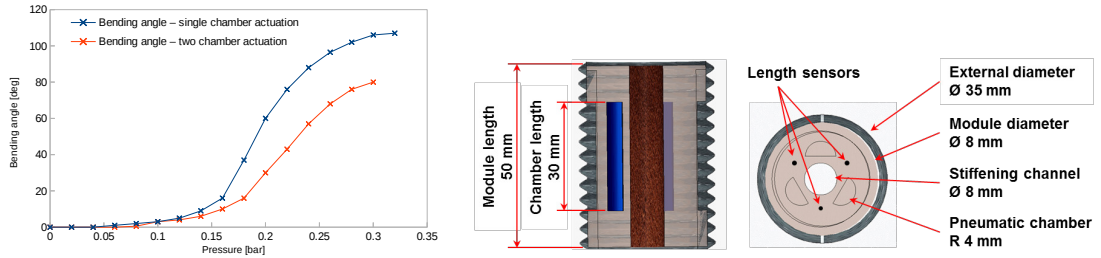
Figure 3.2: Non-linear characteristics of initial STIFF-FLOP prototype. (a) plots, image from [61], (b) STIFF-FLOP design, image from [112]

As shown in the plot, the input pressure range for the initial prototype of the STIFF-FLOP manipulator is approximately 0.3 bar, with most of the bending occurring between 0.15 and 0.25 bar for single chamber actuation and approximately 0.15 and 0.3 bar for double chamber actuation. As a result, a given pressure change in the 0.15-0.3 bar range results in a significantly larger bending change compared to the same pressure change in the 0-0.15 bar range. While model-based control can address the non-linearity, errors in input pressure or variability between actuators can result in significant output errors. This highlights the importance of optimizing the linearity of the response of fluidic actuators. Please refer to Fig. 3.3 for a comparison of linear and nonlinear actuator characteristics. It can be inferred from the observed non-linearity of the response of fluidic actuators that optimizing the linearity of their response is an important objective.
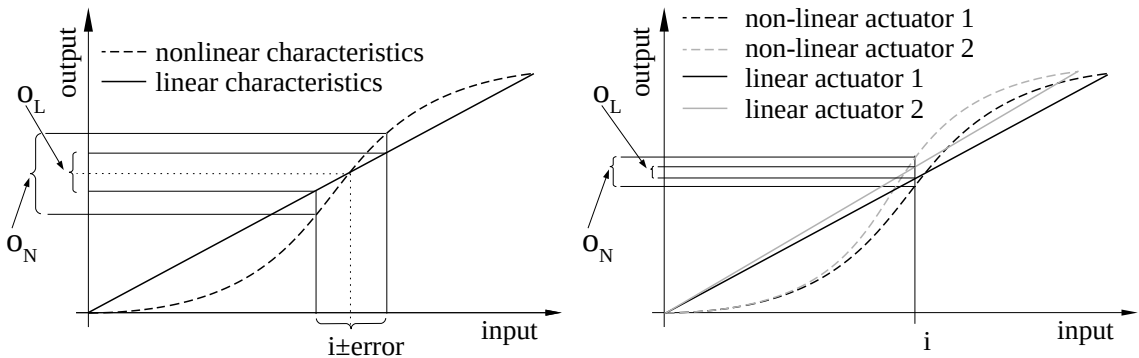
Figure 3.3: Example of linear vs nonlinear characteristic actuators of the same input and output range. (a) variability of the output with respect to the error in the input value, (b) variability in the output with respect to the differences between actuator instances. Note how the corresponding error or variability in the actuators affect the output error for both, linear and nonlinear actuators. i stands for input value and o_l & o_n are outputs of linear and nonlinear actuator respectively.

This section outlines the design choices and fabrication techniques that are implemented

throughout the thesis. The work described in this section is based on research previously published in [113].

3.2.2 Reinforcement

In the case of positive-pressure-driven soft actuators, deformation is caused by the application of internal pressure to a pressure chamber. The pressure acting on the internal chamber surfaces generates forces that stretch the device. As the pressure within a closed volume in a passive state can be considered constant, those forces are distributed equally on the internal surface of the actuation chamber. For that reason, the actuator tends to deform not only in the desired direction but also in all other, often unwanted, directions (ballooning) Fig. 3.4(a). Pneumatic actuators therefore often contain structural elements that are designed to amplify the desired motion and limit any other deformation of the device. These design add-ons can be made of the same material the actuator itself (e.g., geometrical reinforcement via bellows, ribs or groves), Fig. 3.4(b), but can also be constructed from fibre, fabric, paper, or plastic Fig. 3.4(c) and (d).
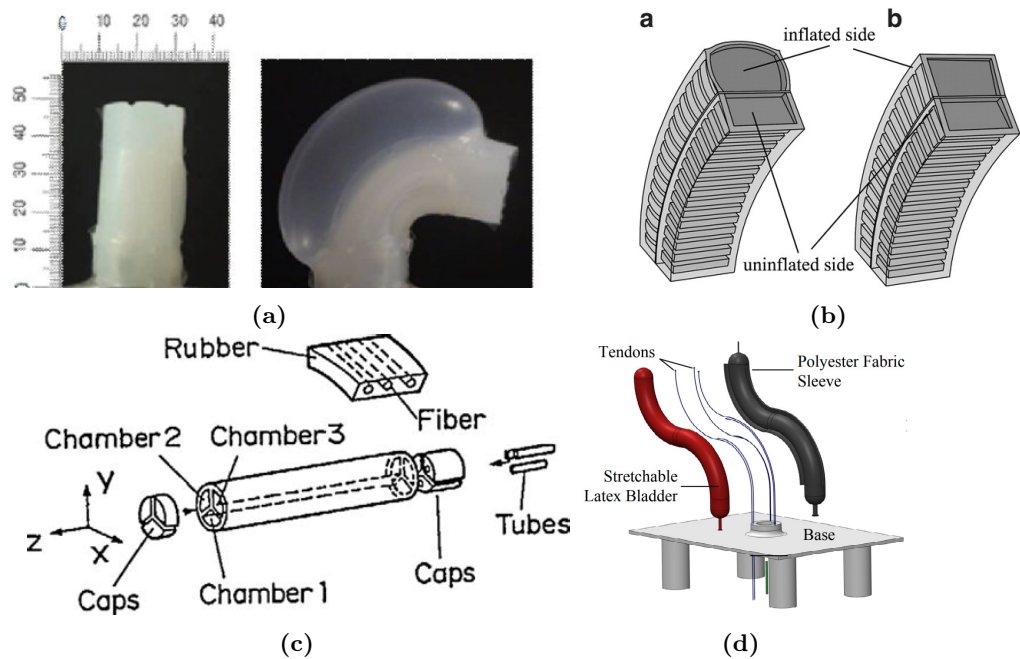
Figure 3.4: Examples of reinforcement. (a) no reinforcement, ballooning. Image from [112], (b) soft actuator reinforced with internal ribs of the same material, image taken from [114], (c) fiber reinforced actuator, image from [69], (d) fabric-reinforced actuator, from [60].

This thesis predominantly explores fibre reinforcement, as it offers many highly desirable features.

Consider a fiber that is flexible but not stretchable, such as a polyester fiber. Such a fiber can restrict tangential extensive forces but cannot resist bending or compressive loads. Therefore, embedding fibers into a soft material of actuators has little effect on its squeezability or passive stiffness response to external loads, but it does reduce material expansion along the fiber direction. Two important factors that influence the behavior of the fiber embedded in the soft fluidic actuator are reinforcement geometry and density.

The reinforcement density

The fibres embedded into the silicone have a constraining effect on silicone deformation. As the silicone is both flexible and stretchable, this effect is strongest in the immediate area of the fibre, though reduces as we move away from it. By way of example, consider a cylindrical actuator reinforced with circles made of a thread as depicted in Fig. 3.5 (b) and (c).
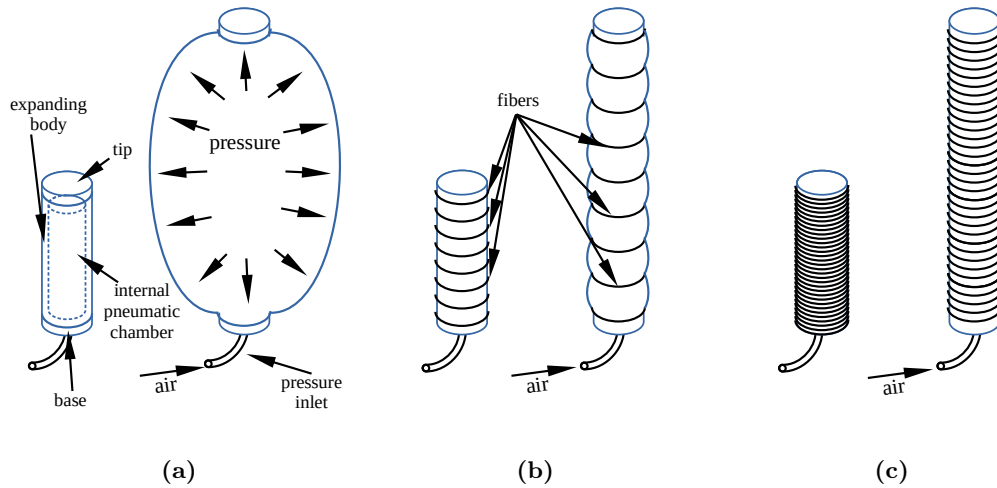
Figure 3.5: Comparison of sparse and dense reinforcement applied to an expanding actuator. (a) No reinforcement, ballooning, (b) sparse reinforced actuator, expansion between the reinforcing rings, (c) dense reinforced actuator, no expansion between reinforcement rings.

When the actuator expands, the distance between subsequent fibres grows accordingly. If the initial reinforcement density is sparse (as shown in Fig. 3.5b), it becomes even sparser during actuation, allowing the pressure to expand the chamber in between the reinforcements (ballooning). Increasing the density of reinforcement threads does improve the situation, as smaller gaps between the threads limit the expansion. Ballooning is a problem, as it induces nonlinear behaviour in the actuator, leading to more intensive wear and tear of the flexible material in the areas in which it expands more (balloons) and also increases stress, resulting in lower operating pressure limits for the device. The conclusion is that the denser

the reinforcement is, the greater the ballooning restraint effect.

On the other hand the ballooning causes the actuator diameter to increase $D_0 \rightarrow D_1$, see Fig. 3.6. Increased diameter causes the cross-section area to grow in a rate proportional to the diameter, $A \propto D^2$. The force generated in the given cross-section is proportional to the pressure and the cross-section area, $F = AP$. As the result, the actuation response is amplified. Assuming the area grows proportionally to the internal pressure, the force in the cross-section would grow in a rate of the square of pressure value $F \propto P^2$.

This could be seen as a means of obtaining actuators capable of generating higher forces and greater extension or bending under the same input pressure. However, it must be noted that the ballooning effect causes the radial dimensions of the actuator to expand during actuation. Therefore, if a higher level of force is required, it would be more appropriate to use a larger actuator retaining the advantages of dense reinforcement such as linearity, reliability, and durability.
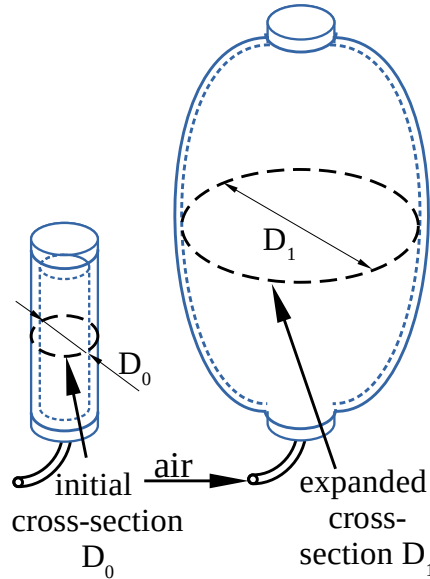
Figure 3.6: Ballooning impact on the actuator geometry

Reinforcement - local interactions

Fibers arranged tightly constrain the strain of the soft material better. On the other hand, when the soft matter of the actuator stretches and fibers move apart, the material in close proximity to the fibers needs to stretch as well. If the fibers are touching each other, the thickness of the silicone in between them is zero at the contact point and close to zero near

that point. Any elongation of the soft material in that region results in notional infinite strain. Infinite strain indicates infinite stress, and in such a case, the adhesion between fibers and the silicone can be easily broken, and the structure of the reinforcement fails. During my research, I tried different kinds of threads, and one of the approaches was to test the thinnest threads possible to increase the density of the reinforcing structure. Those threads were very thin and sleek. The structures made using those threads were failing at a very low number of cycles, and the first symptoms of failure were outer and inner layer separation. An example of such an actuator is presented in Fig. 3.7(d). Note that despite the large expansion (approximately 300%), the reinforcement density remains high.
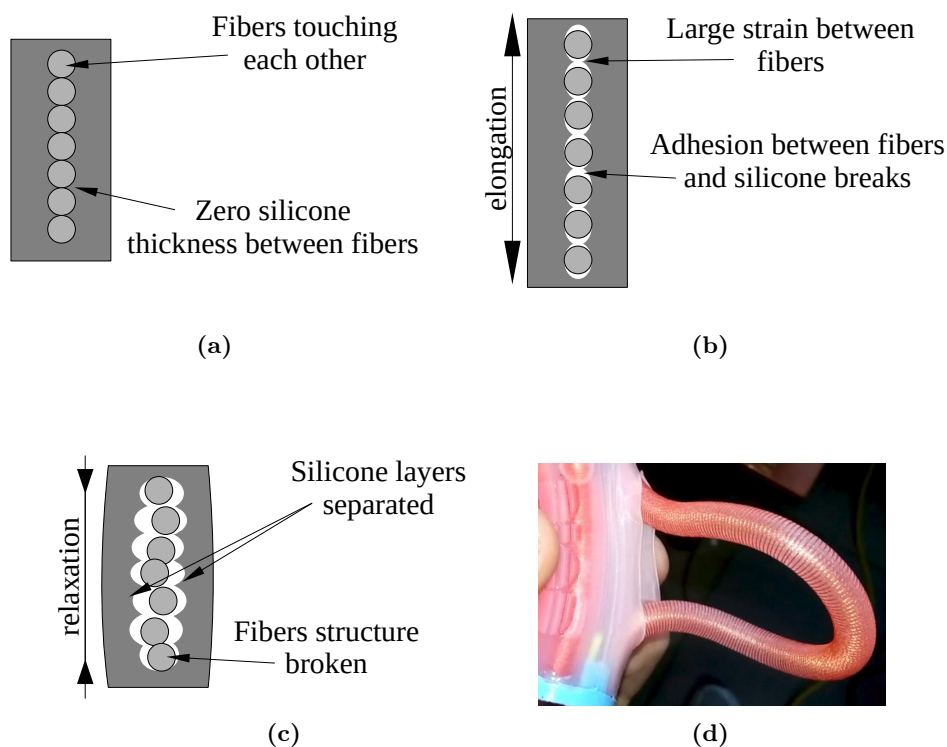
Figure 3.7: Local interactions of sleek, densely arranged fibers. (a) passive state, fibers in contact, (b) material stretched, the adhesion between fibers broken, silicone layers separated, (c) relaxation, material broken, (d) Example of broken actuator (one of STIFF-FLOP chambers) where the internal layer and external layer have separated and broken - fibers still attached to the internal layer.

The problem of an infinitely thin layer of silicone between fibers can be addressed by applying hairy rather than sleek threads. When using hairy threads, the silicone material penetrates the reinforcement structure and creates a mesh, rather than a sharp transition between the silicone and fiber material. Thanks to that, the strain is distributed and stresses are reduced, but also the adhesion between fibers and silicone is improved. Even if the bond

between fiber and silicone is broken locally, there is a high probability that the hair around this region will remain integrated with the silicone and prevent the overall structure from breaking apart (Fig. 3.8).
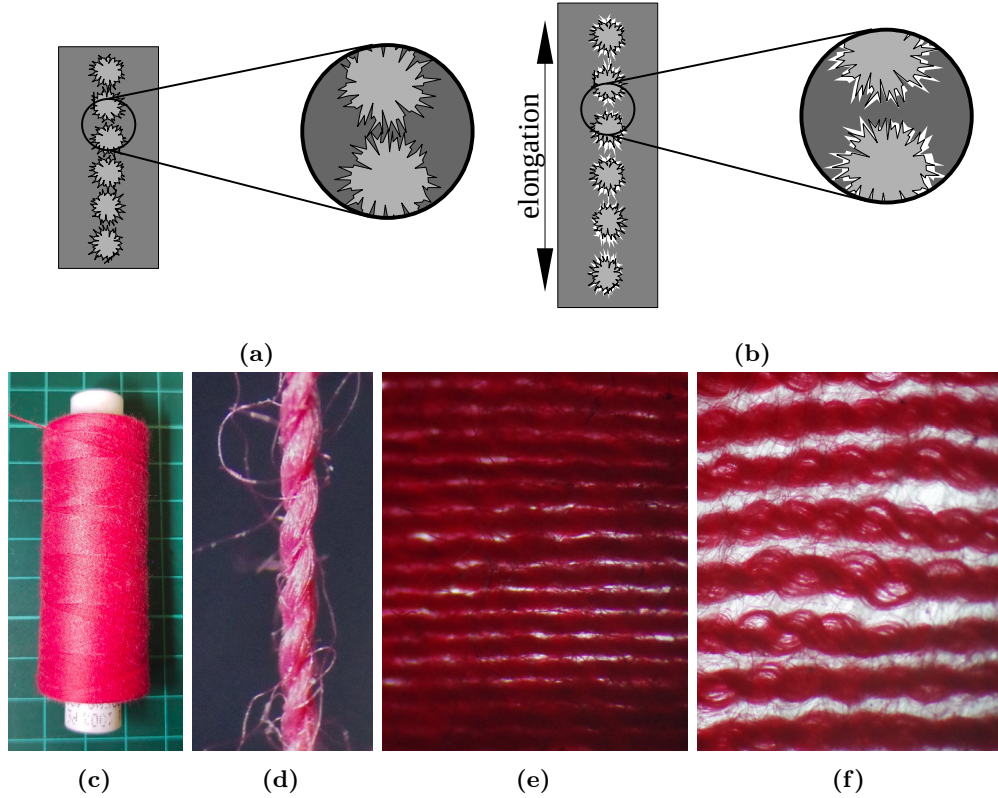
Figure 3.8: Local interactions of hairy, densely arranged fibers. (a) passive state, silicon can penetrate threads and in between them, (b) elongation, the silicone net between fibers stretches, but does not break, fibers kept in place, (c) an example of 'hairy' polyester thread, (d) microscopic image showing a single strand of the thread, (e) silicone reinforced with this thread in passive and (f) stretched state. Note how the thread stretches radially during deformation along with the silicone that penetrated the thread.

It should be noted that in Section 3.5, the interaction of the printed reinforcement and the silicone exhibits similar behavior. Even though the bond between the nylon and silicone material is weak and breaks when the actuator elongates, the overall structure remains intact and prevents the reinforcement from moving from the designed location.

The reinforcement pitch

Most commonly, reinforcement of fibre-reinforced actuators uses single threads. There are no individual rings but consecutive sections of a helix. Thus the actual overall shape of the reinforcement is helical, and the thread is not perpendicular to the actuator axis but inclined to some degree α, Fig. 3.9. It is important to note that this angle α is not constant and

changes as the actuator elongates.
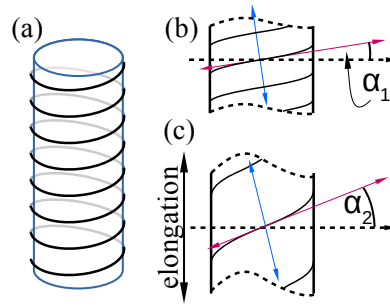
Figure 3.9: The reinforcement in most fibre-reinforced actuators has a helical geometry. (a) The sparser the reinforcement is, the bigger the pitch angle α value. (b) The pitch angle determines the actuator's behaviour. The deformation is constrained only in the direction of the fibre (red axis) and not affected in the perpendicular direction (blue axis). (c) The elongation causes the pitch angle to increase, so the effect increases. From [113].

As already mentioned, the fibres can only constrain expansion in the tangential direction. As they are not perpendicular to the direction of actuation, nor is the tension they generate, and therefore in addition to constraining radial expansion, they also cause the actuator to twist, see Fig. 3.10. Consider an imaginary line cut along the actuator's pressure chamber. If the resulting rectangular membrane is put flat on a surface, it will be seen to contain a set of straight sections of fibres, all parallel to one other. All of them are angled, on account of the original, helical shape of the thread. As only expansion in the direction parallel to the fibres is constrained, if a uniform stretching net force was applied to the membrane, the consequent deformation would change the shape of the membrane, as the deformation direction would be perpendicular to the fibres, as depicted by the green arrow in Fig. 3.10. If the membrane was rolled back up to recreate the chamber and stitched along the cutting line, it would become evident that the line is no longer straight, and that in addition to elongation, the actuator would also have been twisted.
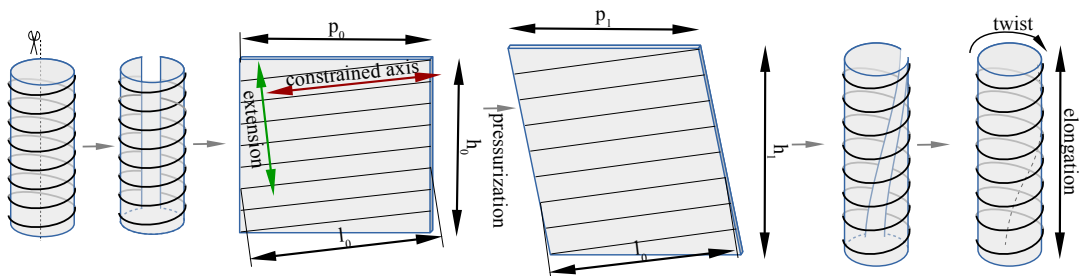
Figure 3.10: Explanation for twisting motion resulting from angled fibres. From [113].

The considered case assumes that the imaginary stretching force is applied uniformly

on the unrolled membrane. In this scenario, the relationship between elongation and twist in the device can be described by the $sin(\alpha)$ and $cos(\alpha)$ functions of the α angle. The elongation of the actuator along its primary actuation axis is proportional to the $cos(\alpha)$ function, while its twist angle is proportional to $\frac{sin(\alpha)}{r}$, where r is the radius of the actuator's chamber. However, in reality, the internal pressure acting on the reinforcement pushes it towards diameter increase, causing the helix to uncoil. This results in normal and shear stresses in the membrane, making the actual case more complicated.

It is important to note that single helical reinforcement can never lead to pure extension as angle α will never be zero. Therefore, some element of twist is inevitable. However, by increasing the reinforcement density, we can reduce α so that $sin(\alpha) \gg cos(\alpha)$, and in doing so reduce the twisting motion to an acceptable level. There may be instances in which twist is desired [56, 67, 115], but often it is not and requires an additional reinforcement helix, in the opposite direction, to compensate [35, 116] - a further reason to consider dense reinforcement.

Interestingly, similar phenomenon can be used to not constrain the radial expansion, but to generate contraction. In case of McKibben muscles, the flexible and extensible actuation chamber is braided with a sheath composed of fibers creating helixes in opposite directions. The steep pitch angle of the fibers allows the actuation chamber to increase its diameter, which due the the fixed length of individual fibers leads to the contraction of the actuator's length, [117]. The 54^o44 pitch angle of the fibers, also referred as a 'neutral angle' is the angle at which the radial and axial forces are in equilibrium and increase in the actuation pressure does not cause any contraction or elongation of the actuator. This is also the reason why the theoretical contraction limit of McKibben actuator is approximately 42%, [117].

3.2.3 The actuation chamber cross-section geometry

The actuation of soft actuators is based on deformation of their soft bodies. The cross-sectional shape of the actuator chamber therefore changes during the actuation process, though in the case of fibre-reinforced actuators, this effect is constrained by fibres. Its perimeter length is constant and has the same value for passive and actuated states. Since the pressure inside the actuation chamber acts to increase the internal volume, the cross-sectional geometry of the chamber will tend towards a shape with the largest area within the constrains of the constant perimeter. That will always be a circular shape, which is indeed the only geometry

that would not undergo change, see Fig. 3.11.
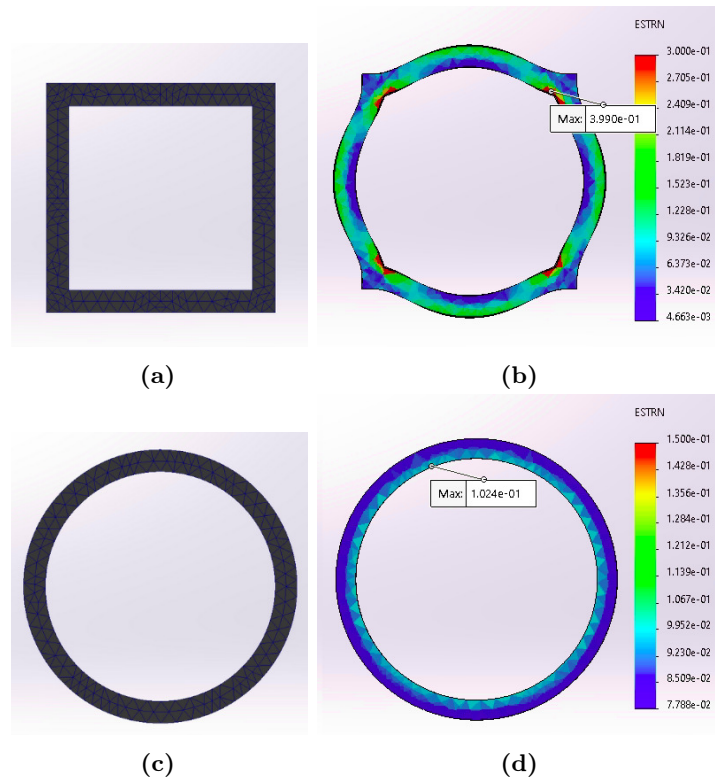
Figure 3.11: Process of pressure chamber deformation during pressurization. Rectangular cross-section (a) converges towards circular when pressurised (b). Note increased strains, especially in corners. Circular cross-section (c) does not change when pressurised (d). Simulation in SolidWorks 2021, standard library rubber material, no reinforcement simulated. Notice approximately 4 times larger strain in case of rectangular cross-section when compared to the circular one (scales are not equal).

The resulting non-linearity in the actuation process creates additional strain, especially in the corners, which increases local stress and the potential for increased wear and tear of the material in those areas.

Such local strain might seem like a relatively insignificant issue, as the hyper-elastic materials used for soft robotics can, in many cases, handle very large deformations. However, it still should be taken into account when designing soft actuators, as cross-sectional deformation could cause severe issues in relation to actuation and interfere with sensors [61].

Another property affected by the variable cross-section is the linearity of the actuator's response, similarly to what was discussed in the case of ballooning. The transformation to a circular cross-section results in the actuaion are's growth, which, in turn, amplifies the response in the actuation region where the cross-section deforms. These processes are discussed in more detail in Section 3.3.

3.2.4 Fabrication

Most fabrication techniques for soft actuators reinforced with fibres involve multiple manual operations. As a general rule, this is somewhat undesirable given that manual steps are a potential source of inconsistency and errors, and labour is a costly element in production. I have therefore proposed several improvements that reduce the amount of the manual work necessary in the manufacture of the device, and that, as a consequence, increase the reliability of the process.

Conceptually, the simplest and most popular way to reinforce a soft actuator with fibres is to create its body and then add the reinforcement. However, this approach is very slow and labor-intensive. Moreover, applying non-stretchable fibres to the soft body of the actuator causes compression of the soft material. This is because the fibre has to be under some tension during the process in order to keep it straight and remain attached to the actuator. A fiber experiencing no tension would become loose, resulting in an uneven distribution on the actuator, as shown in Fig. 3.12.
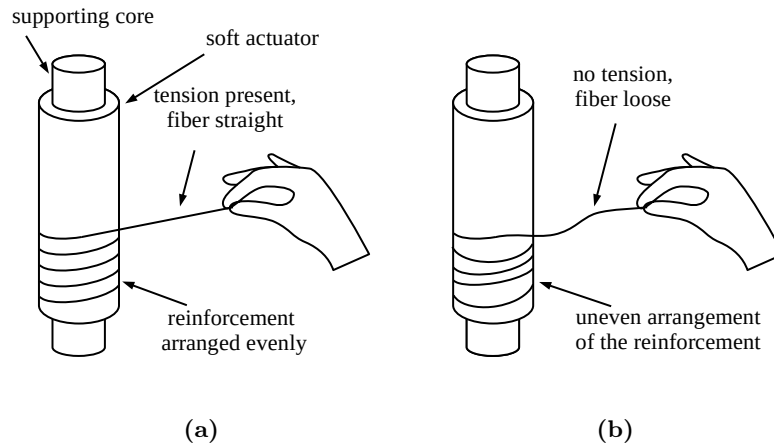
Figure 3.12: Manual winding process, tendon under some tension in (a) vs no tension at all in (b). Some tension is required to keep the thread straight and control the winding process.

It could be argued that the fiber application process could be conducted with a dedicated winding machine, where the tension can be precisely adjusted, but most fabrication processes described in research papers use manual procedures. Therefore, great care needs to be taken during the manufacturing process. Although internal material tension is relatively insignificant when the reinforcement is sparse, it can become problematic if the reinforcement has to be dense - see Fig. 3.13. This is because the tension required to wind the fibre

around the actuator squeezes the soft body of the actuator pushing the material sideways. When the reinforcement is sparse, this might not be considered a significant problem as the additional material has plenty of space between the fibres to spread - see Fig. 3.13a. When the reinforcement is dense, however, and the fibres are close to each other, the material is pushed forward ((1) in Fig. 3.13b) to the point where the internal stress begins to push fibres apart, allowing soft materials to squeeze through and out - see ((2) in Fig. 3.13b). This often results in reinforcement inconsistency and might likely be a reason for later failure.

(a)   **(b)**
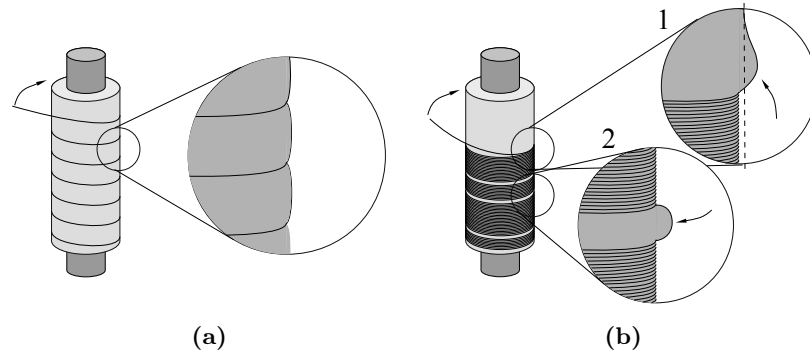
Figure 3.13: Manual thread deployment on the soft body vs stress and deformation. (Fig. 3.13a) sparse reinforcement, pressed material dissipates between fibres, (Fig. 3.13b) dense reinforcement, pressed material is pushed in the direction of winding (1) which leads to potential inconsistencies in the reinforcement (2). From [113].

In view of this, I propose to reverse the order, creating the reinforcement first, and the soft actuator's body thereafter. This can be done using a rigid moulding core - the fibre's tension creates no deformation on the core, and the entire manufacturing process can be automated, see Fig. 3.14.

Once the fibres are wound around the rods (a), they are covered with silicone material (b) and then the core is removed (c). As the friction between the rod and the silicone material is usually significant, extracting the rod could damage the reinforcement by dragging the threads out of the pressure chamber. The cylindrical rods can however be split into three parts to protect the reinforcement structure and facilitate removal. The internal part is removed first (while the external parts are still attached to the reinforcement), after which the other two become loose and can be removed under low tension. If the diameter of the chamber is small, the reinforcement-damage issue can also be solved by using smooth rods (e.g., polished metallic rods) or conical rods (which can be easily removed by pulling out the wider end). Metallic rods are a good solution for cylindrical actuators of standard dimensions. However, other techniques, 3D printing, in particular, allow for much more flexible designs

like curved shapes or variable diameters.

After removing the internal moulding cores a smaller core is inserted into the actuator (d). The volume between the fibres and the core is filled with new silicone material. This creates the actual pressure chamber internal wall. After the material has been cured, all the mould parts are removed, and the actuator is closed at both ends by dip moulding or glueing caps made from stiffer silicone (e).
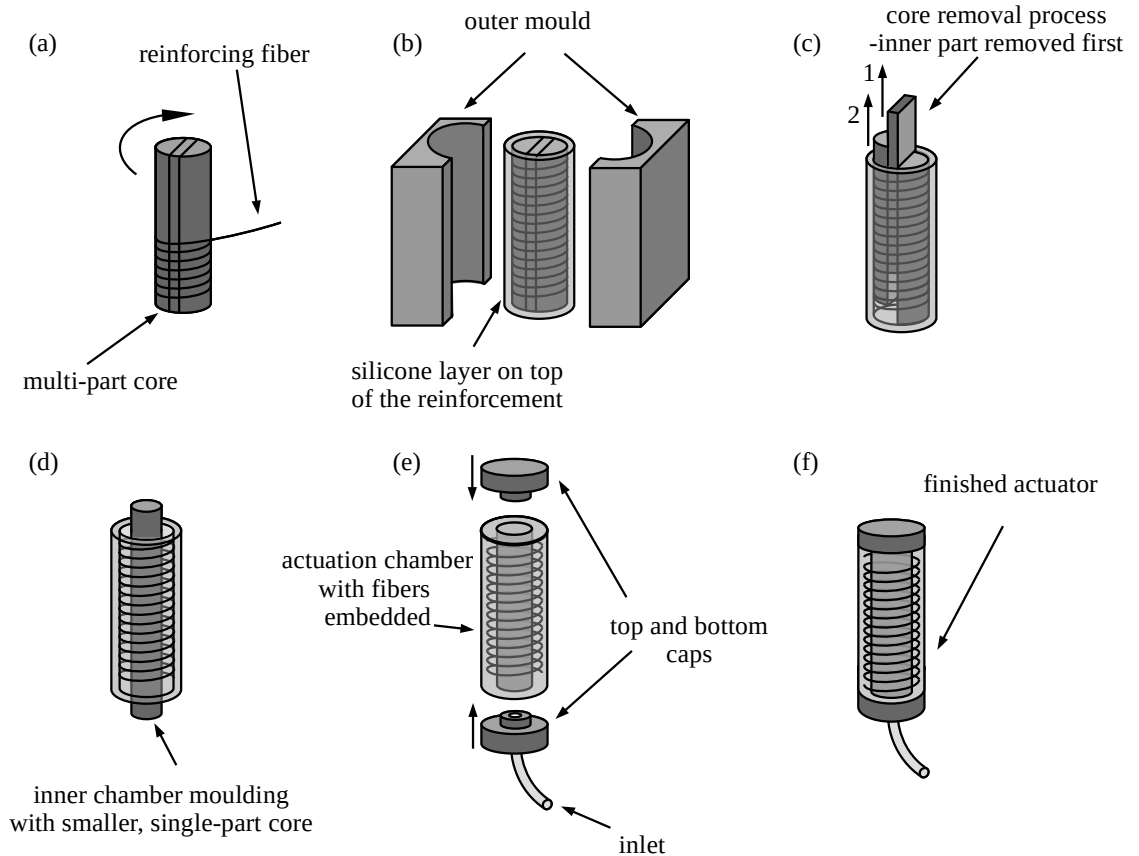
Figure 3.14: The actuator fabrication stages. (a) reinforcement winding using a rigid, multi-part rotating core, (b) external silicone layer casting, (c) core removal, internal core being removed first to prevent damage of fibers, (d) internal silicone layer casting (preventing the reinforcement from being detached from the outer layer), (e) attaching pre-moulded caps, (f) final product.

3.2.5 Summary

The design features (circular cross-section, dense reinforcement) and manufacturing approach outlined in this section are based on the experience I have gained during my research and are complementary to each other. They have been successfully deployed in the studies further described.

The described solutions address the issues I encountered in my research, though these issues are typically found across the literature pertaining to most similar designs.

The following sections of this chapter discuss implementation of the general design described here and expand upon manufacturing techniques by introducing 3D-printing of the reinforcement and additional stiffening structures.

3.3 Rotational actuator

Rotation is a widely used motion type in nature and in human-made devices, involving the movement of one rigid body around a specific axis with respect to another body.

This motion is easy to implement and efficient, which explains why it is extensively utilized by various machines. Electric or combustion motors primarily work through rotation, and if any other kind of motion is required, it is usually generated by a rotating motor and transmitted via a mechanism to produce the desired motion type.

In nature the situation is slightly different, as the motion is in most cases generated by muscles that contract. Their linear motion is applied to bones that pivot around joints, and that way linear motion is transformed into rotation.

Soft robotics muscles have been shown to be capable of generating rotation in a similar way to their biological counterparts [118]. However, in soft robotics, the use of rigid links is often undesired, and a direct rotation generation would be preferable.

In this section, I describe the design of a rotary soft actuator that can be used in applications requiring rotational motion. The actuator's design was utilized to assess the impact of geometry and reinforcement density on the actuation process.

The actuator described in this section has been developed as a potential replacement for traditional electric servomotors used in a robot based on soft-inflatable links [2], Fig. 3.15 and has previously been published in [119].The actuator described in this section has been developed as a potential replacement for traditional electric servomotors used in a robot based on soft-inflatable links
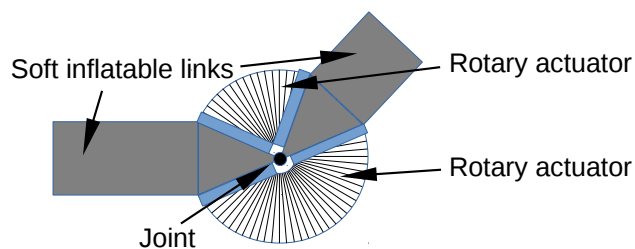
Figure 3.15: The potential application of soft rotational actuator. From [119].

The design and manufacture of this actuator were based on the guidelines described in Section 3.2 The device comprises three main parts: the actuation chamber, the tip, and the base Fig. 3.16, see Fig. 3.16. The actuation chamber is made of soft silicone EcoFlex 0050

(Shore 00-50), while for the base and tip, relatively stiff silicone - SmoothSill 940 (Shore 40 A) - was used. These chosen materials allow the actuation section to deform under pressure while stiffer material used at tip and the base prevent both ends from deformation. The actuation chamber is reinforced with a polyester thread that restrains its radial expansion in a cross-sectional plane.
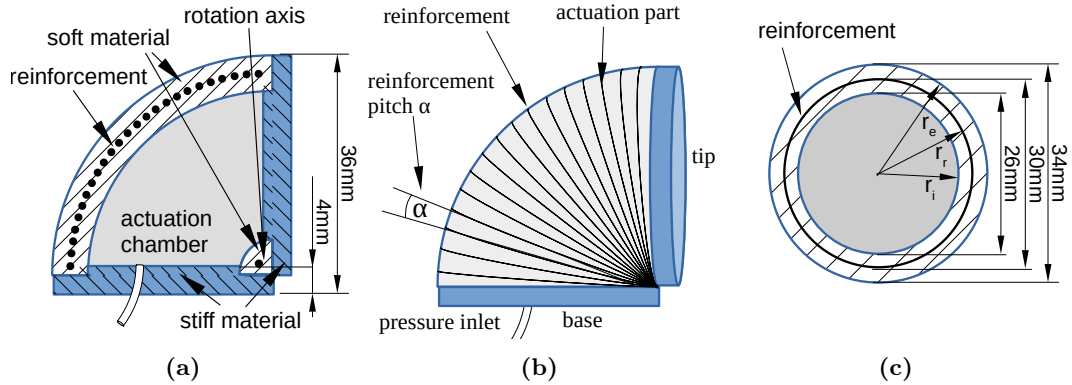
Figure 3.16: Single module design. (a) side view, (b) side cross-section, (c) front cross-section. From [119].

3.3.1 Cross-section geometry and reinforcement density

Due to the reasons explained in Section 3.2.2, a circular cross-sectional shape was chosen for the proposed actuator, as this is the only shape that does not change its geometry during the actuation, see Fig. 3.17 and Section 3.2.3.

The effect of the reinforcement density on the actuation process and the ballooning issue is shown in Fig. 3.18.
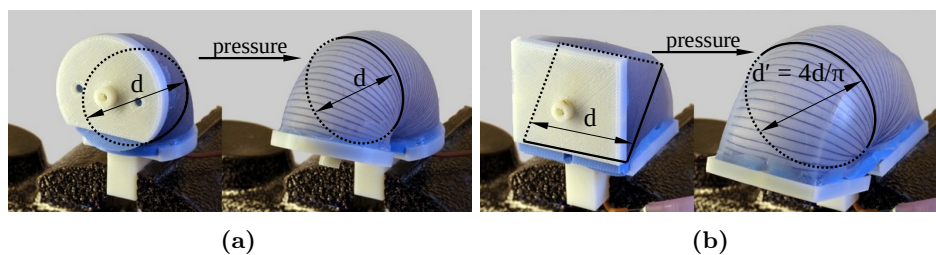
Figure 3.17: Deformation of the actuator cross-section geometry when pressurised: (a) circular cross-section - preservation of circular shape, initial section diameter remains the same after actuation, actuation area remains the same (b) square cross-section - deformation from the square shape (non-pressurised) to a circular shape (pressurised). Dimension changes from d to $d' = \frac{4}{\pi}$ (form perimeter length preservation). Actuation area grows from d^2 to $\frac{4}{\pi}d$ which is by approximately 27%.
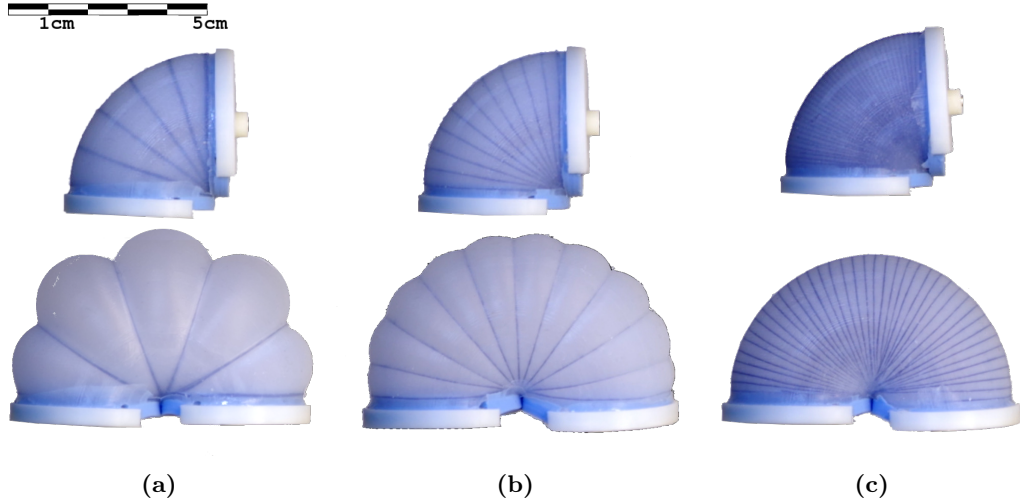
Figure 3.18: Ballooning observed during the actuation process. The more dense the reinforcement, the less deformation is observed. Different angular densities compared: (a) 18°, (b) 9°, (c) 2.25^o. From [119].

3.3.2 Fabrication

The actuator manufacturing process consists of several steps. The first step is the shaping of the reinforcement using a dedicated three-part core, Fig. 3.19(a). The core has tiny grooves that help keep the thread in place. It consists of three parts that can be separated easily and, so facilitates the core's removal after the moulding process is complete. If the core were a single-part body, its removal would not be possible due to the grooves. Once the core is wrapped with the thread, it is then covered with soft silicone, see Fig. 3.19(b). For that manufacturing step, another external two-part mould is used. After the silicone is cured, the external mould is opened, and the three-part core is gently removed from the silicon layer while the thread remains embedded in the silicone. In the third step, the internal layer of the actuation part is created by filling it with the next portion of silicone and putting another smaller core inside. The actuation chamber is then sealed by creating a round cap of stiff silicone using another mould, Fig. 3.19(e) and (f). All mould parts are 3d printed.

3.3.3 Mathematical model

Consider an actuation bending moment resulting from the pressure inside the actuation chamber as M_p. In equilibrium, the actuation bending moment is balanced by stress in the actuator body M_I and the generated torque τ. eq. (3.1), Fig. 3.20a:
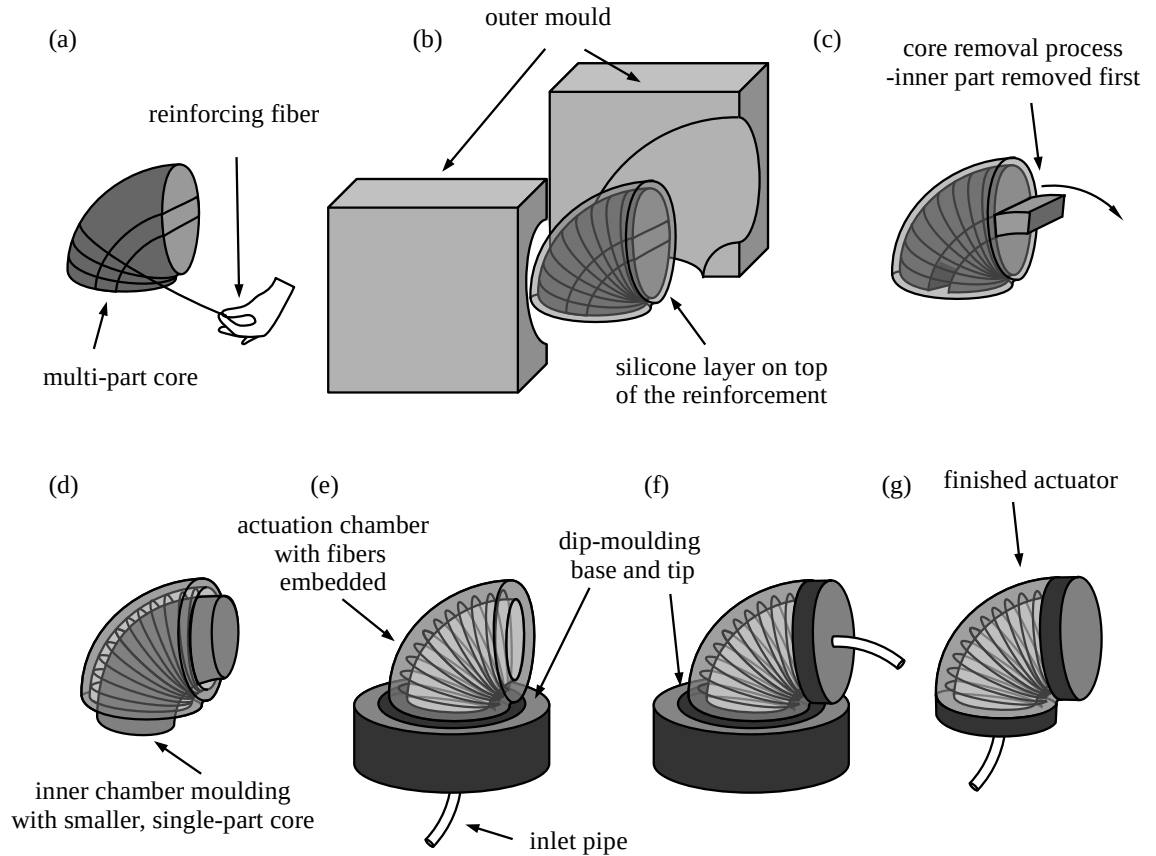
Figure 3.19: Manufacturing process: (a) reinforcement deployment, (b) external layer of active part moulding, (c)core removal, (d) internal layer of active part moulding, (e) and (f) closing both ends of the actuator via dip-moulding, (g) finished actuator.

$$M_p = \tau + M_I \tag{3.1}$$

The bending moment inside the actuation chamber is generated by the pressure acting on the tip and the base of the actuator. Assuming that the base is fixed, the pressure acting on the base does not cause any displacement. That said, the energy accumulated in the actuator as elastic energy is not affected by the pressure acting on the base. Therefore, the impact of the pressure acting on it can be ignored. As the pressure acting on the actuator walls (excluding the base and tip) does not cause any displacement, it too can be ignored based on the same principle. As a result, the only surface that the pressure causes any displacement is the tip of the actuator. The bending moment acting on the tip, in relation to the rotation axis, can be expressed as eq. (3.2):

$$M_p = \int_A pxda = p \int_A xda \tag{3.2}$$

where A corresponds to the internal cross-section area, p denotes the active pressure and x stands for the distance of da from the rotation axis (Fig. 3.20b). As the pressure has a constant value within the chamber, the p variable can be taken outside the integral.
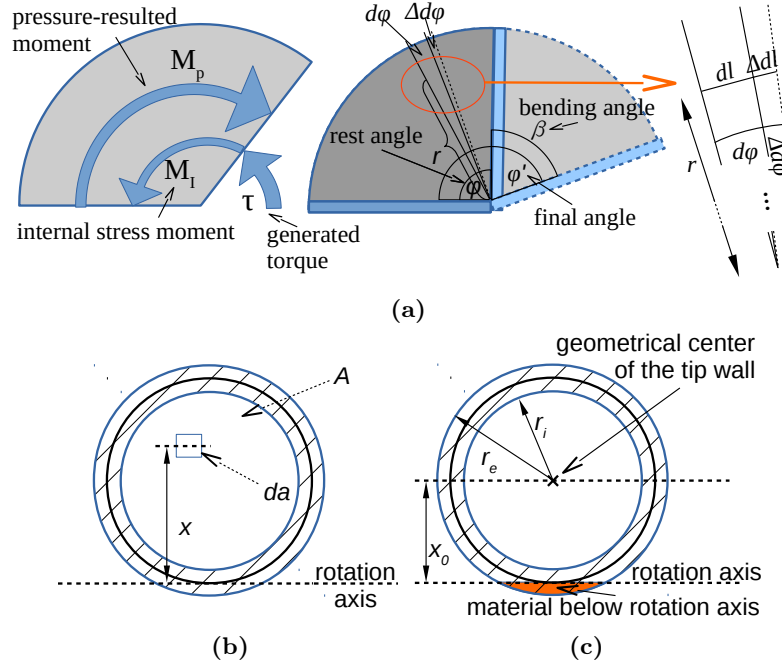
Figure 3.20: Mathematical description of the actuator behaviour, (a) side view, (b) & (c) front view, tip wall of the actuation chamber. From [119].

Introducing a x_0 variable being the distance from the rotation axis to the tip's geometrical centre (Fig. 3.20c), the integral can be written as eq. (3.3)

$$M_p = p \int_A (x - x_0 + x_0)da = p \left(\int_A (x - x_0)da + \int_A x_0 da \right) \tag{3.3}$$

Considering eq. (3.3) and eq. (3.4) , the bending moment is equal to (eq. (3.5)).

$$\int_A (x - x_0)da = 0, \int_A x_0 da = Ax_0 \tag{3.4}$$

$$M_p = pAx_0 = px_0\pi r_i^2 \tag{3.5}$$

Using the same justification as for pressure related to the actuation moment, the internal

stress moment can be calculated as:

$$M_I = \sigma x_0 A_b = \sigma x_0 \pi (r_e^2 - r_i^2) \tag{3.6}$$

where A_b denotes the area of the actuator body in the cross-section.

Putting all the equations together we get eq. (3.7):

$$\tau = p x_0 \pi r_i^2 - \sigma x_0 \pi (r_e^2 - r_i^2). \tag{3.7}$$

The stress variable σ depends on the material properties and strain ε. It can be read from the stress-strain curve of the EcoFlex 0050 material used for the actuator body. This curve was obtained by gradually stretching a specimen while measuring the stretching force value and is presented in Fig. 3.21. The strain ε at a certain point corresponding to actuation angle β can be expressed as:

$$\varepsilon = \frac{\Delta dl}{dl} = \frac{r \Delta d\varphi}{r d\varphi} = \frac{\varphi' - \varphi}{\varphi} = \frac{\beta}{\varphi}. \tag{3.8}$$

where φ and φ' stand for the actuator's rest and active angles, respectively (Fig. 3.20a).

It is important to note that the strain does not depend on the radius r value, which means scaling up or down the given design does not affect the strain in the system. It also does not depend on the x value, meaning it does not depend on the distance from the rotation axis and remains constant throughout the entire actuator volume, with the exception of that part of the flexible actuation chamber below the rotation axis (where the material gets compressed rather than stretched), though this has been ignored on account of its negligible size (shown in orange in Fig. 3.20c).

In regard to the measured characteristics eq. (3.7) can be rewritten as:

$$\tau(p, \beta) = p x_0 \pi r_i^2 - \sigma(\varepsilon(\beta)) x_0 \pi (r_e^2 - r_i^2). \tag{3.9}$$

For a constant angle β the torque is a linear function of pressure $\tau(p, \beta = \beta_0) = p x_0 \pi r_i^2 - c_{\beta_0}$ as the last part of the equation is constant in such cases.

From eq. (3.8) the actuation angle β can be expressed as $\beta = \varphi \varepsilon$, where ε depends on the pressure p and the load τ:
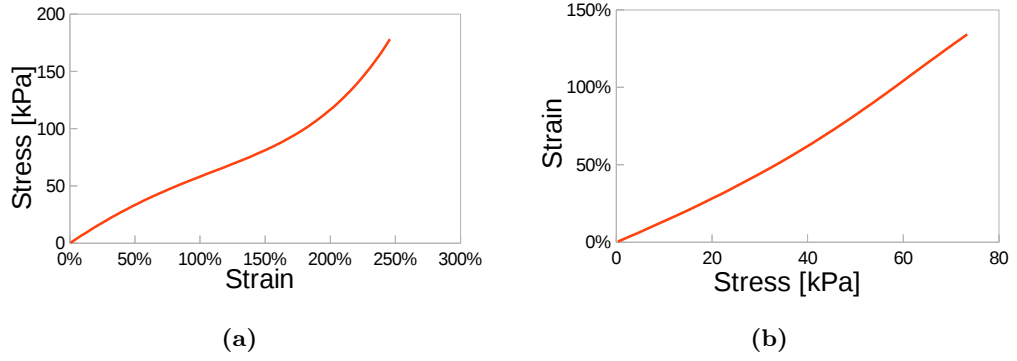
Figure 3.21: Relation between strain and stress of Ecoflex 0050, (a) stress-strain curve, (b) inverted relationship for around 100% deformation (the range of the tested actuator motion). From [119].

$$\beta(p, \tau) = \varphi\varepsilon(\sigma(p, \tau)),$$

$$where : \sigma(p, \tau) = \frac{px_0\pi r_i^2 - \tau}{x_0\pi(r_e^2 - r_i^2)}. \tag{3.10}$$

The final bending angle equation contains the strain ε as a function of stress σ, which is a linear function of pressure p for constant load $\tau = const$. Thus, for constant load, the actuation angle should reflect the inverse stress-strain curve Fig. 3.21b.

3.3.4 Experiments and validation

Bending characterisation

The experimental setup was composed of a pressure source, a pressure gauge and a camera. The actuator was equipped with a lightweight rod attached to its free end to determine its momentary configuration. It was connected to a pressure source through a proportional throttle adjusted to deliver the actuation gas slowly, so the actuation process was very slow and steady. High-speed actuation was not investigated here as that would have additionally involved system dynamics - the pressure measured at the pipe providing fluid to the device would differ from the actual pressure in the chamber, on account of the dynamic pressure distribution in the system. The manometer used in the setup has an accuracy class of 1.6, which means that the maximum possible pressure reading deviation is 1.6% of the sensing range. As a result, the maximum possible pressure reading error is 0.016 bar.

The whole process was recorded on video, and then, using image processing, both the pressure and the bending angle were determined for each recorded video frame. To minimize errors, I used a relatively long focal length lens, and the camera was positioned approximately 1.5 meters away from the actuator. The actuator and pressure indicator planes were positioned perpendicular to the camera's optical axis to ensure accurate measurements. A single frame of the data and the image processed are presented in Fig. 3.22. The use of the analogue pressure indicator eliminated any need for data synchronisation. Each video frame contains both the bending angle and the actuation pressure. Since the bending angle detection required the development of a visual algorithm, the pressure detection was achieved without any additional labour costs. Capturing both values within the same video frame eliminates the need for data synchronisation, simplifying the data processing.
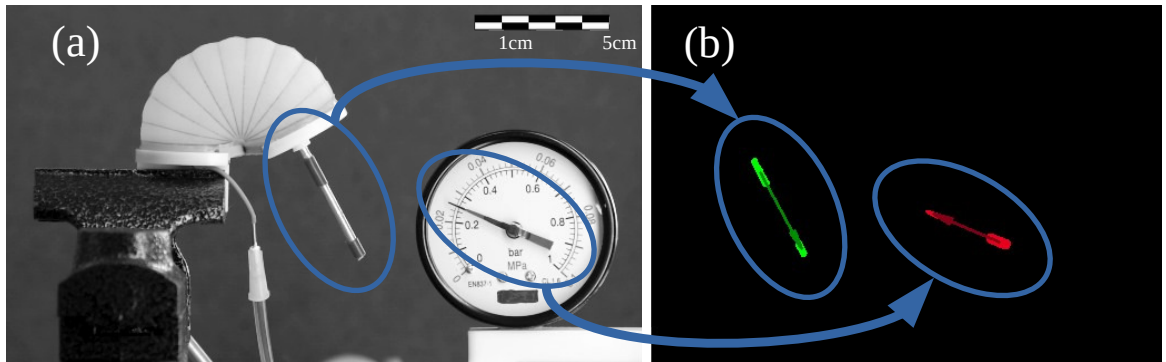
Figure 3.22: (a) Single frame of a recorded sequence, (b) bending angle and pressure indicators detected (green and red consequently) Processed with Blob Detection algorithm from OpenCV library [120]. Image from [119].

In this experimental study, four different actuators were examined. Three of them had circular cross-sections, while one was square. The round actuators were identical apart from the fact that their reinforcement had different numbers of turns - with $\alpha = 2.25^o$, $\alpha = 15^o$ and $\alpha = 18^o$. The square-shaped actuator had similar dimensions and was reinforced with $\alpha = 2.25^o$. All the prototypes had a 90° passive angle. The circular circumference actuators had a 26mm internal and 34mm external diameter, while the square cross-section actuator had 26mm and 34mm internal and external side lengths. In all the cases, the reinforcement was embedded in the middle of the silicone layer. All the used specimens have been presented in Fig. 3.23.

Each actuator was actuated six times at the low speed, from 0 to 90°.

The plots of the bending angle as a function of pressure, with statistical errors included,

(a)   **(b)**   **(c)**   **(d)**
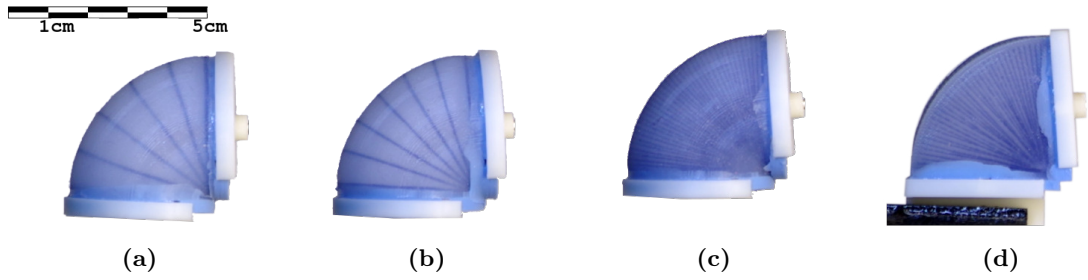
Figure 3.23: Tested rotary actuators. (a), (b) and (c) - circular cross-section, $\alpha = 18^o$, $\alpha = 15^o$ and $\alpha = 2.25^o$, subsequently, (d) square cross-section, $\alpha = 2.25^o$.

are presented in Fig. 3.24. As one can see, none of the characteristics of the tested actuator is linear, and they all reflect a presumed elastomer strain-stress curve, Fig. 3.21.

(a) circular, 2.25^o

(b) circular, 15°

(c) circular, 18°

(d) square, 2.25^o
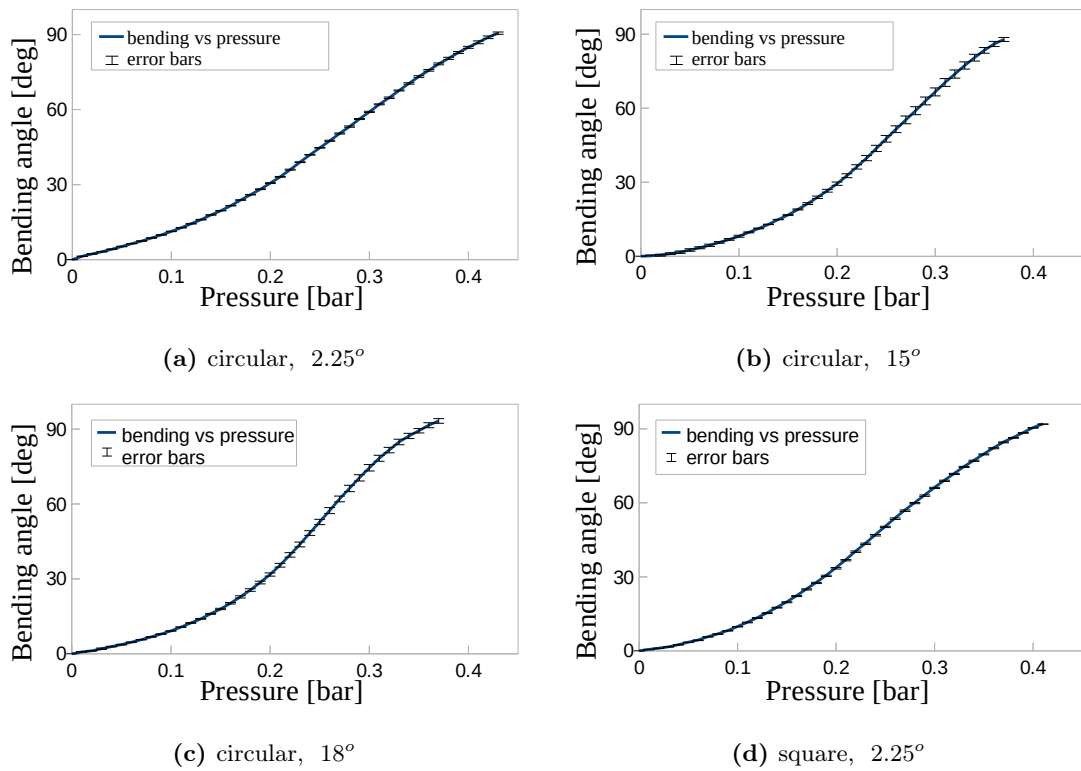
Figure 3.24: Bending angle vs pressure with error bars. Results for various actuators having different cross-section shapes and distances between reinforcement fibres. From [119].

In Fig. 3.25, all the curves are presented in the same plot for comparison purposes. On the left-hand side, all the curves are plotted using the real pressure data. On the right-hand side, the pressure has been normalised for the 90° bending angle limit. The desired linear characteristic has also been presented.

By doing this, we are able to clearly demonstrate that the circular actuator reinforced with the least spacing $\alpha = 2.25^o$ presents the most linear characteristics. It is interesting to note

that the square actuator behaves in a way very similar to the circular one (Fig. 3.25b, red and dark blue lines respectively). The only difference lies in the initial part of the actuation curve. This is because the square shape of the cross-section initially converges to a circle when pressurised. Thus for higher pressures, once its cross-section is almost circular, the actuator presents the very similar actuation properties to a circular one.
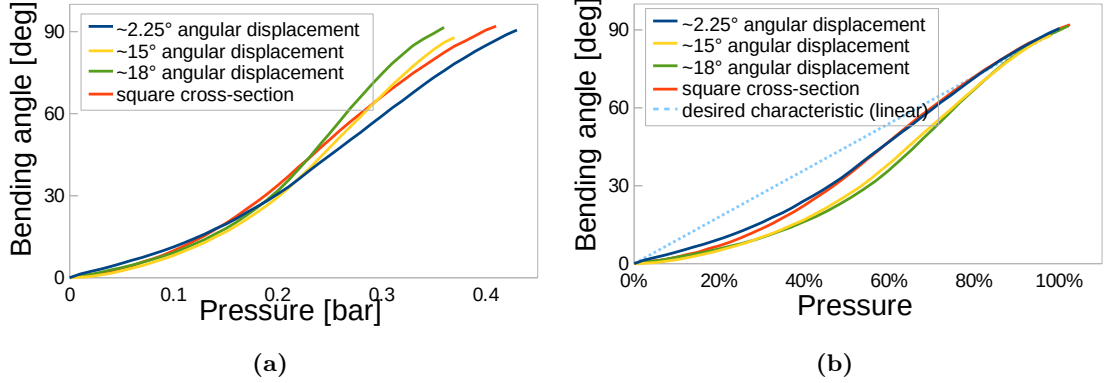
Figure 3.25: Bending angle vs pressure. (a) real data, (b) the $x-$axis has been normalized for comparison purposes. From [119].

The actuator characteristics compared to the model are presented in Fig. 3.26. Statistical evaluation of the tested actuator versions is presented in table 3.3. The experimental data is evaluated with respect to a theoretical linear characteristic for the same range of motion (0° - 90°) and the proposed model having a circular actuator cross-section - Section 3.3.3. As expected, the reinforcement density affects the actuator linearity, and the more reinforcement cycles, the more linear the actuator's behaviour is. Since the actuator manufacturing process is highly imprecise, the actual dimensions may vary. The model's prediction may therefore be better if its geometrical parameters (the actuator dimensions) are slightly adjusted. For that, the inner cross-section radious value has been optimized to minimize the average error and has been estimated to be $25.77mm$ instead of theoretical $26mm$. Such and adjustment reduces the average model error from 3.2^o to 1.83^o.

Torque characterisation

A similar setup was used for torque characterisation. The pressure was determined in the same way as in the bending trials. The torque itself was determined using an electronic scale recorded in parallel with the pressure indicator (Fig. 3.27). The growth of the pressure value inside the actuator causes the bending moment to change, which is reflected in the scale

Table 3.3: Bending linearity error for 0-90° actuation angle.

Actuator geometry, reinforcement spacing	Average deviation from linear characteristic (see Fig. Fig. 3.25b)	Proposed Model Average Error
Circular, 2.25^o	5.8^o	3.2^o
Circular, 15°	10.6^o	5.3^o
Circular, 18°	10.6^o	6.6^o
Square, 2.25^o	6.5^o	-
Circular, 2.25^o, Model adjusted	-	1.8^o

Figure 3.26: Bending experimental data aligned with the model prediction. Actuator diameter in the model adjusted to minimize error. From [119].

reading. Given the radius of the acting force, the torque can then be calculated.

The results of the torque measurement at resting actuator angle (0°) are presented in Fig. 3.28 and a statistical data evaluation is presented in table 3.4. As expected the densely reinforced actuator with the circular cross-section demonstrates the most linear behaviour. This effect is related to the cross-sectional deformation during pressurisation. The cross-section distortion causes its geometry to change, with the effect that torque increases in a nonlinear fashion. To make the plots more comparable in terms of linearity, the torque axis has been normalised for each curve and presented in Fig. 3.29. As discussed in Section 3.3.4, a square-shaped actuator rapidly becomes round under pressure, and this is a likely reason for the higher torque it provides when compared to a similarly reinforced circular one. For the tested dimensions (length of the square cross-section equal to the diameter of the circular one), the active cross-section area in the square-shaped actuator was approximately 27% bigger when passive and approximately 62% bigger when pressurised, than in the circular one. This experiment only measured the stalled torque at rest configuration, and no data
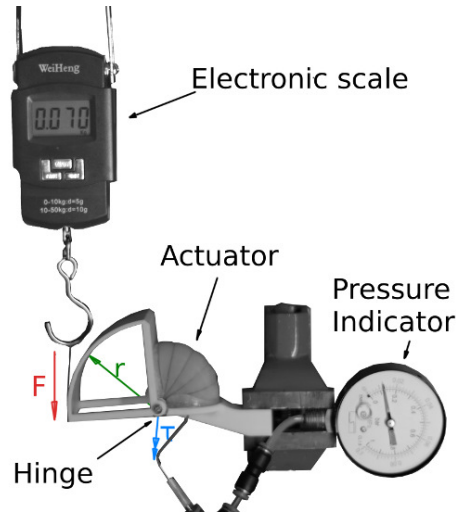
Figure 3.27: Rotary actuation torque test setup

Table 3.4: Blocking torque linearity error for 0 - 0.35bar actuation pressure. Actuation angle: 0°.

Actuator geometry, reinforcement spacing	Average deviation from linear characteristic (see Fig. Fig. 3.29)	Proposed Model Average Error
Circular, 2.25^o	3.6%	3.8%
Circular, 15°	12.4%	7.7%
Circular, 18°	12.1%	6.7%
Square, 2.25^o	6.4%	-

was collected for torque across the stroke or in the time domain.

3.3.5 Summary

This section examines the performance of a fluidic fibre-reinforced rotary actuator. The proposed actuator was tested in terms of bending and torque capabilities, with different versions of the device being compared to one another. I have shown that the densely reinforced, circular cross-sectioned actuator provides more linear behaviour during actuation when compared to both rectangular and sparsely reinforced actuators, even when all other parameters remained the same or very similar. The average deviation of the actuation angle from a reference linear characteristics is approximately 6° with the standard deviation of around 7°. The measured torque deviates less than 4% on average from the behaviour of the ideal actuator. Improved linearity has been achieved by constraining undesirable effects such as changes in cross-section geometry or size.

I have provided an example and justified a hypothesis that the circular actuator's cross-
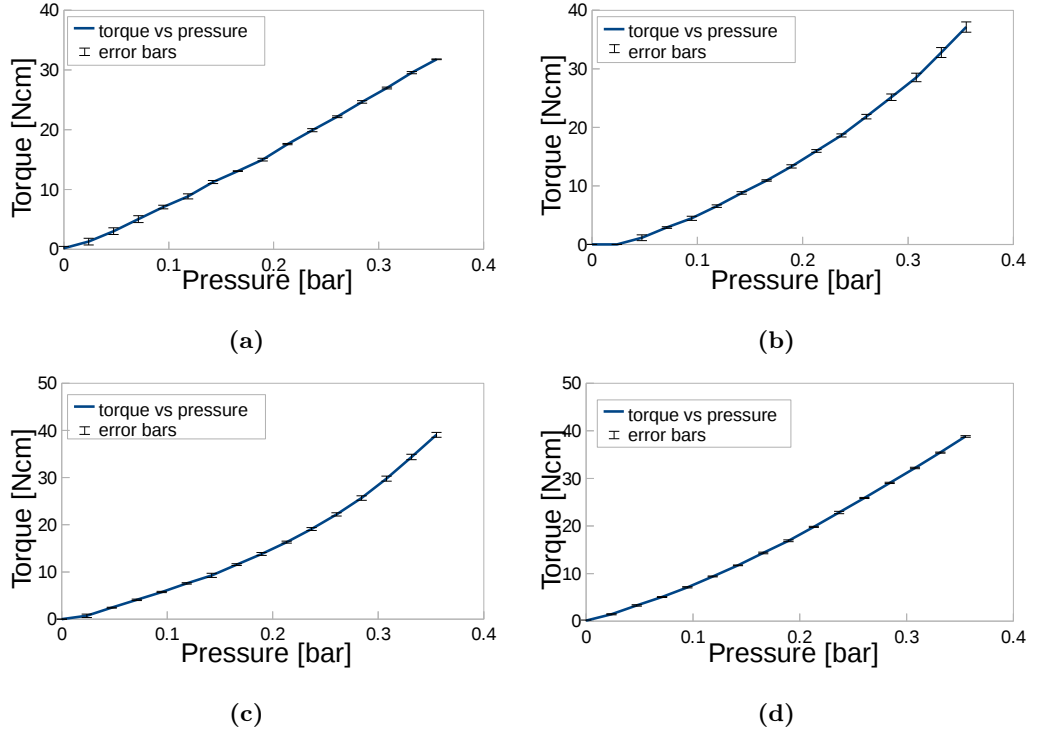
Figure 3.28: Torque vs pressure with error bars. Results for different actuators regarding its cross-section shape and angular distance between reinforcement cycles: (a) circular, 2.25^o, (b) circular, 15°, (c) circular, 18°, (d) square, 2.25^o. Initial configuration of the actuators: 0° actuation angle. From [119].

section shape performs better. I have also validated the hypothesis that an increase in the number of cycles of the reinforcement fibre improves the actuator behaviour.

A mathematical description of the discussed actuator has been proposed, and the gathered data agrees with the model. The predicted bending angle differs, on average, less than 2° from the experimental data, and its standard deviation is equal to 2.2^o.

Limitations

The presented actuator can work only in the positive deformation range. Despite the fact that it is made of soft material, when compressed below its passive angle, it creates significant resistance and buckles. That said, if used in an antagonistic arrangement to drive a rotary joint, as shown in Fig. 3.15, it has to operate around the middle of its range, rather than around its passive angle.

The tip and the base of the actuator are made of stiff silicone. While it is significantly stiffer than the actuation chamber, they still deform under pressure. During experiments, such deformation was causing the parts interfaced with the actuator to detach. In Section 3.5,
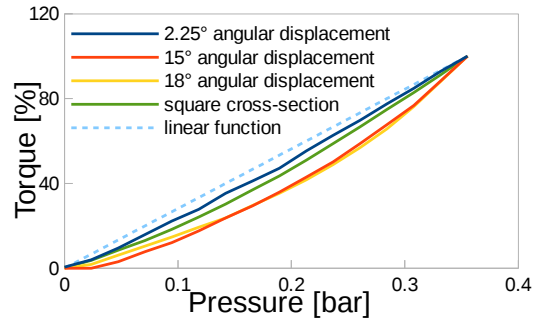
Figure 3.29: Normalised torque plots put on the same graph for comparison purposes.

another interface method was proposed. It is based on shape locking and solves this issue to some extent.

No cyclic nor lifetime tests have been conducted. No destructive tests to define the pressure limits have been conducted either.

The actuator implemented in this section was designed with a specific application in mind, which was an actuator for robotic joints for a manipulator utilising inflatable linkages. The ideas behind it are, however, very general and can be used in a variety of soft actuators. In the following sections, I will present various actuators and robotic devices that are all based on a similar approach and the learnings described in this section.

3.4 Bending actuator with two degrees of freedom

Bending is one of the most popular motion types in soft robotics. It is relatively easy to achieve with various means, and in many cases, can be used straight away. A good example of devices utilizing bending motion is the whole class of soft grippers that use bending actuators to implement robotic fingers. Distributed deformation along with compliance and the soft surface of soft fingers provide distribution of the contact forces on a larger area compared to traditional grippers, and bending motion allows for more reliable grasp postures and wrapping around the handled object rather than relying only on friction forces of parallel grasp.

Just bending, however, is often not sufficient. Another degree of freedom incorporated into the same device could enable various applications.

The human hand is capable of not only grasping but also in-hand manipulation. One of the limitations for robotic grippers to achieve the same level of dexterity is the lack of degrees of freedom. Human hand fingers can not only bend but also vary the direction of bending slightly.

Such a lack of manoeuvrability of single-dof actuators could be addressed by multi-dof actuators, like the STIFF-FLOP module. STIFF-FLOP can bend in any direction and elongate. Its performance is symmetrical in all directions. In the case of many applications, like robotic fingers, a huge part of its workspace would never be used.

It also requires three inputs to be controlled, which might be too complex where simple bending is required.

The gap between single-dof bending actuators and complex multi-dof manipulation modules could be addressed by designing more specific, application-tuned actuators.

In this section, I describe a fibre-reinforced fluidic actuator featuring two degrees of freedom (DOF). This specific actuator was designed as a bending actuator for a swimming octopus robot and is based on learnings from the previous sections. This actuator has been implemented for a very specific task, but it was also used to quantify the effectiveness of three different bending mechanisms: uni-directional bending based on a strain-limiting layer, bending resulting from the actuation chambers located un-symmetrically with respect to the actuator's cross-section, but allowing for multi-directional bending, and the proposed solution that combines those two approaches for improved performance and multi-directional

bending. The work described in this section has been published in [121].

The robot overview

The soft octopus robot is designed for swimming in the water and for being able to advance, turn and twist. For that reason, the tentacles are internally connected and work in two independent groups. Each tentacle has two inner channels that enable it to bend in various directions. Symmetrical actuation of all the tentacle chambers generates a coaxial thrust that pushes the robot forward. The actuation of one group only generates an unsymmetrical thrust that pushes one side of the robot and as a result, the robot turns. Providing pressure to one chamber per actuator causes them to bend to the side, also affecting the robot's motion. One chamber actuation can result in a rotational or twisting motion depending on the chosen pattern. The robot itself is described in more detail in Section 5.2.

The actuator design

The arm of the robot consists of two parts. The active part houses the actuator that generates the bending motion, and the passive part follows the motion imposed by the active part. The active part is assumed to generate the arm motion only, while the motion of the passive part effectively generates the thrust. The design of the arm is presented in Fig. 3.30.
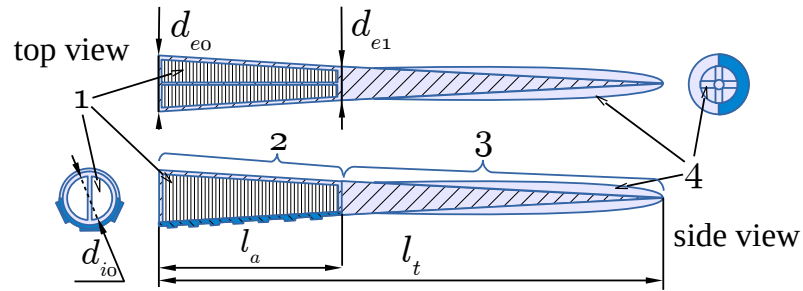
Figure 3.30: The robot's arm design. 1 - actuation chambers, 2 and 3 - active and passive parts of the arm, consequently, 4 - fin-like surfaces. $l_a = 40mm$, $l_t = 140mm$, $d_{i0} = 10mm$, $d_{e0} = 15mm$, $d_{e1} = 9mm$. From [121].

The actuator consists of two independent pressure chambers that tend to elongate when pressurised to enable the intended motion. The inner side of the actuator is covered with stiffer silicone. On account of its mechanical properties, this layer elongates less than the rest of the actuator when pressurised, resulting in bending. The actuation chamber is constrained

by a reinforcement made of polyester thread wound in a tight helix ($\alpha \approx 0.65^o$) and integrated into its wall. In this way, the reinforcement does not restrict elongation of the actuator though efficiently constrains any radial deformation such as ballooning. The actuator structure is presented in Fig. 3.31. The materials used are SmoothOn EcoFlex 00-30 and SmoothOn Smooth Sil 940 for softer and stiffer silicone respectively.
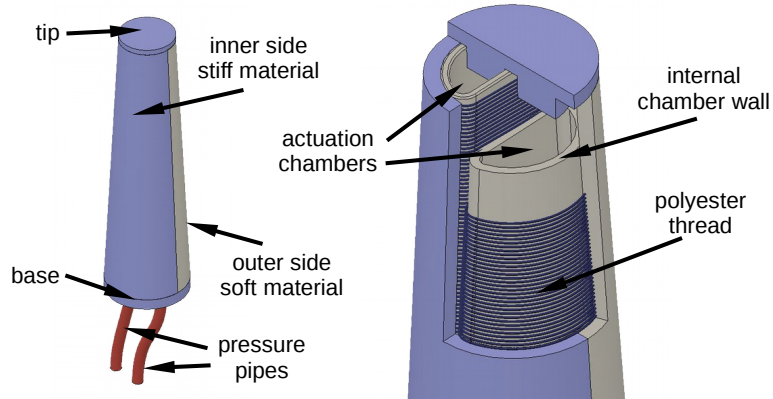
Figure 3.31: The actuator structure. Actuation chambers with reinforcement visible. Stiff silicone denoted in blue, soft in grey colour. From [121].

The inner layer of stiffer material enforces the bending motion of the device when pressure is applied. However, the independent actuation of each pressure chamber influences the direction of the bending plane. The chamber that is pressurised with a higher pressure value tends to elongate more than the another one, thus pushing the corresponding side of the device towards the other side.

The unique feature of this actuator is that it can control the direction in which it bends, known as the bending plane, which is different from other bending actuators.

Other bending actuators with this capability typically use several actuation structures and bend due to asymmetrical actuation of those structures [61, 69]. However, this approach limits the overall area of the actuator that can be used for bending since some actuators must be actuated less than others to achieve bending.

In contrast, the proposed octopus arm actuator uses the entire available volume for bending in the primary direction, which results in greater efficiency. Additionally, the bending plane can still be controlled by adjusting the pressure values on both sides of the actuator.

Therefore, this new actuator design offers high efficiency and greater control over the bending plane, without the limitations of other bending actuators that rely on asymmetrical actuation.

The actuator response for different pressure inputs is presented in Fig. 3.32.
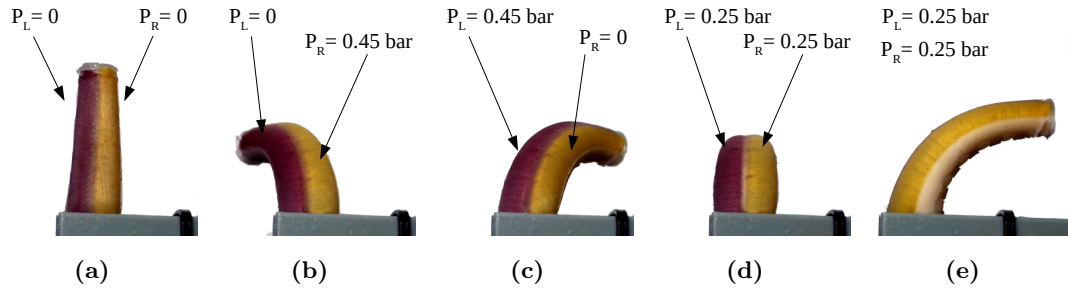
Figure 3.32: The actuator, (a) passive, (b) bent to the left, right chamber pressure higher than left, (c) bent to the right, left chamber pressure higher than right, (d) and (e) symmetrically bent, pressures equal, top view and side view respectively. From [121].

3.4.1 Manufacturing

The actuator is made of silicone material cast in 3D-printed moulds produced by a desktop 3D printer, Zortrax M200. The process consists of several stages as described below:

Step I, reinforcement

In the initial step, the reinforcement is created. It is made of a polyester thread wound around a dedicated 3D printed conical core. Each actuator requires two separate reinforcement structures. The reinforcement is formed manually using a cordless drill that helps to control the pitch and tension of the thread, Fig. 3.33a.

Step IIa, external layer, soft side

The cores with the thread deployed are then inserted into an external mould, and soft silicone is injected. Due to the mould design, only one side of the actuator gets covered in the silicone material.

Step IIb, external layer, stiff side

After the silicone cures, the mould is opened, and the actuator is moved to another mould to add the stiffer part of the external layer. Once in the new mould, stiffer silicone is injected to create the other half of the external layer. Once that is cured, the mould is opened, and the cores gently removed, this process being facilitated by the fact that the cores are conical and can therefore be withdrawn in the direction of the broader end. At this point, the external layer of the actuator, with the reinforcement structure attached to its inner side, is now ready, see Fig. 3.33b.

Step III, internal layer

Although already attached to the actuator, the reinforcement structure remains fragile as it is not fully encased in silicone. Applying any pressure would make the silicone structure extend radially and detach the thread from the silicone surface. A further step is therefore required, in which a smaller semi-conical silicone structure is created using another set of moulds. That structure is then introduced into the actuator, on the underside of the reinforcement, using the same kind of soft silicone, see Fig. 3.33d. Note that the internal layer, in this case, is fabricated separately, outside the actuator and then inserted, again an option presented by the conical rather than cylindrical design. Before insertion, the pre-moulded internal layer is coated with uncured silicone to ensure adhesion between the fibers attached to the internal side of the outer layer and the pre-moulded internal layer. This also provides a seal between the layers. The main advantage of this approach is that every chamber can be examined before assembly, and any defects such as bubbles will be immediately apparent and the unit rejected - an impossibility when chambers are cast directly within the reinforcement.

Step IV, closure

Once the internal layer is attached, the body of the actuator is finished. In the final step, the tip and the base of the actuator are sealed using the same material as in the stiffer internal layer of the actuator. In the base layer, small holes are located so create pathways for the small pressurisation pipes that deliver the actuation fluid.

| (a) | (b) | (c) | (d) |
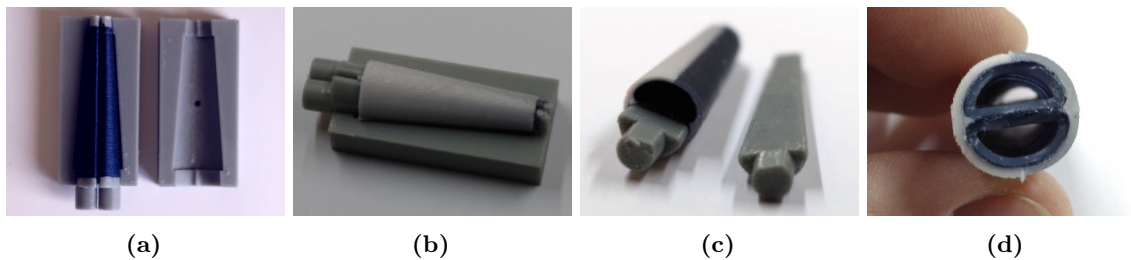
Figure 3.33: Fabrication steps: (a) - reinforcement, (b) - external layer, (c) - reinforcement attached to external layer exposed, (d) - internal chamber layers attached. From [121].

3.4.2 Experimental validation

As explained in previous sections, bending in soft actuators can be induced via constraining elongation on one side or via unsymmetrical actuation.

In this section, the performance of the proposed solution has been validated against the single-DOF bending actuator with a strain-limiting layer and a 2-DOF actuator bending due

to non-symmetrical actuation.

For that purpose, an actuator with the same outer dimensions but exploiting different bending mechanisms has been fabricated. These included the proposed octopus arm actuator with two semi-conical chambers and a stiffer internal layer (Fig. 3.34a), an actuator with only one actuation chamber (Fig. 3.34b), and an actuator with two cylindrical chambers shifted towards the actuator's outer side (Fig. 3.34c). The actuator with a single actuation chamber (b) is expected to generate more bending and exert higher forces than the one with two chambers (a) as it holds a larger actuation cross-section (the chamber separation in the other versions reducing the available space). The drawback is that the bending direction cannot be controlled. Bending in the actuator with shifted chambers (c) is due to unsymmetrical distribution of the pressure inside. This version of the actuator lacks the strain-limiting layer. The actuators and their cross-sections are presented in Fig. 3.34.

(a)   (b)   (c)
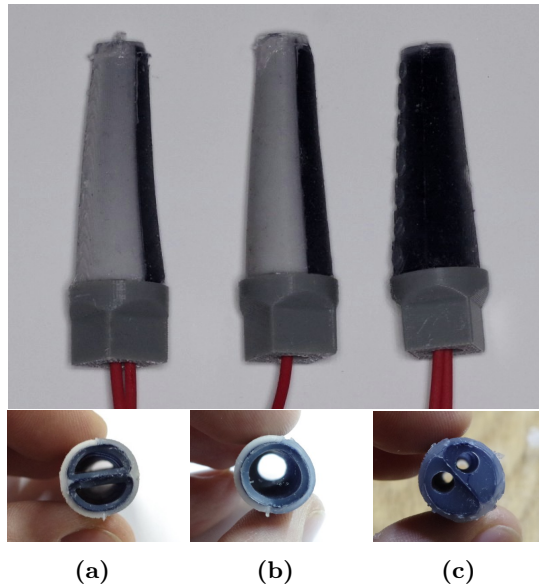
Figure 3.34: Tested actuators (a) - proposed octopus arm actuator, (b) - single DOF actuator, (c) - actuator based on unsymmetrical actuation. All the actuators have same dimensions. From [121].

For the experiment, a simple vision system was used Fig. 3.35a previously referenced in Section 3.3.4. The actuation process for all the actuators was recorded, and using image processing, the pressure value and the bending angle were extracted from the video. Actuation in the range from 0 to 0.4 bar was repeated for each actuator six times. The average actuation curves with statistical errors are presented in Fig. 3.36a. For the blocking force characterisation, the force value was measured at the actuator tip using a custom made 3D printed optical force sensor [122], Fig. 3.35b. The sensor was optimised for small range of

the forces exerted by the actuator and its error was assessed to be within 5% of the measured value. The resulting plots are presented in Fig. 3.36b. The measured deviation of bending plane direction for the proposed actuator is approximately ±28 degrees for pressure equal to 0.4 bar applied to one chamber only.

(a)
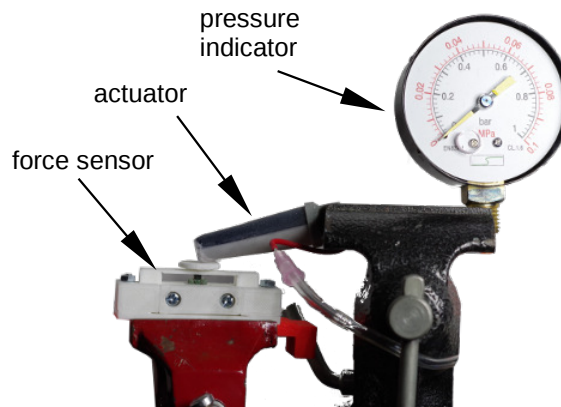
(b)

Figure 3.35: Bending and force measurement, (a) captured and processed frame, (b) force measurement setup. The From [121].

3.4.3 Discussion and conclusions

The experimental data shows that the most effective bending is provided by a single DOF actuator, see Fig. 3.34b. This is due to the greatest possible actuation cross-section area. The proposed octopus arm actuator bends less under the same amount of pressure, as part of the actuation area is occupied by the wall in between the actuation chambers, see Fig. 3.34a. This wall also introduces additional material that stretches during the actuation process, increases the bending stiffness of the device, and further limits the bending deformation. The lowest bending efficiency is provided by the asymmetrical actuator geometry, see Fig. 3.34c, as in that case, we have an even greater decrease in actuation cross-section area alongside
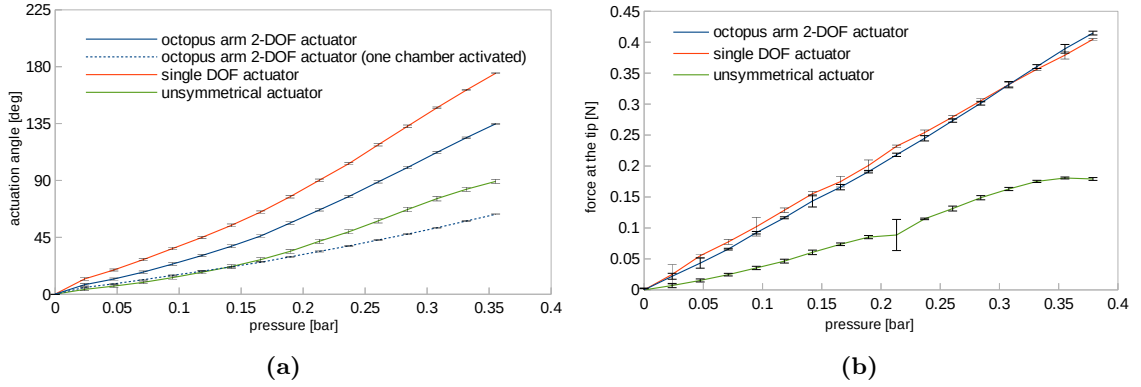
Figure 3.36: (a) Bending vs pressure characteristics of tested actuators, (b) force vs pressure characteristics for the proposed actuator, single DOF actuator and actuator based on unsymmetrical actuation. From [121].

an increase in stiffness. For the same reason, the asymmetrical actuator generates less force than the others. The experimental verification shows that the proposed actuator provides comparable efficiency in generated force to single DOF actuators. However, the bending characteristics are slightly less effective than those with a single DOF actuator. At the same time, it provides a second degree of freedom while outperforming an asymmetrical actuator capable of similar motion.

There are several aspects that have not been properly evaluated. That said, the bending angle with respect to applied pressure for both chambers and single chamber actuation has been characterized. The bending plane angle as a function of pressure in chambers, nor the force generated by the single chamber actuation, has not been characterized. No cyclic tests have been performed.

The actuator design and implementation described in this section is just a specific example of an actuator adjusted for a very specific task, but the outcomes of this work could be applied to many different problems. In this specific example, it was crucial for the actuator to not only bend but also change the bending direction on demand. For that reason, the stability of the cross-sectional geometry was considered not as important, and a single circular cross-section was split into two semi-circular ones, which resulted in slight cross-section deformation when actuation pressure varies in the chambers but allowed for the needed bending plane controllability.

The actuator was designed to be used as an octopus robot arm but could be used in various scenarios such as a manipulation device or a finger in a robotic gripper. A good

example is a gripper device published in [123] in 2020 which uses actuators of similar modality but based on a slightly different mechanical design of parallel pneumatic bellows rather than fiber-reinforced actuators.

The fiber-reinforced actuators described so far have proven their robustness and flexibility in terms of potential applications. They are, however, very labour-intensive to fabricate. Previous sections focused on improvements in the design and fabrication procedure of soft actuators mostly from their performance perspective. The next section focuses on those aspects from the fabrication effort point of view.

3.5 'Instant' soft actuators

One of the issues associated with soft, fibre-reinforced pneumatic actuators is that the fabrication of each design iteration requires a set of moulds to be printed and hours of manual work. Any reinforcement embedded into the actuator adds to the manual work required to manufacture it. Moreover, due to the manufacturing constraints, most of the reinforcement methods proposed so far lead to relatively basic structures that constrain the deformation in a very simple way. Currently, in most cases, the reinforcement is made manually, which results in poor repeatability. Any design adjustment means that the process has to start from scratch, with the redesign and printing of new moulds. Although experience of the process and design improvement mitigated this to an extent, it is still very time-consuming. It is also very restrictive, as a non-experienced technician would not easily be able to replicate the procedure without detailed guidance from someone with the requisite experience.

Over the years of technology development, many complex manufacturing processes become simplified and automated. We now have advanced CNC machines capable of machining complex parts with precision far beyond manual manufacturing techniques. We have additive machines ranging from simple and affordable, hobby-grade 3D printers to very expensive and advanced industrial printers printing in very advanced materials using technologies like laser sintering or ultraviolet-activated resins. Soft technologies, however, are still missing automated fabrication techniques.

An ideal solution would be to fabricate soft robot prototypes using additive methods such as 3D printing. There are technologies that allow printing with very stretchable materials [78, 81, 82], but parts with complex shapes and internal voids are still difficult to achieve with those approaches. In [83], a 3D printer modification allowing for printing with silicone material and reinforcing it with thin layers of filament has been proposed. The structures are printed on a rotating rod, which limits the geometry to cylindrical. In [84], a printing technique combining various materials allowing for printing soft structures reinforced with fibers has been proposed.

There are some commercial 3D printing machines or services that allow for printing soft materials and even combining soft and rigid materials within a single part [124]. However, the physical properties of those materials are still not as good as even cheap platinum cure

silicones.

This chapter proposes a soft robot manufacturing approach that uses robust, high-strain, high-elastic silicone materials and allows the embedding of reinforcement without being overly labour-intensive. The idea uses disposable 3D-printed moulds with embedded reinforcement structures. The moulds and reinforcement structures are printed together such that the reinforcement is over-moulded, becoming a part of the actuator after the external mould is removed. The whole actuator mould can be printed on an affordable desktop FDM (Fused Deposition Modelling) 3D printer. The proposed approach has demonstrated motion performance comparable to fibre-reinforced actuators while enabling faster manufacturing of prototypes and requiring much less manual work in the process. It also potentially paves the way to new reinforcing structures that cannot be achieved through manual fibre deposition or fabric incorporation.

An arbitrary requirement for the design is to be printable using a single extruder FDM printer, as these machines are the most common and affordable 3D printers.

Usage of soft filaments such as nylon allows not only compliant but also squeezable designs.

As the main part of the fabrication process involves filling a 3D printed mould with silicone, waiting for it to cure and then opening it - in a sense like instant food - I have called my approach the 'instant' soft robot.

The work described in this section has previously been published in [125].

3.5.1 The 'instant' actuator design

The simplest possible implementation of the 'instant' robot concept is a linear actuator. It would contain a cylindrical actuation chamber reinforced with circular rings of printed material. The actuator expands when pressurised, but the reinforcing structures constrain the radial expansion, so the only deformation is elongation - just as in fibre-reinforced actuators.

During the printing process, the reinforcing rings are supported by the supporting teeth attached to the inner part of the mould. The printing parameters, including the nozzle distance from the supporting teeth, are adjusted so that the adhesion between rings and the supporting structures is low, and the rings can be easily separated from the mould once the mould is removed. In this way the reinforcing rings break away from the mould and remain

attached to the actuator. This is a standard approach used for removable support structures in FDM 3D printing, ensuring they can be removed without damaging the actual printed object. The correct geometry of the supporting teeth and the distance between them and reinforcement are crucial aspects of the design.

The cross-section of a linear actuator design is presented in Fig. 3.37, and all the crucial design dimensions are presented in Fig. 3.38.

(a)
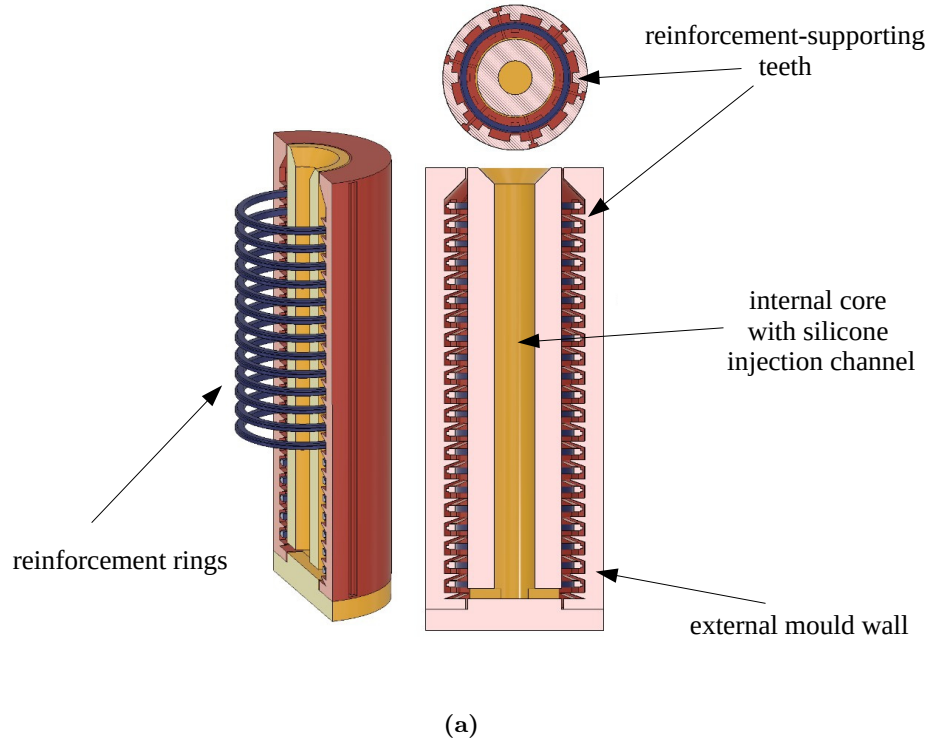
Figure 3.37: Linear actuator mould CAD model. The external wall is in red, the internal core with silicone injection channel in yellow and the reinforcement rings in blue. Supporting teeth visible. From [125].

Adding a vertical continuum layer of 3D printed material connecting the reinforcement rings on one side of the linear actuator results in a strain-constraining structure, turning the linearly extending actuator into a bending one, Fig. 3.39a.

Connecting multiple actuation chambers in parallel leads to a multi-DOF actuator. One of the possible implementations is a 3-DOF manipulation module as shown in Figs. 3.39b and 3.39c.

The manipulation module design above features three identical actuation chambers reinforced with nylon structures. Each module is equipped with a central hollow channel through which pressure cables for subsequent modules can be passed. The reinforcement is
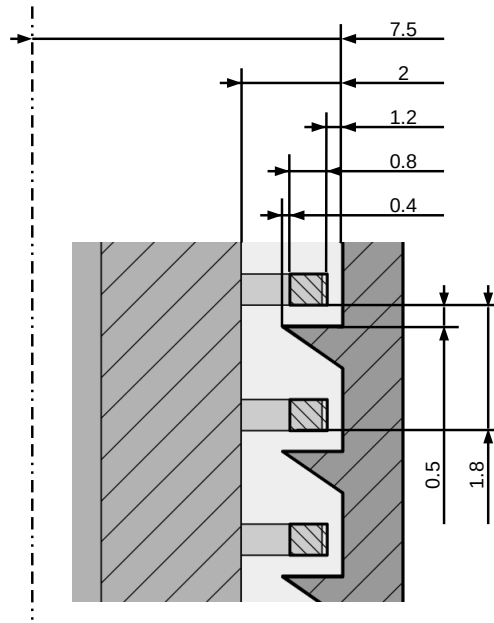
(a)

Figure 3.38: Crucial design dimensions. Dimensions have been tuned to make the reinforcing rings stick to the supporting teeth just slightly and detach when the external mould is broken.

printed from nylon, providing some flexibility, so that the module can be squeezed without breaking, but equally providing enough rigidity so that the pressure chamber geometry does not deform significantly under pressurised despite its non-circular cross-section. This is an important aspect, as an overly deforming chamber would occlude the central channel, thereby affecting the pressure response and making it less linear, see Section 3.2. Some cross-section geometry deformation is nonetheless still visible, resulting in a less linear response than in a module with circular chambers. Due to process limitations, it is impossible to embed circular reinforcement into each chamber, as the reinforcing structure has to be supported by teeth located on the outer wall of the mould or overhung in the air. Overhangs can be only straight lines, so I opted for a circle divided into sections, one section per actuation chamber. I considered a circular cross-section of the rods creating the actuation chambers, but such a modification would not prevent the cross-section from being deformed as the pressure transferred by the silicone would in either case affect the geometry of the reinforcement. Moreover, switching to a circular chamber cross-section would reduce the actuation cross-section.
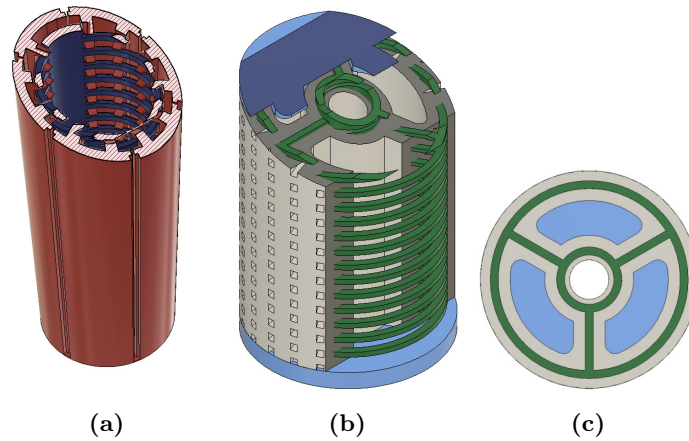
Figure 3.39: 'Instant' actuators design. (a) Bending actuator's mould, continuum layer of 3D printed material (flexible Nylon PA12) exposed in blue (b) Manipulator module, side view, reinforcement exposed in green. Top and bottom sealing in blue. (c) Manipulator module, top view, actuation chambers (in blue) and central channel (in white). From [125].

The manipulation module fabricated using the proposed approach is an alternative to the STIFF-FLOP manipulator [61, 68] providing the same functionality and similar performance while being considerably easier to produce. STIFF-FLOP is a manipulator designed for minimal invasive surgery (MIS), with no rigid components [8]. It is pneumatic pressure-driven and uses no electricity making it MRI-compliant (Magnetic Resonance Imaging). One of the important advantages of STIFF-FLOP is that it is relatively cheap to produce in comparison to other MIS devices and utilises no toxic materials making it an easy-to-use, disposable tool. Using the proposed 'instant' fabrication technique, such a device could become even cheaper to produce, allowing multiple units to be used in a single procedure without significantly increasing costs.

3.5.2 Fabrication

The mould

As mentioned, the moulds for this actuator's fabrication were produced in a 3D printing process. I used an FDM technology printer, a very popular and affordable tool. The design was adjusted for a single nozzle machine, although using more than one material in the same process would make things even more straightforward and enable more complex designs through the introduction of soluble supports.

The moulds were sliced using a Prusa Slicer and printed with a Zortrax M200 machine

[126]. The material used was Nylon PA12 filament. The printing parameters were adjusted to reduce the stringing effect, see Fig. 3.40, and to ensure adhesion of the printed layers, which needs to be strong enough to create a reliable reinforcing structure but weak enough to allow for the separation of the reinforcement when the mould is broken. If adhesion between the outer mould and the reinforcement is too strong, the structure risks breaking away from the actuator body.

(a)   **(b)**
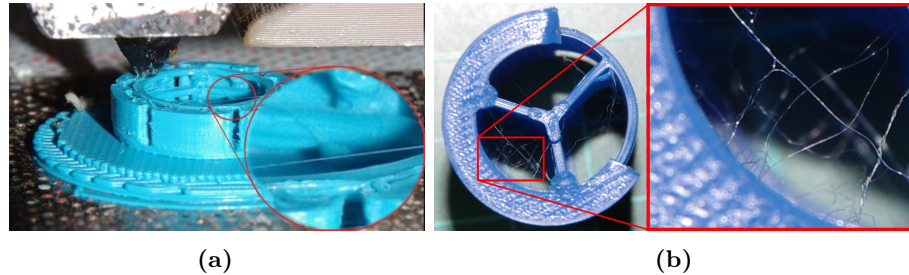
Figure 3.40: (a) Mould being printed, (b) top-view. Some stringing effect visible. From [125].

The reinforcement separation problem could be improved by making gap e (Fig. 3.37(c)) bigger. That said, if the gap is too big, this could lead to the filament not being attached to the supporting teeth at all and consequent print failure.

Given the considerable stringing effect, and that nearly all the prints were affected by some stringing, the design was split, with the outer mould and the internal cores being printed separately. The mould could then be blasted through with hot air, efficiently removing all the string and potential imperfections that could pierce the actuation chamber wall in the final actuator. This "small-feature removal" process has to be quick so as not to affect the actual structure of the mould. Another advantage of splitting the mould design is that the internal cores are not destroyed when the moulds are removed and can therefore be reused.

The main disposable mould of the manipulator module and the internal cores that can be reused are presented in Fig. 3.41.

The actuator

After the mould has been cleaned with hot air, it is assembled (the rods are inserted into the external mould), and filled with silicone by injecting the material through an injection channel. A standard syringe is used for this.

This internal injection channel ensures the silicone material fills the mould from the
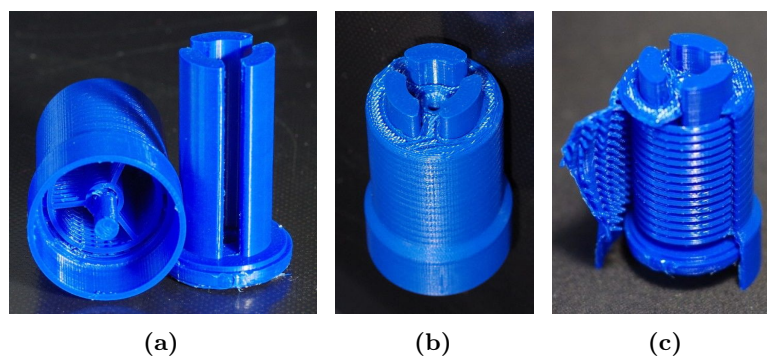
Figure 3.41: 3D printed mould. (a) Mould parts - external single-use part and internal reusable rods. (b) Mould assembled, ready to be filled with silicone, (c), mould broken, internals shown. From [125].

bottom up, helping to efficiently remove all the air from the mould, ensuring bubble-free consistency silicone (it is noted that the silicone must be properly degassed before moulding.) After the silicone has cured, the external mould is broken apart, and the internal rods are pulled out. During this process, the reinforcing rings get separated from the outer mould, remaining embedded in the actuator. The actuator is then sealed at both ends with caps moulded in another fabrication step. The entire procedure is presented in Fig. 3.42.

Finished linear and bending actuators, as well as a manipulation module, are presented in Fig. 3.43.
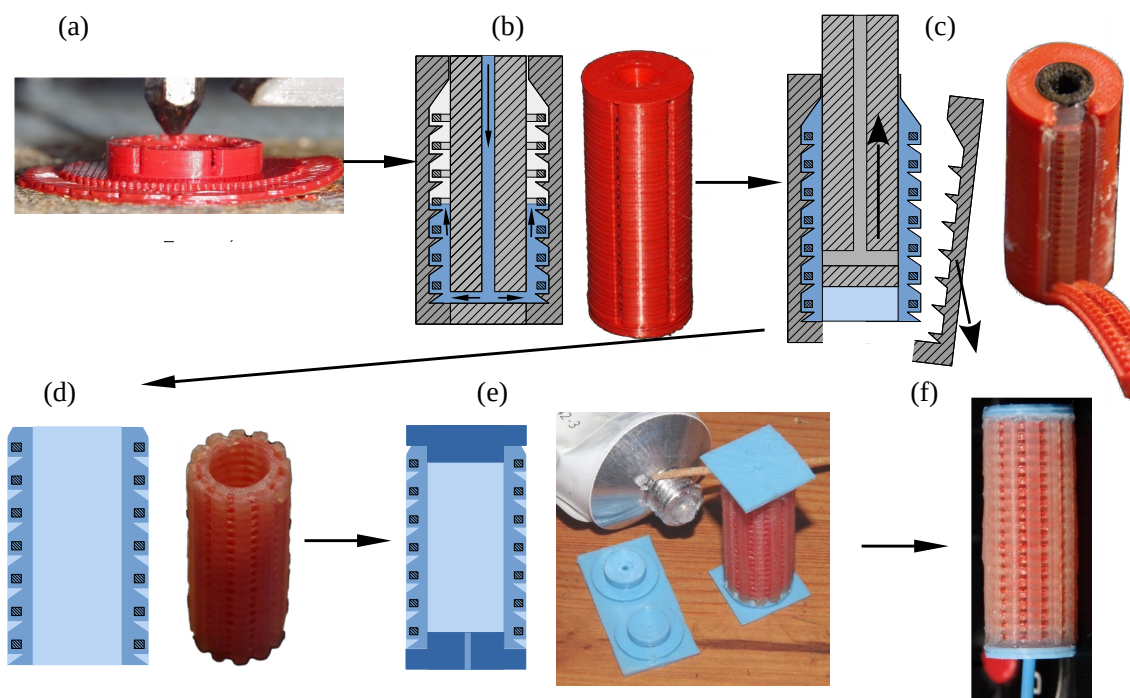
Figure 3.42: Actuator manufacturing. The mould is printed using an FDM printer (a), then assembled and injected with the uncured silicone material (b). After silicone cures, the mould is broken apart and removed (c) while the reinforcement remains attached to the actuator's body (d). Then top and bottom caps are attached (e). In (f) the ready-to-action actuator is presented. From [125].
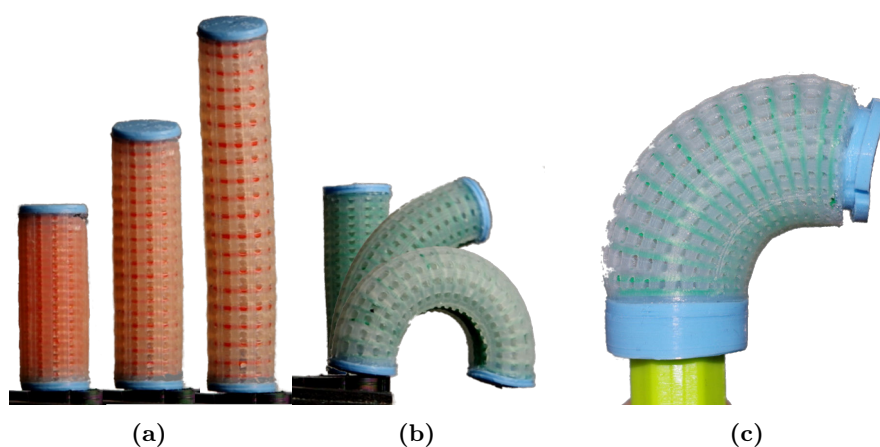
Figure 3.43: 'Instant' actuators, the silicone used SmoothOn Ecoflex 0050 [127], (a) linear expanding actuator, (b) bending actuator, (c) 3-DOF manipulation module. From [125].

3.5.3 Instant soft devices

The manipulation modules can be stacked together to create a soft robotic arm.

The key difference in relation to the manufacturing process between the STIFF-FLOP manipulator and this module, is that I managed to shed the most time-consuming and technically challenging part - the reinforcement fabrication. The old process involved winding polyester threads around cylindrical rods. The cores were composed of 3 parts and were manually wrapped with thread using a drill. There were six identical cores per module required. The new design also resulted in a reduction in the number of moulding steps, again contributing to a decrease in both labour and time, on account of the reduced silicone cures required. It is noted that the old procedure (described in more detail in Section 3.2) has already been optimised for easy, quick, and reliable manufacturing; other procedures proposed for similar actuators are often more labour-intensive.

The STIFF-FLOP manipulator and the new 'instant' manipulator are presented in Fig. 3.44.

An assembled 3-module 'instant' manipulator is presented in Figs. 3.45a and 3.45b. The length of a single 'instant' manipulator module is 38mm, while its diameter is 22mm. The central channel width is 4.5mm.

In parallel to introducing improvements in manufacturing, I have also advanced the design in relation to ease of use of the modules. The STIFF-FLOP manipulator was originally assembled by glueing on attachment rings that were then screwed together. Disassembly operations in case any module needed replacement were time-consuming. Moreover, the attachment rings were rigid, compromising the overall softness of the structure, and potentially limiting applications in which it could be used. In the new design, I equipped the manipulation modules with a base and tip that allows for form-locking the segment ends into each other. This makes the assembly and disassembly processes very simple and straightforward, see Figs. 3.45c and 3.45d.
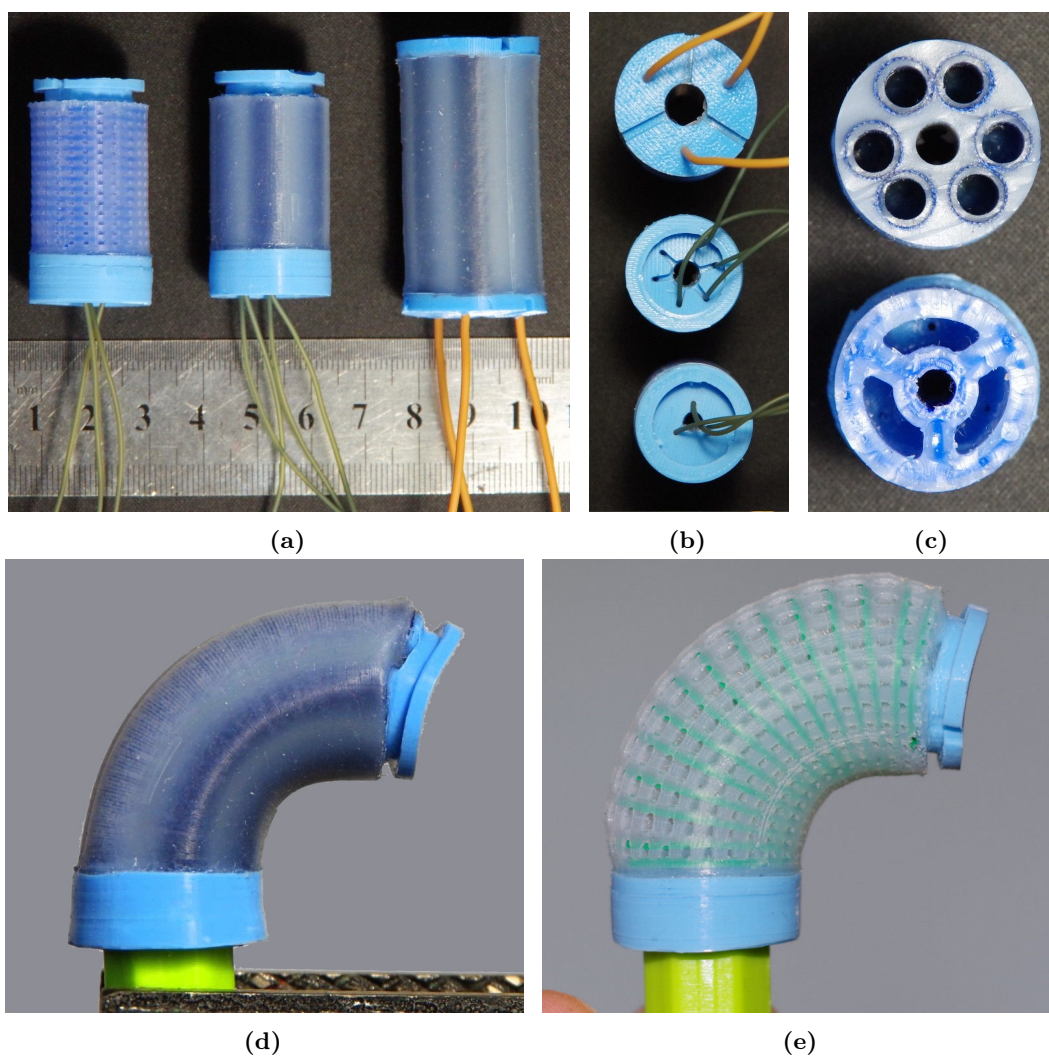
Figure 3.44: (a) 'instant' manipulator (left), STIFF-FLOP-like fibre-reinforced reference (middle) and the actual STIFF-FLOP manipulator (right) modules compared, (b) bottom view, (c) top view, cross-section, (d) actuation of fibre-reinforced and (e) 'instant' modules. From [125].
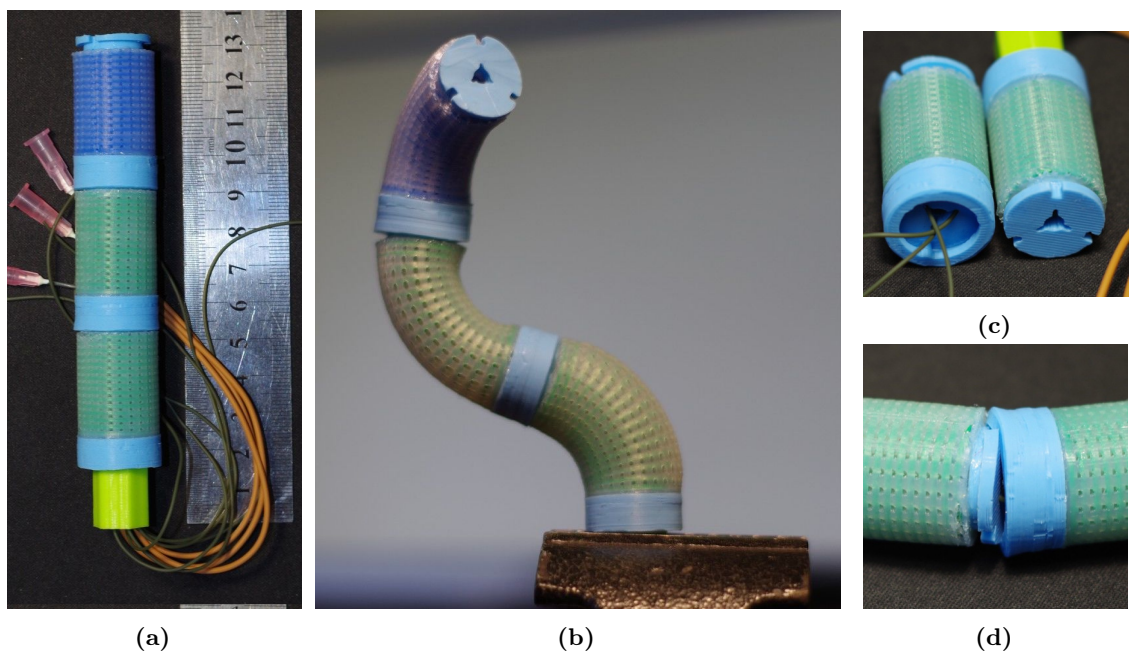
Figure 3.45: (a) and (b) 'instant' manipulator assembled, (c) inlet tubes, (c) and (d) shape locking structure, the connection mechanism. From [125].

3.5.4 Experiments

The proposed actuators and the manipulator module were tested for generated motions and force. A vision-based system equipped with a video camera was used for deformation detection. Colour markers were attached to the actuators and tracked with an image processing algorithm. For force measurement, I used the Robotous RFT40-SA01 force sensor. The pressure was controlled using SMC ITV0050 pressure regulators. For more details on the experimental setup see Section 5.5.

I measured the bending characteristics of the manipulation module and the force it generated in a parallel and perpendicular direction to its central axis with one, two and three chambers actuated. The gathered data was compared with the reference fibre-reinforced STIFF-FLOP design. The external dimensions of the 'instant' and the fibre-reinforced modules match such that they can be easily swapped in the final setup. The cross-sectional area of the actuation chamber is equal in the two designs. The measurement setup is presented in Fig. 3.46.

al

(a)   (b)   (c)
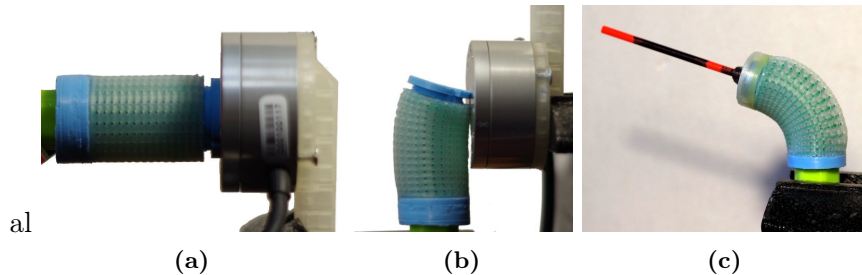
Figure 3.46: Measurement setup. (a) force parallel and (b) perpendicular to the main axis of the manipulation module, (c) bending and elongation characteristics setup. From [125].

Initial tests with modules show that the 'instant' actuator is significantly less stiff than the reference fibre-reinforced module made of the same material. This is due to the fact that the 'instant' actuator contains less silicone on its outer side on account of the reinforcement supporting teeth and the greater volume of the reinforcement itself. The reinforcement material detaches from the silicone wall while the actuator body deforms, making the resulting cross-sectional area of stretched material smaller. Effectively the pressure required to actuate the device is reduced. The bending characteristics of both the fibre-reinforced and 'instant' manipulation modules as well as linear actuators are presented in Fig. 3.47.

On account of the issue mentioned above, I decided to manufacture the proposed manipu-
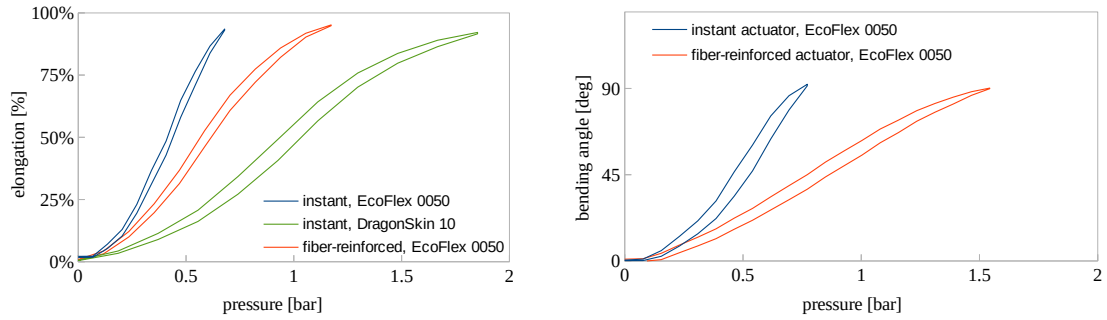
Figure 3.47: (a) Characteristics of 'instant' and fibre-reinforced linear actuators, (b) Bending characteristics of 'instant' and fibre-reinforced manipulation modules. From [125].

lation actuator using stiffer Dragon Skin 10 silicone [128], which shifted the characteristics closer toward to the reference device. The gathered data for the 'instant' actuator (Dragon Skin 10 material) and the fibre-reinforced reference design (EcoFlex 0050 material) are presented in Figs. 3.48 to 3.50.
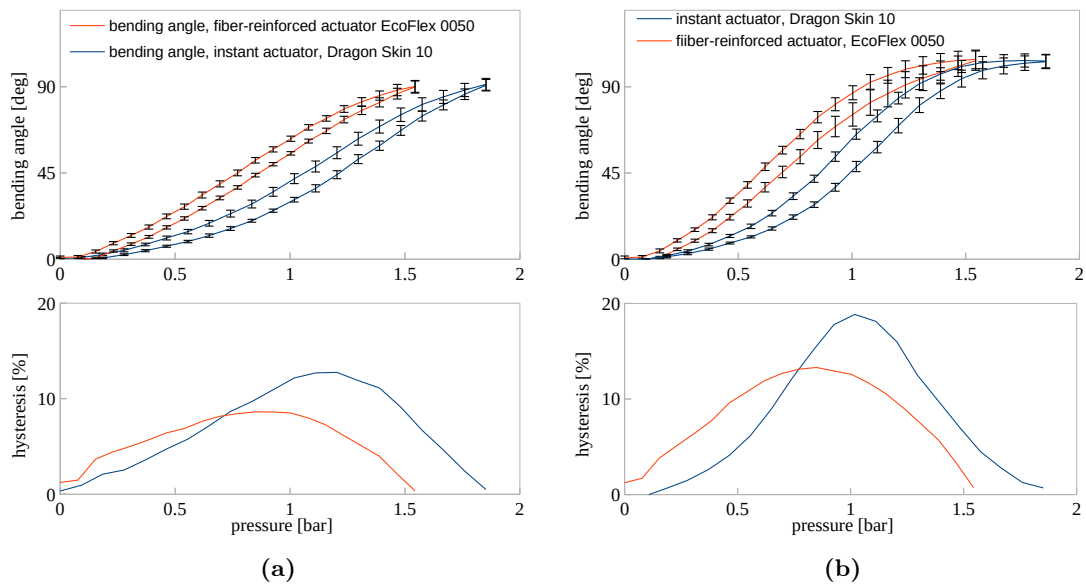
Figure 3.48: The bending characteristics of the manipulator, Fig. 3.46c. (a) single chamber, (b) two chambers activated. The measurement is taken for each chamber three times, 9 measurements in total per module. From [125].

Above a certain pressure value, the compressed gas in the 'instant' manipulation module tends to displace the reinforcement, see Fig. 3.51a-c, creating areas that then balloon, and potentially then burst. Destructive tests show the bursts occur at approximately 2.4 bar pressure at approximately 140 degrees actuation angle for the 'instant' actuator, although the reinforcement started failing earlier, at around 2 bars. I was unable to explode the fibre-reinforced design within the available pressure range (3 bars, approximately 180 degrees), see
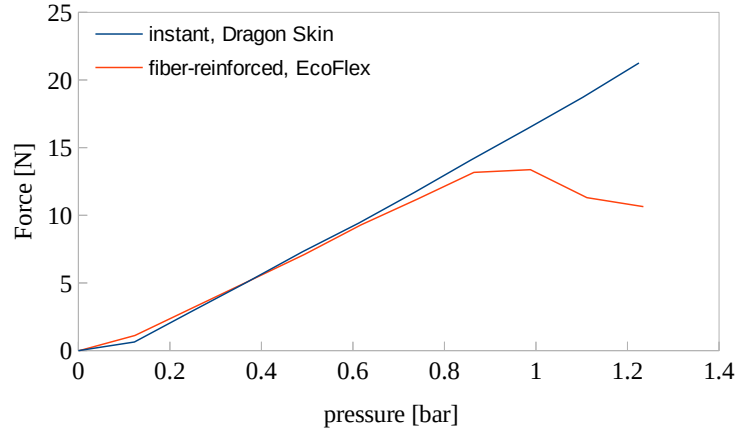
Figure 3.49: The axial force generated by the manipulator along its primary axis, Fig. 3.46a. The reference manipulator started to buckle around 0.8 bar. From [125].
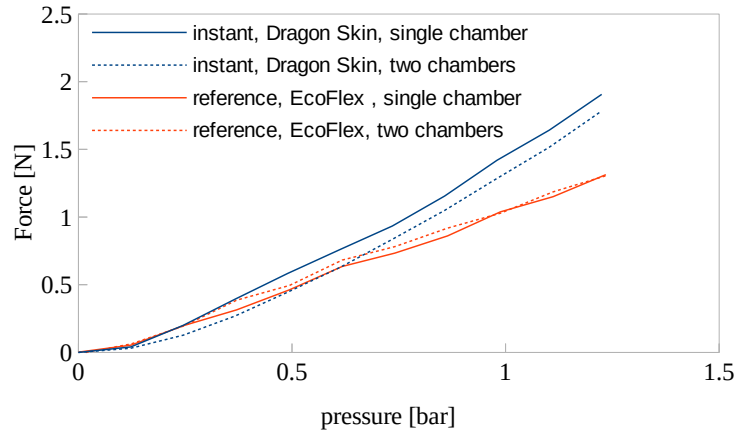
Figure 3.50: The force generated by the manipulator in radial direction, Fig. 3.46b. From [125].

Fig. 3.51(d). In Fig. 3.52 the destructive test data is plotted.

3.5.5 Discussion

The 'instant' actuator, with the same external dimensions and actuation area as the reference fibre-reinforced actuator made of the same material, has a significantly reduced stiffness due to it having less silicone on the outer part of its body - a result of the holes created by the reinforcement-supporting teeth and the volume of the reinforcement itself. For the same reason, the 'instant' actuator requires significantly less pressure to be actuated. This effect can be compensated by using a stiffer material to fabricate the 'instant' actuator.

The 'instant' manipulation module behaviour is less linear than the reference one, and this is probably related to its non-circular pneumatic chamber cross-sections, causing change in the chamber's geometry and resulting in expansion of the actuation area. This does not occur

(a)   **(b)**   **(c)**   **(d)**
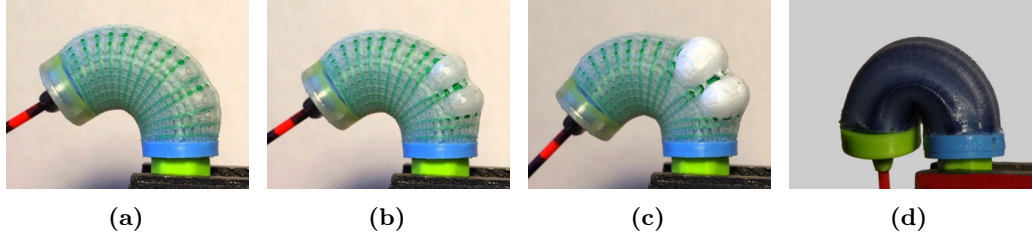
Figure 3.51: Ballooning between reinforcement rings occurs above a certain pressure. (a) at approximately 2 bar the reinforcement starts to displace, (c) at 2.4 the actuator bursts, and (d) reference actuator actuated to 180° with no harm. From [125].

Table 3.5: Manufacturing time comparison, 'instant' vs fibre-reinforced actuators

	STIFF-FLOP	**'instant' manipulator**	**fiber-reinforced linear actuator**	**'instant' linear actuator**
labour time	$\approx$ 3h	$\approx$ 50m	$\approx$ 1h	$\approx$ 40m
skills/experience	high	low	medium	low
mould	34 parts, reusable	6 pats (5 reusable)	10 parts, reusable	4 parts (3 reusable)
moulding steps	3	2	3	2
gluing steps	1	1	1	1
printing time	7h30m	2h40m once & 1h20m per module	3h35m	2h once & 1h20m per actuator

in the reference manipulator's cylindrical chambers, rendering its behaviour significantly more linear.

The deformation of the actuation chambers and the semi-flexible-semi-rigid reinforcement also affects the hysteresis making it slightly more appreciable.

It is also noted that due to the reduced density of the reinforcement, the 'instant' actuator fails at a smaller actuation pressure/angle than the dense reinforced reference module. Still, the 'instant' actuator can efficiently operate up to 90 degrees angle, which makes it a good choice for certain applications. The reinforcing structures themselves never failed in my tests, and the bursts always occurred due to the displacement and ballooning of the silicone body. However, I was able to break the reinforcement by squeezing it repetitively.

The ballooning process in soft actuators can lead to a burst due to a phenomenon known as snap-through instability [129]. This occurs because of the highly nonlinear pressure-to-volume relationship of a flexible inflated membrane, where the pressure initially increases with the inflation volume, but at a certain point, the pressure starts to decrease even as the volume increases. In pressure-driven devices, crossing this turning point means that the volume will continue to increase even if the pressure is not further increased, leading to a burst.

This kind of instability is particularly problematic in systems with many actuation
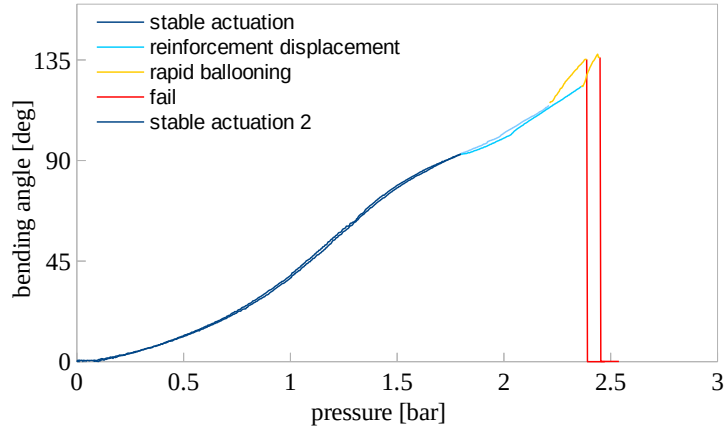
Figure 3.52: Destructive tests of the 'instant' manipulation module. Two chambers were tested, and the third one got damaged while testing the two first ones. Thanks to the automated reinforcement fabrication the characteristics of both chambers are almost perfectly aligned in the stable operational range. From [125].

chambers connected in parallel, where the transition of one actuator through the turning point leads to the rapid transfer of most of the actuation medium from all the other actuators into the given one. This process can be illustrated with an experiment involving two balloons connected to the same tube, where squeezing the inflated balloon causes the other one to inflate rapidly as the fluid is transferred.

One way to mitigate the ballooning problem is through mass-based control, but in cases where the other actuation chambers constitute a reservoir of pressurized gas, even mass-based control would not solve the issue due to the process depicted in the connected balloons experiment.

One drawback of the proposed approach compared to manual fabrication techniques is the disposability of the moulds. In the manual fabrication technique, the moulds are reusable, and their wear is relatively slow. Even 3D-printed moulds, when handled properly, can be used to make any number of actuators. In the 'instant' approach, however, every mould is single-use, resulting in a considerable amount of waste.

While no lifetime tests have been conducted, it is expected that the instant' actuator will have a shorter lifespan than the fiber-reinforced version. This is because the cyclic load on the reinforcing structures is likely to wear and tear them faster than the thread, and similarly, the silicone structure between the reinforcing rings is likely to wear faster due to higher strains.

The actuation properties of the instant linear actuator are very similar to the fibre-

reinforced one. Except for the quantitative difference in the pressure required to achieve an arbitrary elongation, their behaviour in terms of linearity and hysteresis are comparable.

3.5.6 Summary

In this section, I presented a new approach to the design and fabrication of fibre-reinforced actuators. My work extends from the standard fabrication process for fibre-reinforced actuators, automating much of the process and making it less labour-intensive. The actuation performance of the new actuators is comparable to that of previous fibre-reinforced actuators.

It was important for me to develop soft material actuators whose fabrication and use were accessible to soft robotic enthusiasts and researchers who may not have access to specialised equipment. While there are more advanced 3D printing alternatives able to print soft materials directly or even mix stretchable and not-stretchable materials in one process, they are typically either in early development or, on account of their cost, somewhat exclusive and not available to the general robotics community. Using flexible printing materials such as nylon creates actuators that are not only compliant but also squeezable, making these devices entirely soft with no rigid components.

I have designed and fabricated a soft pneumatic linear actuator, a bending actuator, and a 3-DOF manipulation module to demonstrate my approach. Importantly, the manipulation modules can be stacked on top of one another to create a modular, entirely soft manipulator.

The actuators described in this section provide certain motion modalities that correspond to the previously delivered fibre-reinforced actuators. They are simple devices created only as proof of concept. However, the concept could be applied to a variety of designs, custom actuators having very specific dimensions and geometries, or embedded into complex devices. The flexibility of 3D CAD design and 3D printing creates possibilities to utilise this approach to create whole soft robotics systems that could combine 3D printed parts with moulding and could be created with just a few moulding steps. Usage of soluble supports would enable even more complex designs.

The designs of the manipulator module and both the linear and bending actuators are available online at `https://github.com/jfras/instant_soft_robotics`.

3.6 Chapter summary

In this chapter, I present an overview of my research on soft actuators, where I focus on improving their actuation characteristics, specifically the linearity of their response. I aim to optimise the design of the actuators by considering their reinforcement geometry and density, as well as proposing novel fabrication procedures. One of the approaches that I introduce is the concept of 'instant' soft robots that combine 3D printed structures with silicone casting.

The outcomes of this chapter could be summarised in a set of simple rules:

Use reinforcement

Silicone-based actuators are just like balloons. When pressurised, they expand in all the possible directions. This is in general undesired, ballooning weakens the device, make it unstable, non-linear, prone to burst and requires a lot of space to expand, even if only one dimension of the expansion is used. It also requires significantly more medium to fill-up a ballooning actuator. The ballooning effect, however, can be efficiently limited with properly designed reinforcement.

Dense reinforcement is better than sparse

If the reinforcement is sparse, the material between reinforcing structures still can expand. That said, the denser the reinforcement, the better the ballooning is constrained, and the less undesired effects associated with it. When reinforcing with fibres, however, keep in mind that the silicone layers inside and outside of the reinforcement need to be connected. Using hairy threads rather than sleek ones helps to prevent outer and inner silicone layers from detaching from each other.

Use circular cross-sectioin

Circular cross-section is the only one that would not morph into any other shape. When used with reinforcement that fixes the perimeter length, the circular cross-section ensures not only its geometry would not change, but also its area will be constant regardless of the actuation pressure. Constant area makes the actuator's response more linear. Non-circular actuators expand more during the actuation, so that the final force

they generate as a function of pressure can be greater when compared to the circular version with corresponding passive dimensions. In such cases, the expanded dimensions are larger for the non-circular actuator. However, if a larger actuation area is required, a circular actuator with the final dimensions could be used instead of a non-circular but expanding actuator. This would provide the same amount of force or bending while minimizing the disadvantages of non-circular cross-sections.

Create the reinforcement first

If the reinforcement is created first and then covered with external and internal silicone layers, it can be created using rigid (often spinning) cores. Thanks to that, it is significantly easier to manage proper fibre alignment, reduce the labour and required manufacturer skills, as well as improve the final product quality and repeatability.

Consider using 'instant' approach

When labor time is a concern, and some of the performance can be compromised, or when actuator geometry is challenging to create manually, consider the 'instant' approach. 'Instant' approach has proven to provide similar actuation features at significantly reduced fabrication time and requires far less experience and skill to fabricate. Such convenience comes at the cost of a reduced actuation pressure range, slightly lower linearity, and increased hysteresis. Despite these drawbacks, the approach remains usable in various applications.

The research presented in this chapter has its limitations. There are aspects that have not been experimentally quantified, such as the lifespan of proposed devices, cyclic tests that could help determine how their properties change over time, or examination of the actuation pressure limits in most cases. The Mullins effect [130] has been mitigated by actuating the discussed devices several times before experiments, but has not been considered further.

The proposed actuators have limitations that are mostly inherent features of soft-bodied pneumatic robots. The most pronounced failure modes observed in this research are as follows:

Ballooning

If the fibers are arranged too sparsely, or in the case of instant actuators, when the density of the reinforcing rings is limited, there is a risk of an abrupt ballooning effect. When the reinforcement spreads, the soft membrane between them starts to expand radially, which can easily lead to instability and bursting. Even when not unstable, such an effect leads to increased strain and faster wear. For more details, see Fig. 3.51.

Burst

When the tension strength of the material is exceeded, the actuator simply bursts and is permanently broken. This is often preceded by an unstable ballooning phase. See Fig. 3.51.

Leaks

Even if not exploded, it is often the case that some leakages are present in the system. This could be due to not-perfectly air-tight tube connections or some very small holes in the silicone membrane that slowly release the internal pressure of the actuator.

Buckling and twisting

Since the proposed actuators are entirely soft, they can easily buckle or deform in other undesired ways. One of the those failure modes is the twisting of bending actuators around their main axes when more pressure is applied to induce more bending in their primary bending direction. Such an effect leads to decreased bending force and off-axis displacement rather than the expected higher bending forces, see Section 5.1.6. A similar failure occurs in the case of linear pushing actuators that, above a certain pressure, do not generate any more force but buckle, see Fig. 3.49.

Layers detachment

One of the experienced failure modes is the detachment of the inner and outer layers of the actuator structure. If the used reinforcement material cannot be penetrated with the silicone material and arranged too tightly, the local stresses in the close proximity to the fiber gets very high and causes the silicone-fiber bond to break. Since there are

no gaps between fibers, the layers are not interconnected, separate and break, leading to a permanent failure of the actuator. See Section 3.2.2.

Fabrication errors

The fabrication of soft actuators presented in this thesis involves many manual steps (reduced in the 'instant' design, but still present) which are prone to errors. It is often the case that the fibers are not arranged uniformly, or that some air bubble trapped in the silicone is the reason for premature failure of the silicone membrane under pressure. These errors are often invisible prior to the failure of the actuator. This is especially the case for the air bubbles trapped inside the internal layer that are not possible to spot from outside of the actuator.

While the focus of my research has been on the active aspect of soft actuation - generating motion or deformation and exerting forces on the environment - there is another aspect that needs to be addressed: stiffening. Stiffening is one of the approaches to resisting external forces and disturbances or increasing the amount of force that soft robots can generate.

Although soft robots excel at being soft and flexible, they lack the rigidity required to resist external disturbances or generate significant force. Therefore, the concept of stiffening is essential for enhancing the functionality and robustness of soft robots.

In the next chapter, I will briefly discuss some existing approaches to stiffening and highlight some of my concerns regarding them. Additionally, I will present a novel idea to overcome one of the issues associated with these approaches, which can improve the performance of soft robots and enable them to perform more complex tasks in diverse environments.

STIFFENING STRUCTURE INSPIRED BY MAMMALIAN ERECTILE TISSUE

As explained in the one of the introductory Section 2.4, stiffness control is an important issue in soft robotics. While conforming to external forces and objects is effectively the key characteristic of soft robots, they do also need to be able to exert forces. A problem then arises as these are opposing behaviours, Indeed the softer the robot is, the less force it can exert. Soft robots deform significantly and that deformation is distributed, which is the desired effect, but one that also creates an issue.

As an example, in the case of the soft pneumatic gripper depicted in Fig. 4.1 the maximum grasping force it can generate is limited by its stiffness, as increasing the actuation pressure beyond a certain value results not only in the force increase, but in undesired deformation of the fingers as well. Such a deformation is caused by uniformly increasing the actuation bending moment, which leads to a concentration of reaction torque in the base of the finger. That in turn pushes the base of the finger away while the tip of the finger curls, and the grasp transforms from power grasp to pinch grasp.

This kind of problem can be addressed by splitting the finger into independently controlled sections [131] or by pre-programming stiffness in the actuator in order to achieve various bending radii and torque in different places along the finger [132]. The problem is that these solutions are not very flexible (the length of the sections is predefined and needs to be tuned for each application). Additionally, the first solution adds to the control complexity by introducing an additional degree of freedom to the system.
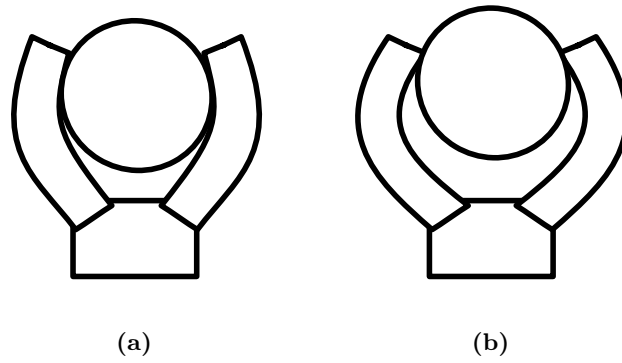
Figure 4.1: Stiffness problem when grasping. (a) moderate actuation pressure, power grasp, (b) actuation pressure increased, fingers deformed (tip curled, base deflected, pinch grasp)

I propose a structure inspired by the mechanical structure of the mammalian penis, in which a soft structure can be effectively stiffened under relatively low blood pressure, thanks to a constant-volume cavity and directional blood flow [133]. One of the main parts of the penis, the corpus cavernosum, is composed of small sinusoids that fill with blood during an erection, trapping the blood inside [20]. Blood, as a liquid, has very low compressibility, so any compression caused by external force generates an increase in pressure that in turn results in high bending resistance of the organ's hydraulic structure despite the relatively low initial pressure.

The proposed structure is composed of small compartments, with each compartment enforcing a directional flow of the actuation medium. Under certain conditions, the outlet of the compartment is closed, while the inlet can accept more actuation fluid all the time. Thanks to this, the structure can be powered with relatively low input pressure, but whenever the compartment is compressed with an external force, the pressure inside it would increase accordingly, with the pressure change remaining local to the disturbance. When the external force is released, the compartment can immediately accept more actuation fluid via the directional input. Such a structure could be used in various ways in soft robotics and beyond to create devices that do not require closed-loop control or sensing to provide complex behaviors and stiff responses along with low actuation pressure requirements. If minimized, the same principle could be used to create smart materials that, in turn, could be incorporated into soft devices to create very complex actuation structures.

The fact that the proposed structure responds to the actuation pressure and external disturbance in a complex way can be used to implement a physical logic element that, in

turn, could be used to embed smart behavior into the body of the device. This would enable
the development of soft robotic systems with inherent adaptive and responsive properties
without the need for complex sensing and control systems, potentially simplifying the overall
design and reducing the required power and computational resources.

As a proof of concept, I have designed a soft pneumatic actuator that can autonomously
stiffen. This design enables the coexistence of high actuation compliance and a stiff response
to disturbances at any operating point. Owing to the intelligent internal structure, the
mechanical resistance of the actuator depends on the direction and characteristics of the
external forces acting on its surface, allowing for an efficient change in compliance on the fly
without locking its shape. Consequently, the proposed actuator can continuously adjust its
shape in one direction gradually, remaining soft and compliant while resisting significantly
higher forces in the opposite direction.

The actuator has an internal structure inspired by the corpus cavernosum sinusoids. It
is composed of individual compartments that trap the actuation fluid inside, increasing the
bending resistance of the device. As the actuation chamber is divided into small distinct
volumes, the local pressure increase resulting from compression of the device can not be
averaged across the chamber. Instead, it is localised in the compressed areas, causing an
increase in pressure, and a consequent increase in stiffness.

Much like with sinusoids during an erection, fluid flow in the proposed actuator is managed
such that during actuation, fluid can flow in but not out, thereby trapping the entire fluid
volume in the actuator. Due to that, if the object moves away from a finger, more fluid flows
into the actuation chamber, and the finger adapts, following the object. If the object pushes
on the finger, the pressure of the trapped fluid increases on account of the deformation,
resulting in an increase in stiffness.

In this section I provide a proof of concept prototype that implements this idea on a
macro scale. Ultimately, the aim would be to identify a material with which to replicate this
on a micro scale - similar to the foam actuation material presented in [59].

4.1 Internal structure

Consider a flexible expanding actuation chamber with a mass of fluid trapped inside. In this scenario, in static conditions, there are three forces in equilibrium. They are the internal pressure, the external disturbance, and the internal stress resulting from the stretch of the material. As the trapped fluid has a constant mass, any external disturbance compressing it causes its volume to decrease, which in turn results in the pressure increase, affecting the stresses in the material and the equilibrium point. Effectively the apparent stiffness of such a structure is higher than it would be when the pressure, rather than its mass, was kept at a constant level.

Consider a flexible but relatively non-stretchable cylinder filled with pressurised gas, see Fig. 4.2a. An external force strong enough to overcome the internal pressure results in the deformation of the structure. Due to the bending moment distribution along the cylinder's length, the deformation is more intense near the cylinder base, and less bending is observed close to the point at which the force is applied. As a result, the compression of the wall on the opposite side to the force application point is higher at the base, see Fig. 4.2b. Consequently, the base's contribution to the internal volume compression is higher than that of the the rest of the pressure chamber as it compresses more in that area. Since the gas can freely travel within the chamber, the compressed volume at the base contributes to the overall compression. As a result, the pressure growth is the same throughout the chamber.

If a specific force value is exceeded, the structure begins to buckle. While in some cases buckling is the desired phenomenon [134, 135], in the case of inflatable cylindrical cantilevers, it causes high strain concentration but also non-linearity and reduction in bending stiffness [136] Fig. 4.2c. In this instance, the volume near the buckled actuator wall is compressed even more, with no significant impact on the pressure, due to the distribution of that compression - as explained above.

A similar process can be observed in soft bending actuators or soft manipulators in which the impact of the force is most pronounced at the base of the device Fig. 4.3

There are several examples of actuators in which a pressurised actuation medium can move freely within the actuation chamber so that the fluid compressed at any one point can move towards non-affected areas [137, 61, 121, 138, 139, 31]. In those designs, the local
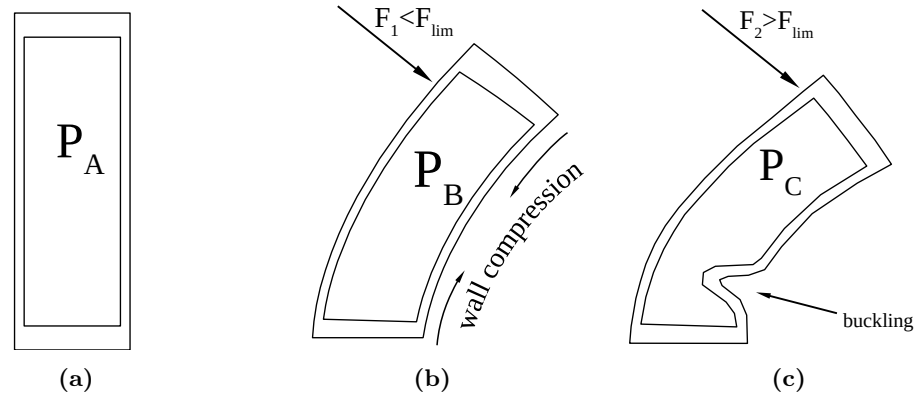
Figure 4.2: An external disturbance on a pressurised cylinder. (a) passive state, (b) the bending motion causes the opposite cylinder side to shorten, the internal volume to shrink and the pressure to grow, (c) force value exceeds a specific value F_lim, no more wall compression is observed, but the structure starts to buckle instead. Internal pressure $P_A < P_B < P_C$

actuation medium compression is distributed throughout the entire volume of the device, reducing the overall pressure increase.
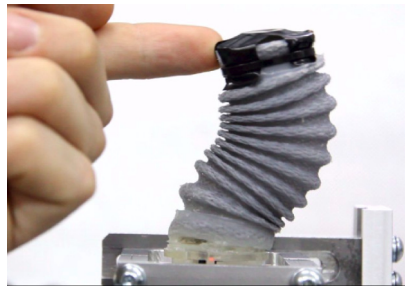
Figure 4.3: An external disturbance on a soft STIFF-FLOP manipulator [61]. The resulting bending moment is the highest in the base as is the deformation.

The ability of the pressurised medium to travel inside the actuation chamber reduces the actuator resistance, as the local, relatively high volume compression is spread evenly throughout the entire volume resulting in a limited increase in pressure. If, however, the gas compression was held within the area in which it originated, the resistance of the actuator would be much more pronounced.

That said, consider an actuator chamber split into smaller volumes, see Fig. 4.4, such that the fluid is unable to move freely between compartments. In this instance, pressure increases proportionally to the local, rather than global, volume change and the resulting pressure will not be homogeneous throughout the actuator, but would increase faster closer to the base. Since the bending moment is greatest near the base, the actuator experiences the greatest volume compression in that area. As a consequence, the base of the actuator stiffens more than the rest of its body, increasing the overall force response.

$$P_A = P_{B1} < P_{B2} < P_{B6} < P_{B7} < P_{B8} < P_{B12}$$

(a)   (b)
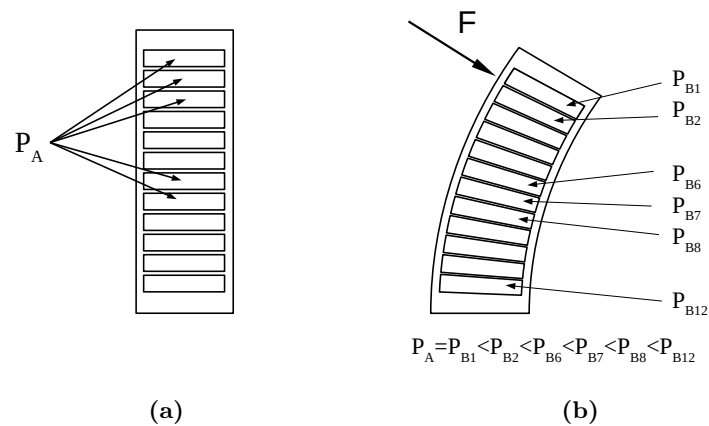
Figure 4.4: In case the internal volume of the actuator is divided into small compartments, the compressed medium can not move inside the actuator leading to pressure increase locally. Thanks to that, the resulting stiffness of the actuator is significantly higher, and buckling is prevented.

A simple implementation of this idea would be to create a complete actuator chamber composed of a series of mini actuation chambers and connect them using dedicated valves, see Fig. 4.5a. Once actuated, all the valves can be closed, ensuring the fluid remains inside the relevant compartments. Creating an array of binary valves and connecting each section via a dedicated tube does not appear feasible. Indeed, any such solution would still only provide two distinct modes of operation - actuation when valves are open and shape-locking when closed.

Assuming that a bending actuator experiences the highest external-force-induced torque at the base, which gradually decreases towards the force-acting point, one might postulate that directional valves could be placed between adjacent compartments without affecting the desired behaviour. Only the top section needs to be supplied with the pressure, and the fluid would then fill subsequent sections in succession. Following any disturbance or impact, the compressed fluid cannot go back towards the top compartment on account of the valve. It is not able to move toward the base either, as the pressure in the lower adjacent compartment would be even higher, see Fig. 4.5b. The final base compartment needs to be connected to the outside environment (i.e. the surrounding atmosphere) with a binary valve to vent the overall structure. This valve would need to remain closed during operation and only open to release the pressure and return the actuator to the relaxed state.
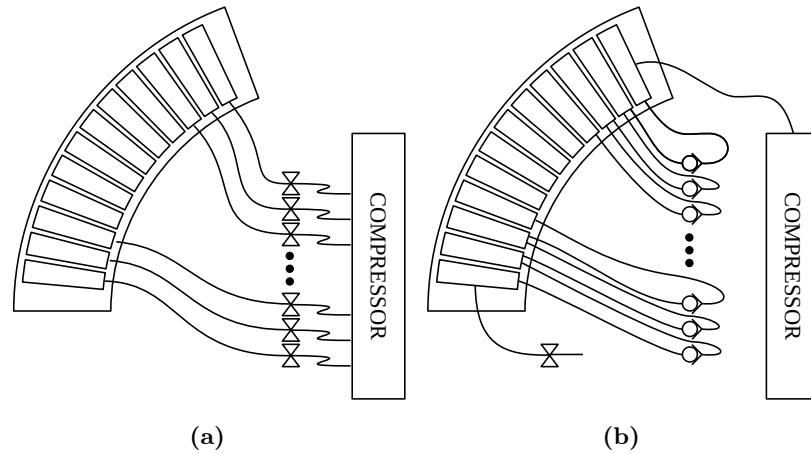
Figure 4.5: (a) each of the compartments of the actuation chamber is connected to the compressor via its dedicated valve. Once pressurised, valves can be closed trapping the medium in the compartments. (b) only the top compartment is connected to the pressure source. Adjacent compartments are connected via check-valves, and the last compartment via a binary valve.

4.2 Principle of stiffness increase

4.2.1 A linear actuator

Consider a flexible cylinder comprising an internal pneumatic chamber reinforced with helical fibre. Assuming the actuator's constituent elastic material shows linear strain-stress behaviour, it will behave like a spring whose elongation is described by the spring equation eq. (4.1), see Fig. 4.6. The stiffness of such an actuator is determined by the spring constant k_0.
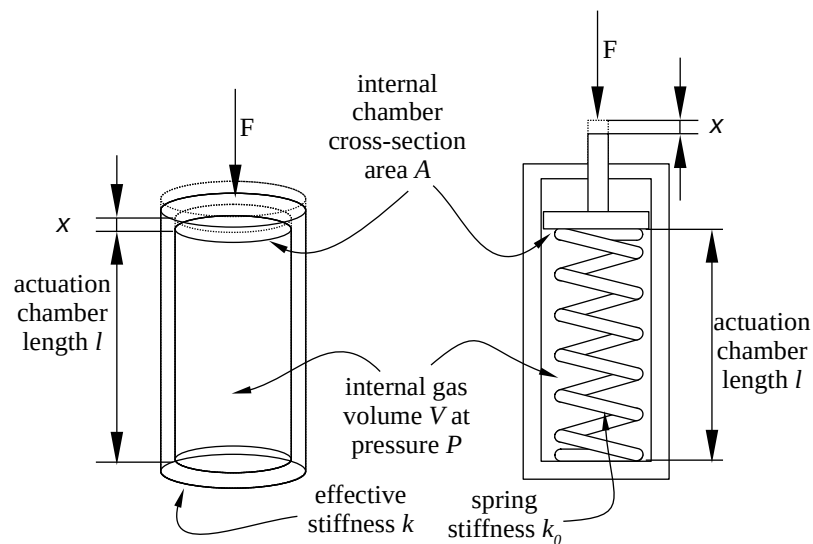
Figure 4.6: The force response for external displacement. The cylindrical linear actuator and an equivalent pneumatic cylinder with a spring in parallel.

$$F = k_0 x \tag{4.1}$$

This cylinder, when pressurised under an external force could be described using eq. (4.2), where F_p and F_e represent pressure-induced force and external force values, respectively.

$$F_e - F_p = k_0 x \tag{4.2}$$

In this case the stiffness, in relation to the external disturbance of the device, can be expressed as eq. (4.3).

$$k = \frac{dF_e}{dx} = \frac{d(k_0 x + F_p)}{dx} \tag{4.3}$$

where F_p represents the pressure-related force and can be expressed as $F_p = AP$. A and P stand for the chamber cross-section area and relative internal pressure value.

The F_p value does not change under constant pressure inside the chamber. In that scenario, the device is powered via a pressure regulator that constantly adjusts to any value changes. In this case effective stiffness $k = k_0$. However, the situation changes if the pressure is initially set but not regulated thereafter. If the mass of the gas inside the chamber and the gas temperature remain constant, the pressures before and after any disturbance (P_0 and P_1 respectively), can be described by the ideal gas law eq. (4.4). As the volume of the chamber is proportional to the length x of the actuator, the equation can be transformed into eq. (4.5)

$$P_0 V_0 = P_1 V_1 \tag{4.4}$$

$$P(x) = \frac{V_0}{V_1} P_0 = \frac{l_{P_0}}{l_{P_0} - x} P_0 \tag{4.5}$$

Taking the above into account in relation to the closed chamber, eq. (4.2) can be reformulated as eq. (4.6) where A denotes the cross-sectional area of the actuator and P_e stands for the atmospheric pressure. Stiffness will therefore be represented by eq. (4.7)

$$F_e + A(P_0 \frac{l_{P_0}}{l_{P_0} - x} - P_e) = k_0 x \tag{4.6}$$

$$k = \frac{dF_e}{dx} = \frac{d[k_0 x - A(P_0 \frac{l_{P_0}}{l_{P_0} - x} - P_e)]}{dx} = k_0 + AP_0 \frac{l_{P_0}}{(l_{P_0} - x)^2} \qquad (4.7)$$

Given that the desired behaviour is the increase in stiffness with respect to the baseline actuator, the stiffness gain can be expressed as eq. (4.8)

$$\frac{k}{k_0} = 1 + \frac{AP_0 l_{P_0}}{k_0 (l_{P_0} - x)^2} \qquad (4.8)$$

where l_{P_0} is the length of the actuator pressurised with pressure $p = P_0$, before the external load is applied. Knowing the parameters of the material used, and the geometry of the actuator, that length can be expressed as a function of pressure as eq. (4.9) where l_0 is the passive length of the device.

$$l_P = l(P) = l_0 + \frac{PA}{k_0} \qquad (4.9)$$

Assuming that the passive length and the fully extended length of actuator l_0 and l_{P_0} respectively, at a given pressure P_0 are predefined by the design requirements, we can express the required stiffness k_0 of the device as follows: eq. (4.10)

$$k_0 = A \frac{P_0 - P_e}{l_{P_0} - l_0} \qquad (4.10)$$

combining eq. (4.10) and eq. (4.8) we get: eq. (4.11)

$$\frac{k}{k_0} = 1 + \frac{(P_0 l_{P_0})(l_{P_0} - l_0)}{(P_0 - P_e)(l_{P_0} - x)^2} \qquad (4.11)$$

which shows that the stiffness increase for an actuator with a predefined length and range is a function of the value of the pressure required to achieve that extension P_0. Stiffness increase for an actuator expanding twice ($l_{P_0} = 2l_0$) depending on the P_0 value and the compression value $\frac{x}{l_{P_0} - l_0}$ has been presented in plots Fig. 4.7

The above reasoning demonstrates that the device's stiffness increases if the mass of the actuation gas is locked within the actuation chamber volume, but also that it is non-linear and increases with the compression of the device. The lower the actuation pressure required to achieve the assumed extension of the actuator, the more pronounced the increase in stiffness.

Taking all the above into account, the actuator design can be tuned to low actuation
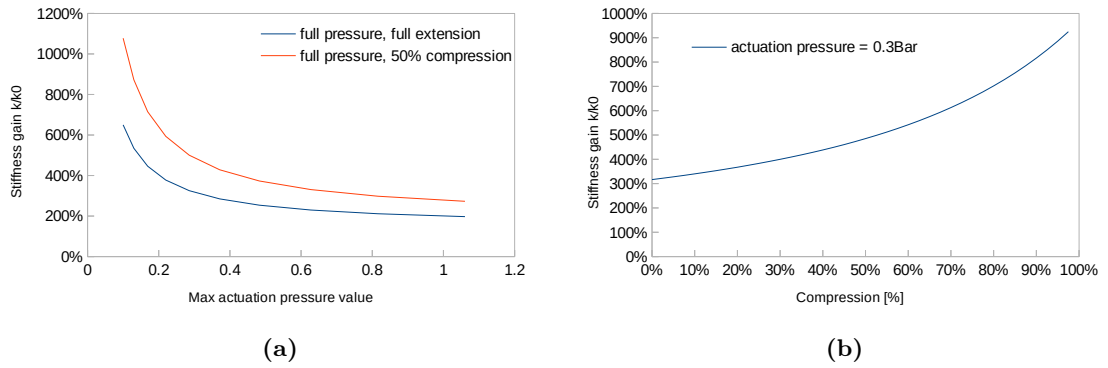
Figure 4.7: (a) stiffness increase vs full actuation pressure for no compression and 50% compression of the device, (b) stiffness increase vs compression for 0.3 bar actuation pressure. Assumed nominal extension of the actuator is $l_{P_0} = 2l_0$ at pressure P_0.

pressures (e.g. increasing the actuation chamber area) to increase its ability to stiffen when the actuation chamber is closed.

4.2.2 A bending actuator

The bending actuator considered here uses similar physical principles, except that the elongation on one side of the actuator is constrained by a strain limiting layer. Similar reasoning can therefore be applied in relation to the bending motion.

In static conditions, the state of the actuator can be described via the equilibrium condition eq. (4.12), Fig. 4.8.
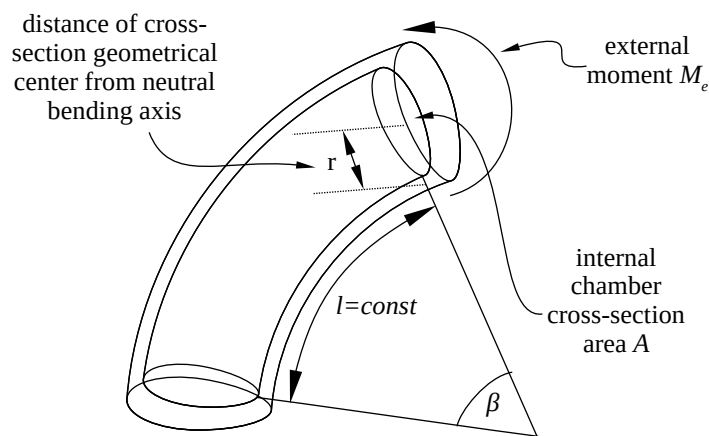
Figure 4.8: Bending actuator geometry

$$M_p + M_e = M_s \tag{4.12}$$

where M_s denotes torque resulting from internal stresses $M_s = \beta EI$, and where β, E and I stand for bending angle, Young modulus and first moment of inertia of the cross-section of the device, respectively. M_p and M_e are the internal force moment and external moment resulting from the pressure inside and external force, respectively.

The apparent bending stiffness k_b of the device relates to the change of the external moment M_e, itself a function of change in bending angle causing a deviation in eq. (4.13).

$$k_b = \frac{dM_e}{d\beta} = \frac{d(\beta EI - M_p)}{d\beta} \tag{4.13}$$

The internal moment M_p depends on the chamber geometry and the internal pressure $M_p = ArP$. The pressure in turn is also affected by the volume change, and can be expressed in terms of the initial pressure and the current bending angle of the device, $P_1 = P_0 \frac{l+r\beta_{P_0}}{l+r+\beta_{P_1}}$. Consequently the derivative eq. (4.13) can be expressed as eq. (4.14)

$$k_b = \frac{Ar^2 P_0(l + r\beta_0)}{(l + r\beta_1)^2} + EI \tag{4.14}$$

Just as with the linear actuator, we can assume that l, EI and β_0 values are set by design requirements, while other values, A, r, and P_0 can be tuned to achieve the requisite bending and passive stiffness levels.

And similarly, we can plot the apparent stiffness gain with respect to the assumed pressure value P_0, Fig. 4.9.

The parameters used for generating the plots above are the actual values used for the prototype described in the following sections. Given the geometry of the actuator, the expected stiffness gain at actuation pressure of 0.3 bar is around 1.8 times the original stiffness and is expected to increase slightly on external disturbance.

4.2.3 Numerical models

The physical properties used in the previous section have been implemented to simulate the bending actuators shape under external loads.

Three distinct scenarios have been taken into account: (a) single actuation chamber, with
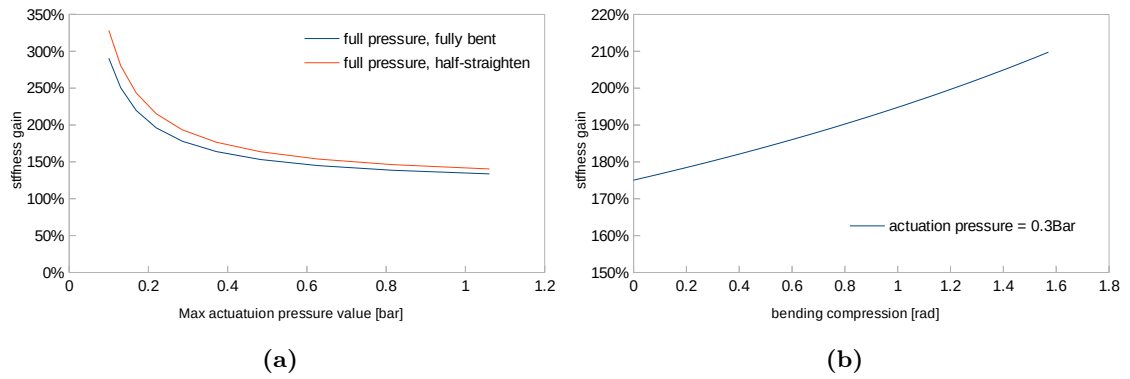
Figure 4.9: (a) stiffness increase as a function of actuation pressure P_0 for fully bent and half straightened (with external force) device, (b) stiffness increase vs compression for 0.3 bar actuation pressure. Assumed nominal bending of the actuator is $\beta_{P_0} = \pi$ at pressure P_0.

pressure regulated at a constant level, (b) single actuation chamber with constant gas mass, but pressure increasing under a load, (c) actuation chamber split into smaller sections, with constant gas mass in each compartment.

The simulation results are consistent with expectations. The closed chamber increases the stiffness of the device significantly and splitting it into smaller compartments amplifies that effect. The amplification is more pronounced the closer to the base the force is acting. This is caused by the fact that the compression happens only in the section between the base and the point at which the force is applied, but is distributed throughout the entire volume in the case of single chamber device.
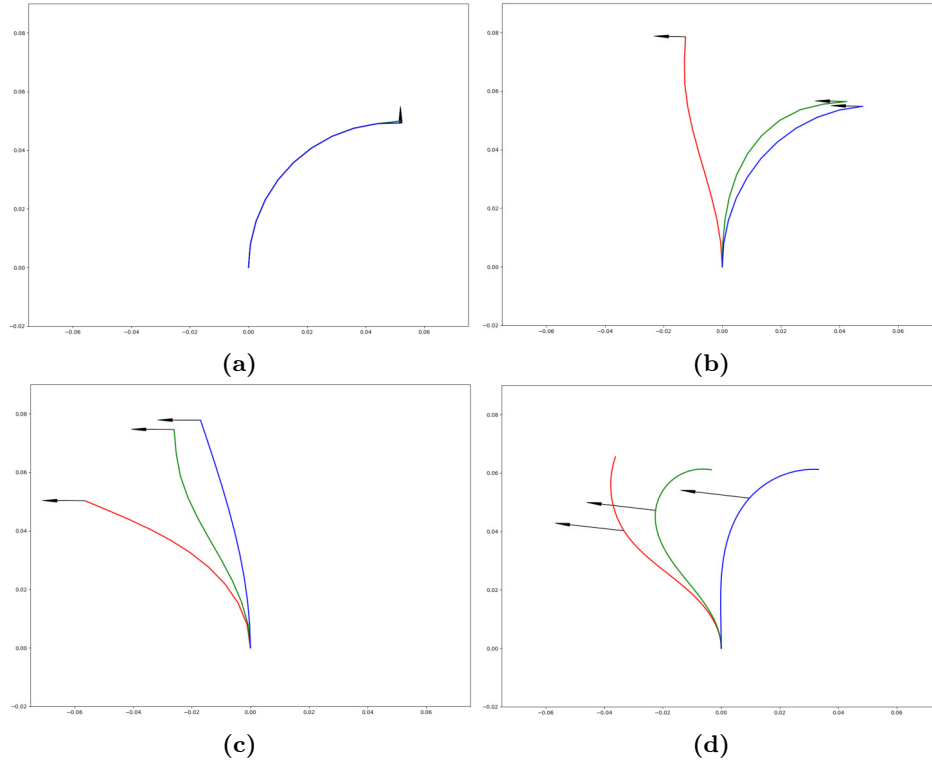
Figure 4.10: Simulation results for (a) only pressure, no force, (b) internal pressure and external force acting at the tip of the actuator, (c) no pressure, a force acting on the tip of the actuator, (d) internal pressure and the external force acting in the body of the actuator. The black arrow represents the external force acting on the actuator. Red colour: actuator with a single chamber and fixed pressure. Green colour: actuator with a single chamber and fixed mass. Blue colour: actuator with the split chamber and fixed mass in each section independently.

4.3 Design

The ideal implementation of the presented idea would be a material composed of microscopic cells, with each cell capable of stopping the outflow of the actuation medium so that it can freely enter but exit only on demand. To the best of the authors' knowledge, no such engineering material exists. Therefore we propose a simplified model at the macroscopic level that simulates the desired behaviour.

The proof-of-concept design features a few common elements to many of the devices already produced; the main part of the actuator is a cylindrical pneumatic chamber with fibres embedded into its wall, arranged in such a way as to enable elongation but limit radial expansion [61]. As the cross-section of the chamber is circular, and its perimeter has a constant length regardless of the pressure, its geometry remains circular during the pressurisation process [113].

The core part of the design, and indeed the main difference with respect to previous
designs, are the dividers. The dividers split the overall volume of the chamber into smaller
individual actuation chambers. Each division features a check valve that allows the pressurised
medium to flow in one direction only. The top compartment is supplied with the actuation
pressure, while the bottom one can be opened or closed to vent the device or to keep it
pressurised, see Fig. 4.11.

(a)   (b)
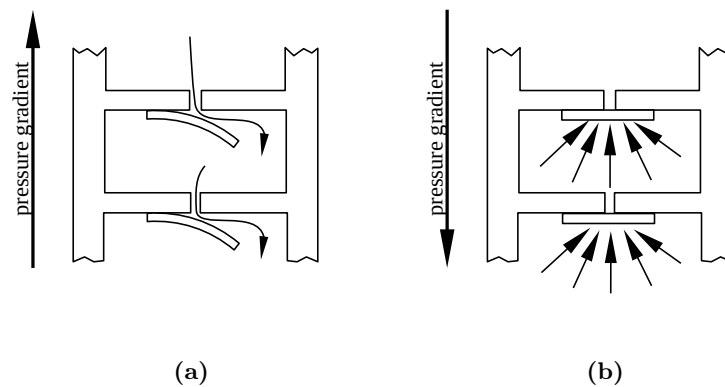
Figure 4.11: Compartments of the actuation chamber connected via check valves. (a) The check-
valves enable the flow from top to bottom, (b) but restrict it in the opposite direction.

This system is not without its drawbacks. Any check-valve requires some pressure
gradient to open (cracking pressure). While this may not be an issue towards the top of the
actuator, under low actuation pressures, the threshold may not be reached between the lower
compartments.

The built-up pressure difference between the top and bottom compartment was large
enough to cause a visible difference in the first prototypes, and for that reason, the design
has been adjusted. Additional check-valves connecting each of the compartments with the
pressure supply were added so that each compartment could be provided with the same
input pressure. At the same time, the fluid flow remains possible in one direction only, from
the pressure supply towards the chamber and then from the upper compartments to lower
compartments, see Fig. 4.12. Given that each compartment is pressurised equally, the real
actuation pressure differs only marginally from the supplied pressure.

Pressurisation and venting cycles, as well as the valves' working principle, are demonstrated
in Fig. 4.13. The valves are created by overlaying a small hole with a thin silicone membrane.
Since the silicone membrane tends to adhere to the material surrounding the hole, it creates
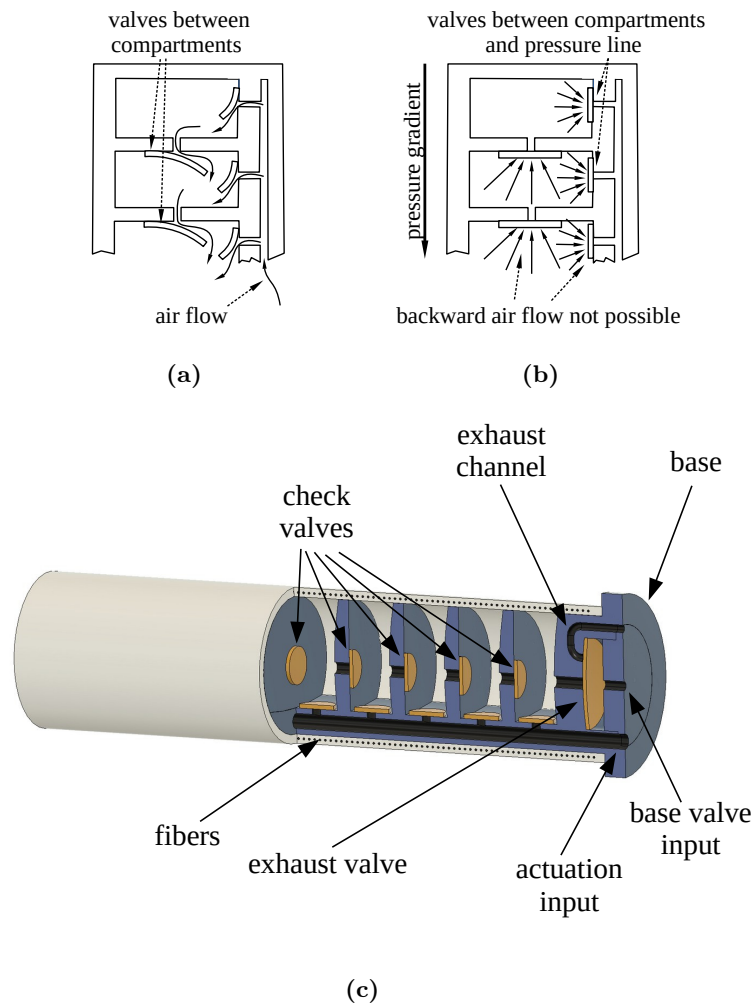
Figure 4.12: Additional valves between each compartment and the supply pressure channel helps
to distribute the actuation pressure uniformly. (a) the check-valves enable the flow from the supply
channel and from the top to bottom, (b) but restrict it in the opposite direction, (c) cad model of
the design.

a seal when there is pressure from outside. However, when there is pressure from within,
acting on the membrane through the hole, the slight adhesion is overcome, and the membrane
deflects, opening up the channel. Once the flow stops, the membrane re-seals the hole.

4.4 Fabrication

The proof-of-concept prototype was designed by casting silicone in 3D-printed moulds. The
fabrication process consists of the following steps - creation of the external sleeve containing
the reinforcing fibres, moulding of the internal structure, arrangement of the membranes
constituting the internal valves, and eventually assembly of all the parts.

The external sleeve is made in three steps. Initially, the thread is wrapped around a
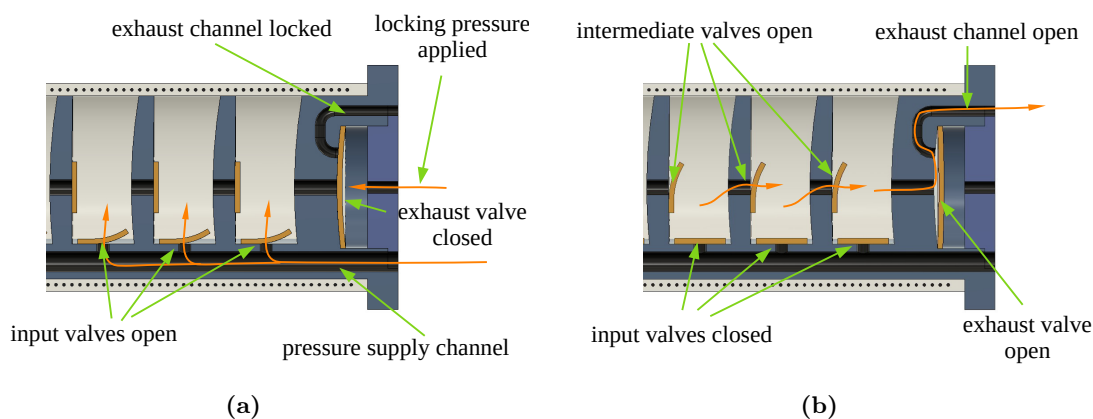
Figure 4.13: Actuation cycle: (b) pressurization, (c) venting.

cylinder, then placed into a mould and covered with a layer of silicone. Once the silicone
has cured, the cylinder is replaced with another cylinder of smaller diameter and an internal
layer of silicone is created. When the internal silicone is cured, the resulting structure is cut
along a straight line and peeled off the cylinder. For the external sleeve, SmoothOn Ecoflex
0030 silicone was used. The sleeve is cut because it needs to be sealed against the internal
structure in the subsequent steps. If it were not cut, applying glue between the sleeve and
compartments would not be possible. Since the sleeve is cut, it is feasible to apply glue on
the compartment edges and then wrap the internal structure with the sleeve.

The internal structure is moulded in a multi-part mould, see Fig. 4.14 using relatively stiff
silicone SmoothOn Smooth Sill 950. Once out of the mould, uncured silicone is dispensed
with a brush onto the surface areas surrounding the holes in order to create a smooth surface
- a necessary step to ensure valves are airtight once fitted. Once surfaces have been prepared,
small pieces of soft silicone sheeting made of Ecoflex 0050 are placed on top of each of the
holes to create the actual valves; the internal structure of a physical prototype is shown in
Fig. 4.15.
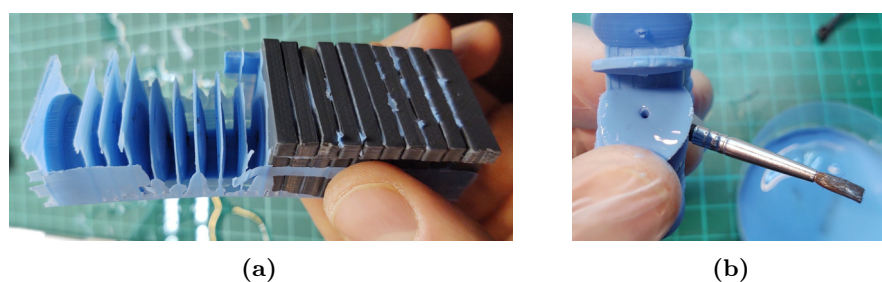
Figure 4.14: (a) demoulding of the internal structure, (b) smoothing surfaces to create valves.
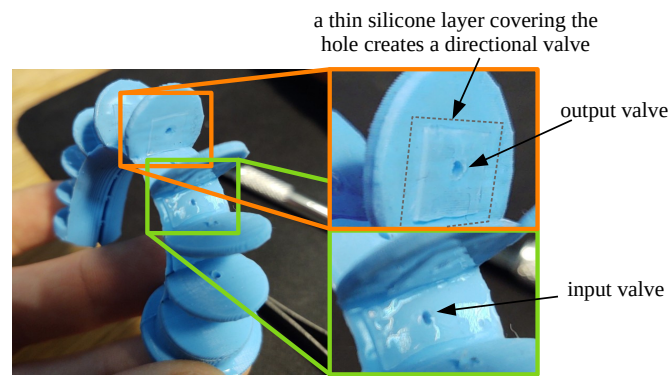
(a)

Figure 4.15: Implementation of the valves. Input and output valves exposed

The final step is to apply the prepared external layer. For that process, Smooth-On
Sil-Poxy adhesive is applied to the edge of all the dividers to ensure each compartment is
appropriately sealed, and that the medium can only flow in the desired direction through the
one-way-valves, see Fig. 4.16.

(a)
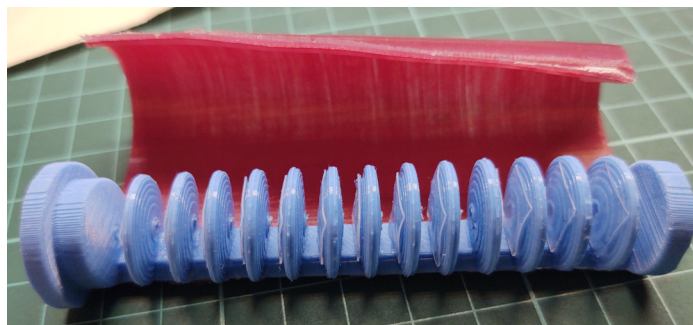
Figure 4.16: Application of the external layer.

The finished actuator is shown in Fig. 4.17.
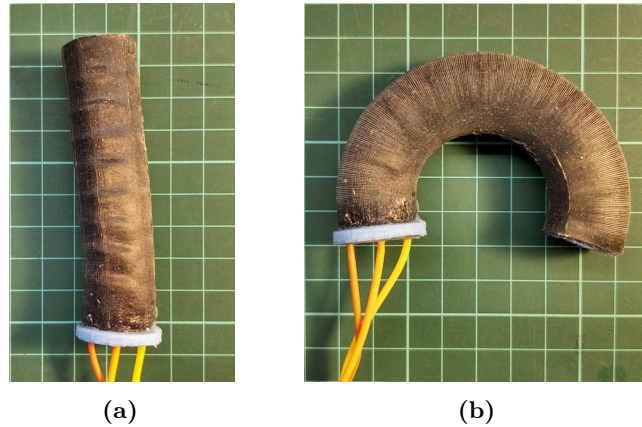
Figure 4.17: Finished actuator, (a) passive state, (b) actuated.

4.5 Results

In order to validate the simulated results, experimental data was collected.

4.5.1 Force response

The test setup consisted of two pressure regulators controlling the pressure inside the actuation
chamber and the outlet valve, a Cartesian positioning system with a force sensor attached
that is used to create the deflection and measure the reaction forces, and all the electronics
required to actuate and record the data including an Arduino and Raspberry Pi boards. As
a positioning system, an adapted Saintsmart CNC3018 machine was used. For experimental
reasons, the original spindle was replaced with a Robotous RFT40-SA01 6 axis force/torque
sensor to collect the force data, see Fig. 4.18.

The test procedure involved actuation up to the requisite pressure value, closing the main
venting valve so that the pressurised medium could not escape, moving the force sensor along
the predefined trajectory and recording the reaction forces of the actuator with respect to
the position of the force sensor. This procedure was repeated in several trials to cover the
complete sampling area.

(a)　　　　　　　　　　　　　　(b)
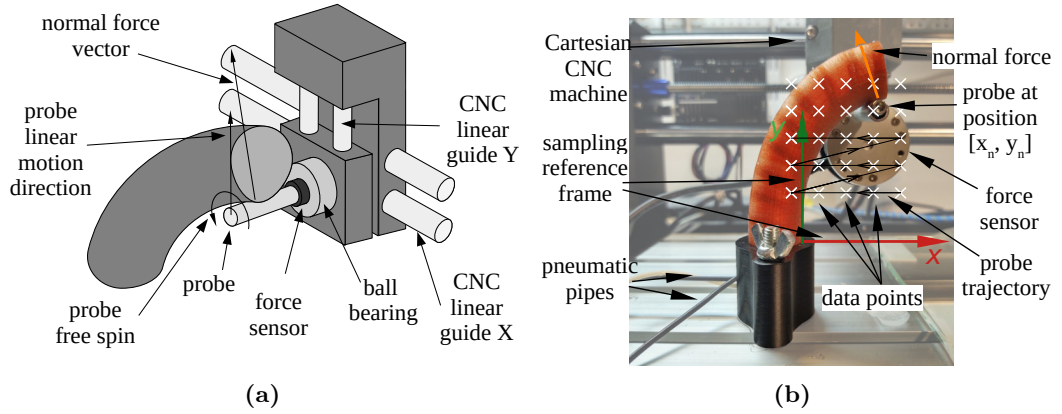
Figure 4.18: Test setup used for data collection. (a) Schematics showing the setup, (b) actual setup with data sampling points presented, along with the tool path used to collect the data. Please note that the reference frame is attached in the actuator base, while the samples are collected staring from $x = -10, y = 30$

The normal force value as a function of XY (position of the probe) with respect to the base of the actuator is presented in Fig. 4.19

(a)　　　　　　　　　　　　　　(b)
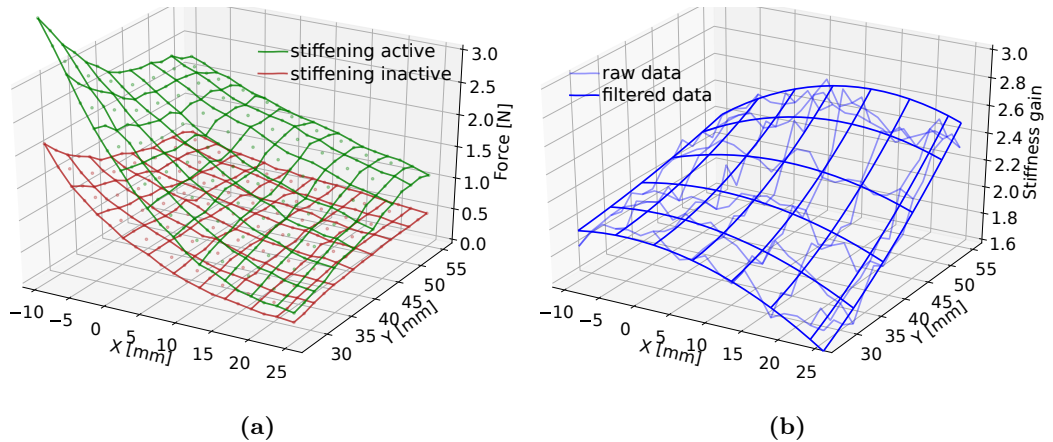
Figure 4.19: Normal force value with respect to the probe position for a fully actuated finger. (a) The samples have been collected for the stiffening mechanism engaged (green) and disengaged (red). (b) Stiffness relative increase (dimensionless value). Note the vertical axis ranges from 1.6 to 3.0.

4.5.2 Grasping force

The force response presented in the previous section accounts for the force applied in the normal direction with respect to the deformed finger axis. In a real-world scenario, more than one finger would be acting in opposition, as seen in Fig. 4.20. In such cases, the friction effect comes into play, causing the tangential resistive force at the contact point F_f. This force is proportional to the normal force, $F_f = \mu F_n$, where μ represents the friction coefficient.

By summing up the reaction force vectors F_f and F_n, we obtain the force vector F, which

can be represented by components parallel and perpendicular to the motion direction, F_y and F_x. Note that the second contact point creates similar vectors F_y' and F_x', where $F_x' = -F_x$. The opposing vector components F_x and F_x' cancel out, while the F_y and F_y' components add up.

In my test, the probe was attached via ball bearings. As a result, the friction effect was reduced when moving on the actuator surface, since the probe rolled rather than slid on it, and only the normal reaction force was captured. However, if we assume a sliding motion, the friction coefficient would become significant, and the actual force required to pull an object from a gripper composed of such fingers can be calculated using eq. (4.15). The resultant forces for various μ values are presented in Fig. 4.21. Note that the calculated force value is 'per finger'.

$$F_y = sin(\varphi)F_n + cos(\varphi)\mu F_n \tag{4.15}$$
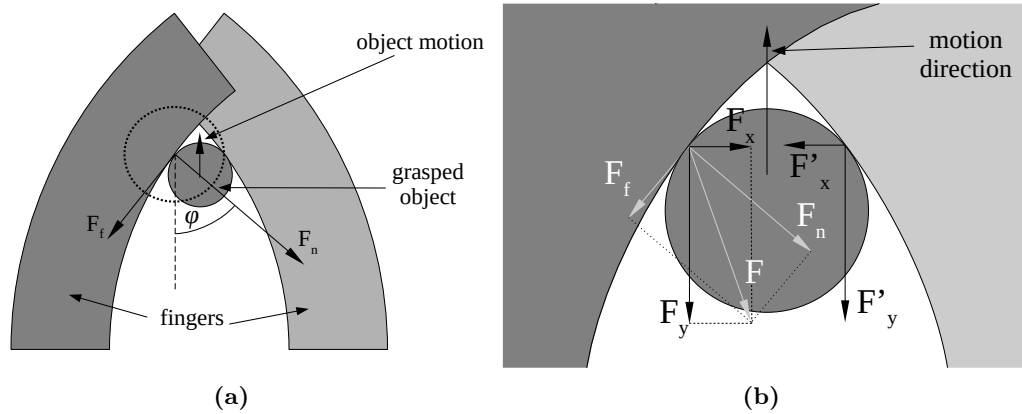
Figure 4.20: Grasping with stiffening actuators. The grasping force F_y results not only from the normal forces F_n, but also from the friction F_f.
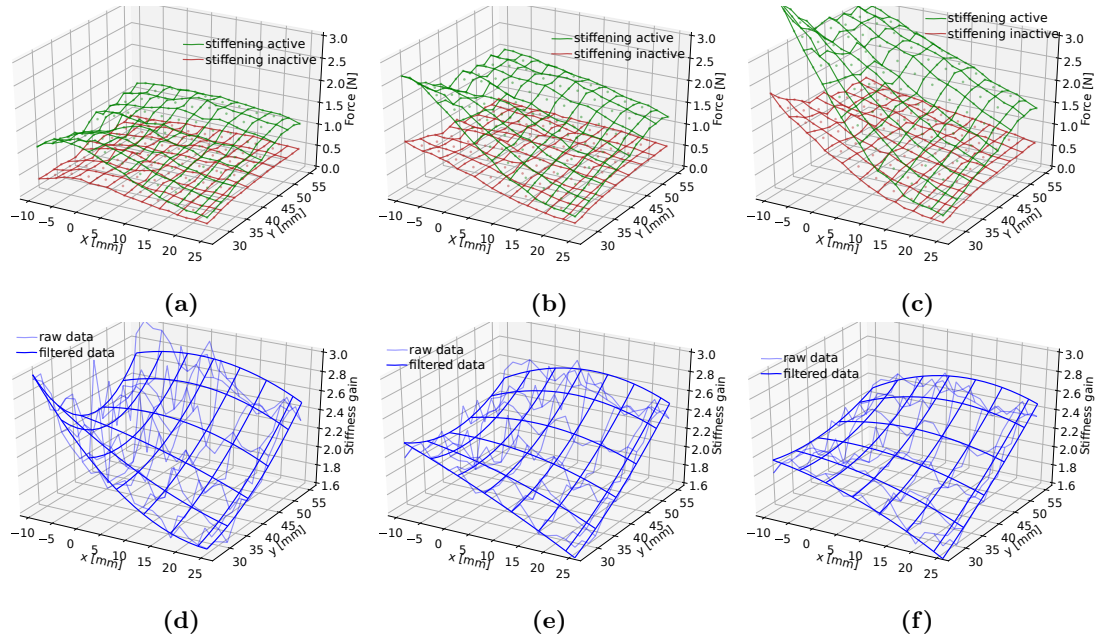
Figure 4.21: Force required to displace an object out of the gripper as a function of the location of the object with respect to the finger. (a), (b) & (c) the calculated forces, (green with stiffening system engaged and red - disengaged), (d), (e) & (f) stiffness gain. The data was plotted for three assumed friction coefficients : $\mu = 0.1$, $\mu = 0.5$ and $\mu = 1.0$ for (a), (b) & (c) respectively.

4.6 Single stiffening cell as a logic element

A check valve, by design, transfers fluid in one direction. If pressure is applied in the opposite direction, it simply remains closed and no flow is possible. This behavior corresponds to the behavior of a diode in electric circuits. Single cell of the proposed structure could be considered as a capacitive element connected via diodes and resistors, as shown in Fig. 4.22. Diodes represent the check valves, while resistors represent the resistance of the pneumatic channels and finite valve dimensions.

(a)

(b)
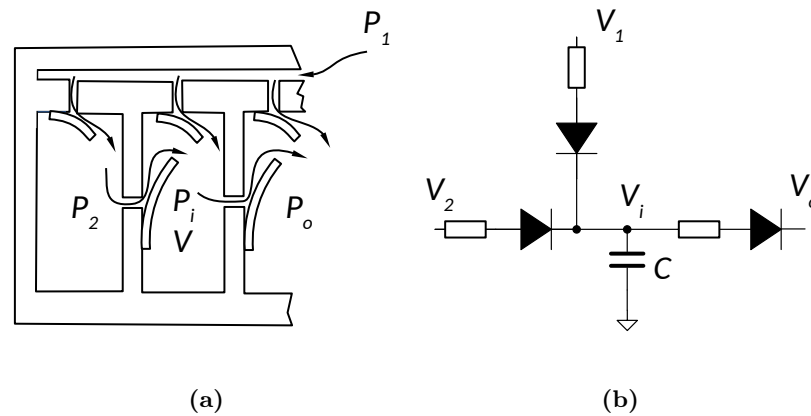
Figure 4.22

In such a circuit, the internal pressure of the given cell would be expressed as V_i, while the internal cell volume V corresponds to the capacitance of the capacitor C. Any external disturbance compressing the cell volume causes the capacitance to decrease, which, given a constant electric charge, causes the voltage V_i to increase accordingly. If the voltages V_1 or V_2 are greater than the internal voltage V_i, then the current would flow and the capacitor charge would increase. If, in turn, the output voltage V_o is lower than the internal voltage V_i, the capacitor would discharge proportionally to the voltage difference. Each diode requires some voltage V_f to start conducting any current (Forward voltage), which corresponds to the check valve cracking pressure.

The last compartment of the actuator is connected to the atmosphere via a channel that can be closed with pressure applied to a dedicated chamber in the actuator base. This element could be expressed as an NMOS transistor (n-type MOSFET) that opens when no voltage is applied to the gate terminal and closes otherwise. The overall actuator equivalent circuit can be expressed as Fig. 4.23.
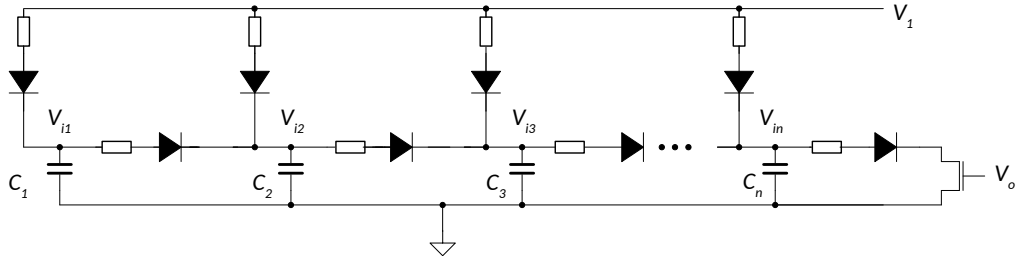
Figure 4.23: An electronic circuit that is equivalent to the beiding actuator's internal structure

Electric diodes can be used to implement simple *diode logic* [140]. Since diode logic allows for creating AND and OR gates, and capacitors could be considered as memory elements, the proposed structure could potentially be used to create simple logic functions implemented directly into the devices physical structure.

4.7 Discussion

In this chapter, I have proposed a novel smart structure capable of soft actuation and stiff responses despite low actuation pressure. The idea is inspired by mammalian erectile

tissue that is capable of trapping blood, which drastically increases the stiffness of the penis structure despite relatively low actuation pressure.

While the idea was incorporated into a bending actuator to prove the concept, it could be abstracted to a more general mechanism. Currently, the structure is composed of macroscopic cells that can lock the actuation medium under certain conditions and release it when conditions change. Ideally, the structure would be miniaturized to create a smart material composed of microscopic cells. This material would offer varying mechanical properties in response to external disturbances along different axes, which could be controlled by an external input signal. As a result, the material could be used to enhance local interaction forces without locking its shape.

The proposed structure has the potential to be used in various scenarios in soft robotics, including improving existing soft actuators and devices as shown in this chapter. Additionally, it could be utilized in the creation of novel actuation modes and devices, offering new possibilities for soft robotic applications.

A single cell of the proposed structure could be considered as a logic element that executes a specific function: when the condition of the pressure gradient is met, it fills up with fluid, and when the pressure gradient reverses, it locks and remains pressurized until another pressure-releasing condition is met. The check valves themselves can be considered fluidic diodes, passing signals in one direction and stopping them in the reverse direction. Diode logic could be implemented using these elements, leading to some level of intelligence embodied within the structures of soft robots.

To prove the concept as a stiffening mechanism, I have implemented fluidic soft actuators that can significantly improve their apparent stiffness while maintaining their actual stiffness and actuation pressure range at a low level.

The experiments conducted gave results similar to what was expected based on calculations, showing a significant improvement in force response when the stiffening mechanism was engaged.

The proposed actuator can be utilised in several designs but is especially suitable for soft gripper fingers.

The main difference in comparison with other stiffening principles proposed in soft robotics is that actuation and stiffening work in a complementary way, without influencing each other.

This means that even if stiffening is engaged, actuation can still proceed, as more actuation fluid is freely transferred into the actuation chamber. In other designs stiffening inhibits actuation.

The proposed actuator has several limitations. Firstly, the stiffness increase is dependent on the actuation pressure range and is more pronounced at lower pressures. That said, in case of applications requiring high actuation pressures, the stiffening effect for bending actuators is expected to be small (according to eq. (4.14), it converges to around 117% of the original stiffness at high actuation pressures for the tested bending actuator geometry). In theory, this issue could be addressed by using a non-compressible actuation fluid, such as hydraulic actuation.

The manufacturing process of the actuator is labor-intensive and prone to manufacturing errors. There is no efficient way to test the subsequent manufacturing steps, and the device can be tested only when completed. Consequently, if there is any leakage between compartments, this will be detected only at the very end of the process and cannot be easily fixed. The manufacturing failure rate in my case was approximately 50%.

The lifetime in terms of the number of cycles has not been tested; however, during my tests, I observed that internal compartments lose their air-tightness over time. This could be explained by post-curing shrinkage of the used materials. Smooth Sil rubber experiences significantly larger shrinkage than EcoFlex material, resulting in a significant shrinkage ratio difference between the compartment wall and the silicone sheet that creates the check valve - causing leakages. Consequently, the lifetime of prototypes was limited to several days or a few weeks. If these actuators are to be used in actual devices, this problem would need to be addressed.

Additionally, the proposed actuator inherits standard limitations of soft actuators: at certain pressures, it buckles and twists instead of applying more force on the external object.

This chapter concludes my research on soft actuation, and the forthcoming chapters will showcase a series of demonstrators and devices that are built using the soft actuators I have developed. Although some aspects, such as stiffening, were not incorporated into these demonstrators due to the chronological order of my research, it is important to note that the stiffening actuator detailed in this chapter is the culmination of my PhD work. Unfortunately, due to temporal limitations, I was unable to incorporate the stiffening actuator into any

functioning device.

Soft Robotic Systems

Whilst earlier sections concentrated on soft actuators and their specific characteristics, this chapter delves into various robotic systems that implement the actuation principles discussed. The majority of devices examined in the subsequent sections serve as demonstrators; however, in Section 5.4, a practical upper-limb assistive device is introduced.

The demonstrators primarily explore soft grasping and underwater locomotion. The research presented in this chapter has been disseminated through numerous publications: [141, 142, 143].

5.1 Prosthetic hands

One possible application of fibre-reinforced actuators lies in the realm of grasping devices. In this section, I introduce a soft hand designed with a potential application as a prosthetic hand, created to showcase the capabilities of fibre-reinforced actuators. The hand was fabricated using the techniques outlined in preceding sections.

5.1.1 Motivation

Grasping devices are not only used in robotic applications, but also in applications such as wearable prosthetic devices that help amputees compensate for missing limbs.

Traditional rigid robotic prosthetic devices can be expensive due to their complex and sophisticated mechanisms. They contain a wide range of precise mechanical and electrical elements and require complex control techniques to enable even simple manipulation tasks. They are made of rigid and heavy materials and actuated by the power of electric motors. Due to their lack of mechanical compliance, any flexibility in such devices requires the addition of compliant features (such as springs) or for complex sensing to be embedded into their construction (to achieve software-controlled compliance).

In recent years some new prosthetic hands based on 3D printing technology have been proposed. Those projects aim to make prostheses simpler to fabricate, more affordable and ultimately more accessible [144, 145]. Nonetheless, they are still rigid in nature.

Over the last years, some examples of hands made of soft and compliant materials have also been presented. The Pisa/IIT Soft Hand [146] uses elastic tendons to operate its rigid-component fingers. By exploiting grasp synergies and flexible tendons, a single motor is sufficient to actuate all the fingers and to achieve a variety of grasps that adapt to the environment. Another compliant hand driven by shape memory alloy is presented in [147]. It can also passively adapt to the environment while offering sensing capabilities, without the need for any sophisticated control mechanisms.

A pneumatic soft hand composed of PneuFlex actuators is proposed in [35, 42]. It contains one actuator per finger, each individually controlled, one for the thumb and two for the palm. Another hand with a similar working principle is presented in [148]. It incorporates sensing capabilities using light-based sensors integrated into its fingers. Even though several devices
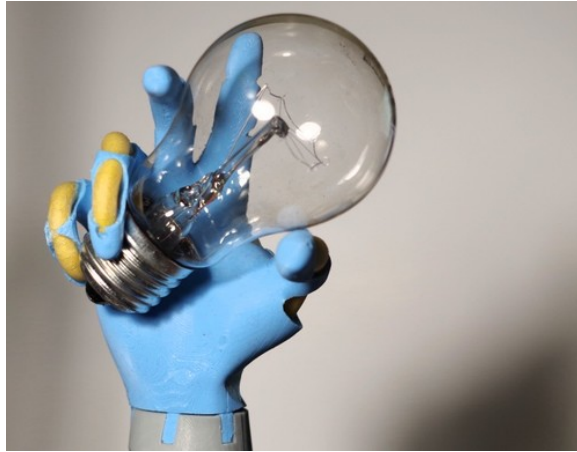
Figure 5.1: Soft pneumatic hand. From [142].

with human hand morphology have been proposed [149, 150], very few of them offer a real human-like shape and appearance [15], which is deemed a significant issue when the device is to be used as a prosthetic system [151].

In this section, I present a prosthetic device designed to closely resemble the human hand in shape and replicate some of the mechanisms inherent in a natural hand, Fig. 5.1. It offers six degrees of actuation that can be operated in groups for simplicity or controlled separately for enhanced manipulation precision. Each finger has one actuator to achieve bending, while the thumb is equipped with two actuators to make it capable of apposition and opposition modes. Since all the fingers can operate within the same actuation group, the costs of the final system can be further reduced.

The prosthetic hand described here is based on a 3D scan of a real human hand, ensuring that the design's proportions and shape are anatomically accurate. The shape, configuration and size of the hand can be easily modified to meet the needs of each patient. Low fabrication costs make it affordable and especially suitable for child amputees who require frequent device changes due to their body growth. It is worth noting that because it is made of soft materials, it is also considered safer than traditional prostheses.

Grasping capability is evidently the most crucial requirement; however, other primary objectives of the work outlined in this thesis were to emulate the appearance and behaviour of the human hand. This is predicated on the assumption that similar behaviour (finger synergy) and morphology (closely matched geometry) would facilitate the transfer of human hand strategies to the robotic system. Furthermore, a more human-like geometry and appearance

could potentially enhance the experience of future amputees when compared to prostheses with a more machine-like appearance [151]. Safety and affordability were also important factors considered during the development process.

Subsequent to the publication of the work described herein, several soft-material-based hands have been proposed, which reasonably resemble the human hand in shape [14, 13]. To the best of my knowledge, the design proposed in this thesis offered the most human-like appearance at the time of publication. For a more detailed comparison of other devices, refer to table 5.1 in Section 5.1.8.

The work described in this section has previously been published in [142] and [141].

5.1.2 Mechanical structure

The hand contains six independent pressure-driven soft, flexible actuators. Each finger uses one actuator and thus can be controlled independently from the other fingers. In addition, the thumb is equipped with two actuators allowing it to bend and change its pose between opposition and apposition. The overall structure of the hand is presented in Fig. 5.2.
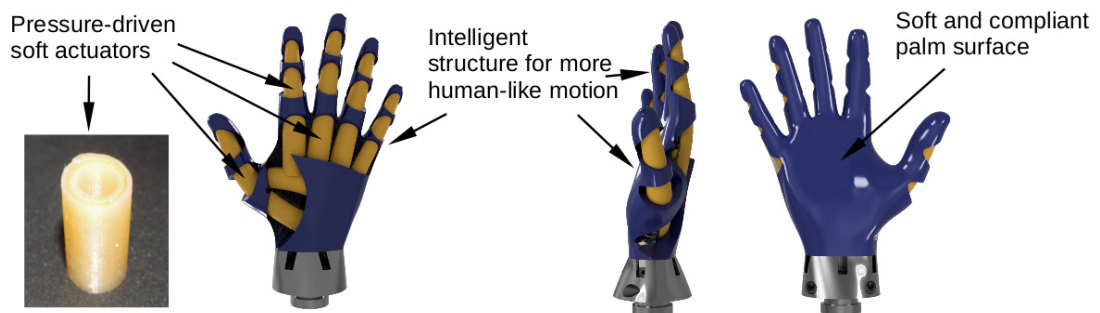
Figure 5.2: The mechanical structure of the hand. From [142].

The hand is designed to be easily manufactured without need of any expensive equipment. It is made of two kinds of two-component silicone reinforced with polyester thread. The main part of the device, a rubber exoskeleton, is made of relatively stiff silicone SmootOn SmoothSill 940 (Shore A40), while the actuators are fabricated from the far softer SmoothOn EcoFlex 0050 (Shore 50 scale 00). This combination of materials allows us to 'pre-program' the fingers' mechanical properties into the hand structure and transform the linear deformation of the actuators into the required curling motion of the fingers.

In this section, I present a prototype that is 100 mm in length, measured from the wrist to the ring finger's tip - a size that corresponds to the hand of a 2 to 3 year old child.

Actuator Design

The actuator is a pneumatic, fibre-reinforced conical tube, as discussed in Section 3.2. The linear expansion of the actuator is converted into a bending motion using the exoskeleton finger structure with its appropriately designed stiffness distribution, i.e., one side of the finger is made of a stiffer material than the other.
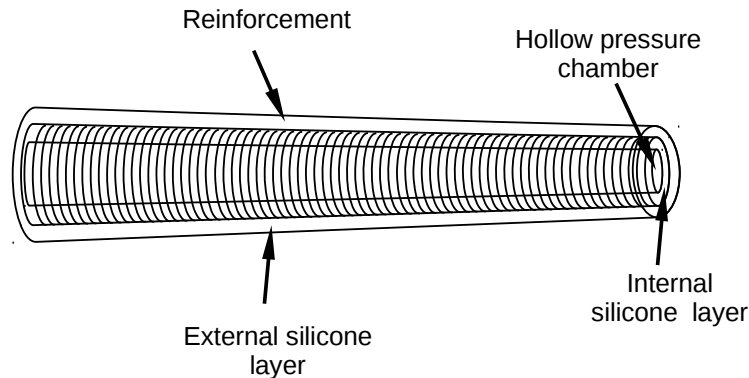
Figure 5.3: Structure of the actuator. From [142].

The structure of the actuator is presented in Fig. 5.3. The slight pitch of the reinforcing helix ($\alpha \approx 0.6^o$) guarantees that its impact on the elongation capabilities is minimised. The internal layer creates an airtight membrane that transfers the pressure onto the reinforcement, and the external one prevents the reinforcement from detaching from the actuator and keeps it in the desired shape. The bottom and the tip of the actuators are sealed using stiff silicone SmootSill 940. A 1.2mm-diameter channel is integrated into the actuator base, as a pressure inlet.

Overall design

The hand structure is essentially defined by an exoskeleton structure made of stiff silicone - see Fig. 5.4. The exoskeleton constrains all the actuators and creates the palm and fingers' surface. The exoskeleton is based on a 3D scan of a human hand to be as bio-realistic as possible. The finger lengths and location of joints are therefore anatomically accurate. The exoskeleton is designed to constrain the deformation of the actuators in areas that correspond to bones and to transfer longitudinal motion into bending motions in the regions corresponding to the finger joints. This behaviour is achieved by making the exoskeleton out of a material with a significantly higher stiffness than that of the actuators. The actuators,

made of soft material, elongate when pressurised. They are, however, attached on one side to the exoskeleton which is far less stretchable or extendable. As a result, the side attached to the exoskeleton expands less than the free side, and consequently, the finger bends. As the hand is made without any rigid components, bending is not limited to discrete joints but distributed along the whole finger.

The soft rotational joint described in Section 3.3 was also considered as an actuator for the design presented here as finite joints lead to more human-like hand motions. However, this would have required a separate actuator for each joint, making the overall design and fabrication process significantly more complex. I therefore discounted its use for the prosthetic hand.

As mentioned, each finger can be controlled independently, but can also operate in groups efficiently and synergistically as they are flexible and compliant. The control complexity of dexterous manipulation is therefore reduced as the hand structure and its compliance simplifies interaction with objects.
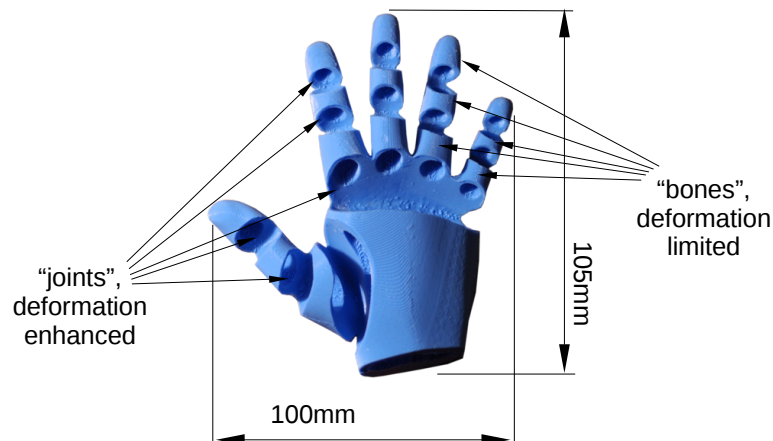
Figure 5.4: Exoskeleton. Defines the hands' shape and generates bending motion. From [142].

The exoskeleton fuses the fingers so that they affect each other - much like the fingers of a human hand do. For example, the actuation of the index finger causes the middle finger to move slightly, the actuation of the middle finger makes the index and the ring finger move too, and so on, see Fig. 5.10. For that reason, the synchronous actuation of all the fingers results in more bending and higher grasping forces than the actuation of separate fingers, again, just as in a human hand [152, 153]. An additional actuated joint is embedded into the

thumb's base to change the thumb operating mode between opposition and apposition.

5.1.3 Manufacturing

The manufacturing process used here follows the approach presented in Section 3.2. It consists of several moulding steps and involves a set of 3D printed moulds.

Actuators

It starts with the manufacture of the actuators. Reinforcement is wound around conical 3D printed cores which are then inserted into a dedicated mould. The mould is then filled with silicone creating a thin layer on the outer side of the reinforcing helix. When the silicone has cured, the cores are removed. The actuators are then filled with new silicone material, and another set of cores is inserted to create a thin layer of silicone inside the reinforcement - see Fig. 5.5.

The next manufacturing steps focus on sealing both ends of the actuator. The base of the actuator contains the pressure inlet, which is created by inserting a 1.2-mm diameter rod into the sealing mould. The pressure is provided to the actuator through 2-mm diameter tubes that combined with the 1.2-mm diameter hole in the actuator base, create a reliable and tight seal. Although this seal is secure, the tubes are nonetheless glued to prevent them from being pulled out - see Fig. 5.6. It is noted that similar designs ([35, 56]) use the manual reinforcement winding approach, which has certain drawbacks in comparison to the design presented here (refer Section 3.2). The enhancements represent a step toward industrial manufacturing as most of the processes can be easily automated.

The Hand

The prefabricated actuators are arranged inside the main mould that creates the exoskeleton. There are specially designed sockets that keep the actuators in position and ensure that stiff silicone does not cover the joint areas. This is a crucial aspect of the process, as in the areas covered with non-stretchable silicone, expansion is significantly limited. As a consequence, the shape and arrangement of sockets define the joints' positions and 'pre-program' the finger motion. The main mould is shown in Fig. 5.7.

Since some hand areas require enhanced flexibility (i.e. *metacarpophalangeal joint* - the
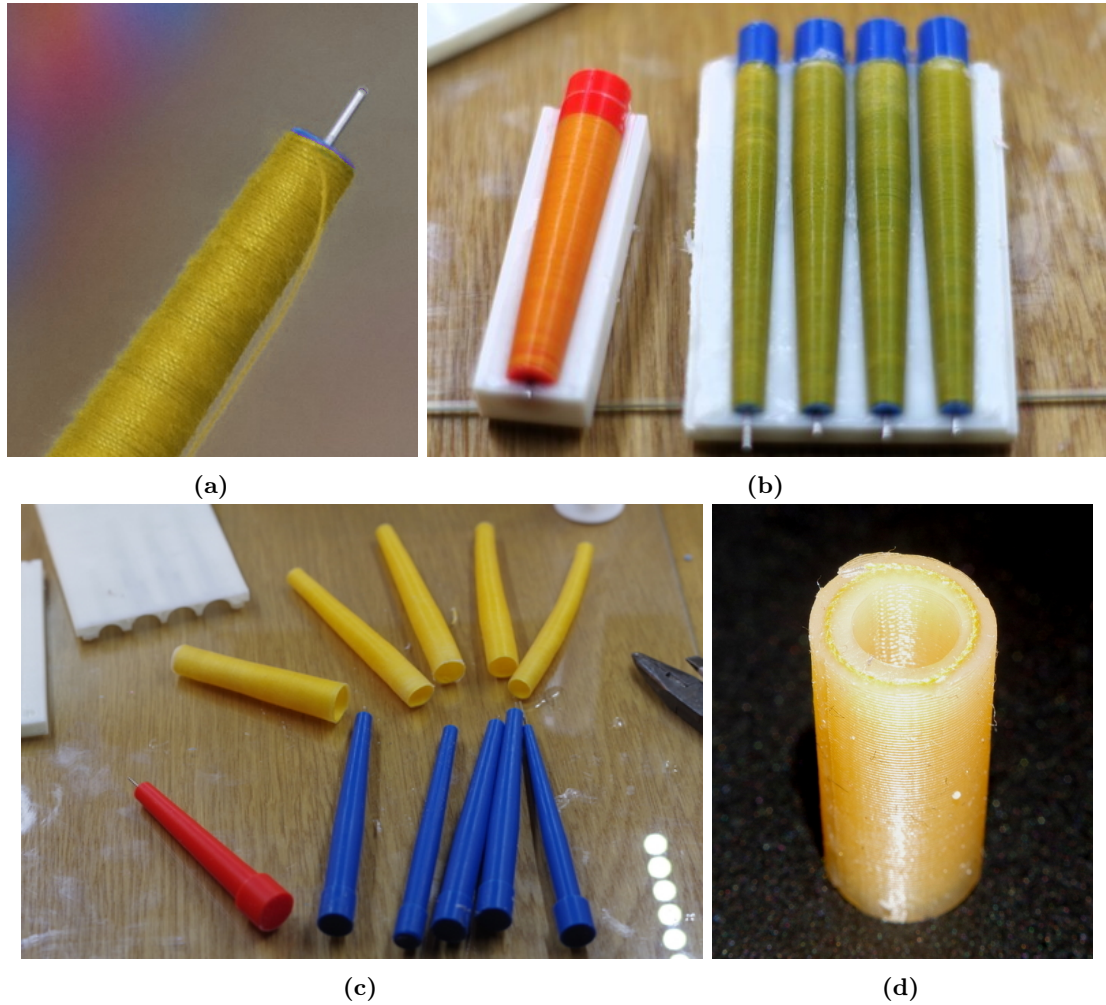
Figure 5.5: Actuator manufacturing. (a) thread winding for reinforcement, (b) actuators in mould, (c) external silicone layer cured - cores removed, (d) internal layer created - a cross-section of the actuator. From [142].

base joint of all the fingers and *carpometacarpal joint* - the base thumb joint), there are auxiliary structures made of soft silicone deployed into the main mould together with the actuators. Before filling the mould with the stiffer silicone, all parts are glued to the mould using softer silicone. This operation reduces the risk of stiff silicone penetrating undesired areas during the injection operation. The mould is then filled with stiff silicone (SmoothSill 940) by syringing the material through a small hole on the upper part of the mould. The filled mould and the hand formed from the mould are shown in Fig. 5.8.

5.1.4 Kinematics

The hand has six actuators, one per finger and two for the thumb - see Fig. 5.9. Each finger can be controlled separately, but as the whole hand structure is compliant and adapts to the
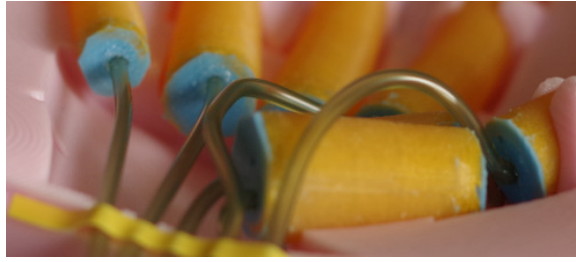
Figure 5.6: Fingers bases with pressure pipes connected. The actuator pressure inlets are 1.2mm in diameter, and the pipe diameters are 2mm. From [142].
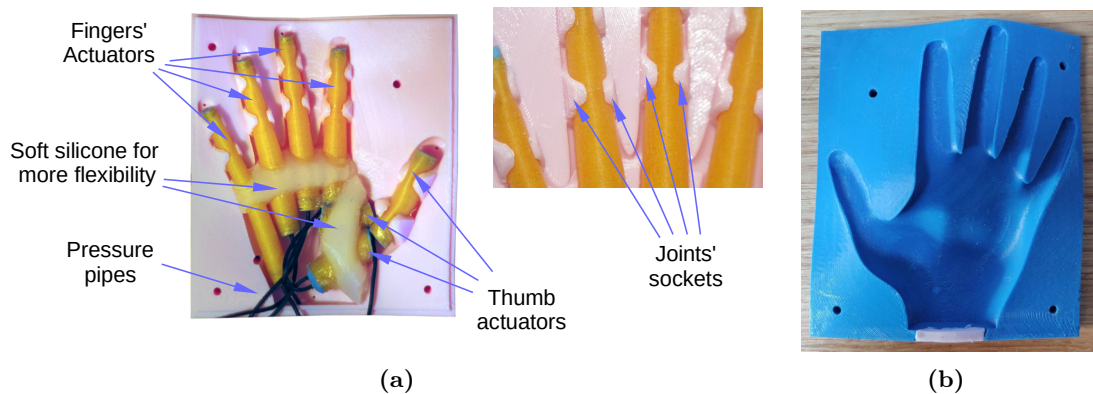
Figure 5.7: (a) Alignment of pneumatic actuators in the main mould, (b) other side of the mould. From [142].

object being handled, they can be actuated in groups, i.e., synergistically, reducing control requirements.

The hand is designed to mimic the human hand in terms of appearance and fingers actuation. The exoskeleton is designed to fuse the fingers at their bases, leading to interference between finger movements, as is the case for human hands. For example, in Fig. 5.10 only the middle finger is actuated in both the real and prosthetic hand, but movement of adjacent fingers can be observed in both cases.

To further increase the bio-mimetic aspect of the hand, a second actuator was added to the thumb allowing it to work in apposition or opposition modes as shown in Fig. 5.11.

5.1.5 Control

The hand is driven by pneumatic pressure. For the presented prototype a custom control unit has been developed - see Fig. 5.12c, and Section 5.5 for more information. Each pressure controller is controlled independently with PWM signals and provides pressures from 0 to 0.2 MPa. The controller can be commanded by a joystick or mimic the operator's hand
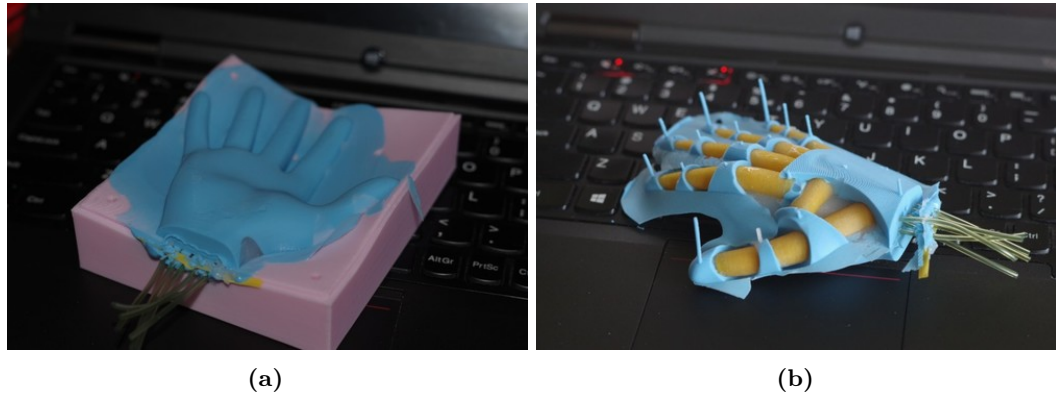
Figure 5.8: Main open (a) and demoulded hand with degassing channels visible (b). From [142].
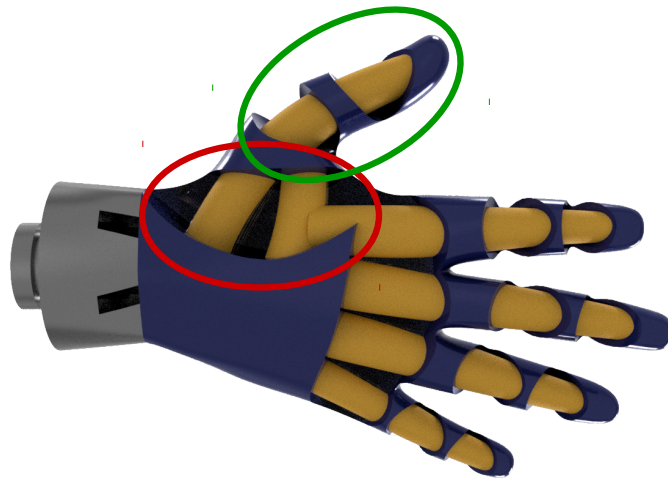
Figure 5.9: The degrees of actuation. One actuator per finger and two for the thumb: thumb actuation in green, thumb mode control (apposition/opposition) in red. From [142].

using a LeapMotion controller as in Fig. 5.12b. This type of interface allows for smooth and natural control that is very useful for development purposes but not very useful in the target system as it requires a healthy hand for command input. For the final application, an EMG interface or similar will need to be developed to control the hand directly from the activities of the remaining muscles of the amputee. The software developed for prototyping enables the creation of a sequence of different pressure values that can be applied in a specific order. Desired grasp motions can be saved and loaded from a file. The control methods are shown in Fig. 5.12.
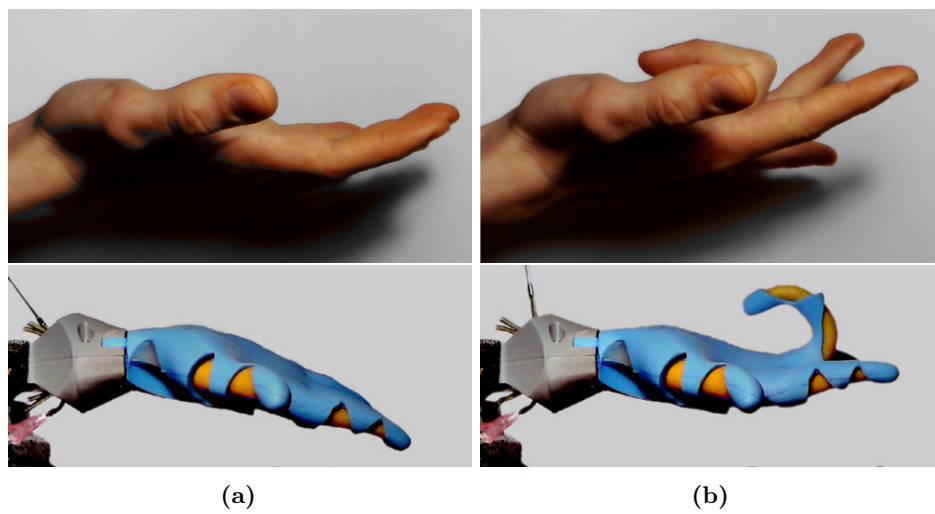
Figure 5.10: Influence of the middle finger actuation on other fingers. (a) hand passive, (b) only middle finger active but index and ring fingers affected. From [142].
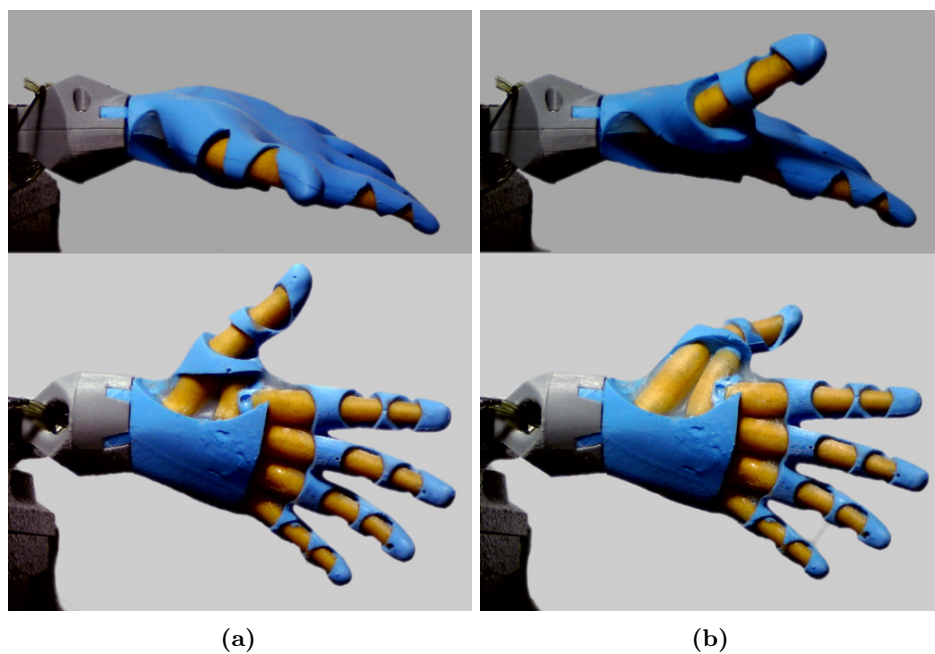
Figure 5.11: The thumb in different modes. (a) apposition and (b) opposition mode. From [142].
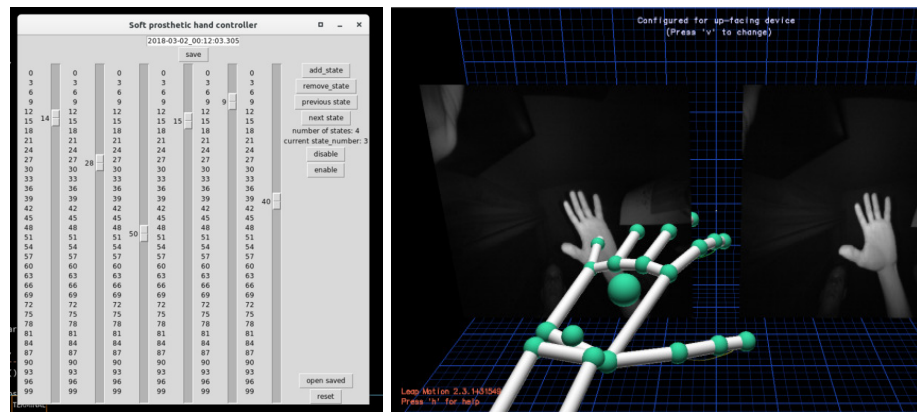
(a)

(b)

(c)

Figure 5.12: (a) Slider-based controller, (b) LeapMotion-based hand tracking (c) The control unit. From [142].

5.1.6 Experiments

Bending and force test

The hand has been tested in terms of forces and bending angles generated by the fingers as a function of pressure. During the tests, the hand was observed with a camera. For each finger, the hand's orientation was adjusted so that the bending plane of the examined finger was always parallel to the camera imaging plane. A colour marker attached to the fingertip was tracked using an image processing algorithm during the actuation process. The pressure was tracked with the same camera using the same techniques - see Fig. 5.13. The actuation process was repeated six times and recorded at 60 frames per second. Each frame of the recorded video was processed, and the value of the actuation pressure and the corresponding bending angle was determined. For bending and force evaluation, two scenarios were tested: individual actuation of each finger separately and simultaneous actuation of all the fingers.

The force assessment used the same experimental setup and a custom 3D-printed force sensor [122]. The generated forces were measured for each finger separately in each scenario. The results of all the performed tests are presented in Fig. 5.14, Fig. 5.15 and Fig. 5.16. Graphs indicate the average of all trials for each configuration.
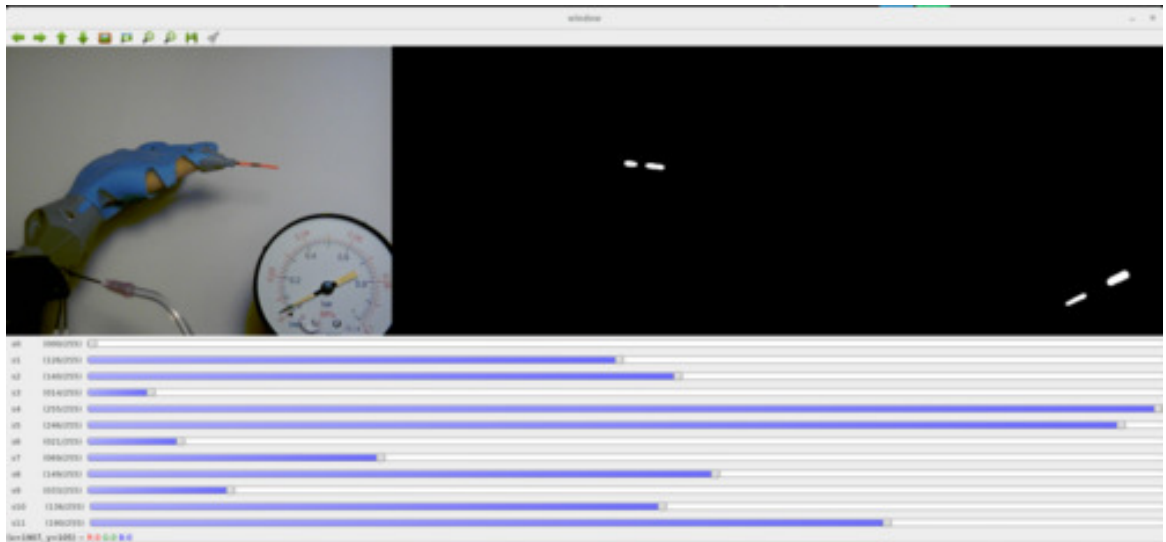
Figure 5.13: Finger bending tracking software. PS3-eye camera image at 60 frames per second is used to extract the bending angle and pressure value for each recorded frame. From [142].
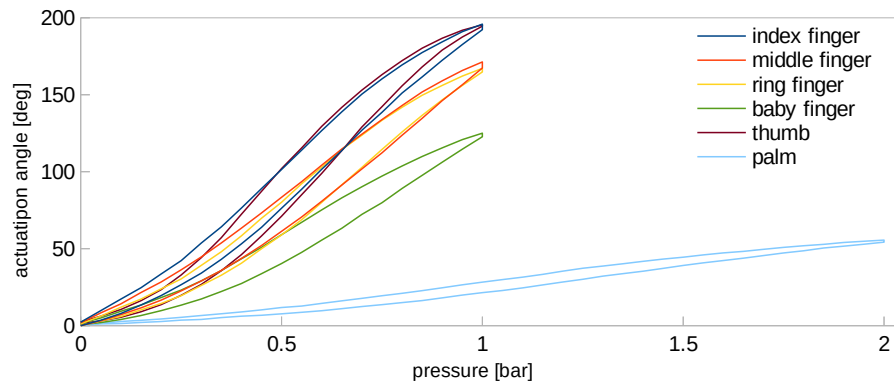
Figure 5.14: Actuation angle vs actuation pressure, whole actuation cycles. From [142].
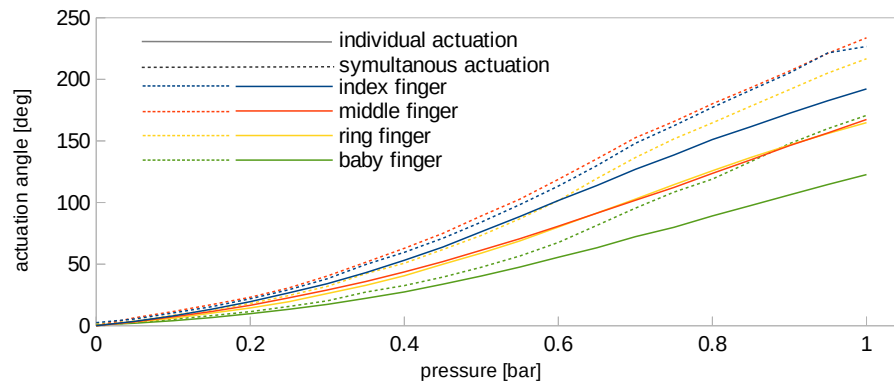
Figure 5.15: Actuation angle vs actuation pressure, single finger actuation compared to the simultaneous actuation (all the fingers together). Only pressurisation is shown. From [142].
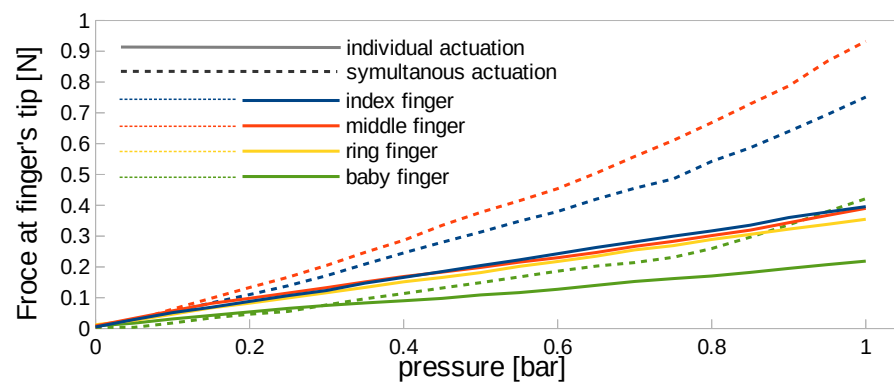
Figure 5.16: Experimental results. Force measured at the fingertip vs actuation pressure, comparing individual fingers and whole hand actuation. Note that during the simultaneous actuation the ring finger force sensor failed - no data was gathered. From [142].

Grasping tests

One of the tests conducted was the estimation of maximum payload. A cylinder was placed in the hand and pulled out multiple times while the pulling force was measured. The forces required to extract the object in the direction indicated in Fig. 5.17 ranged between 7 and 10 Newtons, with the lowest recorded value being 6N. Thus, the maximum payload can be estimated to be 500g assuming some safety margin.

(a)
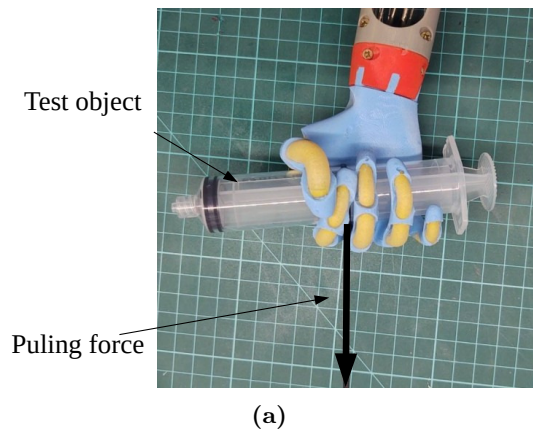
Figure 5.17: (a) Puling force test. A plastic cylinder is placed in the hand and pulled-out while the pulling force is recorded. The max value is considered as the required pulling force.

Preliminary grasping postures tests were performed. During these experiments, I was trying to demonstrate different kinds of grasps for different objects. The grasp postures have been chosen from the postures described in the literature and referenced as Kapandji score test [154, 35, 155, 156]. To investigate the hand's capabilities, I tried a number of those, the results of which are presented in Fig. 5.18.

Figure 5.18: Grasping tests, (a) various grasping postures picked from Kapandji score test [154], images from [142], (b) an exemplary load applied to the hand. Total mass of the object and syringe 550g. In both cases all the actuators are connected to the same pressure source.

One of the observed grasping issues is finger twisting. This is an inherent feature of soft bending actuators: beyond a certain actuation pressure, instead of providing additional bending force, they begin to twist to the side. This failure mode constitutes the actual pressure limiting factor, rather than the pressure value that would lead to a burst. The twisting process is presented in Fig. 5.19.
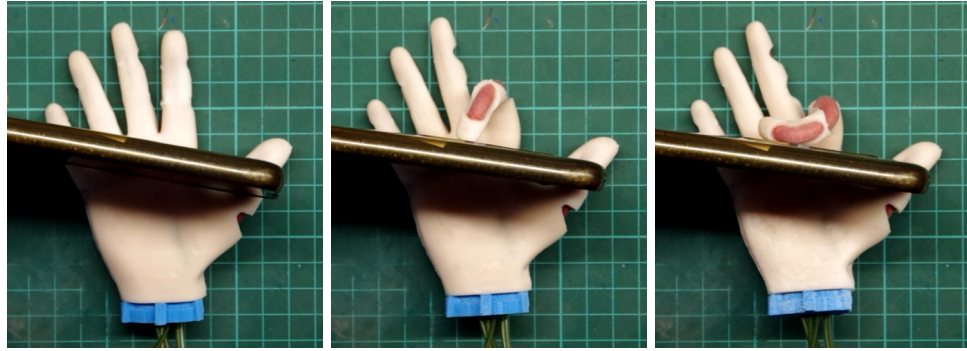
Figure 5.19: One of the failure modes: increasing pressure above a certain pressure leads not to higher forces, but to twisting of a finger.

5.1.7 Adult-size hand

After initial tests with the child-sized prototype, I spent a considerable amount of time designing and fabricating an adult-size version of the device. Due to the substantial increase in the volume, it became possible to embed more complex actuation mechanisms into the larger prototype, and so the adult-sized version comprised an additional actuator per finger making actuation of the metacarpophalangeal joint independent from the actuation of the rest, resulting in an 11 DOF system (similarly to double-compartment actuators described later in [13]) - see Fig. 5.20.
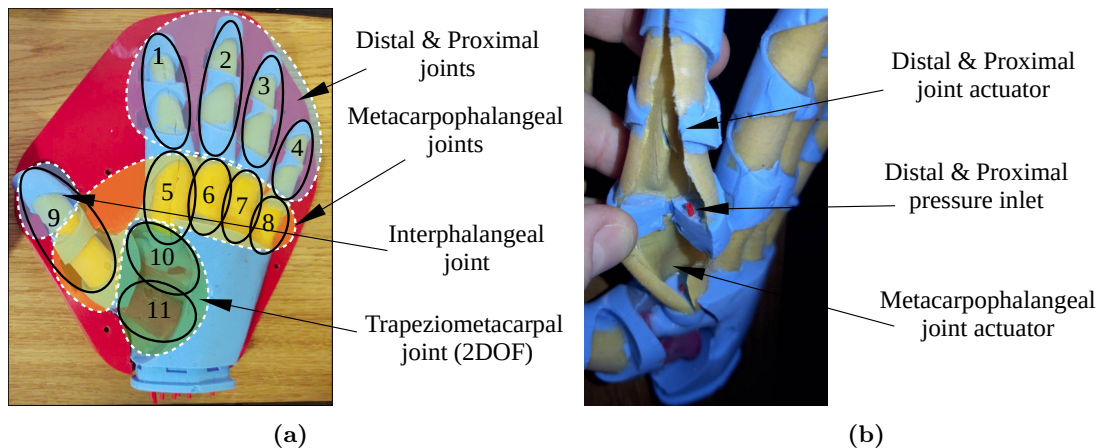
Figure 5.20: (a) Adult-size hand prototype degrees of freedom. Metacarpophalangeal joint and proximal & distal joints actuated separately, (b) index finger cut to show internal structure and individual actuators.

The hand was designed, along with all the required moulds and a single prototype was fabricated. However, the further development of the project was interrupted in early 2022 by the Covid 19 outbreak and has never been finalised. A photo of the full-size prototype is presented in Fig. 5.21.
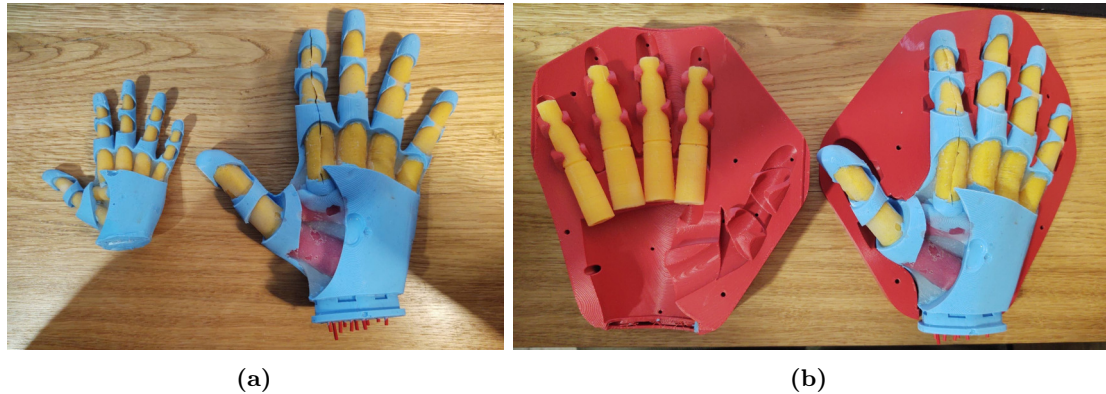
Figure 5.21: Adult-size hand prototype. (a) small hand and big hand prototypes comparison, (b) hand prototype and set of moulds. From [142].

5.1.8 Discussion

Test outcomes

The tests show that the hand is capable of a range of motions. The bending tests prove that individual fingers influence adjacent fingers when pressurised, eliciting natural finger motion. This is especially notable in the case of activation scenarios when not all the fingers are directly activated. Simultaneous actuation results in a significantly higher force exerted by each finger, which is helpful when trying to lift heavy objects. Some actuation hysteresis was observed.

Grasping tests show that the hand is capable of efficiently grasping various objects. A passive adaptation capability was observed during those tests. It is noted that the hand was able to hold the test objects despite its small size. It should be noted that the depicted items were not grasped but rather placed and then held by the hand. Pressures were tuned for each individual object. I anticipate that an adult-sized hand would offer similar dexterity while exerting higher grasping forces.

The overall payload of the hand, assessed in a pull-out test with a 24mm cylinder, is approximately 0.5kg. This means the hand can lift approximately seven times its own weight.

The table 5.1 provides a brief comparison of the proposed hand with other anthropomorphic designs. Note that the table is divided into two parts: soft material hands, and hands claiming some degree of 'softness' or flexibility but constructed from rigid components. Each section is sorted by date. Only anthropomorphic designs are considered. When comparing to other soft devices, bear in mind that the described design was developed in late 2016 and published in

2017, while the larger version was developed in early 2020 but never finalised. Large-DOF devices, such as RBO Hand 3 [13, 14], were published in 2021 and '22, meaning that no soft pneumatic hand with more than 10 DOF was available when I was working on the large version of my design, which comprised 11 DOF and featured double-compartment fingers, similar to RBO Hand 3 published in '22.

Limitations

Actuation of the thumb is insufficient. For the range of actuation pressure, the palm actuator is unable to fully move the thumb from apposition to opposition mode. Although this joint is powered by two separate actuators, they are interconnected and controlled by a single pressure regulator. In the subsequent iteration, the exoskeleton thickness was reduced in the actuation region, and the actuators' cross-sectional area was enlarged. The actuators were also divided into two independent actuators, which should collectively enable greater thumb mobility in terms of bending range and add the missing degree of freedom.

Another limitation is that beyond a certain pressure value, fingers cease to provide additional grasping force and instead start to twist and buckle. This issue could be addressed to some extent by employing the stiffening structures described in chapter 4, which would increase finger stiffness at the same actuation pressure level. The breaking pressure value has not been quantified, but it is considerably higher than the useful pressure range.

When controlling the hand with the LeapMotion controller, it became apparent that it does not work correctly in certain configurations. Its performance is highly dependent on lighting conditions and the kind of gestures performed, some of which are impossible to achieve using LeapMotion. The most problematic cases occur when fingers are not fully visible from the LeapMotion's perspective, requiring the software to estimate the actual hand configuration, often inaccurately. It also struggles with gestures where fingers touch each other, such as pinch grasps, typically outputting a similar hand configuration but with a large gap between fingertips. Consequently, pinch grasps were not truly feasible using this type of interface. Nonetheless, it remains useful for other test scenarios, and its interface is easy to operate even for inexperienced users.

Table 5.1: Comparison of various soft and flexible anthropomorphic hands.

	device	year published	cost	DOF	actuation technology	mass (g)	payload (kg)	payload to mas	control complexity	anthropomorphic appearance
soft material — before 2017	Cosmetic Prosthetic Hand [15]	2005	N/A	11	1 DC motor + tendons	N/A	N/A	N/A	low	★★★
	ISR-SoftHand [150]	2014	€400-800	10	3 servomotors + tendons	530	1.8	3.4	medium	★★
	Ohio State University soft robotic hand [147]	2015	N/A	5	5 Antagonistic SMA actautors	282	N/A	N/A	low	★
	RBO Hand 2 [42]	2015	$100 materials + 2 days labour	7	7 PneuFlex	178	0.5	2.8	low to high	★
	Cornell soft prosthetic hand [148]	2016	N/A	5	5 fabric reinforced pneumatic	na	N/A	N/A	low	★
	Presented hand small [141, 157, 142]	2017	$10 materials + 2 days labour	6	6 fiber reinforced actuaros	70	0.5	7.1	low to high	★★★
soft material — after 2017	BCL-26 [158]	2019	N/A	26	22 fiber reinforced chambers	N/A	2	N/A	high to very high	★★
	X-Limb [16]	2020	$200	13	5 DC motors	253	2	7.9	low	★★★
	Presented hand large	2020 - never finished	$30 materials + 2 days labour	11	11 fiber reinforced actuaros	285	N/A	N/A	low to high	★★★
	Hand with human-inspired palm [14]	2021	€100-€150	20	hybrid-bending soft finger	300	N/A	N/A	high to very high	★★
	RBO Hand 3 [13]	2022	<$250	16	5x PneuFlex (4x double-compartment) 7x bellow actuator	N/A	3.9	N/A	high to very high	★★
rigid material	Ultralight Anthropomorphic Hand [149]	2001	N/A (low)	13	flexible fluidic joints	N/A (low)	N/A	N/A	low	★
	Shadow Dexterous Hand [159]	2004-now	N/A (high)	20	20 DC motors + tendons	4300	5	1.2	very high	★★
	Pisa IIT hand [146]	2014	N/A	19	1 DC motor + flexible tendons	N/A	2	N/A	low	★
	UC Softhand [160]	2015	$300	10	3 DC motors + tendons	280	0.74	2.6	medium	★

5.2 Soft Octopus

Soft robotics has offered solutions beyond the niche fields of robotic arms and grippers, having entered into the realm of mobile robots, with bio-inspired systems that can walk, crawl, jump, roll or swim [161, 31, 162, 106]. One specific area, underwater exploration, can benefit hugely from soft robotic solutions, as soft robots are able to mimic the very complex movements of aquatic creatures [163, 110]. Indeed several octopus-inspired robots have already been developed. In [105] the eight-arm octopus-like robot presented is able to swim using sculling movements of its arms, while in [104] the device, whose soft arms enable it to mimic octopus crawling locomotion - see [164]. In both cases, the arms are made of flexible material, though the rest of the robot body is rigid. The arms are driven by electrical motors embedded in their bases to achieve locomotion - each arm itself is only a passive extension of a rigid shaft attached to a motor. Involving electric motors in the design leads to an end-product that is largely rigid, and therefore somewhat distant in nature to its biological role model. Their tendon-based actuation is another aspect in which these robots differ significantly from their biological counterparts.

In this section, I present an entirely soft octopus robot (Fig. 5.22) whose locomotion is achieved through fluidic actuation. It has eight arms that actively deform and bend during the actuation cycle. The actuator designed specifically for this robot is described in more detail in Section 3.4. The swimming action is caused by direct deformation of the active parts of its arms, using fluidic actuation chambers. Its arms or tentacles make use of a novel type of soft continuum fluidic actuator that can bend in a range of directions, with bend angles a function of the chamber pressures. The robot can therefore offer a range of motions, including forward propulsion, turning and rotation around the primary axis, that hitherto have not been achieved in these kind of devices.

The work described in this section has previously been published in [143].

5.2.1 Design

As in other designs described here, the octopus arms are made of two types of silicone - SmoothOn Ecoflex 0030 and Smooth-Sil 940. A polyester thread is used to reinforce the outer walls of the chambers. Each arm contains active parts (actuation chambers) and passive

(a) **(b)**
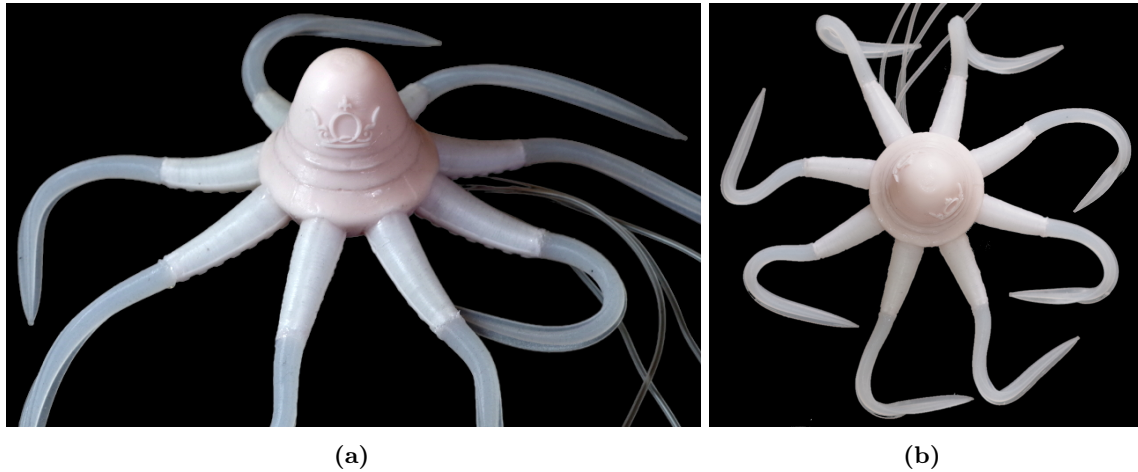
Figure 5.22: The octopus robot. (a) - side view, (b) - top view. From [143].

parts (extended tails). The passive part of each arm is not actuated but is designed to generate thrust while moving. When actuated, the active part of the arm experiences a curling motion, which in itself would not cause any significant thrust. The arms are therefore extended by long tails that are pushed through the water, amplifying the active part's motion and achieving the requisite forward thrust. The main body of the robot is entirely made of Smooth-Sil 940.
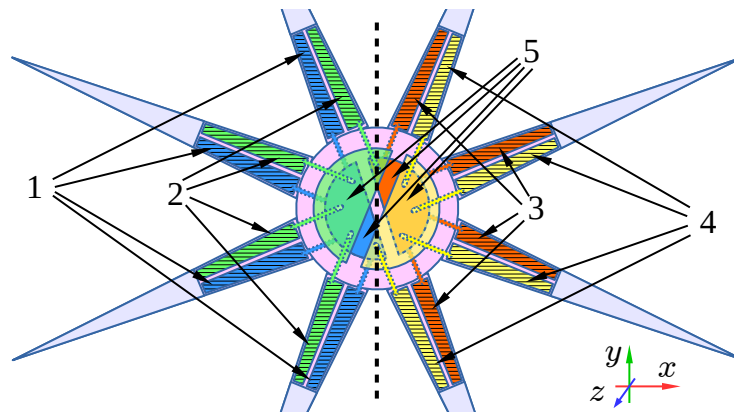
Figure 5.23: The robot's design. 1,2,3 and 4 - independent actuator groups, 5 - internal pressure distribution chambers. Body diameter: 55 mm, body height: 53 mm, total diameter with arms straighten: 335 mm. From [143].

In the design, I ensured each side of the robot could be actuated independently to enable the robot to turn. For that reason, four arms are grouped together. As each arm has two degrees of freedom, two arm groups require four independent pressure inputs. The actuation fluid is delivered through flexible pipes and distributed between the arms by internal channels within the robot body. The structure and distribution of the arms are designed to allow

the robot to swim forward, change its course of direction, and rotate around the z axis to navigate the three-dimensional space effectively. The structure and the dimensions of the assembled robot are shown in Fig. 5.23. Robot behaviour as a function of the pressure in the respective actuator groups is shown in Fig. 5.24.

(a)
(b)
(c)

(d)
(e)
(f)
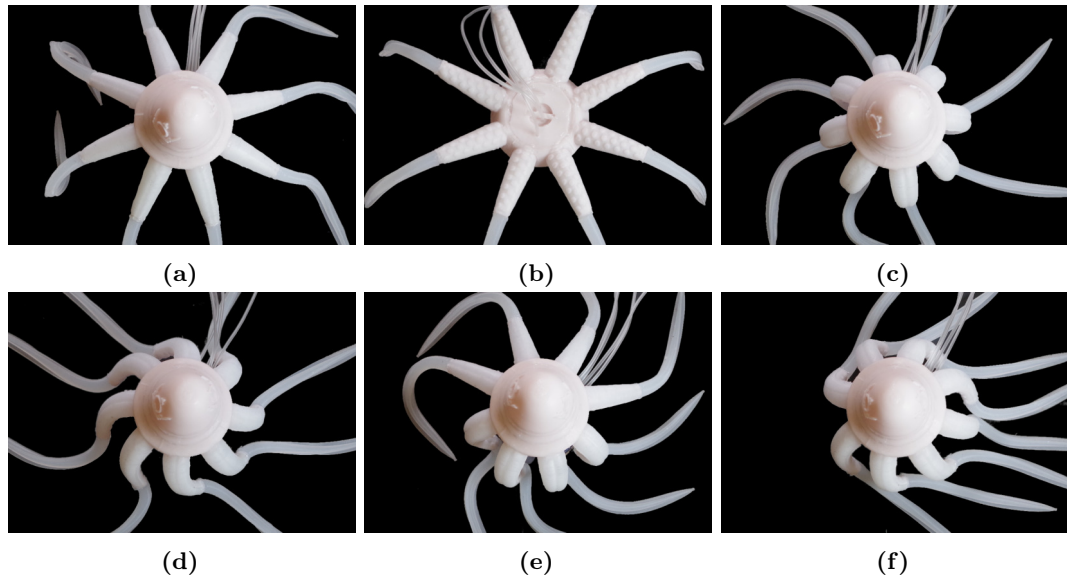
Figure 5.24: Different actuation patterns. (a),(b) - passive robot, top and bottom view, respectively, (c) - same pressure for all actuation chambers, forward movement, (d) - axial activation symmetry ($2^{nd}+4^{th}$ actuation groups), rotation along Z axis, (e) - one side activation ($1^{st}+2^{nd}$ actuation groups), rotation around y axis, (f) - two sides activation, ($1^{st}+4^{th}$ actuation groups), rotation around x axis. From [143].

5.2.2 Manufacturing

The robot is made in a similar way to the other designs described in this thesis. Fabrication of the body is a multi-staged process, as described below. The manufacturing procedure for the arms is outlined in Section 3.4.

The main part of the body is cast in the dedicated mould as seen in Fig. 5.25a. The main part of the body contains eight sockets for the arms with two pressure channels per arm - see Figs. 5.25b and 5.25c. The arms are connected to the body with the same material as used in the body itself (Smooth-Sil 940).

The body consists of several empty chambers that ultimately connect to the arms. The chambers are open after the first casting step - the mould used for that procedure is shown in Fig. 5.25a. Once the silicone is cured, the arms are connected, and all connections checked. Provided the seals are all tight, the top and bottom chambers of the body are closed - the
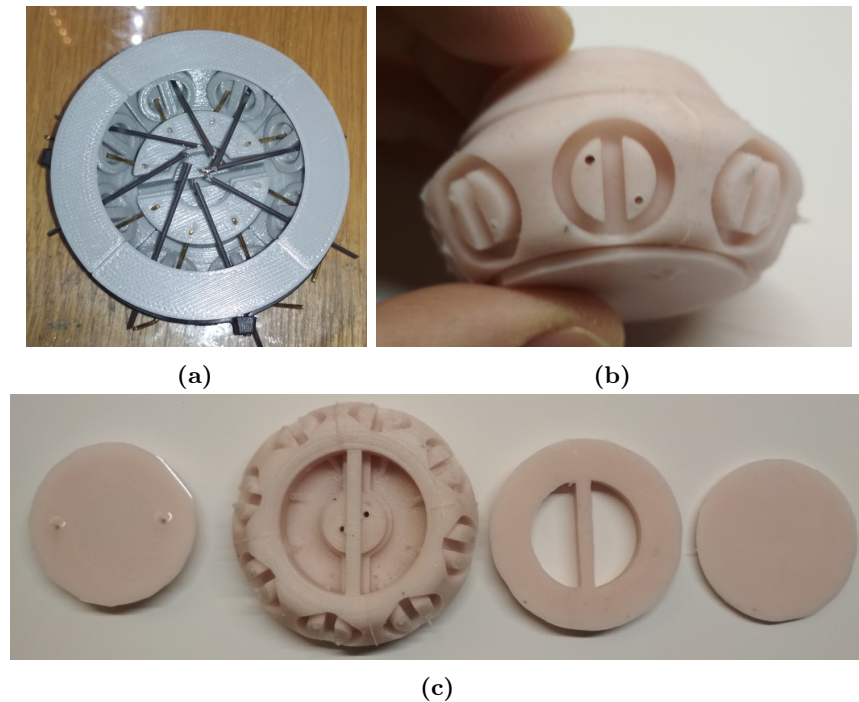
Figure 5.25: The robot's body. (a) Mould, (b) body assembled, arm socket with two separate pressure inlets presented (c) parts of the body, internal distribution chambers visible (compare Fig. 5.23). From [143].

final step of the fabrication procedure. The assembled robot is presented in Fig. 5.22. Its weight is approximately 120g.

5.2.3 Tests

Although the end-goal environment for the robot is water, its actuation system was tested with air. This is due to the high water viscosity generating resistance and reducing the actuation medium flow, in turn resulting in very slow robot actuation. Air actuation, however, causes actuators to change their volume significantly while their weight varies only slightly. The additional air volume in the robot body increases its buoyancy such that it floats. For that reason, the velocity tests were performed on the water surface. For the force tests, the robot was fixed to a lever that kept it below the water surface despite the buoyancy issue.

Test setup

All the experiments were conducted in a water tank made of transparent acrylic glass. The robot was powered by pressurised air supplied through 1 m long and 2 mm wide flexible tubes. The pressure was regulated at the tube inlet with a Camozzi k8p pressure regulator.
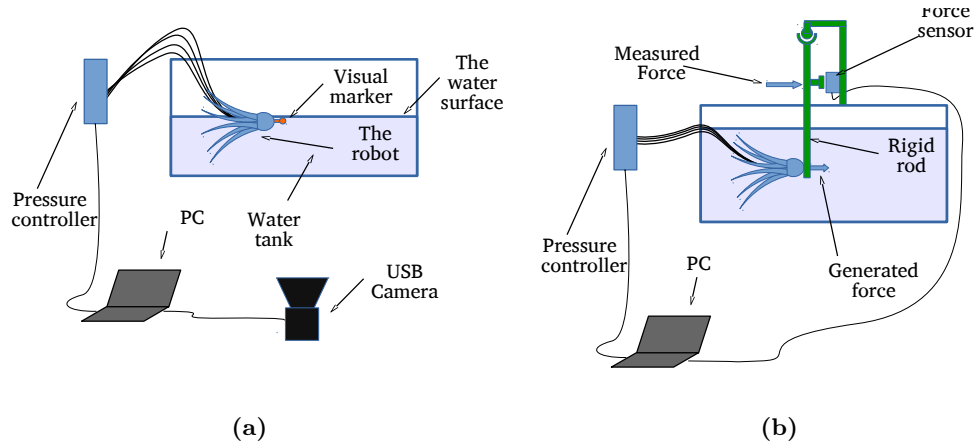
Figure 5.26: Test setup. (a) velocity test setup, (b) force test setup. From [143].

For all the actuation trials, just one tube was used to pressurise the robot. Using a small connector, the pressurised air was then distributed to the relevant chambers to activate the desired actuator groups (groups 1 - 4 for velocity and force tests, 1 and 3 for twist motion, 1 and 2 for turning motion - see Fig. 5.23).

Velocity test

For the velocity measurements, the robot was allowed to move freely within the tank, powered by a sequence of pressure pulses of a given frequency and a given pressure value. While progressing through the tank, the octopus robot was filmed, and, to simplify motion tracking, it had a coloured marker attached - see Fig. 5.26a. Using image analysis techniques, the robot position was extracted from the recorded image sequence and correlated to pressure data. The robot replicates the *arm swimming* pattern of the octopus. [165] defines arm swimming pattern as undulated motion of the arms in synchrony. Those undulations consist of a power (closing) and a recovery (opening) stroke of the arms. A sequence of frames extracted from the recording is shown in Fig. 5.27. The results are shown in Fig. 5.28a. The data presents three full actuation cycles using averages with error bars from six trials.

Force test

The robot was tested for force generation during actuation. The setup used is presented in Fig. 5.26b. The robot was attached to the lower end of a rod suspended on a hinge, with only the lower end of the rod below the water surface. A point on rod, one third of the way down its length, was aligned to abut a force sensor, which was activated when the rod was
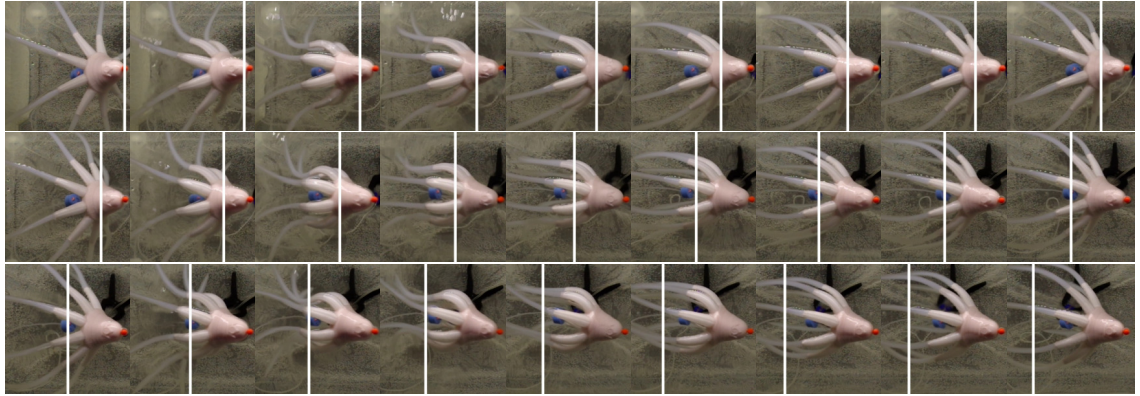
Figure 5.27: Movement of the robot, *arm swimming* pattern [165]; forward motion, three cycles presented. Video recorded at 30 fps. Every fifth frame is shown. White line indicates the tip position in the first frame and remain constant in space through all the other frames. From [143].

pushed toward it - see Fig. 5.26b. For the experiment, a single axis force sensor was used. During actuation, the robot exerted a force on the rod that was transferred to the sensor. Knowing the sensor position and the length of the rod, the measured force was calculated.

The recorded forces are presented in Fig. 5.28b

Manoeuvring capability evaluation

The turning and twisting manoeuvres have not been quantified, but some preliminary tests have been done. To achieve certain motion types, specific sections of the arms or group of arms were actuated, and the resulting manoeuvres recorded from above. For twisting motion, all the arms were actuated, but only one side of them was pressurised. Both sets of arms had the same chamber actuated simultaneously, i.e. either the left or right side, depending on the spin direction. For the turning motion, only one arm group was activated, but in this case, both chambers of each active arm were used. The test shows that the robot is capable of the assorted motion types - see Fig. 5.30 and Fig. 5.29.

5.2.4 Limitations and Discussion

The initial test shows that the robot is capable of manoeuvring in a number of fundamental ways - it can proceed, twist and turn. For the tested actuation pattern, which is a sequence of pressure pulses of 1 bar value, 1.5 s period, and 0.3 s pulse time, the average velocity of the robot is approximately 3.8 cm/s and around 9 cm/s at the peak value. This pattern was chosen to show the current design's capabilities. The pressure was set to a safe level and was

(a)

(b)
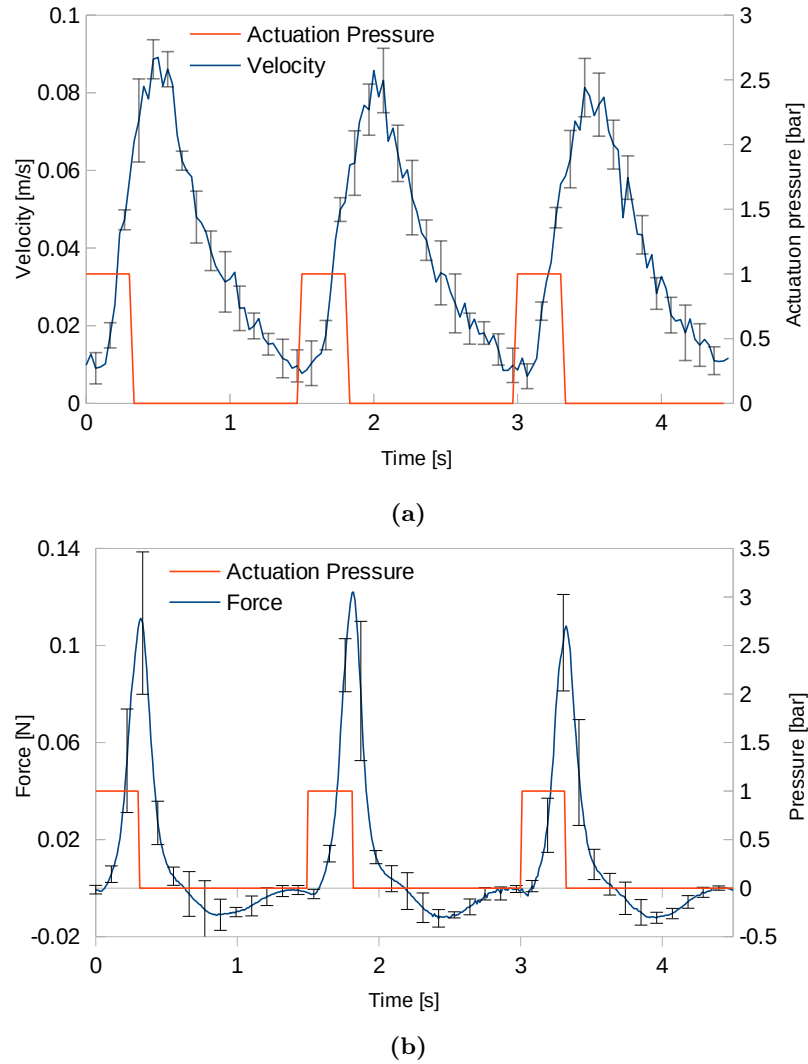
Figure 5.28: (a) velocity test result, (b) force test results. The plot presents average velocity values of 6 trials with error bars. Three complete actuation cycles are shown. From [143].

removed when a significant velocity was achieved. The next pulse was applied when velocity dropped to near zero. The thrust generated by the robot actuated in the same manner but at a fixed position (no velocity with respect to the water) is, on average, approximately 0.011 N and around 0.11 N at the peak value. The generated force has a low value but is sufficient to drive the robot.

The possible reasons for the low force value include a small actuator area, along with long and soft levers of the arms, and a relatively slow actuator response that reduces the relative speed of the arms with respect to water, which in turn limits the drag and thrust. If the force were insufficient to drive the device, several adjustments could be attempted, such as moving the power source closer to the robot to reduce dynamic losses in the actuation pipes,
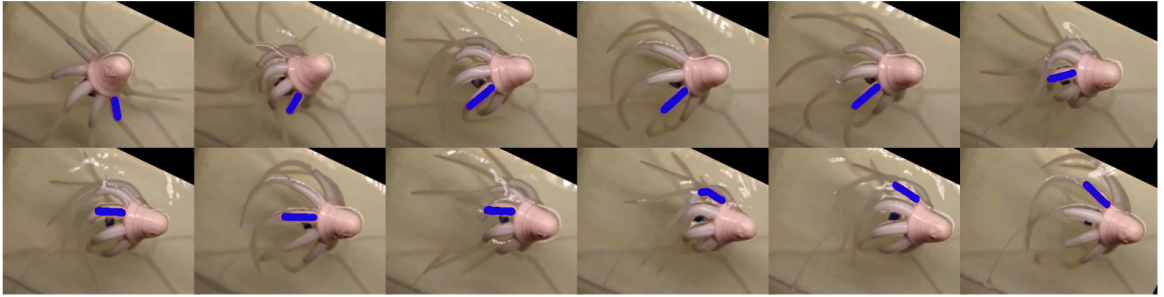
Figure 5.29: Movement of the robot; twisting motion. Three actuation cycles are presented. For better clarity of the twisting motion shown in the static figure, one of the arms is coloured blue. From [143].
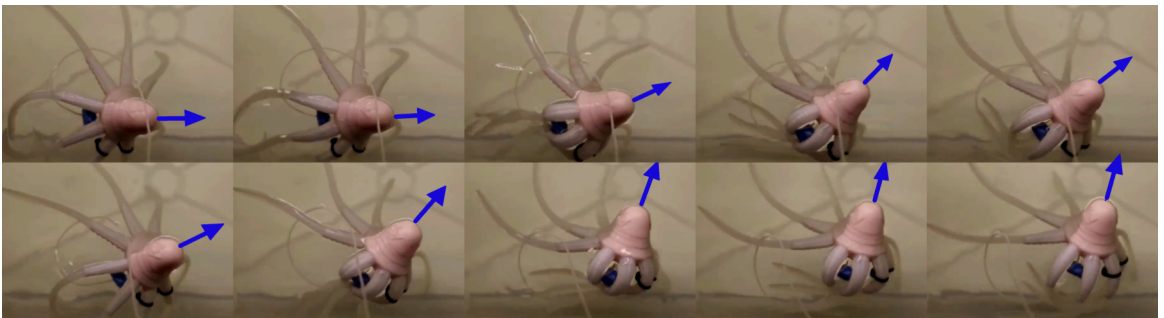
Figure 5.30: Movement of the robot; turning motion. Two cycles are presented. For better clarity of the robot's dynamics, the direction of the robot is marked in blue. From [143].

adjusting the arms' geometry, or increasing the actuator size. It is also worth noting that a low force value is not necessarily a drawback, as higher force generation could potentially incur additional costs, such as increased energy consumption and a drop in efficiency.

As the robot is powered by external pressure controlled via a regulator connected to the robot with a relatively thin and long pipe, its value in the actuators varies from (is considerably smaller than) the requested delivery pressure. This is due to the regulators' limited flow, the air viscosity and compressibility. The measurements of the pressure near the regulator outlet and the robot inlet are presented in Fig. 5.31. As demonstrated, the pressure at the robot level is significantly different from the requested one. Not only is it lower in the active state, but the venting process is also slow. The drag in the pipes and viscosity of the actuation fluid cause a significant delay and loss of dynamics. As a result, the overall range of available actuation frequencies is reduced with respect to the robot itself. Such a significant disparity must be considered when designing robot control algorithms and is a clear drawback of having an external power source. One potential improvement is moving the power source as close to the actuators as possible or using different sizes of pressure pipes.

This kind of effect is expected in all air-pressure-driven systems, but it has the most

significant impact on devices where system dynamics play a role, like in the discussed octopus where arm speed and beating frequency are important. The beating frequency issue is discussed in more detail in Section 5.3.
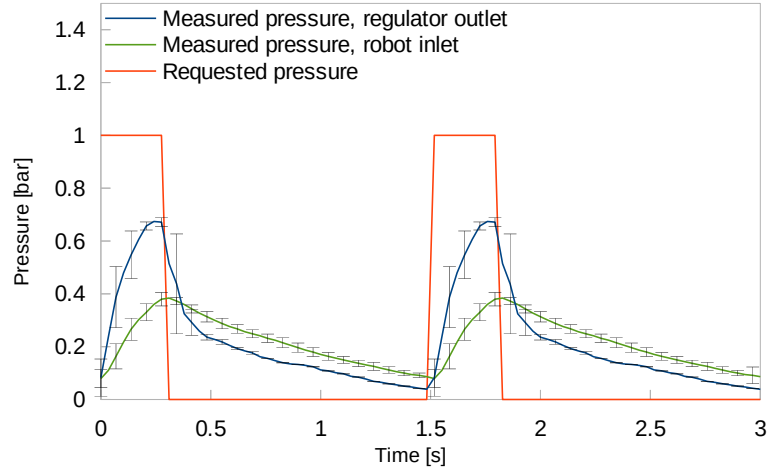
Figure 5.31: The disparity between requested and actual pressures in the system. From [143].

For proof of concept, the system was powered with pressurised air - this proved a useful way to show feasibility but limits real-world applicability. Ultimately, the end-goal system would need a liquid medium such as water or oil. In this way the control mechanism would be volume based rather than pressure based, and, as a result the robot's buoyancy would be unaffected.

The performance of the proposed demonstrator is within the range of other robots resembling octopus-like swimming with arms described in the literature. The overall average speed of 32mm/s is similar to another soft octopus robot driven with shape memory alloys [166]. While other designs outperform the proposed device in terms of absolute velocity (180mm/s) [167], it is worth noting that in this case, the robot is driven with conventional servomotors, is substantially larger, and is equipped with a flexible net that, along with the arm swimming pattern, creates a propulsion jet. The speed expressed in B_L (body lengths) per second of the described robot is approximately 0.22 (for the body length assuming the distance from the tip of the head to the end of the arms in the stroke - when the body length is the longest), with other robots reporting values ranging from 0.19 [105] up to 0.5 for [167]. However, it is unclear how the robot body length is measured in most cases. Most of the reported octopus robots use conventional actuators (servomotors), and to the best of my knowledge, only one other design uses soft actuators [166]. There are other robots resembling

octopus or squid in appearance but swimming due to jet propulsion with arms added for different purposes (e.g. crawling and manipulation [168]); they have not been considered in the following comparison. Octopus-inspired robots that perform crawling [104] or climbing [169], etc., but can't swim, have not been included in the following comparison. Swimming octopus robots' motion parameters are presented in table 5.2. No lifetime cyclic test has been conducted, and the breaking pressure has not been assessed.

Table 5.2: Swimming robots resembling octopus morphology powered with arms

	Robot	B_L(mm)	B_L/s	v (mm/s)	No of arms	deg. of actuation	3D swimming	Actuation method
soft actuation	Proposed Soft octopus	total - 175 arms - 140	0.22 0.27	38	8	4	+	fiber reinforced pneumatic actuators
	Octobot [166]	total - N/A arms - 79	N/A 0.32	25	8	1	-	shape memory alloy
conventional actuation	8-arm robotic system [105]	total - N/A arms - 200	0.19	98.6	8	8	+	electric serovomotors
	Octopus with compliant web [167]	total - N/A arms - N/A	0.5	180	8	8	+	electric servomotors
	Variable morphology robot [170]	total - N/A arms - 300	N/A $\sim$ 0.3	$\sim$ 100	8	8	+	electric servomotors
	Kraken [171]	total - 500 arms - 300	N/A $\sim$ N/A	N/A	4	4	+	stepper motors

5.3 Soft Fish

Another bio-inspired concept for a soft swimming robot is a fish robot. There are examples of soft robotic swimming fish [110, 163, 172] but to the author's best knowledge, at the time of development of the following design, there were no others that were driven with soft silicone-based fibre-reinforced actuators.

5.3.1 Design

The robot contains a fixed head section, an actuated tail, and a fin. The tail consists of an actuator and a flexible but passive section, Fig. 5.32. The active section has an asymmetric pair of fluidic actuators that extend when pressurised. As they are located on the sides, actuation of one side of the robot results not only in elongation but also in bending towards the non-actuated side of the fish - see Fig. 5.33. Applying and releasing the pressure in a periodical manner on both sides creates a heaving motion of the robot's tail. The flexible structure of the tail allows the fin to adapt to the water flow.
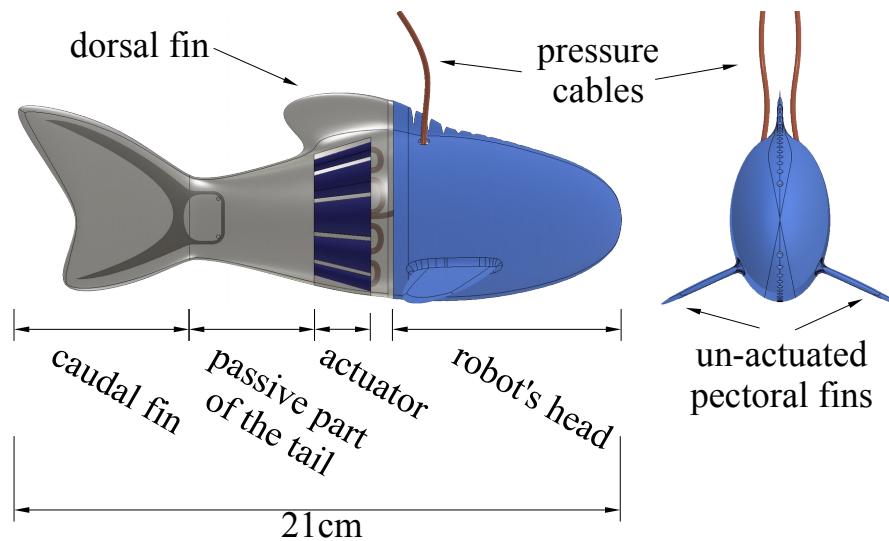
Figure 5.32: Robot's design.

My focus in this project concerned the rear part of the robot only. The head of the robot is a 3D printed part designed with a view to potentially house any requisite electronics, hydraulic pumps or batteries. With a potential increase in head size necessary for this, it seems likely that the rear section of the robot would need to be scaled up to match.

(a)   (b)
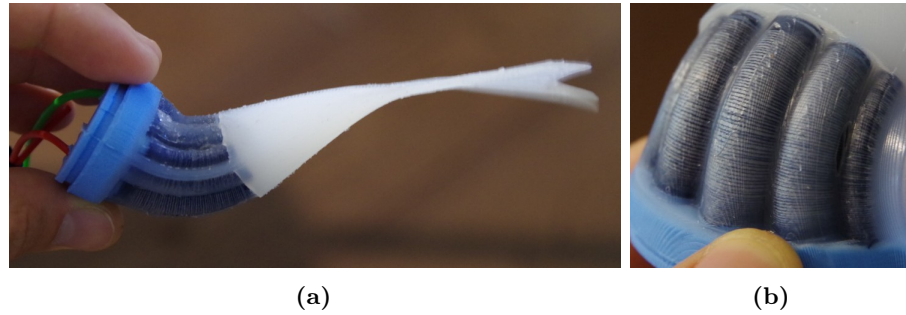
Figure 5.33: Bending of the tail, (a) bottom view, (b) the actuator zoomed-in, fibres visible.

Tail

The tail consists of an active part and a passive, flexible part. The active part deforms when pressurised and bends the tail sideways. The passive part of the tail deforms during the movement, assuring the fin travels through the water and also rotates so that it not only pushes the water to the side but also generates a thrust. The fin attached to the tail is responsible for the actual thrust generation. The active part of the tail is approximately 15% of the overall length of the rear part of the robot. Each side of the active part contains five connected actuators - see Fig. 5.34b. Although each actuator is conical in shape, they all have different dimensions, so as to fit better within the tail's geometry. The tail's cross-section is elliptical and becomes thinner towards the dorsal fin. While each side of the tail consists of many actuators, not all of them need to be actuated simultaneously, though for the purposes of this study, they are set to work in unison. Indeed they could be actuated separately to control the thrust not only in the horizontal plane but also vertically.

(a)   (b)   (c)
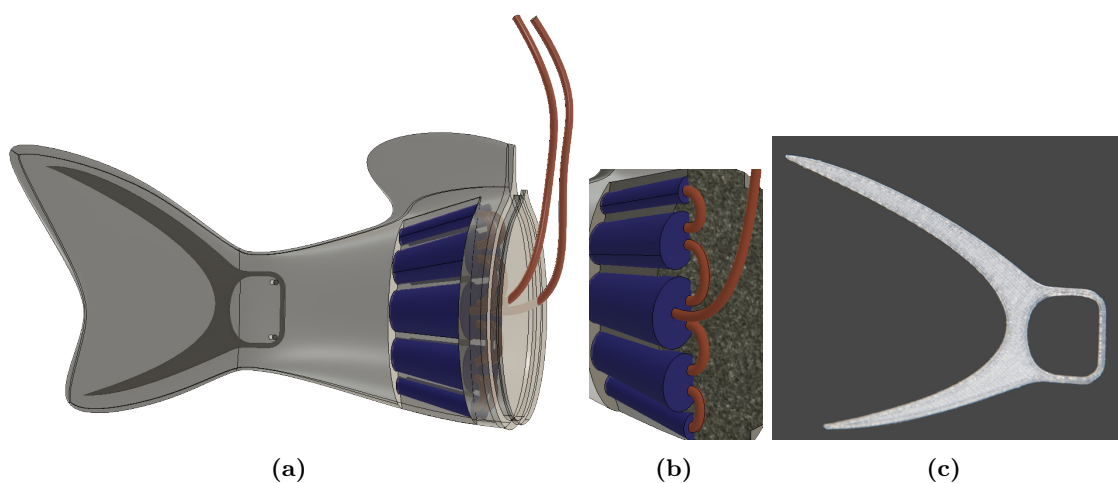
Figure 5.34: (a) Section view on the actuators and (b) connections between them, (c) a 3D printed nylon structure supporting the caudal fin of the robot.

Caudal fin

The caudal fin is made of the same material as the tail. Since it is very soft silicone, I added a 3D printed structure to increase the fin's rigidity - see Fig. 5.34c. I used Nylon filament for that part, ensuring that the fin remains flexible. The 3D printed part is covered with silicone creating a thin membrane stretched across the nylon component from one end to another. Because of the outer silicone membrane, the caudal fin can adapt to the water flow, even during the actuation.

Similar designs

Researchers from MIT have developed a robotic fish SoFi, driven by a soft tail that deforms when the pressurised medium is transferred from one side of the tail to the other [110, 173]. In the SoFi robot, however, the actuation chambers take up almost all of the volume of the tail, are not reinforced with fibres and are not divided into any sections enabling separate actuation. For that reason, SoFi has additional actuators for the pectoral fins to control pitch - a feature that would not be necessary in my design. My understanding is that the application of fibre reinforcement would improve the robot's efficiency as it effectively reduces any radial expansion of the actuators (a problem that is clearly observable in the footage of actuated SoFi prototype - see [174]). Another design difference - the inclusion of a passive deformable flexible part of the tail, helps create the desired swimming behaviour - see [172]; with a short tail, fine-tuning the swimming behaviour becomes considerably more difficult. Furthermore, smaller actuation volumes mean that there is less fluid to transfer between the chambers, which in turn could help to increase the beating frequency. On the other hand, smaller chambers mean higher pressures are needed to produce equivalent tail bending and actuation torque. Nevertheless, commercial miniature pumps are able to provide high pressures although flow rates are relatively low. Specifically, commercial pumps of the dimensions required by my design offer flow rates lower than what is required to provide a beating frequency of 1.7Hz for my system (e.g. [175]). That said, they do offer up to 8bar pressure - considerably more than the 1.8bar currently demanded by my fish design. High-pressure low-volume chambers do therefore seem to be a better choice than low-pressure high-volume actuators.

5.3.2 Fabrication

For the fabrication of my robot fish, I used a manufacturing process similar to the one described in previous chapters; rods with the fibre wound around them are placed into the moulds and are covered with a silicone layer that bounds the fibre creating the external layer of the actuator. Once the silicone has cured, the rods are removed. To make the removal step easier and mitigate damage to the fragile structure of the reinforcement (at this stage, it is quite delicate as it is not embedded into, but rather just attached to the silicone surface), the rods are split into three parts and the inner part of the rod removed while the external parts remain attached to the thread preventing it from being pulled away from the actuator. Having removed the internal part, the outer parts are loosened and can be removed easily. It is noted that by using conical rods instead of cylindrical ones, the removal of the internal parts is even further simplified, as they can be easily withdrawn in the thin end to thick end direction, mitigating the need to be split into three parts. A partially manufactured actuator with the conical rod still embedded is shown in Fig. 5.35a. The next step is to create the actual pressure chamber, which is the internal part of the actuator, and which is made in a separate mould. Once the inner part of the actuator cures, it is inserted into the external layer of silicone created in the previous step with the fibre already attached. The actuator is then sealed at both ends using caps cast in a stiffer silicone material, one of which has openings for the insertion of pressure pipes. A set of 5 actuators for each side of the robot is then connected and inserted into the tail mould - see Fig. 5.36. The set of moulds for the right side of the robot is shown in Fig. 5.35b.

(a)   (b)
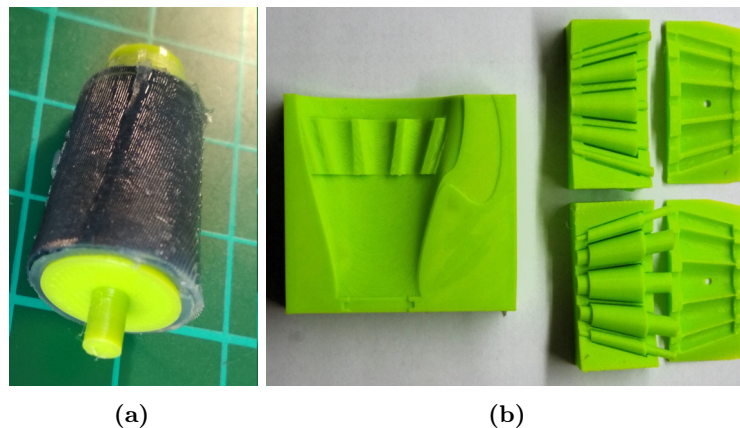
Figure 5.35: Manufacturing. (a) partially manufactured actuator, (b) set of moulds for one side of the robot.
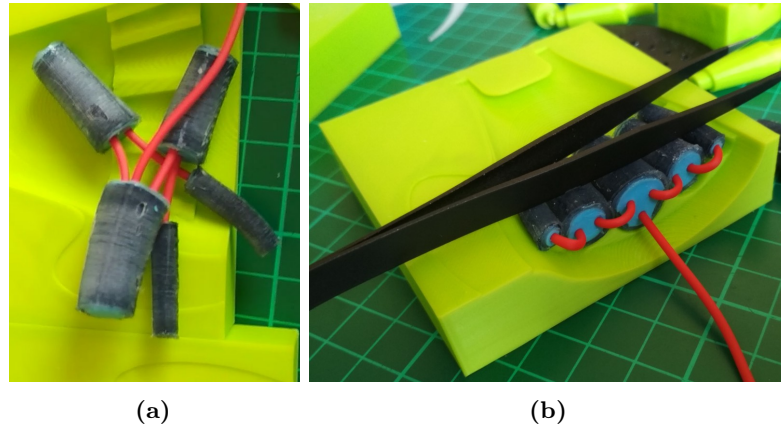
Figure 5.36: (a) set of actuators ready to be deployed, already connected, (b) actuators arranged inside the tail mould.
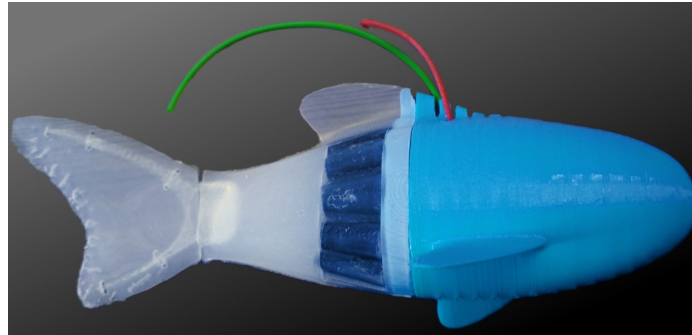
Figure 5.37: Assembled soft fish robot

5.3.3 Experimental validation

Experimental validation of the design comprised two sets of trials. Firstly the thrust generated by the robot was measured, and secondly, the speed of the robot was assessed. The force was characterised as a function of actuation pressure amplitude and frequency, while the velocity test was conducted for just one beating frequency selected from the force trials.

Force measurement

The force was measured using a Robotous RFT40-SA01 sensor. The experiment was repeated for various pressure amplitudes and beating frequencies. The chosen tail motion was a sinusoidal wave. In the experimental setup, the robot was submerged in water while attached to a float and a weight, ensuring that it stays at a constant depth and maintains its orientation during the experiment - see Fig. 5.38. The robot's mounting point was aligned with its yaw rotation axis. The mount did not constrain the yaw rotation, so the robot was able to oscillate as though it was not attached to the sensor. This is important as in real conditions,

an element of the force generated by the fin would be consumed by the oscillations of the robot's body. Also, the head rotation affects the orientation of the tail and, ultimately, the generated force. As the force sensor used was not water-proof, the force generated by the robot had to be transferred to the sensor by way of a lever. The robot was attached to the lever using a flexible element to reduce vibrations. Force was measured for at least five complete actuation cycles (more cycles for higher frequencies).

The data collected from the tests is presented in Fig. 5.39.
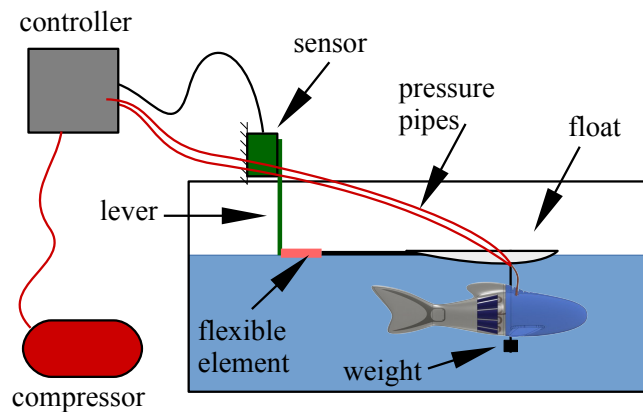
Figure 5.38: Force measurement setup
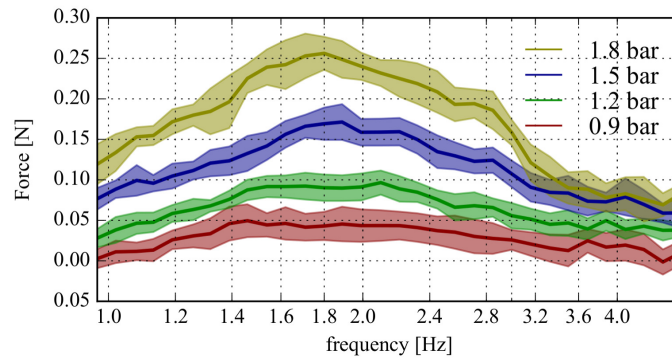
(a)

Figure 5.39: Force generated by the robot for various actuation amplitudes vs frequency of actuation. Data was collected from seven trials for each amplitude. Average and standard deviation plotted. Yellow, blue, green and red colours denote various pressure amplitudes.

Experimental data shows that the generated force increases along with the actuation pressure. It also shows that the efficiency of the actuation depends on the beating frequency, and for all the tested amplitudes the highest efficiency is within a similar range of frequencies. Those results agree with the research described in [176].

To investigate how much the yaw angle oscillation of the robot's body affects the generated force, the experiment was repeated with the tail itself fixed firmly to the same lever. The shape of the measured curves is very similar to what had been previously observed, although the frequencies are shifted, and the force values are much higher - see Fig. 5.40. Note the logarithmic scale at the x-axis in the presented plots.
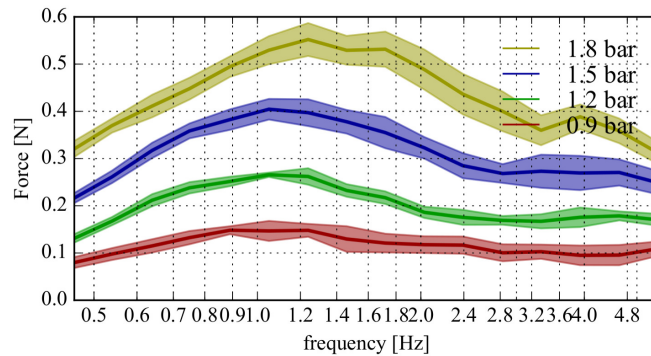
(a)

Figure 5.40: Force generated by the tail of the robot rigidly attached to the sensor for various actuation amplitudes vs frequency of actuation. Data was collected from five trials for each amplitude. Average and standard deviation plotted. Yellow, blue, green and red colours denote various pressure amplitudes.

These results suggest that reduction in body oscillation would be beneficial in terms of robot motion effectiveness.

Velocity

As the robot is attached to an external pressure source, its movement is inevitably constrained to some extent. The robot's motion, for example, is affected by the rigidity of the tubing used for pressure connection and the drag it creates. Moreover, since the current design uses air as an actuation means, it is not possible to balance the robot as its buoyancy changes during the actuation cycle. For this reason, to keep its pitch and depth at a constant level, an additional float is attached to the robot, changing its inertia and creating extra drag. The measured velocity is therefore not the true velocity the robot would achieve under real, untethered conditions.

In order to measure the velocity, colour markers were attached to the robot's body and the motion filmed from above. By extracting the markers from the footage it was then possible to calculate the approximate velocity of the robot. Four different actuation amplitudes were

tested, always using the 1.7Hz beating frequency that generated the best results in force tests. The results are presented in Fig. 5.41. This is the first evaluation of the fish swimming in water; the acquired data is not statistically significant but shows the velocity is approximately proportional to the actuation amplitude over the tested range.
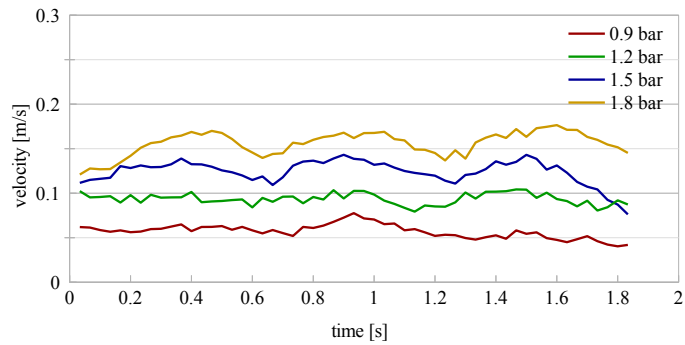
Figure 5.41: Velocity measured for various pressure amplitudes. Actuation frequency 1.7Hz. Three full actuation cycles are presented.

The swimming process is shown in Fig. 5.42.
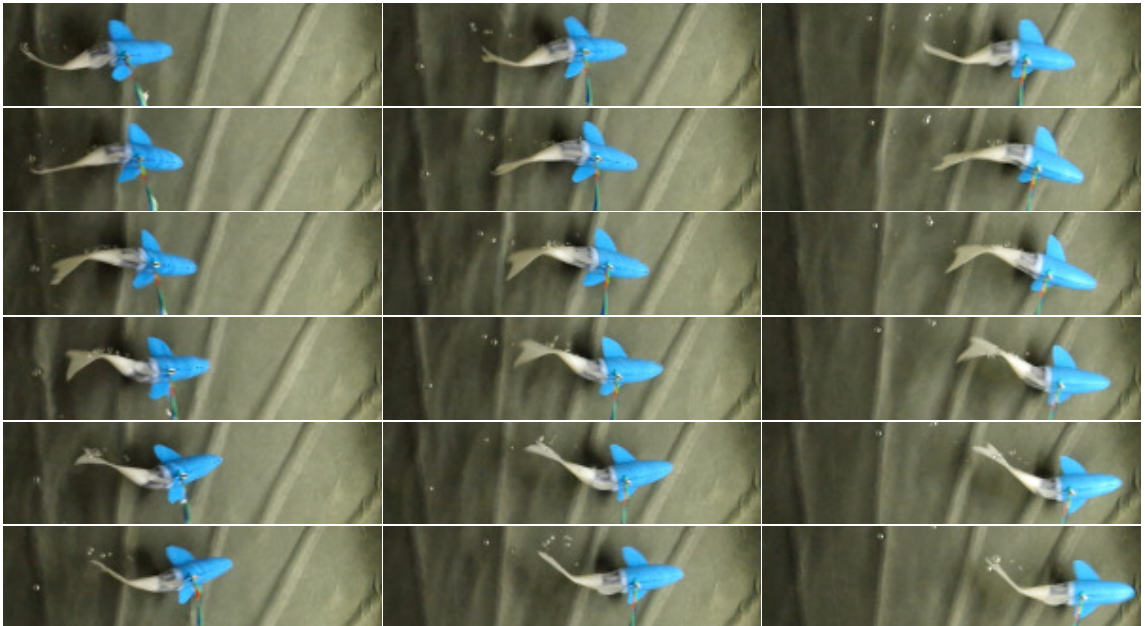
Figure 5.42: Three full actuation cycles (each column shows a single cycle). Beating frequency 1.7Hz, pressure amplitude 1.8bar

5.3.4 Discussion

The robot requires an external pressure source (compressor) and is controlled by two pressure regulators. During the actuation process, air travels from the compressor to the regulators

and then to the robot via relatively thin pressure pipes. This process takes time, and some pressure is lost due to the viscosity, compressibility and the mass of the air that has to be moved in and out, meaning the actual actuation pressure differs from the requested pressure, as seen in Fig. 5.31.

The gathered data shows the behaviour of the whole system, complete with compressor, regulators and pipes. The efficiency drop for frequencies higher than 1.5Hz is most likely related to the inertia of the pressure supply system and not the robot itself: the viscosity and inertia of the actuation fluid, along with the limited flow of the pressure regulators and the drag created in the pressure tubes, result in reduced dynamics of the actual device. The pressure at the actuator level is significantly different from the pressure at the regulator output and from the requested pressure. As a result, the amplitude of oscillations drops significantly above a certain frequency (cut-off frequency). The pressure-drop effect has been examined in the case of the octopus robot, see Fig. 5.31.

It is also noted that the controlled value in this setup is the pressure at the regulator outlet and that it is not possible to ensure that this pressure is reached inside the actuator (for higher frequencies, there may not be enough time for the air to travel through the piping). Furthermore, the pressure inside the actuator, even if it does reach the requested value, may not necessarily correspond with the tail amplitude, as this is highly dependent on the tail inertia and drag generated by the surrounding water.

The current robot design features a set of 5 actuators per side, which enables actuation of the tail in two directions (vertically as well as horizontally) and potentially 3D navigation without the need to articulate other fins. The current prototype provided proof of concept, though not without failings - in its present form it can swim forward with no issues but can barely turn. Furthermore, the pneumatic actuation system creates imbalance as the variable volume of the actuation chambers affects the robot's buoyancy.

To put the described fish robot demonstrator into context, several other soft robotic fishes have been presented in table 5.3.

It is noted that some of them are claimed to be 'soft' while using traditional actuators (servomotors). Apparently, one of the most popular actuation methods for swimming fish robots are electroactive polymers, but there are examples of pneumatic and hydraulic mechanisms too. The typical swimming speeds of these robots range from as low as 0.25 B_L

Table 5.3: Comparison of soft and compliant swimming fish robots

	Robot	B_L (m)	B_L/s	v (m/s)	Thrust (N)	Maneuverability	Actuators
soft actuators	Proposed soft fish	0.21	0.71	0.15	0.25	2D	Pneumatic Fiber Reinforced
	Manta robot [31]	0.15	0.67	0.1	N/A	1D	Pneumatic Fiber Reinforced
	SoFi '14[110]	0.34	0.44	0.15	N/A	2D	Pneumatic PneuNet
	SoFi '18[177]	0.47	0.5	0.235	N/A	3D	Hydraulic PneuNet
	Flexi-Tuna [178]	0.33	2.70	0.89	0.185	2D	Pneumatic McKibben
	Electro-ionic fish [179]	0.09	0.69	0.06	18m	2D	Dielectric Elastomer
	Biomimmetic fish [180]	0.15	0.25	0.032	0.5m	2D	Dielectric Elastomer
	Micro-robot fish [181]	0.15	0.75	0.112	N/A	2D	Dielectric Elastomer
DC motors	Variable stiffness fish [182]	0.32	0.55	0.176	1.5	1D	Servomotor + cables
	OpenFish [172]	0.42	2.02	0.85	N/A	1D	Servomotor + cables
	Compliant Robotc Tuna[183]	0.27	0.37	0.1	N/A	2D	Servomotor + cables
	Wire-driven Fish [184]	0.31	2.15	0.665	N/A	3D	Servomotor + cables

for one of the electroactive polymer designs up to 2.7 B_L for a McKibben muscles powered device. The most similar design, SoFi, uses positive pressure driven PneuNet actuators and reaches the same velocity of 15cm/s and slightly slower body length per second. However, this is a self-contained device powered with water pressure, rather than air, while the proposed design has an external power source and is actuated with air.

SoFi uses soft pneumatic (or hydraulic - depending on implementation) PneuNet actuators [12] that are arranged in antagonistic pairs. PneuNet is a network of interconnected cavities that expand when pressurised. One side of the actuator is equipped with a strain-limiting layer, so that the expansion causes elongation on the other side of the actuator, and consequently bending. The radial deformation of the actuator is limited by compartment dividers made of the same flexible material. For this reason, the radial expansion is reduced, but still present, when compared to virtually no radial expansion in the case of circular fibre reinforcement actuators used in the proposed design.

The actuators in the case of SoFi occupy approximately 57% of the robot length, while in my design they are reduced to 10% of the length. There is, however, a difference in SoFi's pneumatic and hydraulic designs, as the pneumatic one is optimised for escape manoeuvres and uses only one pair out of two for forward swimming. The other half deforms passively in that process, similarly to the passive part of the tail in my design. In such a case, the active actuation part of SoFi constitutes approximately a quarter of the robot's body length. The hydraulic version, however, has only one actuation pair spanning the entire tail volume. The overall SoFi actuation volume is approximately 110ml per side, while the proposed robot requires approximately 6ml of pressurised medium.

Due to the significant reduction of the actuator volume, the approximated energy required to actuate the tail in my design is significantly smaller. It is not clear, however, for what actuation range the energy consumption in SoFi was calculated, and it is noted that the SoFi robot is significantly larger than my design. The energy consumption might not be that significant if the same conditions were met (sizes, actuation range).

The energy consumption for proposed fish was calculated at 60° actuation angle. In such case the actuation pressure is ≈ 1 bar and the actuation volume is ≈ 6ml. The approximated elastic energy stored in the system in such case is ≈ 0.3 J according to eq. (5.1)[110], where $W_{elastic}$ is the energy, V is the final actuation volume and P is pressure. This value is based on assumed linear volume-pressure relationship. The actual shape of the curve was not measured. Only the elastic energy required to bend the tail compared.

$$W_{elastic} = \int_0^V P(v)dv \tag{5.1}$$

Both designs operate at very similar beating frequencies and achieve very similar velocities. The SoFi robot swims at slightly lower velocities relative to body length, but it is a self-contained system with the power source onboard, while my design has an external power source.

A detailed comparison between SoFi and the proposed design has been summarised in table 5.4.

In my tests, I have not gathered life-time information. The breaking pressure is approximately 2 bar, which corresponds to approximately 100° bending angle (tested on one prototype only).

Table 5.4: Comparison SoFi robot and proposed Soft Fish

	SoFi 2014	SoFi 2018	Proposed Fish
Overall Length (cm)	33.9	47	20
Overall Fork Lenght (cm)	30.5	N/A	15
Acuatior length (cm)	15.9	N/A	2
Max tail bending angle (deg)	>140	N/A	60
Actuation volume (ml)	110	N/A	6
No. of actuators	4	2	10
No. of actuation groups	4	2	2
Actuation Pressure (bar)	0.6	N/A	1
Actuation Elastic Energy (J)	2.89	N/A	$\approx$0.3
Beating frequency (Hz)	1.67	1.4	1.7

Only forward swimming has been tested; the turning motion has not been quantified. During the tests, the varying buoyancy of the fish was compensated with a weight attached to its body and a float on the surface.

The described fish robots conclude the demonstrators I have developed during my PhD. Soft hands, the octopus, and the fish were designed primarily to create a pleasant visual experience and showcase the actuators' performance, proving that they can be used in realistic scenarios. While these devices could be developed further towards their target applications, they remain only demonstrators at this stage.

In the following section, however, I describe an actual upper-limb assistance device that has been specifically designed for a particular patient and successfully deployed.

5.4 Icarion Semi-Passive Exoskeleton[*]

In 2019 a small start-up company contacted me regarding a product they were developing. Their idea was to create a compact, wearable, active arm exoskeleton that could be worn under clothing. The goal was to improve quality of life for people with disabilities by increasing the range of everyday activities they could perform without assistance. The solution was to provide patients with a device that offered very low interference with their appearance (meaning no bulky mechanical parts mounted around their limbs) and that was wearable for an extended period without causing fatigue or requiring frequent battery recharge. The device needed to flex or extend patients' joints on request. Depending on individual patients' needs, various levels of forces were required, as in some cases, the force should only assist the movement, while in others, the entire flexing force would be generated by the device. The force range needed to account for potential objects held by the patient. The device needed to be slim, lightweight, ergonomic, and power-efficient. The goal was to initially augment the elbow joint and then, based on the learnings, design devices for other joints.

5.4.1 Requirements

To meet the high-level requirements for supporting everyday activities and rehabilitation, more detailed technical requirements were assessed. These requirement values stem from the analysis of use cases conducted in collaboration with the patient and their doctor and assume tasks like handling a glass of beverage, TV remote, or mobile phone usage. The requirements take into account safety measures such as the maximum force transferred via the patient's elbow and safe pressure ranges. Most of the data is the property of the company, but overall requirements have been summarised in table 5.5.

5.4.2 System architecture

The primary component of the device is a passive bracket attached to the patient's upper limb, while the actuation part exerts forces on the bracket to aid in operating the limb. The system also includes a control unit that generates the actuation pressures based on user input, with force sensors operated by the user's leg to increase or decrease the operating

---

[*]The intellectual property described in this chapter belongs to Icarion Sp. z o. o. company. Thanks to Bartłomiej Gaczorek and the Icarion company for permission to share this work.

Requirement	Target Value	First Prototype Value
Actuation pressure range	3 bar	3 bar
Wearable part weight	as lightweight as possible	250 g
Time to recharge	one day	battery - one day air pressure - 1 hour
Elbow torque	5 Nm	1.1 Nm
Passive actuator length	90 mm	90 mm
Actuator extension	100%	100%

Table 5.5: Elbow assistive device requirements and first prototype parameters

pressure, and a pressure tank containing pressurised gas, as shown in Fig. 5.43. Due to the low-pressure storage used in the initial prototype, the system also employed an integrated compressor to recharge the pressure tank when needed. The entire system is integrated with the user's wheelchair, so the only additional payload carried by the patient is the wearable part of the device. The force-sensing input interface is fixed to the wheelchair frame and operated via movements of the patient's knee.

(a)
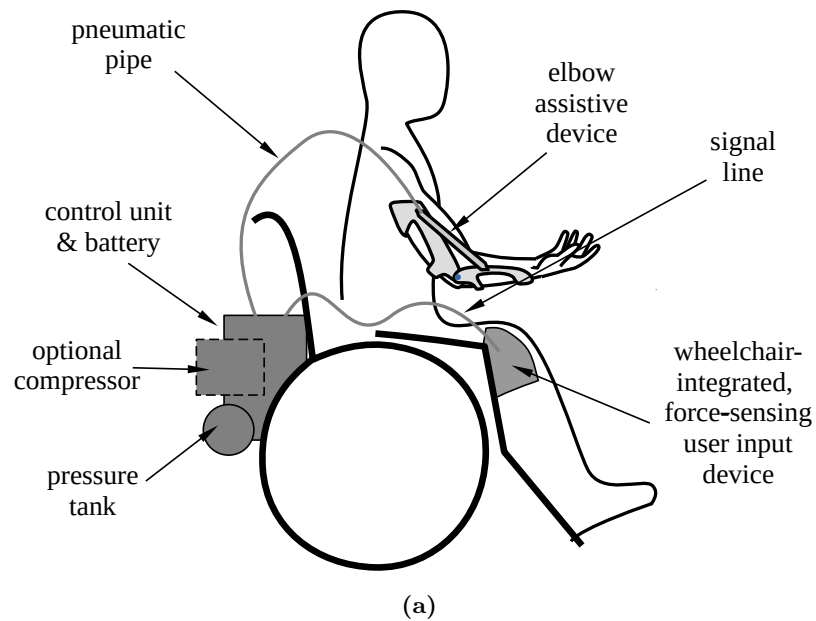
Figure 5.43: Overall architecture of the device.

The actual prototype is presented in Fig. 5.44.
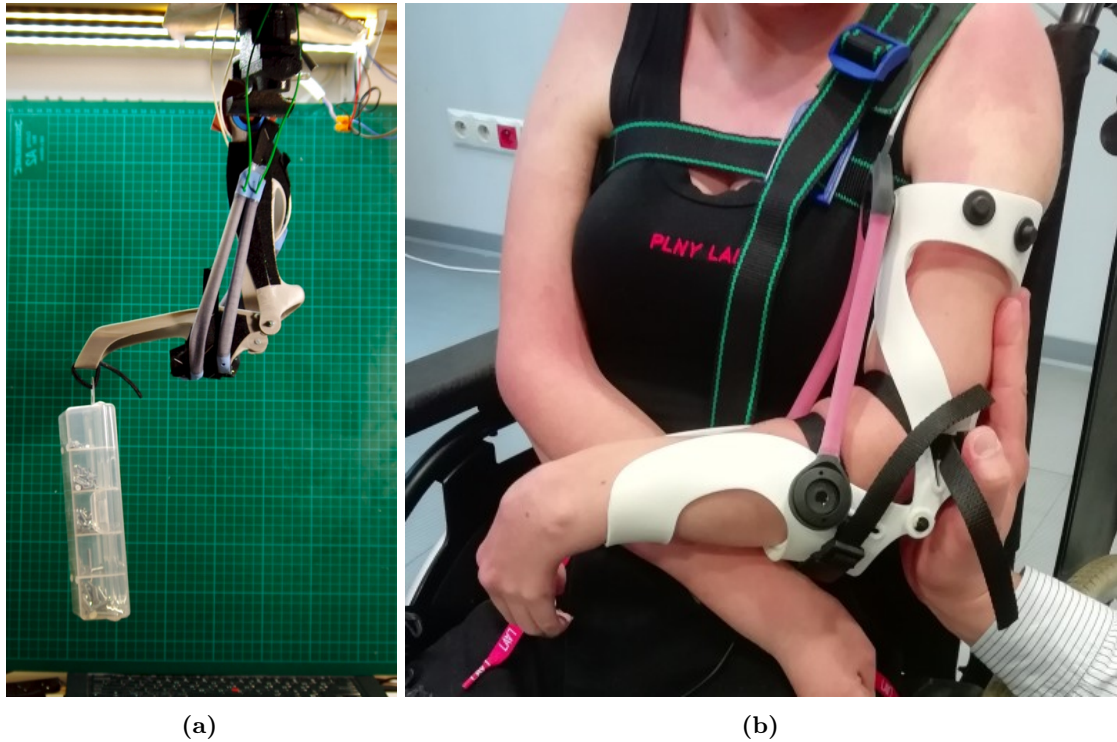
Figure 5.44: (a) A prototype of the arm exoskeleton device during tests (b) final prototype worn by patient.

5.4.3 Actuator

To satisfy the design requirements, the correct actuator technology needed to be selected. Moreover, the actuators had to have a good force-to-weight ratio, sufficient stroke and be soft. McKibben actuators and fibre reinforced linear pneumatic actuators were both considered.

McKibben actuators provide a very high power-to-mass ratio but have a very limited stroke [185]. Limited stroke forces the actuator to act on a short lever to generate the requisite amount of rotation. This is not ideal, as a short lever requires higher forces for actuation, which in turn means that higher forces are transferred via the joint. Since the device needs to be slim and lightweight, it relies on the patient's body along with the structural elements of the device. That said, the forces and bending moments in the system are transferred partially via the device and partially via the patient's bones and joints. In such a case, high actuation forces are undesirable as they put the patient at risk of high forces being transferred via their joints. Along with that, mechanical parts themselves would need to be bulkier to handle these higher forces, as shown in Fig. 5.45.

Due to the above limitations, fibre reinforced actuators were chosen for further development.
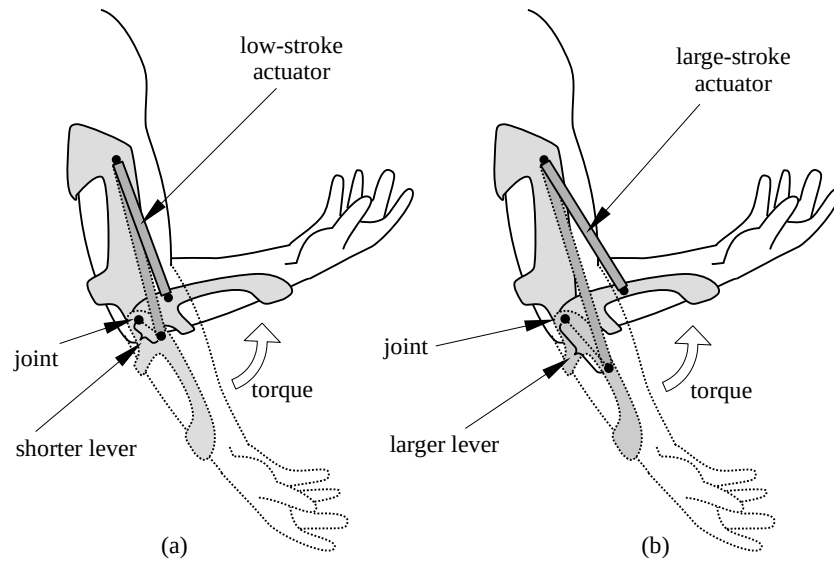
Figure 5.45: The stroke of the actor determines its alignment with the joint, which affects the forces transferred by the joint. (a) Low-stroke actuator, (b) large-stroke actuator.

A significant difference when compared to McKibben actuators is that fibre-reinforced actuators expand when pressurised and passively return when pressure is released. Since the kinematics of the device requires pulling actuators, fibre reinforced actuators in this type of design work in a passive manner, like springs that can be actively released, much as in [186]. This feature is another advantage of fibre reinforced actuators, as the maximum force they provide is physically limited. With McKibben actuators, the force generated increases with the pressure value, and so, should it encounter a failure in pressure reduction or a bug in the software, the potential consequences for the patient could be disastrous. Our system ensures the safety force levels are never exceeded despite any such failures in the system.

The actuator design is similar to the actuators used for most of the projects described in this thesis - see chapter 3; a flexible tube reinforced with fibres that elongates when pressurised and contracts when pressure is released. Due to its simple geometry, the behaviour of such an actuator can be easily adjusted, in terms of dimensions and force profile, for a specific user.

Hooke's law can approximate the force and displacement of such an actuator (assuming linear characteristics of the silicone) eq. (5.2),

$$F = xk \tag{5.2}$$

where F denotes the force acting on the actuator, and x is the displacement. In the

case of this actuator, F is composed of two factors - the internal force $F_p = PA_i$ generated by the pressure inside the actuator and the external force exerted by the actuator upon the outer world F_e. k in turn is determined by the material properties (elastic modulus E) and cross-sectional area of the silicone A_s and the initial length of the actuator l, eq. (5.3), Fig. 5.46.

$$A_i P + F_e = \frac{EA_s}{l} x \qquad (5.3)$$
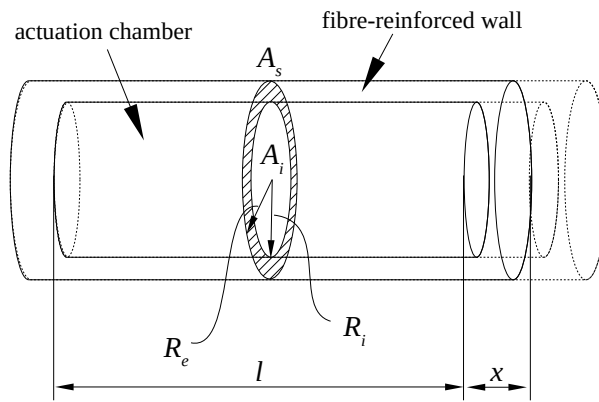
Figure 5.46: The Icarion actuator schematic. l - passive length, x - displacement, R_i and R_e radii internal and external respectively, A_s and A_i - cross-section area of the silicone and actuation chamber respectively.

When the pressure-resulting force is less than the force resulting from the stretch of the material, the device will exert a force on the user's limb. The maximum force that can be generated occurs when the internal pressure is off eq. (5.4).

$$F_{e,P=0} = \frac{EA_s}{l} x \qquad (5.4)$$

Using the above equation, knowing the required range of forces F_e, for the required range of motions under a given range of actuation pressures, the actuator's geometry can be tweaked to satisfy those requirements.

By putting the requested forces $F_e = F_0$ and $F_e = F_1$, as well as the required lengths of the actuator l_0 and l_1 on a plot, we can determine the actuator's required stiffness k and passive length l, Fig. 5.47
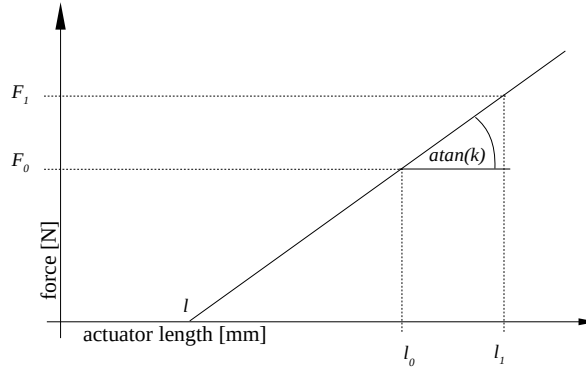
Figure 5.47: The required forces and displacements on the plot.

This, in turn, allows us to determine the overall actuator geometry.

$$A_s = \frac{lk}{E} \tag{5.5}$$

$$A_i = \frac{F_1}{P_{max}} \tag{5.6}$$

so that

$$R_i = \sqrt{\frac{A_i}{\pi}} \tag{5.7}$$

$$R_e = \sqrt{\frac{A_e}{\pi} - R_i^2} \tag{5.8}$$

5.4.4 Results

The first prototype of the device was delivered to the patient and tested for several weeks with good results. The battery lasted between 15 and 28 hours. The pressure tank used had a volume of 2 liters and was charged up to 3.5 bar, lasting between 30 and 60 minutes. When the pressure level dropped, it was automatically recharged with an integrated compressor. The patient reported that after short training, she was able to operate the device without explicitly thinking about the leg actions needed to induce the required elbow motions. The patient reported that the device was helpful in many situations, but there were scenarios that

required more degrees of freedom actuation (such as the shoulder joint) in which the device was not helpful, though it did not cause any additional effort either. The patient reported that full desired functionality would require the shoulder to be assisted as well.

During the wear and tear tests, the actuators were tested for several thousand cycles with no visible wear. The target tank pressure was 200 bars and was estimated to be sufficient for approximately 2000 actuation cycles.

The first prototype's torque was significantly lower than the target value. This design choice was made because higher torque would require larger actuators, which in turn would consume more air. The patient did not need such high assistive torques for operation, as 1.1 Nm was already sufficient. The initial prototype operated with a low-pressure source (3.5 bar) and an integrated compressor, whereas the target system was designed to use only a high-pressure source. This should allow for the use of larger actuators without compromising operation time and should enable the removal of the compressor from the system.

5.4.5 Summary

My contribution to this project was the actuator design and fabrication as well as the control unit prototype, in terms of both the electronics and firmware along with integration of the input devices.

When this text was initially written, the first prototype of the device had undergone testing by the first user. After several weeks of use, the user reported a substantial improvement in their mobility, and the device had not experienced any system failures.

There were plans in place to improve the device based on feedback from both users and doctors. Unfortunately, the decision was made to end the project due to technical difficulties and lack of further funding.

5.5 Pressure control system

An element common to the various systems presented is a pressure control box. The box was developed explicitly for the prosthetic hand project (Section 5.1), but used extensively for the other projects too. It was designed as a standalone device that could work in several modes. The simplest mode was to generate a requested sequence of pressures in a loop for demonstration purposes. In this mode, a soft device, say the hand, could re-play the recorded sequence of movements in a loop. In another mode it could be used in remote control via a gamepad, web interface, or external program running on a PC. This could be a simple application with sliders, where each slider corresponds to a single pressure output, or a more sophisticated controller such as LeapMotion. To satisfy all those goals, the internal control unit comprised two parts - a Raspberry Pi computer and Arduino micro-controller. The Raspberry Pi board was responsible for communication via the Ethernet port, handling game-pad input or playing the pre-recorded sequence of pressures, as well as exposing the WiFi interface alongside a webpage composed of sliders that could be operated via any browser, laptop or mobile device. The Arduino board was generating PWM (Pulse Width Modulation) signals for pressure regulators. The reason to delegate the PWM generation to Arduino is that the Raspberry is not a real-time system, and the PWM signals it provides are subject to fluctuations making the pressure output unstable.

A diagram showing the structure of the device is presented in Fig. 5.48, and the actual device is shown in Fig. 5.49.

Device	Function	Model	Units
High level controller	Web interface UDP interface Gamepad interface Control signals values calculation	Raspberry Pi 3B	1
Low level controller	Realtime PWM signal generation	Arduino clone, ATMega328P-A	1
Pressure regulators	Pressure control	Camozzi k8p	6

Table 5.6: The hardware used in the pressure controller
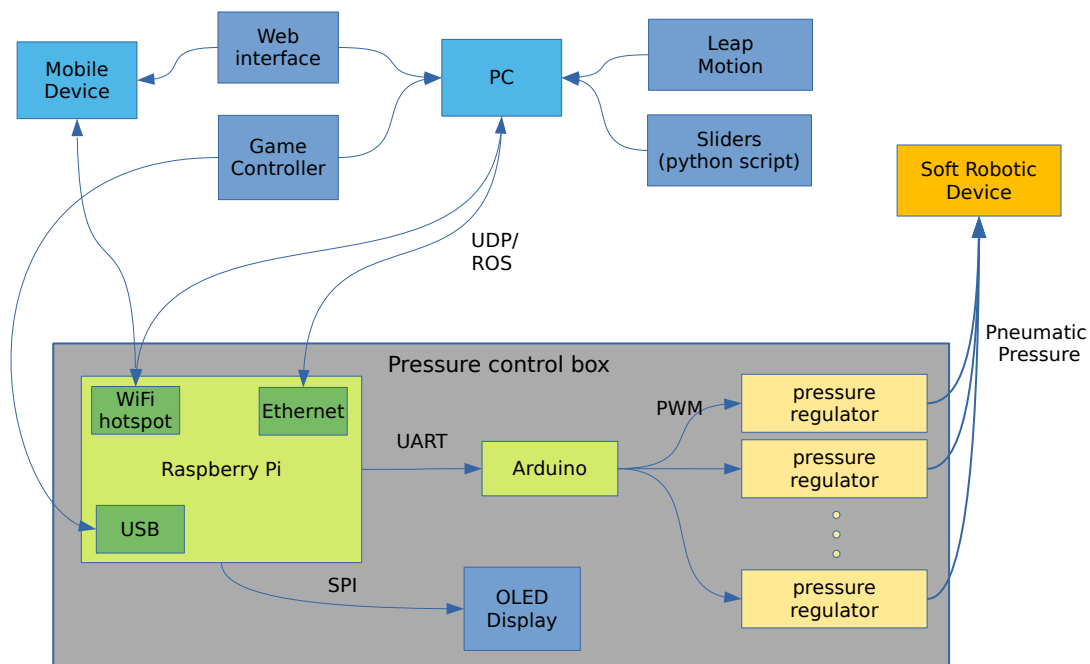
Figure 5.48: The pressure control box block diagram.

Figure 5.49: The pressure control box along with soft hand and Leap motion controller.

6

CONCLUSIONS

In this thesis, I have summarised the outcomes of my PhD research. The focus throughout was on soft mechanical structures actuated with pressurised fluids and their optimisation in terms of mechanical design and fabrication.

I have presented various actuators and the mathematics that underlie their functioning. I have created a new stiffening mechanism, that allows for simultaneous actuation and stiffening and calculated how much stiffening is expected depending on the actuator geometry and physical properties.

Finally, I have created several soft robotic devices and systems, including demonstrators such as hands, swimming octopus and fish robots, as well as a real-life semi-passive orthotic device.

While implementing specific actuators and devices, this work aims to address general problems in soft robotics. The performance of soft actuators is an important issue that will become increasingly important as soft material robotic technology reaches consumer-level readiness. Currently, most soft robotic devices and applications are still in the research phase, where energy efficiency and ease of use are secondary issues. However, when companies begin selling their soft actuators to other tech companies as a power source for more complicated devices, or sell soft robotic devices themselves, performance, robustness, and ease of use, including linearity of their responses, will become increasingly important.

Reliable actuators require not only proper design but also relevant fabrication techniques. The highly manual fabrication approach that is most popular in the literature is not only inefficient, but also prone to human errors, and the quality of the final product can vary

significantly. If soft actuators are to become more popular and accessible to engineers, we need more automated and reliable fabrication techniques.

Finally, stiffness controllability is a growing concern in the case of soft actuation. Soft actuators are intrinsically soft, but when they need to exert forces, such softness becomes an issue. Existing stiffening approaches are usually some form of state transition, such as the actual transition from liquid to solid or solidification of granular medium via jamming. This process, however, limits further actuation and requires more complicated control strategies. I believe that the preferred stiffening technology should coexist with actuation in a way that the shape of the device is not locked and can be further adjusted.

6.1 Contributions

In Section 1.2, I asked three questions about soft robotics design, fabrication, and stiffening techniques. These questions have been addressed by advancing the state of the art with the contributions outlined below.

6.1.1 Design and Fabrication

Fibre-reinforced actuators

The concept of soft robotics is relatively new, and manufacturing methods and design paradigms are therefore shifting an developing at a pace - indeed as yet, there are no well-established rules or best practice guidelines for soft robot design or manufacture. In this work, I have proposed several innovations in relation to the design and fabrication of soft-bodied, fibre-reinforced actuators. I identified circular cross-sectional geometry as the ideal shape of the actuation chambers in applications where the linearity of the actuator response is important. Any non-circular geometry displays a tendency toward circularity during pressurisation, leading to non-linearity in the initial part of the actuation process. I also proposed the application of dense rather than sparse reinforcement. Even if dense enough to prevent actuator damage, sparse reinforcement may not constrain ballooning sufficiently and thus affect the linearity of the actuator's response. Sparse reinforcement often requires contrary helical fibres to cancel torsion created while the actuator is expanding. In the case of dense reinforcement, this effect is negligible as the pitch of the thread is minimal. Dense

reinforcement is however problematic for most common fabrication techniques. To overcome this issue, I proposed another improvement, which was to revert the standard fabrication process order and complete the process of applying the reinforcement before creating the body of the actuator. This can be done by wrapping a rigid rod with a thread by spinning the rod on a spindle while progressively applying the thread. This process is fast, reliable and labour efficient. The rod with the tread is then covered with silicone, and the internal layer is created afterwards, enabling the production of denser reinforcement, with more even thread arrangement than with previous techniques.

'Instant' soft robots

To simplify the manufacturing process further and to improve the repeatability of actuator performance, I developed a new design for soft structures that I refer to as *instant soft robots* - so-called as the idea is based on disposable moulds that dramatically reduce the fabrication time. This is effectively the time it takes to fill a 3D printed structure with silicone and allow it to cure (once cured the mould can be broken-off and disposed of, while all the crucial reinforcing structures remain integrated with the silicone).

My research on the design and fabrication of fiber-reinforced actuators has the potential to make an impact not only within the field of soft robotics but also in other areas where actuation technology is utilized. The advancements proposed can improve the reliability and characteristics of soft actuators, making them a more appealing alternative to traditional actuation methods. Additionally, the simplified fabrication techniques developed can increase the availability of soft actuators, potentially leading to the introduction of soft technology in new applications. This represents a qualitative change in the field and highlights the potential for further innovation and integration of soft robotics technology in various industries.

The potential impact of this "instant" soft robot design extends beyond the current field of soft robotics as well, as the simplified manufacturing process and improved repeatability of actuator performance can make soft robots more accessible to a wider range of industries and applications. The reduced fabrication time and simplified process, along with publicly available CAD files, could make it easier and more cost-effective for companies and makers to incorporate soft robotics technology into their projects, products, and services.

6.1.2 Stiffening

The biggest advantage of soft-bodied robots - mechanical compliance - is, simultaneously, one of their major limitations. Although soft and compliant, which is a huge bonus in terms of robot access and working in delicate and fragile environments, their inability to exert significant force is potentially problematic.

I proposed a stiffening structure inspired by the mammalian penis. The structure is designed to direct the flow of the actuation fluid to, and then ensure it cannot escape from, those areas in which stiffening is required. This mechanism can be activated on-demand, and the increased stiffness can be applied in one direction while other dimensions remain compliant. In this way, the stiffening effect does not act against the actuation mechanism, as is the case in all other stiffening systems proposed for soft robots.

I was able to implement this mechanism into a bending actuator, demonstrating proof of concept. The test data shows that activation of the stiffening structure causes the apparent stiffness to double compared to the non-activated mechanism, which is consistent with expectations. A higher stiffening ratio could be achieved by adjusting the geometry of the device or using hydraulic actuation.

This work has the potential to improve the ability of soft-bodied robots to increase the range of possible interaction forces, broadening the possible application space and improving the performance of devices that are already based on soft technologies. Since this idea uses actuators that are backward compatible with previous fiber-reinforced actuators, in terms of their outer shape and structure, the existing designs could be easily adjusted for this kind of actuation.

Even though this stiffening actuator renders itself as an ideal candidate for grasping devices, the soft hand presented here had been developed before the stiffening actuator and for that reason uses standard bending actuators.

6.1.3 Soft robotic systems

I designed and constructed various robotic systems able to demonstrate proof-of-concept for the actuators I developed. These included soft hands, a swimming octopus and fish robots. All of them could be controlled via the pressure driver that I designed, offering several

interfaces for user convenience.

Beyond that, I played a part in creating a real-life arm exoskeleton that passed through the initial several-week-long deployment, reporting very good results in relation to significantly improved mobility. My involvement included the development of the soft actuation mechanism, the creation of a prototype of the pressure control unit, complete with electronics and firmware, and the integration of the technical elements into the system.

6.2 Future work and open questions

There are several possible routes to take in relation to developing the research work of this thesis, the most obvious one being to create a grasping device with an internal stiffening structure. This could offer better grasping performance than currently provided by soft grippers.

Although the demonstrators I produced were just demonstrators - necessary to establish proof of concept - each of them was made with a specific application in mind. The soft hand could be further developed to deliver a real prosthesis that could be worn and used by amputees. That would require the development of some user input interface and a portable pneumatic power source would need to be created. Swimming robots could be equipped with onboard hydraulic power sources and sensors for several applications, from marine life research to military reconnaissance.

The work presented here can also serve as a foundation for the development of more advanced features, such as embodied intelligence. The proposed stiffening structure has been implemented using individual cells, each having directional inputs and outputs and reacting to disturbances depending on those input and output pressures. If arranged in more complex structures, such cells could be used to implement smart behaviours or perform embodied computations. That said, the stiffening structure has shown potential, but there is much more to explore.

REFERENCES

[1] Kaspar Althoefer. "Antagonistic actuation and stiffness control in soft inflatable robots". In: *Nature Reviews Materials* 3.6 (2018), p. 76.

[2] Agostino Stilli, Helge A Wurdemann, and Kaspar Althoefer. "A novel concept for safe, stiffness-controllable robot links". In: *Soft robotics* 4.1 (2017), pp. 16–22.

[3] Thomas George Thuruthel, Yasmin Ansari, Egidio Falotico, and Cecilia Laschi. "Control strategies for soft robotic manipulators: A survey". In: *Soft robotics* 5.2 (2018), pp. 149–163.

[4] Brennan T Phillips, Kaitlyn P Becker, Shunichi Kurumaya, Kevin C Galloway, Griffin Whittredge, Daniel M Vogt, Clark B Teeple, Michelle H Rosen, Vincent A Pieribone, David F Gruber, et al. "A dexterous, glove-based teleoperable low-power soft robotic arm for delicate deep-sea biological exploration". In: *Scientific reports* 8.1 (2018), p. 14779.

[5] K Althoefer. *Neuro-fuzzy path planning for robotic manipulators*. 1996.

[6] Matteo Cianchetti, Cecilia Laschi, Arianna Menciassi, and Paolo Dario. "Biomedical applications of soft robotics". In: *Nature Reviews Materials* 3.6 (2018), pp. 143–153.

[7] Jelizaveta Konstantinova, Ali Shafti, and Kaspar Althoefer. *Soft and Stiffness-controllable Robotics Solutions for Minimally Invasive Surgery: The STIFF-FLOP Approach*. River Publishers, 2018.

[8] A. Arezzo, Y. Mintz, M. E. Allaix, S. Arolfo, M. Bonino, G. Gerboni, M. Brancadoro, et al. "Total mesorectal excision using a soft and flexible robotic arm: a feasibility study in cadaver models". In: *Surgical Endoscopy* (2016), pp. 1–10.

[9] Mauro Verra, Andrea Firrincieli, Marcello Chiurazzi, Andrea Mariani, Giacomo Lo Secco, Edoardo Forcignanò, Anastasios Koulaouzidis, Arianna Menciassi, Paolo Dario, Gastone Ciuti, et al. "Robotic-assisted colonoscopy platform with a magnetically-actuated soft-tethered capsule". In: *Cancers* 12.9 (2020), p. 2485.

[10] Agostino Stilli, Arianna Cremoni, Matteo Bianchi, Alessandro Ridolfi, Filippo Gerii, Federica Vannetti, Helge A Wurdemann, Benedetto Allotta, and Kaspar Althoefer. "AirExGlove—A novel pneumatic exoskeleton glove for adaptive hand rehabilitation in post-stroke patients". In: *2018 IEEE International Conference on Soft Robotics (RoboSoft)*. IEEE. 2018, pp. 579–584.

[11] A. Stilli, L. Grattarola, H. Feldmann, H. A. Wurdemann, and K. Althoefer. "Variable Stiffness Link (VSL): Toward inherently safe robotic manipulators". In: *2017 IEEE International Conference on Robotics and Automation (ICRA)*. May 2017, pp. 4971–4976. DOI: `10.1109/ICRA.2017.7989578`.

[12] Filip Ilievski, Aaron D Mazzeo, Robert F Shepherd, Xin Chen, and George M Whitesides. "Soft robotics for chemists". In: *Angewandte Chemie* 123.8 (2011), pp. 1930–1935.

[13] Steffen Puhlmann, Jason Harris, and Oliver Brock. "RBO Hand 3: A platform for soft dexterous manipulation". In: *IEEE Transactions on Robotics* 38.6 (2022), pp. 3434–3449.

[14] Haihang Wang, Fares J Abu-Dakka, Tran Nguyen Le, Ville Kyrki, and He Xu. "A novel soft robotic hand design with human-inspired soft palm: Achieving a great diversity of grasps". In: *IEEE Robotics & Automation Magazine* 28.2 (2021), pp. 37–49.

[15] Maria Chiara Carrozza, Giovanni Cappiello, Giovanni Stellin, Franco Zaccone, Fabrizio Vecchi, Silvestro Micera, and Paolo Dario. "A cosmetic prosthetic hand with tendon driven under-actuated mechanism and compliant joints: ongoing research and preliminary results". In: *Robotics and Automation, 2005. ICRA 2005. Proceedings of the 2005 IEEE International Conference on.* IEEE. 2005, pp. 2661–2666.

[16] Alireza Mohammadi, Jim Lavranos, Hao Zhou, Rahim Mutlu, Gursel Alici, Ying Tan, Peter Choong, and Denny Oetomo. "A practical 3D-printed soft robotic prosthetic hand with multi-articulating capabilities". In: *PloS one* 15.5 (2020), e0232766.

[17] Jr. Schulte H F. "Characteristics of the McKibben artificial muscle, The Application of External Power in Prosthetics and Orthotics". In: (1961), pp. 94–115.

[18] SM Hadi Sadati, Seyedeh Elnaz Naghibi, Ali Shiva, Ian D Walker, Kaspar Althoefer, and Thrishantha Nanayakkara. "Mechanics of continuum manipulators, a comparative study of five methods with experiments". In: *Towards Autonomous Robotic Systems: 18th Annual Conference, TAROS 2017, Guildford, UK, July 19–21, 2017, Proceedings 18.* Springer. 2017, pp. 686–702.

[19] J. Fras, Jan Czarnowski, Mateusz Macias, and Jakub Glowka. "Static modeling of multisection soft continuum manipulator for stiff-flop project". In: *Recent Advances in Automation, Robotics and Measuring Techniques.* Vol. 267. Springer, 2014, pp. 365–375.

[20] Kirk A. Keegan and David F. Penson. "Chapter 28 - Vasculogenic Erectile Dysfunction". In: *Vascular Medicine: A Companion to Braunwald's Heart Disease (Second Edition).* Ed. by Mark A. Creager, Joshua A. Beckman, and Joseph Loscalzo. Second Edition. Philadelphia: W.B. Saunders, 2013, pp. 341–348. ISBN: 978-1-4377-2930-6. DOI: `https://doi.org/10.1016/B978-1-4377-2930-6.00028-8`. URL: `http://www.sciencedirect.com/science/article/pii/B9781437729306000288`.

[21] *Evening Standard: Scientists develop robo-octopus that mimics real sea creature.* `https://www.standard.co.uk/tech/scientists-develop-robooctopus-that-mimics-real-sea-creature-a4192871.html`. Accessed: 2022-07-03.

[22] *Evening Standard: 'Robohand' developed for children who have lost a limb.* `https://www.standard.co.uk/tech/robohand-developed-for-children-who-have-lost-a-limb-a3566456.html`. Accessed: 2022-07-03.

[23] *UT2 Magazine:SOFT MACHINE.* `https://issuu.com/ut-2_publication/docs/ut3_six__2019_issuu`. Issue 6 2019, pp. 52-53, Accessed: 2022-07-03.

[24] *Mashable: Scientists built a robot octopus that moves its tentacles like the real thing.* `https://mashable.com/video/robot-octopus-moves-like-the-real-thing`. Accessed: 2022-07-03.

[25] *BBC Sunday Morning Show: Soft proshtetic hand and soft octopus.* `https://www.sems.qmul.ac.uk/news/5020/`. Accessed: 2022-07-03.

[26] *The Progress 1000: London's most influential people 2019.* `https://www.standard.co.uk/news/the1000/the-progress-1000-london-s-most-influential-people-2019-technology-engineering-a4248211.html`. Accessed: 2022-07-03.

[27] Jianglong Guo, Chaoqun Xiang, Tim Helps, Majid Taghavi, and Jonathan Rossiter. "Electroactive textile actuators for wearable and soft robots". In: *2018 IEEE International Conference on Soft Robotics (RoboSoft)*. IEEE. 2018, pp. 339–343.

[28] J. K. Paik and R. J. Wood. "A bidirectional shape memory alloy folding actuator". In: *Smart Materials and Structures* 21.6 (2012), p. 065013.

[29] H. Yin and Q. Sun. "Temperature variation in NiTi shape memory alloy during cyclic phase transition". In: *Journal of materials engineering and performance* 21.12 (2012), pp. 2505–2508.

[30] Mikołaj Rogóż, Hao Zeng, Chen Xuan, Diederik Sybolt Wiersma, and Piotr Wasylczyk. "Light-driven soft robot mimics caterpillar locomotion in natural scale". In: *Advanced Optical Materials* 4.11 (2016), pp. 1689–1694.

[31] Koichi Suzumori, Satoshi Endo, Takefumi Kanda, Naomi Kato, and Hiroyoshi Suzuki. "A bending pneumatic rubber actuator realizing soft-bodied manta swimming robot". In: *Robotics and Automation, 2007 IEEE International Conference on*. IEEE. 2007, pp. 4975–4980.

[32] Matthew A Robertson and Jamie Paik. "New soft robots really suck: Vacuum-powered systems empower diverse capabilities". In: *Science Robotics* 2.9 (2017), eaan6357.

[33] Josie Hughes, Utku Culha, Fabio Giardina, Fabian Guenther, Andre Rosendo, and Fumiya Iida. "Soft manipulators and grippers: a review". In: *Frontiers in Robotics and AI* 3 (2016), p. 69.

[34] Yufei Hao, Zheyuan Gong, Zhexin Xie, Shaoya Guan, Xingbang Yang, Ziyu Ren, Tianmiao Wang, and Li Wen. "Universal soft pneumatic robotic gripper with variable effective length". In: *2016 35th Chinese Control Conference (CCC)*. 2016, pp. 6109–6114. DOI: `10.1109/ChiCC.2016.7554316`.

[35] Raphael Deimel and Oliver Brock. "A novel type of compliant and underactuated robotic hand for dexterous grasping". In: *The International Journal of Robotics Research* 35.1-3 (2016), pp. 161–185.

[36] Ho Choi and Muammer Koc. "Design and feasibility tests of a flexible gripper based on inflatable rubber pockets". In: *International Journal of Machine Tools and Manufacture* 46.12-13 (2006), pp. 1350–1361.

[37] Kevin C Galloway, Kaitlyn P Becker, Brennan Phillips, Jordan Kirby, Stephen Licht, Dan Tchernov, Robert J Wood, and David F Gruber. "Soft robotic grippers for biological sampling on deep reefs". In: *Soft robotics* 3.1 (2016), pp. 23–33.

[38] *Soft Robotics Inc.* `https://www.softroboticsinc.com/`. Accessed: 2022-06-17.

[39] *Soft Gripping Wagard GmbH.* `https://soft-gripping.com/imprint/`. Accessed: 2022-06-17.

[40] *OnRobot soft grippers.* `https://onrobot.com/en/products/soft-gripper`. Accessed: 2023-01-29.

[41] *Festo Multi Choice Gripper.* `https://www.festo.com/net/SupportPortal/Files/333986/Festo_MultiChoiceGripper_en.pdf`. Accessed: 2022-06-17.

[42] Raphael Deimel and Oliver Brock. "Soft hands for reliable grasping strategies". In: *Soft Robotics.* Springer, 2015, pp. 211–221.

[43] Michael Rybski, Moshe Shoham, and Gershon Grossman. "Robotic manipulators based on inflatable structures". In: *Robotics and computer-integrated manufacturing* 12.1 (1996), pp. 111–120.

[44] N Salomonski, M Shoham, and G Grossman. "Light robot arm based on inflatable structure". In: *CIRP annals* 44.1 (1995), pp. 87–90.

[45] Hye-Jong Kim, Akihiro Kawamura, Yasutaka Nishioka, and Sadao Kawamura. "Mechanical design and control of inflatable robotic arms for high positioning accuracy". In: *Advanced Robotics* 32.2 (2018), pp. 89–104.

[46] Sebastien Voisembert, Alain Riwan, and Nazih Mechbal. "Numerical evaluation of a new robotic manipulator based on inflatable joints". In: *2012 IEEE International Conference on Automation Science and Engineering (CASE)*. IEEE. 2012, pp. 544–549.

[47] *Otherlab, M3 Robots*. https://www.otherlab.com/blog-posts/m3-robots. Accessed: 2022-06-17.

[48] Siddharth Sanan, Michael H Ornstein, and Christopher G Atkeson. "Physical human interaction for an inflatable manipulator". In: *2011 annual international conference of the IEEE engineering in medicine and biology society*. IEEE. 2011, pp. 7401–7404.

[49] Nathan S Usevitch, Zachary M Hammond, Mac Schwager, Allison M Okamura, Elliot W Hawkes, and Sean Follmer. "An untethered isoperimetric soft robot". In: *Science Robotics* 5.40 (2020), eaaz0492.

[50] Quanxia Lyu, Shu Gong, Jialiang Yin, Jennifer M. Dyson, and Wenlong Cheng. "Soft wearable healthcare materials and devices". English. In: *Advanced Healthcare Materials* 10.17 (Sept. 2021). ISSN: 2192-2640. DOI: 10.1002/adhm.202100577.

[51] Chia-Ye Chu and Rita M Patterson. "Soft robotic devices for hand rehabilitation and assistance: a narrative review". In: *Journal of neuroengineering and rehabilitation* 15.1 (2018), pp. 1–14.

[52] Panagiotis Polygerinos, Zheng Wang, Kevin C Galloway, Robert J Wood, and Conor J Walsh. "Soft robotic glove for combined assistance and at-home rehabilitation". In: *Robotics and Autonomous Systems* 73 (2015), pp. 135–143.

[53] Ye Ding, Myunghee Kim, Scott Kuindersma, and Conor J Walsh. "Human-in-the-loop optimization of hip assistance with a soft exosuit during walking". In: *Science robotics* 3.15 (2018), eaar5438.

[54] Tiana M Miller-Jackson, Rainier F Natividad, Daniel Yuan Lee Lim, Luis Hernandez-Barraza, Jonathan W Ambrose, and Raye Chen-Hua Yeow. "A Wearable Soft Robotic Exoskeleton for Hip Flexion Rehabilitation". In: *Frontiers in Robotics and AI* 9 (2022).

[55] Emanuele Pulvirenti, Richard S Diteesawat, Helmut Hauser, and Jonathan Rossiter. "Towards a Soft Exosuit for Hypogravity Adaptation: Design and Control of Lightweight Bubble Artificial Muscles". In: *2022 IEEE 5th International Conference on Soft Robotics (RoboSoft)*. IEEE. 2022, pp. 651–656.

[56] Kevin C Galloway, Panagiotis Polygerinos, Conor J Walsh, and Robert J Wood. "Mechanically programmable bend radius for fiber-reinforced soft actuators". In: *Advanced Robotics (ICAR), 2013 16th International Conference on*. IEEE. 2013, pp. 1–6.

[57] Y. Sun, Y. S. Song, and J. Paik. "Characterization of silicone rubber based soft pneumatic actuators". In: *International Conference on Intelligent Robots and Systems*. Nov. 2013, pp. 4446–4453. DOI: 10.1109/IROS.2013.6696995.

[58] Ian D Walker. "Continuous backbone "continuum" robot manipulators". In: *ISRN Robotics* 2013 (2013).

[59] Aslan Miriyev, Kenneth Stack, and Hod Lipson. "Soft material for soft actuators". In: *Nature Communications* 8.1 (2017), p. 596.

[60] A. Stilli, H. A Wurdemann, and K. Althoefer. "Shrinkable, stiffness-controllable soft manipulator based on a bio-inspired antagonistic actuation principle". In: *International Conference on Intelligent Robots and Systems*. IEEE. 2014, pp. 2476–2481.

[61] J. Fras, J. Czarnowski, M. Macias, J. Glowka, M. Cianchetti, and A. Menciassi. "New STIFF-FLOP module construction idea for improved actuation and sensing". In: *International Conference on Robotics and Automation*. IEEE. 2015, pp. 2901–2906.

[62] R.H. Gaylord. *Fluid actuated motor system and stroking device.* http://www.google.com/patents/US US Patent 2,844,126. 1958.

[63] Glenn K. Klute and Blake Hannaford. "Fatigue characteristics of McKibben artificial muscle actuators". In: *IROS*. 1998.

[64] Shoichiro Koizumi, Shunichi Kurumaya, Hiroyuki Nabae, Gen Endo, and Koichi Suzumori. "Recurrent Braiding of Thin McKibben Muscles to Overcome Their Limitation of Contraction". In: *Soft Robotics* 7.2 (2020), pp. 251–258.

[65] Krishna Manaswi Digumarti, Andrew T Conn, and Jonathan Rossiter. "Euglenoid-inspired giant shape change for highly deformable soft robots". In: *IEEE Robotics and automation letters* 2.4 (2017), pp. 2302–2307.

[66] Erik H Skorina, Ming Luo, Wut Yee Oo, Weijia Tao, Fuchen Chen, Sina Youssefian, Nima Rahbar, and Cagdas D Onal. "Reverse pneumatic artificial muscles (rPAMs): Modeling, integration, and control". In: *PloS one* 13.10 (2018), e0204637.

[67] Fionnuala Connolly, Panagiotis Polygerinos, Conor J. Walsh, and Katia Bertoldi. "Mechanical Programming of Soft Actuators by Varying Fiber Angle". In: *Soft Robotics* 2.1 (Mar. 2015), pp. 26–32. URL: http://online.liebertpub.com/doi/pdfplus/10.1089/soro.2015.0001.

[68] J. Fras, Mateusz Macias, Jan Czarnowski, Arianna Brancadoro Margherita Menciassi, and Jakub Glowka. "Soft Manipulator Actuation Module – with Reinforced Chambers". In: *Soft and Stiffness-controllable Robotics Solutions for Minimally Invasive Surgery: The STIFF-FLOP Approach*. Ed. by Jelizaveta Konstantinova, Ali Shafti, and Kaspar Althoefer. River Publishers, 2018. Chap. 3.

[69] K. Suzumori, S. Iikura, and H. Tanaka. "Development of flexible microactuator and its applications to robotic mechanisms". In: *International Conference on Robotics and Automation*. IEEE. 1991, pp. 1622–1627.

[70] T. Noritsugu, M. Ku Ota, and S. Yoshimatsu. "Development of Pneumatic Rotary Soft Actuator". In: *Transactions of the Japan Society of Mechanical Engineers Series C* 66.647 (2000), pp. 2280–2285. DOI: 10.1299/kikaic.66.2280.

[71] Nicholas W Bartlett, Michael T Tolley, Johannes TB Overvelde, James C Weaver, Bobak Mosadegh, Katia Bertoldi, George M Whitesides, and Robert J Wood. "A 3D-printed, functionally graded soft robot powered by combustion". In: *Science* 349.6244 (2015), pp. 161–165.

[72] Zachary M Hammond, Nathan S Usevitch, Elliot W Hawkes, and Sean Follmer. "Pneumatic reel actuator: Design, modeling, and implementation". In: *2017 IEEE International Conference on Robotics and Automation (ICRA)*. IEEE. 2017, pp. 626–633.

[73] Elliot W Hawkes, Laura H Blumenschein, Joseph D Greer, and Allison M Okamura. "A soft robot that navigates its environment through growth". In: *Science Robotics* 2.8 (2017), eaan3028.

[74] T Abrar, F Putzu, A Ataka, H Godaba, and K Althoefer. "Highly Manoeuvrable Eversion Robot Based on Fusion of Function with Structure". In: *2021 IEEE International Conference on Robotics and Automation (ICRA)*. IEEE. 2021, pp. 12089–12096.

[75] Taqi Abrar, Fabrizio Putzu, Jelizaveta Konstantinova, and Kaspar Althoefer. "EPAM: Eversive pneumatic artificial muscle". In: *2019 2nd IEEE International Conference on Soft Robotics (RoboSoft)*. IEEE. 2019, pp. 19–24.

[76] Francois Schmitt, Olivier Piccin, Laurent Barbe, and Bernard Bayle. "Soft robots manufacturing: a review". In: *Frontiers in Robotics and AI* 5 (2018), p. 84.

[77] Ahmed Hassan, Hareesh Godaba, and Kaspar Althoefer. "Design Analysis of a Fabric Based Lightweight Robotic Gripper". In: *TAROS*. 2019.

[78] TJ Wallin, J Pikul, and RF Shepherd. "3D printing of soft robotic systems". In: *Nature Reviews Materials* (2018), p. 1.

[79] J. H. Pikul, S. Li, H. Bai, R. T. Hanlon, I. Cohen, and R. F. Shepherd. "Stretchable surfaces with programmable 3D texture morphing for synthetic camouflaging skins". In: *Science* 358.6360 (2017), pp. 210–214. ISSN: 0036-8075. DOI: `10.1126/science.aan5627`. eprint: `http://science.sciencemag.org/content/358/6360/210.full.pdf`. URL: `http://science.sciencemag.org/content/358/6360/210`.

[80] Wookeun Park, Seongmin Seo, and Joonbum Bae. "A Hybrid Gripper with Soft Material and Rigid Structures". In: *IEEE Robotics and Automation Letters* (2018).

[81] S. Walker, O.D. Yirmibeşoğlu, U. Daalkhaijav, and Y. Mengüç. "14 - Additive manufacturing of soft robots". In: *Robotic Systems and Autonomous Platforms*. Woodhead Publishing, 2019, pp. 335–359. DOI: `https://doi.org/10.1016/B978-0-08-102260-3.00014-7`.

[82] Bryan N Peele, Thomas J Wallin, Huichan Zhao, and Robert F Shepherd. "3D printing antagonistic systems of artificial muscle using projection stereolithography". In: *Bioinspiration & biomimetics* 10.5 (2015), p. 055003.

[83] Oisín Byrne, Fergal Coulter, Mark Glynn, James F.X. Jones, Aisling Ní Annaidh, Eoin D. O'Cearbhaill, and Dónal P. Holland. "Additive Manufacture of Composite Soft Pneumatic Actuators". In: *Soft Robotics* 5.6 (2018). PMID: 30148682, pp. 726–736. DOI: `10.1089/soro.2018.0030`.

[84] M. Schaffner, J. Faber, L. Pianegonda, et al. "3D printing of robotic soft actuators with programmable bioinspired architectures". In: *Nature Communications* 9 (Dec. 2018). DOI: `10.1038/s41467-018-03216-w`.

[85] Vincent Wall, Raphael Deimel, and Oliver Brock. "Selective stiffening of soft actuators based on jamming". In: *2015 IEEE International Conference on Robotics and Automation (ICRA)*. IEEE. 2015, pp. 252–257.

[86] Yonghua Chen, Yunquan Li, Yingtian Li, and Yizhong Wang. "Stiffening of soft robotic actuators—Jamming approaches". In: *2017 IEEE International Conference on Real-time Computing and Robotics (RCAR)*. IEEE. 2017, pp. 17–21.

[87] Allen Jiang, Asghar Ataollahi, Kaspar Althoefer, Prokar Dasgupta, and Thrishantha Nanayakkara. "A variable stiffness joint by granular jamming". In: *International Design Engineering Technical Conferences and Computers and Information in Engineering Conference*. Vol. 45035. American Society of Mechanical Engineers. 2012, pp. 267–275.

[88] Yingtian Li, Yonghua Chen, Yang Yang, and Ying Wei. "Passive particle jamming and its stiffening of soft robotic grippers". In: *IEEE Transactions on robotics* 33.2 (2017), pp. 446–455.

[89] Huy Hoang Huynh, Dong Han, Kazuhiro Yoshida, Michael De Volder, and Joon-wan Kim. "Soft actuator with switchable stiffness using a micropump-activated jamming system". In: *Sensors and Actuators A: Physical* (2022), p. 113449.

[90] Inrak Choi, Nick Corson, Lizzie Peiros, Elliot W Hawkes, Sean Keller, and Sean Follmer. "A soft, controllable, high force density linear brake utilizing layer jamming". In: *IEEE Robotics and Automation Letters* 3.1 (2017), pp. 450–457.

[91] A Clark and N Rojas. "Design and workspace characterisation of malleable robots". In: ().

[92] SM Hadi Sadati, Yohan Noh, S Elnaz Naghibi, Althoefer Kaspar, and Thrishantha Nanayakkara. "Stiffness control of soft robotic manipulator for minimally invasive surgery (MIS) using scale jamming". In: *International Conference on Intelligent Robotics and Applications*. Springer. 2015, pp. 141–151.

[93] Hwayeong Jeong and Jung Kim. "Echinoderm inspired variable stiffness soft actuator with connected ossicle structure". In: *2019 International Conference on Robotics and Automation (ICRA)*. IEEE. 2019, pp. 7389–7394.

[94] Francesco Visentin, Saravana Prashanth Murali Babu, Fabian Meder, and Barbara Mazzolai. "Selective Stiffening in Soft Actuators by Triggered Phase Transition of Hydrogel-Filled Elastomers". In: *Advanced Functional Materials* 31.32 (2021), p. 2101121. DOI: `https://doi.org/10.1002/adfm.202101121`. eprint: `https://onlinelibrary.wiley.com/doi/pdf/10.1002/adfm.202101121`. URL: `https://onlinelibrary.wiley.com/doi/abs/10.1002/adfm.202101121`.

[95] Yegor Piskarev, Jun Shintake, Vivek Ramachandran, Neil Baugh, Michael D Dickey, and Dario Floreano. "Lighter and Stronger: Cofabricated Electrodes and Variable Stiffness Elements in Dielectric Actuators". In: *Advanced Intelligent Systems* 2.10 (2020), p. 2000069.

[96] Yegor Piskarev, Jun Shintake, Christophe Chautems, Jonas Lussi, Quentin Boehler, Bradley J Nelson, and Dario Floreano. "A Variable Stiffness Magnetic Catheter Made of a Conductive Phase-Change Polymer for Minimally Invasive Surgery". In: *Advanced Functional Materials* (2022), p. 2107662.

[97] Tingchen Liao, Manivannan Sivaperuman Kalairaj, Catherine Jiayi Cai, Zion Tsz Ho Tse, and Hongliang Ren. "Fully-Printable Soft Actuator with Variable Stiffness by Phase Transition and Hydraulic Regulations". In: *Actuators*. Vol. 10. 10. Multidisciplinary Digital Publishing Institute. 2021, p. 269.

[98] Ali Shiva, Agostino Stilli, Yohan Noh, Angela Faragasso, Iris De Falco, Giada Gerboni, Matteo Cianchetti, Arianna Menciassi, Kaspar Althoefer, and Helge A Wurdemann. "Tendon-based stiffening for a pneumatically actuated soft manipulator". In: *IEEE Robotics and Automation Letters* 1.2 (2016), pp. 632–637.

[99] Victoria Oguntosin, Ayoola Akindele, and Enock Oladimeji. "Gesture-based control of rotary pneumatic soft robot using leap motion controller". In: *2019 6th International Conference on Soft Computing & Machine Intelligence (ISCMI)*. IEEE. 2019, pp. 169–174.

[100] Nathan S Usevitch, Allison M Okamura, and Elliot W Hawkes. "APAM: antagonistic pneumatic artificial muscle". In: *2018 IEEE International Conference on Robotics and Automation (ICRA)*. IEEE. 2018, pp. 1539–1546.

[101] Brian H Do, Valory Banashek, and Allison M Okamura. "Dynamically Reconfigurable Discrete Distributed Stiffness for Inflated Beam Robots". In: *arXiv preprint arXiv:2002.04728* (2020).

[102] Rolf Pfeifer, Max Lungarella, and Fumiya Iida. "The challenges ahead for bio-inspired'soft'robotics". In: *Communications of the ACM* 55.11 (2012), pp. 76–87.

[103] Sangbae Kim, Cecilia Laschi, and Barry Trimmer. "Soft robotics: a bioinspired evolution in robotics". In: *Trends in biotechnology* 31.5 (2013), pp. 287–294.

[104] M Cianchetti, M Calisti, L Margheri, M Kuba, and C Laschi. "Bioinspired locomotion and grasping in water: the soft eight-arm OCTOPUS robot". In: *Bioinspiration and Biomimetics* 10.3 (2015), p. 035003. URL: http://stacks.iop.org/1748-3190/10/i=3/a=035003.

[105] M. Sfakiotakis, A. Kazakidi, N. Pateromichelakis, and D. P. Tsakiris. "Octopus-inspired eight-arm robotic swimming by sculling movements". In: *2013 IEEE International Conference on Robotics and Automation.* May 2013, pp. 5155–5161. DOI: 10.1109/ICRA.2013.6631314.

[106] Alireza Ramezani, Soon-Jo Chung, and Seth Hutchinson. "A biomimetic robotic platform to study flight specializations of bats". In: *Science Robotics* 2.3 (2017). DOI: 10.1126/scirobotics.aal2505. eprint: http://robotics.sciencemag.org/content/2/3/eaal2505.full.pdf. URL: http://robotics.sciencemag.org/content/2/3/eaal2505.

[107] Sina Sareh, Kaspar Althoefer, Min Li, Yohan Noh, Francesca Tramacere, Pooya Sareh, Barbara Mazzolai, and Mirko Kovac. "Anchoring like octopus: biologically inspired soft artificial sucker". In: *Journal of the royal society interface* 14.135 (2017), p. 20170395.

[108] William M. Kier. "The Musculature of Coleoid Cephalopod Arms and Tentacles". In: *Frontiers in Cell and Developmental Biology* 4 (2016), p. 10. ISSN: 2296-634X. DOI: 10.3389/fcell.2016.00010. URL: https://www.frontiersin.org/article/10.3389/fcell.2016.00010.

[109] William McMahan, V Chitrakaran, M Csencsits, D Dawson, Ian D Walker, Bryan A Jones, M Pritts, D Dienno, M Grissom, and Christopher D Rahn. "Field trials and testing of the OctArm continuum manipulator". In: *Proceedings 2006 IEEE International Conference on Robotics and Automation, 2006. ICRA 2006.* IEEE. 2006, pp. 2336–2341.

[110] Andrew D Marchese, Cagdas D Onal, and Daniela Rus. "Autonomous soft robotic fish capable of escape maneuvers using fluidic elastomer actuators". In: *Soft Robotics* 1.1 (2014), pp. 75–87.

[111] Matteo Cianchetti, Tommaso Ranzani, Giada Gerboni, Thrishantha Nanayakkara, Kaspar Althoefer, Prokar Dasgupta, and Arianna Menciassi. "Soft robotics technologies to address shortcomings in today's minimally invasive surgery: the STIFF-FLOP approach". In: *Soft robotics* 1.2 (2014), pp. 122–131.

[112] Matteo Cianchetti, Tommaso Ranzani, Giada Gerboni, Iris De Falco, Cecilia Laschi, and Arianna Menciassi. "STIFF-FLOP surgical manipulator: Mechanical design and experimental characterization of the single module". In: *2013 IEEE/RSJ international conference on intelligent robots and systems.* IEEE. 2013, pp. 3576–3581.

[113] J. Fras and Kaspar Althoefer. "Soft fiber-reinforced pneumatic actuator design and fabrication: Towards robust, soft robotic systems". In: *Annual Conference Towards Autonomous Robotic Systems.* Springer. 2019, pp. 103–114.

[114] Wen Zhou and Yiqing Li. "Modeling and analysis of soft pneumatic actuator with symmetrical chambers used for bionic robotic fish". In: *Soft robotics* 7.2 (2020), pp. 168–178.

[115]   Joshua Bishop-Moser, Girish Krishnan, Charles Kim, and Sridhar Kota. "Design of soft robotic actuators using fluid-filled fiber-reinforced elastomeric enclosures in parallel combinations". In: *Intelligent Robots and Systems (IROS), 2012 IEEE/RSJ International Conference on*. IEEE. 2012, pp. 4264–4269.

[116]   Panagiotis Polygerinos, Zheng Wang, Johannes TB Overvelde, Kevin C Galloway, Robert J Wood, Katia Bertoldi, and Conor J Walsh. "Modeling of soft fiber-reinforced bending actuators". In: *IEEE Transactions on Robotics* 31.3 (2015), pp. 778–789.

[117]   Bertrand Tondu. "Modelling of the McKibben artificial muscle: A review". In: *Journal of Intelligent Material Systems and Structures* 23.3 (2012), pp. 225–253.

[118]   Bertrand Tondu, Serge Ippolito, Jérémie Guiochet, and Alain Daidie. "A seven-degrees-of-freedom robot-arm driven by pneumatic artificial muscles for humanoid robots". In: *The International Journal of Robotics Research* 24.4 (2005), pp. 257–274.

[119]   J. Fras, Y. Noh, H Wurdemann, and K. Althoefer. "Soft fluidic rotary actuator with improved actuation properties". In: *International Conference on Intelligent Robots and Systems*. IEEE. 2017.

[120]   G. Bradski. "The OpenCV Library". In: *Dr. Dobb's Journal of Software Tools* (2000).

[121]   J. Fras, M. Macias, Y. Noh, and K. Althoefer. "Fluidical bending actuator designed for soft octopus robot tentacle". In: *2018 IEEE International Conference on Soft Robotics (RoboSoft)*. IEEE. 2018, pp. 253–257.

[122]   Y. Noh, Akihiro Shimomura, Masanao Segawa, Hiroyuki Ishii, J. Solis, Atsuo Takanishi, and Kazuyuki Hatake. "Development of Tension/Compression Detection Sensor System designed to acquire quantitative force information while training the airway management task". In: *2009 IEEE/ASME International Conference on Advanced Intelligent Mechatronics*. July 2009, pp. 1264–1269. DOI: 10.1109/AIM.2009.5229798.

[123]   Sylvain Abondance, Clark B Teeple, and Robert J Wood. "A dexterous soft robotic hand for delicate in-hand manipulation". In: *IEEE Robotics and Automation Letters* 5.4 (2020), pp. 5502–5509.

[124]   Callum McGuire and Davide Marini. "Inkbit Q&A–Taking 3D printing to the next level". In: *Reinforced Plastics* 65.3 (2021), pp. 142–144.

[125]   J. Fras, J Glowka, and K Althoefer. "Instant soft robot: A simple recipe for quick and easy manufacturing". In: *2020 3rd IEEE International Conference on Soft Robotics (RoboSoft)*. IEEE. 2020, pp. 482–488.

[126]   *Zortrax M200 Product page*. https://zortrax.com/pl/3d-printers/m200/. Accessed: 2019-11-08.

[127]   *Ecoflex 00-50 Product page*. https://www.smooth-on.com/products/ecoflex-00-50/. Accessed: 2017-09-15.

[128]   *Dragonskin Product page*. https://www.smooth-on.com/products/dragon-skin-10-fast/. Accessed: 2017-09-15.

[129]   T Wang, F Xu, Y Huo, and Michel Potier-Ferry. "Snap-through instabilities of pressurized balloons: Pear-shaped bifurcation and localized bulging". In: *International Journal of Non-Linear Mechanics* 98 (2018), pp. 137–144.

[130]   WV Mars. "Evaluation of a Pseudo-Elastic Model for the Mullins Effect". In: *Tire Science and Technology* 32.3 (2004), pp. 120–145.

[131]   Clark B Teeple, Theodore N Koutros, Moritz A Graule, and Robert J Wood. "Multi-segment soft robotic fingers enable robust precision grasping". In: *The International Journal of Robotics Research* 39.14 (2020), pp. 1647–1667.

[132]   Xingxing Ke, Jiajun Jang, Zhiping Chai, Haochen Yong, Jiaqi Zhu, Han Chen, Chuan Fei Guo, Han Ding, and Zhigang Wu. "Stiffness Preprogrammable Soft Bending Pneumatic Actuators for High-Efficient, Conformal Operation". In: *Soft Robotics* (2021).

[133]   DA Kelly. "Axial orthogonal fiber reinforcement in the penis of the Nine-banded Armadillo (Dasypus novemcinctus)". In: *Journal of Morphology* 233.3 (1997), pp. 249–255.

[134]   S. Janbaz, F. S. L. Bobbert, M. J. Mirzaali, and A. A. Zadpoor. "Ultra-programmable buckling-driven soft cellular mechanisms". In: *Mater. Horiz.* 6 (6 2019), pp. 1138–1147. DOI: 10.1039/C9MH00125E. URL: http://dx.doi.org/10.1039/C9MH00125E.

[135]   Chao-Yung Yeh, Shih-Chien Chou, Hsin-Wei Huang, Hung-Chen Yu, and Jia-Yang Juang. "Tube-crawling soft robots driven by multistable buckling mechanics". In: *Extreme Mechanics Letters* 26 (2019), pp. 61–68. ISSN: 2352-4316. DOI: https://doi.org/10.1016/j.eml.2018.12.004. URL: https://www.sciencedirect.com/science/article/pii/S2352431618302220.

[136]   S.L. Veldman, O.K. Bergsma, and A. Beukers. "Bending of anisotropic inflated cylindrical beams". In: *Thin-Walled Structures* 43.3 (2005), pp. 461–475. ISSN: 0263-8231. DOI: https://doi.org/10.1016/j.tws.2004.07.015. URL: https://www.sciencedirect.com/science/article/pii/S0263823104001703.

[137]   A. Stilli, L. Grattarola, H. Feldmann, H. A. Wurdemann, and K. Althoefer. "Variable Stiffness Link (VSL): Toward inherently safe robotic manipulators". In: *2017 IEEE International Conference on Robotics and Automation (ICRA)*. May 2017, pp. 4971–4976. DOI: 10.1109/ICRA.2017.7989578.

[138]   P. Polygerinos, Z. Wang, J. T. B. Overvelde, K. C. Galloway, R. J. Wood, K. Bertoldi, and C. J. Walsh. "Modeling of Soft Fiber-Reinforced Bending Actuators". In: *IEEE Transactions on Robotics* 31.3 (June 2015), pp. 778–789. ISSN: 1552-3098. DOI: 10.1109/TRO.2015.2428504.

[139]   B. Mosadegh, P. Polygerinos, C. Keplinger, S. Wennstedt, et al. "Pneumatic Networks for Soft Robotics that Actuate Rapidly". In: *Advanced Functional Materials* 24.15 (2014), pp. 2163–2170. ISSN: 1616-3028. DOI: 10.1002/adfm.201303288. URL: http://dx.doi.org/10.1002/adfm.201303288.

[140]   Robert Haydn Wilkinson. "A method of generating functions of several variables using analog diode logic". In: *IEEE Transactions on Electronic Computers* 2 (1963), pp. 112–129.

[141]   J. Fras and K. Althoefer. "Bio-mimetic pneumatic soft prosthetic hand". In: *UK-RAS Conference on 'Robotics and Autonomous Systems', Bristol*. UK-RAS, 2017.

[142]   J. Fras and K. Althoefer. "Soft biomimetic prosthetic hand: Design, manufacturing and preliminary examination". In: *2018 IEEE/RSJ International Conference on Intelligent Robots and Systems (IROS)*. IEEE. 2018, pp. 1–6.

[143]   J. Fras, Y. Noh, Macias M., H Wurdemann, and K. Althoefer. "Bio-inspired octopus robot based on novel soft fluidic actuator". In: *International Conference on Robotics and Automation*. IEEE. 2018.

[144]   "e-NABLE Project". In: (). http://enablingthefuture.org, accessed 2018-07-31.

[145]   "Open Bionics". In: (). https://openbionics.com/, accessed on 2018-07-31.

[146] Manuel G Catalano, Giorgio Grioli, Edoardo Farnioli, Alessandro Serio, Cristina Piazza, and Antonio Bicchi. "Adaptive synergies for the design and control of the Pisa/IIT SoftHand". In: *The International Journal of Robotics Research* 33.5 (2014), pp. 768–782.

[147] Yu She, Chang Li, Jonathon Cleary, and Hai-Jun Su. "Design and fabrication of a soft robotic hand with embedded actuators and sensors". In: *Journal of Mechanisms and Robotics* 7.2 (2015), p. 021007.

[148] Huichan Zhao, Kevin O'Brien, Shuo Li, and Robert F Shepherd. "Optoelectronically innervated soft prosthetic hand via stretchable optical waveguides". In: *Sci. Robot.* (2016).

[149] Stefan Schulz, Christian Pylatiuk, and Georg Bretthauer. "A new ultralight anthropomorphic hand". In: *Robotics and Automation, 2001. Proceedings 2001 ICRA. IEEE International Conference on.* Vol. 3. IEEE. 2001, pp. 2437–2441.

[150] Mahmoud Tavakoli and Anibal T de Almeida. "Adaptive under-actuated anthropomorphic hand: ISR-SoftHand". In: *Intelligent Robots and Systems (IROS 2014), 2014 IEEE/RSJ International Conference on.* IEEE. 2014, pp. 1629–1634.

[151] Mike Kaczkowski. "Cosmesis is Much More Than Appearance... It's Function". In: *inMotion* 9 (1999), pp. 1–48.

[152] Vladimir M Zatsiorsky, Zong-Ming Li, and Mark L Latash. "Enslaving effects in multi-finger force production". In: *Experimental brain research* 131 (2000), pp. 187–195.

[153] Marco Santello and John F Soechting. "Force synergies for multifingered grasping". In: *Experimental brain research* 133 (2000), pp. 457–467.

[154] Adalbert I Kapandji. "Clinical evaluation of the thumb's opposition". In: *Journal of Hand Therapy* 5.2 (1992), pp. 102–106.

[155] Thomas Feix, Roland Pawlik, Heinz-Bodo Schmiedmayer, Javier Romero, and Danica Kragic. "A comprehensive grasp taxonomy". In: *Robotics, Science and Systems: Workshop on Understanding the Human Hand for Advancing Robotic Manipulation.* Vol. 2. 2009, pp. 2–3.

[156] Thomas Feix, Javier Romero, Heinz-Bodo Schmiedmayer, Aaron M Dollar, and Danica Kragic. "The grasp taxonomy of human grasp types". In: *IEEE Transactions on Human-Machine Systems* 46.1 (2016), pp. 66–77.

[157] Jan Fras and Kaspar Althoefer. "Soft pneumatic prosthetic hand". In: *Towards Autonomous Robotic Systems: 19th Annual Conference, TAROS 2018, Bristol, UK July 25-27, 2018, Proceedings 19.* Springer. 2018, pp. 112–120.

[158] Jianshu Zhou, Xiaojiao Chen, Ukyoung Chang, Jui-Ting Lu, Clarisse Ching Yau Leung, Yonghua Chen, Yong Hu, and Zheng Wang. "A soft-robotic approach to anthropomorphic robotic hand dexterity". In: *Ieee Access* 7 (2019), pp. 101483–101495.

[159] R Walker. "Shadow dextrous hand technical specification". In: *Shadow Robot Company* 388 (2021).

[160] Mahmoud Tavakoli, Rafael Batista, and Lucio Sgrigna. "The UC softhand: Light weight adaptive bionic hand with a compact twisted string actuation system". In: *Actuators.* Vol. 5. 1. MDPI. 2015, p. 1.

[161] Robert F. Shepherd, Filip Ilievski, Wonjae Choi, et al. "Multigait soft robot". In: *Proceedings of the National Academy of Sciences* 108.51 (2011), pp. 20400–20403. DOI: 10.1073/pnas.1116564108.

[162] M. Calisti, G. Picardi, and C. Laschi. "Fundamentals of soft robot locomotion". In: *Journal of The Royal Society Interface* 14.130 (2017). ISSN: 1742-5689. DOI: `10.1098/rsif.2017.0101`.

[163] Yong Zhong and Ruxu Du. "Design and Implementation of a Novel Robot Fish with Active and Compliant Propulsion Mechanism." In: *Robotics: Science and Systems.* 2016.

[164] M Cianchetti, A Arienti, M Follador, B Mazzolai, P Dario, and C Laschi. "Design concept and validation of a robotic arm inspired by the octopus". In: *Materials Science and Engineering: C* 31.6 (2011), pp. 1230–1239.

[165] Asimina Kazakidi, Michael Kuba, Alex Botvinnik, Michael Sfakiotakis, Tamar Gutnick, Shlomi Hanassy, Guy Levy, John A Ekaterinaris, Tamar Flash, Binyamin Hochner, et al. "Swimming patterns of the octopus vulgaris". In: *22nd Annual Meeting NCM Society.* 2012, pp. 23–29.

[166] Faheem Ahmed, Muhammad Waqas, Bushra Shaikh, Umair Khan, Afaque Manzoor Soomro, Suresh Kumar, Hina Ashraf, Fida Hussain Memon, and Kyung Hyun Choi. "Multi-material bio-inspired soft octopus robot for underwater synchronous swimming". In: *Journal of Bionic Engineering* 19.5 (2022), pp. 1229–1241.

[167] Michael Sfakiotakis, Asimina Kazakidi, Avgousta Chatzidaki, Theodoros Evdaimon, and Dimitris P Tsakiris. "Multi-arm robotic swimming with octopus-inspired compliant web". In: *2014 IEEE/RSJ International Conference on Intelligent Robots and Systems.* IEEE. 2014, pp. 302–308.

[168] Andrea Arienti, Marcello Calisti, Francesco Giorgio-Serchi, and Cecilia Laschi. "Posei-DRONE: design of a soft-bodied ROV with crawling, swimming and manipulation ability". In: *2013 OCEANS-San Diego.* IEEE. 2013, pp. 1–7.

[169] Kazuyuki Ito, Yoshihiro Homma, and Jonathan Rossiter. "The soft multi-legged robot inspired by octopus: climbing various columnar objects". In: *Advanced Robotics* 34.17 (2020), pp. 1096–1109.

[170] Thibaut Paschal, Jun Shintake, Stefano Mintchev, and Dario Floreano. "Development of bio-inspired underwater robot with adaptive morphology capable of multiple swimming modes". In: *2017 IEEE/RSJ International Conference on Intelligent Robots and Systems (IROS).* IEEE. 2017, pp. 4197–4202.

[171] Yara Almubarak, Michelle Schmutz, Miguel Perez, Shrey Shah, and Yonas Tadesse. "Kraken: A wirelessly controlled octopus-like hybrid robot utilizing stepper motors and fishing line artificial muscle for grasping underwater". In: *International Journal of Intelligent Robotics and Applications* 6.3 (2022), pp. 543–563.

[172] Sander van den Berg. "Design of a high speed soft robotic fish". MA thesis. Postbus 5,2600 AA Delft,The Netherlands: Delft University of Technology, 2019.

[173] R. K. Katzschmann, A. d. Maille, D. L. Dorhout, and D. Rus. "Cyclic hydraulic actuation for soft robotic devices". In: *2016 IEEE/RSJ International Conference on Intelligent Robots and Systems (IROS).* Oct. 2016, pp. 3048–3055. DOI: `10.1109/IROS.2016.7759472`.

[174] *MIT News material about SoFi robot, starting from 25s.* URL: `https://youtu.be/BSA_zb1ajes?t=25` (visited on 09/15/2019).

[175] *Flowlink company page, micro gear pumps.* URL: `https://www.flowlink.nl/product-detail/c-series-micro-gear-pumps/` (visited on 09/15/2019).

[176] Pablo Valdivia y Alvarado and Kamal Youcef-Toumi. "Performance of Machines with Flexible Bodies Designed for Biomimetic Locomotion in Liquid Environments". In: vol. 2005. May 2005, pp. 3324–3329. DOI: 10.1109/ROBOT.2005.1570623.

[177] Robert K Katzschmann, Joseph DelPreto, Robert MacCurdy, and Daniela Rus. "Exploration of underwater life with an acoustically controlled soft robotic fish". In: *Science Robotics* 3.16 (2018), eaar3449.

[178] Sijia Liu, Yingjie Wang, Zhennan Li, Miao Jin, Lei Ren, and Chunbao Liu. "A fluid-driven soft robotic fish inspired by fish muscle architecture". In: *Bioinspiration & Biomimetics* 17.2 (2022), p. 026009.

[179] Tiefeng Li, Guorui Li, Yiming Liang, Tingyu Cheng, Jing Dai, Xuxu Yang, Bangyuan Liu, Zedong Zeng, Zhilong Huang, Yingwu Luo, et al. "Fast-moving soft electronic fish". In: *Science advances* 3.4 (2017), e1602045.

[180] Jun Shintake, Vito Cacucciolo, Herbert Shea, and Dario Floreano. "Soft biomimetic fish robot made of dielectric elastomer actuators". In: *Soft robotics* 5.4 (2018), pp. 466–474.

[181] Zhenlong Wang, Guanrong Hang, Jian Li, Yangwei Wang, and Kai Xiao. "A micro-robot fish with embedded SMA wire actuated flexible biomimetic fin". In: *Sensors and Actuators A: Physical* 144.2 (2008), pp. 354–360.

[182] Kangkang Li, Hongzhou Jiang, Siyu Wang, and Jianmin Yu. "A soft robotic fish with variable-stiffness decoupled mechanisms". In: *Journal of Bionic Engineering* 15 (2018), pp. 599–609.

[183] Anirban Mazumdar, Pablo Valdivia Y Alvarado, and Kamal Youcef-Toumi. "Maneuverability of a robotic tuna with compliant body". In: *2008 IEEE International Conference on Robotics and Automation*. IEEE. 2008, pp. 683–688.

[184] Yong Zhong, Zheng Li, and Ruxu Du. "A novel robot fish with wire-driven active body and compliant tail". In: *IEEE/ASME Transactions on Mechatronics* 22.4 (2017), pp. 1633–1643.

[185] Patrick van der Smagt, F Groen, and Klaus Schulten. "Analysis and control of a rubbertuator arm". In: *Biological Cybernetics* 75.5 (1996), pp. 433–440.

[186] Elliot W Hawkes, David L Christensen, and Allison M Okamura. "Design and implementation of a 300% strain soft artificial muscle". In: *2016 IEEE International Conference on Robotics and Automation (ICRA)*. IEEE. 2016, pp. 4022–4029.